Spring 1-1-2013

Nonisothermal Behavior of Compacted Silt Under High Suction Magnitudes

Nahed Alhadi Alsherif
University of Colorado at Boulder, nahed.alsherif@colorado.edu

NONISOTHERMAL BEHAVIOR OF COMPACTED SILT UNDER HIGH SUCTION MAGNITUDES

by

Nahed Alsherif

M.S., Tripoli University - Libya

B.S., Tripoli University - Libya

A thesis submitted to the

Faculty of the Graduate School of the

University of Colorado in partial fulfillment

of the requirement for the degree of

Doctor of Philosophy

Department of Civil, Environmental, and Architectural Engineering

2014

This thesis entitled:

Nonisothermal Behavior of Compacted Silt

under High Suction Magnitudes

written by Nahed Alsherif

has been approved by the Department of Civil, Environmental, and Architectural Engineering

_____

Professor John McCartney (committee chair)

_____

Professor Dobroslav Znidarčić

_____

Professor Ning Lu

Date_____

The final copy of this thesis has been examined by the signatories, and we find that both the content and the form meet the acceptable presentation standards of scholarly work in the above mentioned discipline.

Nahed Alsherif (Ph.D. Civil Engineering, Department of Civil, Environmental, and Architectural Engineering)

Nonisothermal Behavior of Compacted Silt under High Suction Magnitudes

Thesis directed by Professor John S. McCartney

ABSTRACT

An improved understanding of the thermo-hydro-mechanical behavior of unsaturated soils under elevated temperatures and high suction magnitudes is needed to interpret the behavior of thermally-active geotechnical systems where very dry conditions may be encountered. Examples of relevant thermally-active geotechnical systems include ground-source heat exchangers, energy foundation systems, heat dissipation embankments, containment systems for nuclear waste, or backfills for buried electric cables. Important variables governing the performance of these systems include the change in volume and shear strength of a soil element during changes in suction or temperature. Further, the role of effective stress under high suctions and temperatures needs to be established to understand if it is possible to extend thermo-hydro-mechanical constitutive models developed for saturated soils to unsaturated soils.

A new triaxial cell was developed in this study to understand the effects of heating and cooling on the volume change and shear strength of unsaturated silt under high suction magnitudes. The triaxial cell incorporates the vapor flow technique of Likos and Lu (2003) to control high suction magnitudes, and builds upon concepts developed by Uchaipichat and Khalili (2009) for elevated temperature testing including a set of resistance heaters in the cell, a glass cell, cell fluid circulation, and redundant approaches to measure specimen volume change. Three series of triaxial compression tests were performed on specimens of compacted silt under the same high suction magnitude but following different temperature application paths. The testing

series involved ambient temperature conditions, application of a change in temperature before application of suction, and application of a change in suction before application of a change in temperature.

The results from isothermal tests on the compacted silt were used to evaluate the role of effective stress state at high suctions. Further they were used to interpret the role of suction-induced hardening in unsaturated soils. A brittle-stress strain curve was observed in all tests performed on unsaturated silt under high suctions. A sharp decrease in shear stress was observed after reaching the peak shear strength and it was not possible to reach critical state conditions at larger displacements. As expected, the tests on unsaturated silt under high suctions had significantly higher shear strength than the soil under saturation conditions for the same consolidation stresses. In this case, application of suction likely led to an increase in the preconsolidation stress of the soil, and the peak shear strength values were used to estimate the change in preconsolidation stress using established constitutive relationships for unsaturated soils. The stress state in the unsaturated specimens was successfully described using the single-value effective stress principle using the suction-stress characteristic curve predicted from the shape of the soil water retention curve (SWRC). The suction stress characteristic curve (SSCC) was observed to increase significantly with increasing suction, and did not tend toward an asymptotic value for the range of suctions investigated in this study. This confirms that the application of high suctions can have a major impact on the effective stress state and the associated shear strength of the soil. The results indicate the importance of carefully understanding the shape of the SWRC before estimating the SSCC.

The results from nonisothermal tests indicate that the path of testing has a major impact on the volume change and shear strength of compacted silt under high suction magnitudes. The

change in temperature led to an increase in shear strength when it was applied after the change in suction, which was contradictory to observations for tests on compacted silt under low suctions reported in other studies. The reason for the contradictory behavior is likely due to the lower degree of saturation of the specimens tested following the S-T path, and it is hypothesized that the degree of saturation has a different effect on the stress state at high suction magnitudes near residual saturation conditions than for nearly-saturated soils. When a high suction magnitude was applied after a change in temperature, a lower shear strength was observed than the tests performed under ambient temperature, which is possibly due to a greater amount of softening occurred during heating at low suction values. A cyclic heating-cooling test performed on a soil that was brought to suction equilibrium before heating indicates that the shear strength after cooling was greater than that of the ambient temperature test. The effects of testing paths were attributed to relative effects of hardening during suction application and softening during heating, and thermo-elasto-plastic constitutive models were used to explain the effects of temperature on the peak shear strength of unsaturated soils.

ACKNOWLEDGEMENT

The author wishes to thank her advisor, Professor John Scott McCartney, for his guidance, assistance, and positive attitude, which helped immensely through the completion project. Special recognition is given to Professors Dobroslav Znidarčić, Richard Regueiro, Harihar Rajaram, and Ning Lu for serving on my thesis committee. Deserving of additional thanks for their enthusiasm and assistance are the many geotechnical engineering students and professors at the University of Colorado Boulder, whom there are far too many to list. A special thanks goes to Adel Sasi, and my family, who have inspired me to achieve my goals. Funding from Libyan government and NSF CMMI 1054190 is greatly appreciated.

Table of Contents

List of Tables

List of Figures

1. INTRODUCTION

1.1.Motivation and Problem Statement

An improved understanding of the thermo-hydro-mechanical behavior of unsaturated soils during application of elevated temperatures and high suction magnitudes is needed to interpret the behavior of thermally-active geotechnical systems located above the water table that may experience very dry soil conditions. These include ground-source heat exchangers (Preene and Powrie 2009), energy foundation systems (Brandl 2006; Laloui et al. 2006; Adam and Markiewicz 2009; Bourne-Webb et al. 2009; McCartney and Murphy 2012), heat dissipation embankments (McCartney 2012; Coccia and McCartney 2013), soil-borehole thermal energy storage systems (Sibbitt et al. 2012; McCartney et al. 2013a); containment systems for nuclear waste (Gens et al. 1998; Kanno et al. 1999), and backfills for buried electrical cables (Abdel-Hadi and Mitchell 1981; Brandon et al. 1989). When these thermally-active geothermal systems are operated in heating mode, thermally induced water flow will cause the soil nearest to the heat exchangers to dry, potentially to the point that very high suction magnitudes may be encountered.

The shear strength and volume change behavior of unsaturated soils under high suction magnitudes due to changes in temperature remain largely uncertain due to the lack of supporting experimental data in the literature. Several studies have been performed to understand the effects of high suction magnitudes on the isothermal behavior of unsaturated soils (Blatz and Graham 2000; Nishimura and Fredlund 2000; Lloret et al. 2003), and experimental procedures and advanced triaxial testing devices have been developed to evaluate the shear strength of unsaturated soils under high suction values (Delage et al.1987; Cui and Delage 1996; Blatz and Graham 2000; Cunningham et al. 2003; Nishimura and Fredlund 2003). Other studies have

evaluated the non-isothermal behavior of unsaturated soils subjected to low suction magnitudes in terms of shear strength (Uchaipichat and Khalili 2009) and volume change (Saix 1991; Saix et al. 2000; Romero et al. 2003; Tang and Cui 2005; Uchaipichat and Khalili 2009; Gens 2010). However, none of these studies have directly dealt with testing of unsaturated soils under high suction magnitudes and elevated temperatures. Although data is available on the thermo-hydro-mechanical response of compacted silt under low suction magnitudes (Uchaipichat and Khalili 2009), the behavior of compacted silt under high suctions may differ. Specifically, the pore water under very low degrees of saturation (less than 5%) may have different effects on the effective stress state and the thermal volume change response than under higher degrees of saturation. Small changes in volume of the pore water during temperature changes may lead to large changes in suction at the tail-end of the soil-water retention curve (SWRC), and the soil may retain less water under high suction magnitudes (Grant and Salehzadeh 1996; Romero et al. 2003). Further, the role of suction and degree of saturation in the definition of effective stress at high suction magnitudes and nonisothermal conditions is uncertain, as most studies linking these variables involved verification using results from tests involving suction magnitudes less than 500 kPa (Lu et al. 2010). Due to the lack of experimental data on shear strength and volume change under high suctions and nonisothermal conditions, the suitability of extending effective stress-based thermo-elasto-plastic constitutive relationships developed for saturated soils to unsaturated conditions has not been assessed.

Constitutive models for saturated soils indicate that temperature will lead to a change in volume that is sensitive to the initial stress state. Specifically, normally consolidated, saturated soils generally experience a contraction in volume during heating, likely due to the greater coefficient of thermal expansion of pore water compared to that of the soil skeleton (Campanella

and Mitchell 1968). During heating, both the water and particles expand, but the water expands approximately 7 to 10 times more (McKinstry 1965; Mitchell and Soga 2005), creating a pressure gradient that leads to consolidation and permanent contraction. Overconsolidated soils typically experience expansion during heating, as the role of the pore water becomes less relevant for the tightly packed arrangement of particles typical of overconsolidated soils. The impact of temperature on the shear strength of soils is generally believed to be due to changes in the preconsolidation stress and yield function of the soil with temperature (Houston et al. 1985; Eriksson 1989; Hueckel et al. 1990; Cui et al. 2000; Hueckel et al. 2009). In most saturated soils and unsaturated soils under low suction magnitudes, an increase in temperature leads to a decrease in the preconsolidation stress if the specimen is subsequently loaded (Tidfors and Sällfors 1989). The effects of the reduction in the preconsolidation stress on the shape of the yield surface may lead to a decrease in the peak shear strength for some stress states (Uchaipichat and Khalili 2009). However, the critical state shear strength is typically unaffected by temperature.

At high suction magnitudes, several aspects are expected to play a different role than under low suctions. The role of pore water in the thermo-mechanical response of soils may be different under high suction magnitudes than under saturated conditions or low suction magnitudes. Specifically, the volume change of the pore water during heating will likely not lead to changes in degree of saturation or changes in suction for very dry conditions. However, the pore water should still play an important role in the inter-particle interactions and corresponding effective stress. Similar to low suction magnitudes, temperature may have an impact on the preconsolidation stress for high suction magnitudes. Accordingly, a difference in the overall thermal response of unsaturated soils under high and low suction magnitudes is expected. The

van der Waals attraction forces are expected to play an important role in the inter-particle stresses in fine grained soils under low degrees of saturation (Lu and Likos 2006). Several studies have found that the shear strength of soils can be significantly greater in the residual saturation range than that in the funicular range (Blatz et al. 2002; Nishimura and Fredlund 2000). This is confirmed by a reduction in volume and behavior similar to overconsolidated, saturated soils or even rock in the case of very high suction values. It is well established that saturated soils with a high overconsolidation ratio (OCR) will expand elastically during heating, while saturated soils with a low OCR may contract permanently during heating (Baldi et al. 1988; Cekeravac and Laloui 2004). However, the role of stress state under high suction magnitudes is not well understood. Although it is expected that application of high suction magnitudes will lead to an increase in effective stress as well as an increase in the preconsolidation stress, the relative increases in each of these values will lead to different OCR values.

1.2.Objectives of the Study

The primary objective of this research project is to understand the nonisothermal shear strength and deformation behavior of unsaturated silt under high suction magnitudes. Specifically, this study will involve an investigation of the effects of temperature changes on the soil-water retention curve (SWRC), volume change parameters, shear-stress strain curves, and shear strength failure envelope parameters for unsaturated soils under high suction magnitudes. An understanding of the inter-relationships between these variables also helps improve our understanding of the effective stress in unsaturated soils under different conditions, and helps to develop nonisothermal elasto-plastic constitutive relations for unsaturated soils. Although a range of constitutive relationships have been developed for saturated soils (Hueckel and Baldi

1990; Cui et al. 2000; Laloui and Cekerevac 2003; Abuel-Naga et al. 2009; Hueckel et al. 2009), the behavior of unsaturated soils in nonisothermal conditions has not been thoroughly investigated. Accordingly, more research is needed to understand if these constitutive relationships can be extended to soils under high suction magnitudes.

1.3 Approach

To accomplish the objective of this study, a new triaxial cell was developed to measure the shear strength of unsaturated soils under elevated temperatures and high suction magnitudes. Specifically, the vapor flow technique developed by Likos and Lu (2003) was employed in the triaxial cell to control high suction magnitudes, and a temperature control system to apply elevated temperatures. The vapor flow technique is used to control the total suction in a soil specimen by modulating the relative humidity within a silt specimen using a mass flow control system with relative humidity feedback. This system mixes water-saturated and dry air to a given proportion, after which this air is passed through the soil specimen until reaching relative humidity equilibrium. Further, the details of the triaxial cell were defined based on the experience of Uchaipichat and Khalili (2009), including the use of a set of resistance heaters within the triaxial cell, a glass pressure cell, cell fluid circulation, and redundant approaches to measure specimen volume change.

The experimental program includes performing two sets of anisotropic consolidated-drained triaxial tests under different temperatures. The first set is a set of isothermal anisotropic consolidated-drained triaxial tests that was performed on compacted silt specimens under different combinations of total suction and net normal stress. The results from the triaxial tests are used to investigate the effective stress principle in unsaturated soils through the concept of the suction-stress characteristic curve (SSCC). Specifically, these results were analyzed to

examine the applicability of predicting SSCC using parameters from SWRC models fitted to data defined at low suction magnitudes. The second set of tests is divided into two groups of nonisothermal anisotropic, consolidated-drained triaxial tests which were performed following two different testing paths to investigate the influence of temperature and high suction on the shear strength and volume change parameters of unsaturated soils during shearing. Finally, one test was performed under nonisothermal condition with heating cooling cycle to investigate the effects of temperature cycle on soil volume change behavior.

The research program involves the following major tasks:

1. Design, calibrate, and verify the performance of a triaxial apparatus for testing shear strength properties of unsaturated soils under high suction magnitudes and elevated temperature.
2. Perform a comprehensive experimental program to investigate the influence of temperature, high suction and net normal stress on the peak shear strength parameters, volume change parameters and soil water retention curve parameters of unsaturated silt.
3. Evaluate the effective stress in compacted silt specimens under low degrees of saturation and assess the implications of using a single SWRC curve over the full range of saturation.
4. Evaluate the role of temperature on the shape of the SWRC under high suction magnitudes.
5. Understand the nonisothermal shear strength and deformation behavior of unsaturated silt under high suction magnitudes in terms of the volume change curves during suction and temperature application, the shear stress-strain curves, and the shear failure envelopes.
6. Use constitutive models available in literature for water retention, effective stress, and elasto-plastic stress-strain behavior to evaluate the experimental results.

1.4. Thesis Organization

The structure of the thesis is as follows: A literature review focused on the experimental and theoretical investigations relating to the effects of temperature and suction on soil behavior is presented in Chapter 2. The vapor flow technique used to control high suction magnitudes in unsaturated soils, as well as the effects of temperature on the vapor equilibrium technique, are also reviewed in this chapter. The effects of high suction and elevated temperature on the soil water retention curve (SWRC) of unsaturated soils are also reviewed. As an understanding of the stress state in unsaturated soils is critical to interpretation of the triaxial test results, a discussion on the principle of effective stress is presented, along with a discussion on how the effective stress is linked with the SWRC. Next, a review of volume change behavior of soils due to suction and temperature change is considered, and the effects of suction and temperature on the shear strength of unsaturated soils are reviewed. Finally, constitutive models that have been proposed in the literature for capturing the effects of temperature and suction on the volume change and shear strength behavior of unsaturated soils are presented.

The geotechnical properties of the soil used in this study, Bonny silt, is described in Chapter 3. These include the grain size distribution, compaction characteristics, saturated shear strength parameters, hydraulic properties, thermal conductivity, air permeability, and isothermal volume change properties. Details of the thermo-hydro-mechanical triaxial cell and suction control system developed as part of this research project are provided in Chapter 4. The experimental equipment and an assessment of the suction application are described first. Next, detailed description of the calibration tests is presented, including thermal calibration test performed to account for thermal volume change of the triaxial cell with its different

components, and relative humidity calibration test performed to account for the relative humidity.

The experimental program and test procedures followed in this research program are described in Chapter 5. The sample preparation and the sample set up are described first. Then, the experimental procedures followed for performing both isothermal and non-isothermal tests are presented in addition to showing all measurements during all testing stages. Finally, corrections to triaxial data are presented along with the analysis steps. The results of the experimental investigation on effects of high suction and elevated temperature on soil behavior are presented in Chapter 6. The experimental results from isothermal anisotropic consolidated-drained triaxial tests are presented first, followed by the experimental results from nonisothermal anisotropic consolidated-drained triaxial tests.

The results obtained from the isothermal and nonisothermal anisotropic consolidated-drained triaxial tests to evaluate the soil water retention curve and effective stresses relationship at high suction magnitudes are discussed and analyzed in Chapter 7. A theoretical assessment of constitutive models available in literature using the experimental results is provided in this chapter. The main conclusions of this research effort are summarized in Chapter 8.

2. LITERATURE REVIEW

2.1.Introduction

The first section of this chapter includes a summary of the vapor equilibrium technique (VET), which is the basis of the vapor flow technique used to control suction in the new triaxial cell in this study. This section also discusses the limitations and relevant laboratory apparatus used for application of the VET. Next, the role of high suction and elevated temperature on the soil water retention curve (SWRC) of unsaturated soils are reviewed in Section 2.3. As an understanding of the stress state in unsaturated soils is critical to interpretation of the triaxial test results, a discussion on the principle of effective stress is presented in Section 2.4, along with a discussion on how the effective stress is linked with the SWRC. A review of volume change behavior of soils due to suction and temperature change is considered in Section 2.5, the effects of suction and temperature on the shear strength of unsaturated soils are reviewed in Section 2.6. This includes a discussion of a preliminary testing program performed by the author (Alsherif and McCartney 2012) to understand this behavior. Constitutive models that have been proposed in the literature for capturing the effects of temperature and suction on the volume change and shear strength behavior of unsaturated soils are presented in Section 2.7.

2.2.Vapor Equilibrium Technique for Control of High Suction Magnitudes

2.2.1 General

The vapor equilibrium technique has been used in several studies to control the total suction in unsaturated soils (Tessier 1984; Delage et al. 1998; Romero 1999; Delage and Cui 2000; Villar 2000; Blatz et al. 2008). This technique involves the use of saturated salt solutions to control the relative humidity of the air within a closed chamber. If a soil specimen is suspended above the air within the chamber, the relative humidity within the chamber will cause

evaporation or condensation of water from the soil pores. The basis of the vapor equilibrium technique is Kelvin's law, which relates the total suction in the soil with the relative humidity of the air in closed environmental chamber containing saturated salt solutions, as follows:

$$\psi = \frac{\rho_w RT}{M_w} \ln(R_h) \qquad \text{Eq. 2.1}$$

where ψ is the total soil suction (kPa), R is the universal (molar) gas constant, equal to 8.31432 J/molK, T is the absolute temperature in Kelvin, M_W is the molecular mass of water vapor equal to 18.016 g/mol, ρ_w is the density of water (kg/m^3), and R_h is the relative humidity of the pore air in decimal form. The relative humidity is related to the total suction in the soil, not the matric suction. The matric suction is associated with capillarity effects in the soil, while the total suction incorporates the effects of both capillarity and osmotic potential.

2.2.2 Laboratory Equipment for Vapor Equilibrium Application

The vapor equilibrium technique has been originally incorporated into laboratory test equipment to measure the mechanical properties of unsaturated materials under various stress paths and initial conditions. Oedometers have been modified to control high total suction in the wetting condition by many researchers to examine the swelling behavior of unsaturated clay (Jenning and Burland1962; Matyas and Radhakrishna 1968; Fredlund and Morgenstern1977; Esteban 1990). In these studies, suction was not directly controlled, where the specimen was placed in the oedometer in initial unsaturated condition and wetted until the metric suction is equal to zero. An improvements to the testing apparatus have been achieved by many others to control the suction applied and overcome the limitation of the testing technique (Escario1969; Escario and Sáez 1986; Belanteur et al. 1997; Villar 1999; Cuisinier and Masrouri 2004; and Hoffman et al. 2005). Due to difficulties in controlling the stress state in oedometer tests, several other studies have incorporated the vapor equilibrium technique into triaxial cells for application

of high suctions (Blatz and Graham 2000; Nishimura and Fredlund 2003). The suction was applied in this triaxial cell by either circulating air vapor through the pedestal base porous stone as shown in Figure 2.1, where vapor exchange takes place between the specimen and the circulating air, or by placing the entire cell within a relative humidity control chamber.

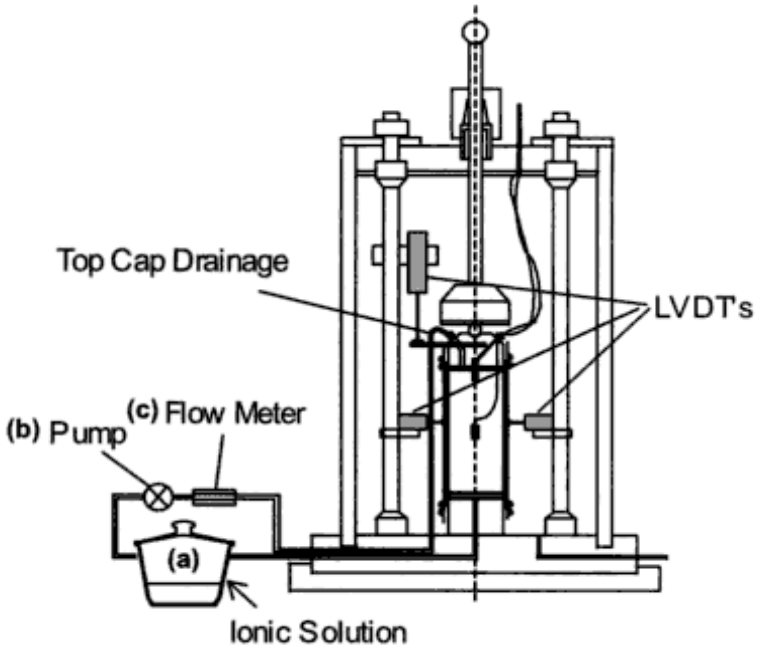

Figure 2.1: Triaxial equipment with vapor equilibrium technique for suction control (Blatz and Graham 2000)

Although the vapor equilibrium technique using the saturated salt solutions is a simple approach to control the total suction in these testing apparatus, it may be time consuming due to the slow rates of evaporation and condensation. In addition, the change in the salt solution concentration and the solubility of the salt due to temperature increase over time would change the target suction applied to the soil specimen. Test results obtained using this technique have shown a sensitivity to air temperature (Tang and Cui 2005). Tang and Cui (2005) performed a calibration tests for several saturated salt solutions to account for the effect of temperature on the relative humidity and consequently on the suction applied. They found that changes in

temperature from 20 to 80 °C can lead to changes in suction from 82 to 184 MPa for a saturated solution of $Mg(NO_3)_2$. This increase in suction due to increasing temperature and their coupled effect on the shear strength of unsaturated soil under high suction values was pointed out by Alsherif and McCartney (2012) and they suggested further investigation.

To speed up the rate of evaporation, a circulation system was used to force the air to flow through the soil specimens using an air flow pump (Cunningham et al. 2003; Nishimura and Fredlund 2003; Blatz and Graham 2003). The effect of using the circulation system on the target suction applied was assessed by Pintado et al. (2009) using the same odometer apparatus that used by Lloret et al. (2003). Their test results indicate that the time needed to reach equilibrium can be shortened from weeks to days by using air circulation. They also stated that necessary precautions should be taken because equilibrium suction could differ from the applied suction due to the gas pressure difference between the boundaries. They suggested some precautions such as keeping the air pressure difference smaller than 10 kPa between boundaries to improve the accuracy of results and using soils with high air permeability to help reducing this differential pressure. Soils having high air permeability would easily allow the forced air to go through the soil and the pressure difference between the bottom and top of the soil specimen will be at minimum level. Greater values of air permeability for compacted soils occur for lower values of initial degree of saturation, or by drying the soil specimen to a low degree of saturation before placement in the testing device.

2.2.3. Vapor Flow Technique

Due to the issues noted with the use of saturated salt solutions to independently control the temperature and suction in soils, an alternative approach involving vapor flow control may be more appropriate. The suction control system proposed by Likos and Lu (2003) shown in

Figure 2.2, is particularly suited for this application. They developed a system to control the relative humidity of pore air flowing through a soil specimen by using mass flow controllers to mix water-saturated and dry air to a known proportion for the measurement of total suction characteristic curve of unsaturated clay. The equilibrium water content of soil samples placed on an electronic balance in the controlled humidity environment is measured as water is adsorbed or desorbed the “humid” gas.

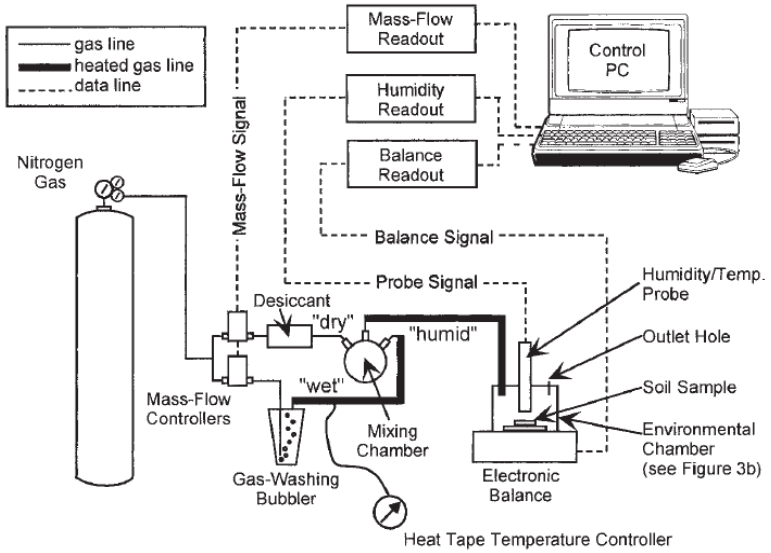

Figure 2.2: Vapor flow technique for control of high suction (Likos and Lu 2003)

Likos and Lu (2003) proved the validity of the test technique by comparing their test results with results obtained from tests using non-contact filter paper technique performed on the same clay as shown in Figure 2.3. This figure shows an agreement between results obtained by both testing technique. The advantages of the new system over existing suction measurement techniques are that it is fully automated, has a much broader measurement range and is capable of determining both wetting and drying characteristics in significantly less time. However, this technique has been employed only in measurement of total suction characteristic curve under

isothermal conditions, and yet not used to assess the thermo-hydro-mechanical properties of unsaturated soils in the relatively high suction range.

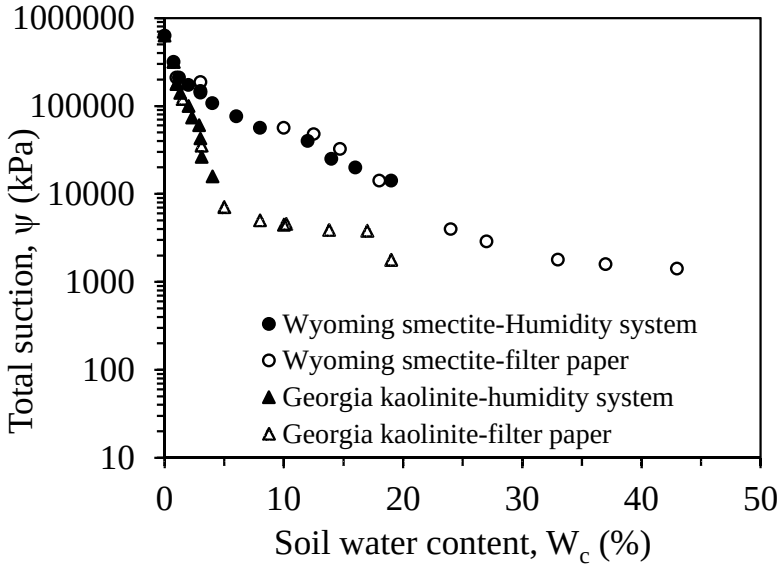

Figure 2.3 Comparison of non-contact filter paper measurements and automated humidity system measurements for Wyoming smectite and Georgia kaolinite (Likos and Lu 2003)

2.3.Soil Water Retention in Unsaturated Soils at High Suctions

2.3.1.General Comments

The amount of water stored in a soil system and its relation to the applied matric suction is an important aspect to define soil condition. The relationship that relates the degree of saturation or water content to the matric suction is described as the soil water retention curve (SWRC). Points on the SWRC be defined by relating the equilibrium suction with the gravimetric water content or degree of saturation at equilibrium. Points on the SWRC in the low suction range are usually defined, using the axis translation technique, as the equilibration degree of saturation at which no more water can be extrapolated from the soil system under particular applied matric suction. Points on the SWRC in the high suction range are defined using vapor equilibrium technique by converting the equilibrium relative humidity to total suction using Kelvin's equation (Eq. 2.1).

The gravimetric water content following the vapor equilibrium testing technique in defining points on SWRC is calculated after each period of time, as follows (ASTM D6836):

$$w_i = w_o + \frac{M_i - M_o}{\rho_d V} \qquad \text{Eq. 2.2}$$

where w_i is the gravimetric water content corresponding to the i^{th} measurement of suction, w_o is the gravimetric water content for the first suction measurement, M_o is the mass of the specimen for the first suction measurement (kg), M_i is the mass of the specimen for the i^{th} suction measurement (kg), ρ_d is the dry density at which the specimen was prepared (kg/m^3), V is the volume of the specimen (m^3). The degree of saturation corresponding to the measured gravimetric water content is calculated as follows:

$$S = \frac{w}{\frac{\rho_w}{\rho_d} - \frac{1}{G_s}} \qquad \text{Eq. 2.3}$$

where S is the degree of saturation, G_s is the specific gravity and ρ_w is the water density (kg/m^3). During the equilibration process, it is important to maintain the temperature constant, as the relative humidity is particularly sensitive to temperature. The equilibrium state can be achieved when there is no further change in the degree of saturation along with no further change in relative humidity for two or three following measurements at the ambient temperature.

Brooks and Corey (1964), van Genuchten (1980), and Fredlund and Xing (1994) have developed constitutive relationships to represent the change in water storage of soils as a function of suction. They proposed various equations, each with set of fitting parameters, to match as smoothly and accurately the experimental data points as possible. van Genuchten (1980) proposed a hyperbolic function with two fitting parameters α_{vG} and N_{vG} to characterize the SWRC of a soil in terms of degree of saturation, given as follows:

$$S_r = \frac{S_{res} + (S_{sat} - S_{res})}{\left(1 + [\alpha_{vG}\psi]^{N_{vG}}\right)^{1-\frac{1}{N_{vG}}}} \qquad \text{Eq. 2.4}$$

where S_r is the degree of saturation, S_{res} is the residual degree of saturation and S_{sat} is equal to 1, ψ is suction applied, and N_{vG} and α_{vG} are empirical parameters used to fit the SWRC to experimental data. α_{vG} is typically considered to be the inverse of air entry suction and N_{vG} is a parameter related to the pore size distribution and the slope of the SWRC for suctions between the air entry suction and the residual degree of saturation. An example of the soil water retention curve by Sillers et al. (2001) showing the entire different saturation regions is presented in Figure 2.4. This figure presents the variation of saturation with increasing suction and how to define the air entry suction value.

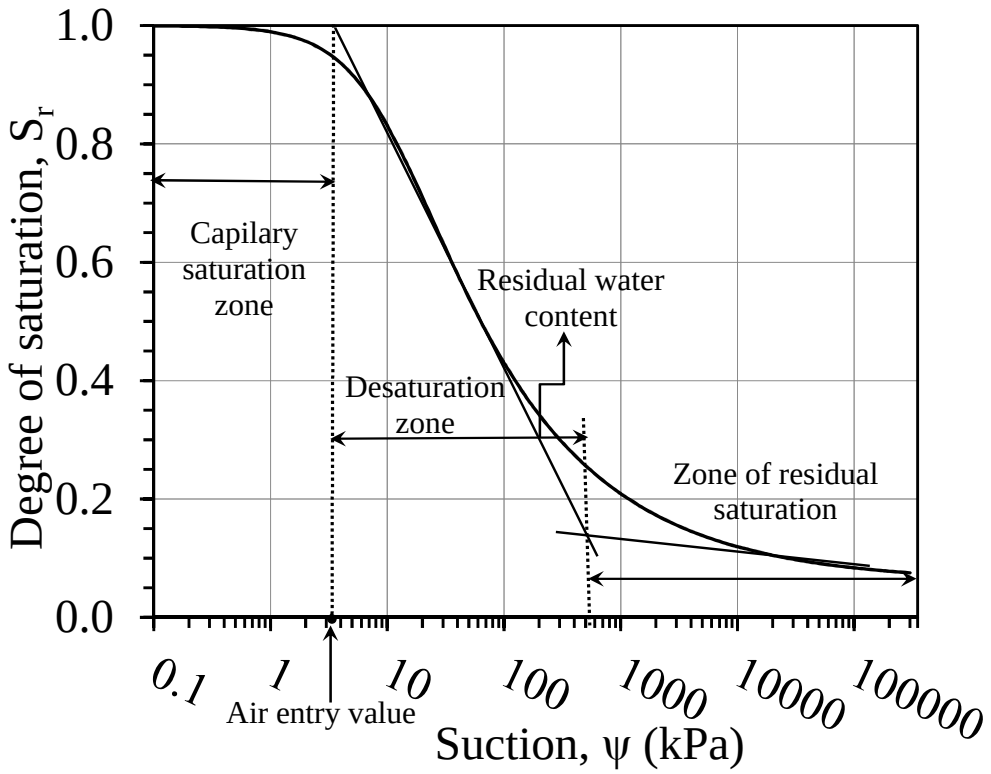

Figure 2.4: SWRC defined for the entire range of suction under isothermal condition showing the regions of de-saturation (Sillers et al. 2001)

2.3.2. Influence of Temperature on SWRC

The effect of temperature on the SWRC of compacted soils under high suction magnitudes has been investigated in several studies. This is important to consider as changes in the SWRC may affect the mechanical Behavior of unsaturated soils (Romero et al. 2001; Uchaipichat and Khalili 2009). Early studies in the area of soil physics by Grant and Salehzadeh (1996) and She and Sleep (1998) observed that an increase in temperature leads to a decrease in degree of saturation for a given suction. They attributed this shift to changes in the soil-water contact angle, a reduction in the interfacial tension between air and water, and thermal expansion of air entrapped within the soil pores. They observed that the change in contact angle primarily led to a reduction in the air entry suction. A shift in the SWRC to lower degrees of saturation for elevated temperatures was also reported in studies that involved control of the stress state and measurement of volume change as shown in Figure 2.5, including Romero et al. (2001), Salager et al. (2007), and Uchaipichat and Khalili (2009) for low suction values and Olchitzky (2002), Romero et al. (2003), Imbert et al. (2005), Tang and Cui (2005), and Villar and Gomez (2007) for high suction values. Romero et al. (2003) found that the density of the soil does not affect the SWRC at low degrees of saturation. Olchitzky (2002) compared his results with a prediction based on a reduced interfacial tension, and found that this reduction was not sufficient to explain the change in water retention with temperature. Uchaipichat and Khalili (2009) observed that the SWRC under different temperatures is independent of stress level for low suction magnitudes.

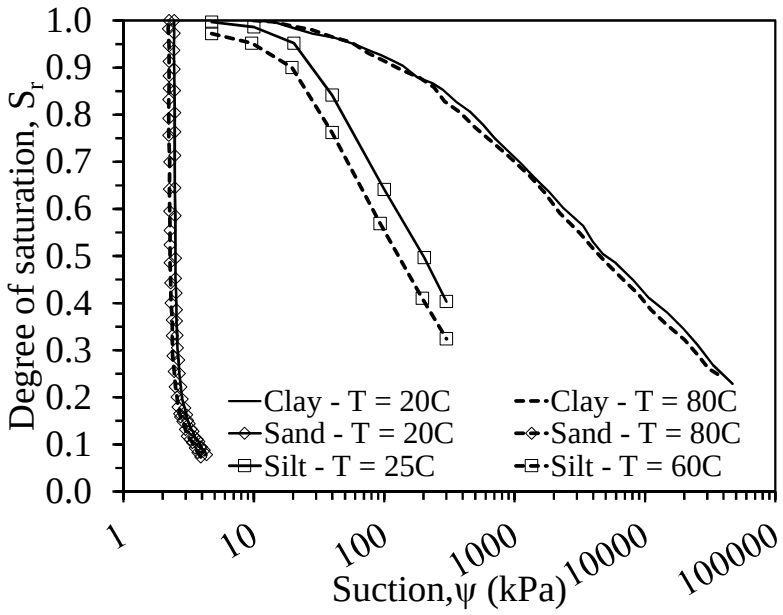

Figure 2.5: Soil water retention curves for Boom clay (Romero et al. 2003), sand (Thomas et al. 2001) and compacted silt (Uchaipichat and Khalili 2009) at different temperatures

2.4.Stress State in Unsaturated Soils

Many of the previous studies on the principle of effective stress in unsaturated soils used the axis translation technique to characterize the shear strength or volume change of soil specimens having relatively high degrees of saturation (Khalili et al. 2004; Lu and Likos 2006; Khalili and Zargarbashi 2010; Alonso and Romero 2011). At these relatively high degrees of saturation, typically greater than 0.5, the water phase is usually connected through the specimen. Khalili and Khabbaz (1998), Lu and Likos (2006), Kayadelen et al. (2007), and Lu et al. (2010) have shown experimentally and analytically that the soil-water retention curve (SWRC) and the effective stress are functionally related, and these relationships are assumed to hold over the whole range of saturation. Lu et al. (2010) proved that the van Genuchten (1980) SWRC model can be used to define the effective stress in both unsaturated sands and clays, and derived analytical expressions for clays that show that effective stress increases monotonically with increasing suction for the case of constant net normal stress.

Despite the strong evidence supporting a relationship between the SWRC and effective stress, this relationship has not been fully verified at high suction magnitudes (or low degrees of saturation) where the water phase is not continuous. This is a critical gap in the literature because it is common practice to extrapolate the shape of the SWRC fitted to data at high degrees of saturation to the entire range of degree of saturation. Even when SWRC data is defined at high suctions using separate tests, the uncertainty in the data may be particularly high due to specimen variability, changes in volume, large changes in suction with relatively small changes in relative humidity of the pore air, and issues with defining thermodynamic equilibrium (Blatz et al. 2008; Delage et al. 2008).

Bishop (1959) formulated a relationship for the effective stress in unsaturated soils that incorporated a soil-specific effective stress parameter χ to account for the impact of the amount of pore water, as follows:

$$\sigma' = (\sigma - u_a) + \chi(u_a - u_w) \qquad \text{Eq. 2.5}$$

where the difference between the total normal stress σ and the pore air pressure u_a is referred to as the net normal stress σ_n, and the difference between the pore air pressure u_a and the pore water pressure u_w is referred to as the suction ψ, and χ is referred to as the effective stress parameter. Skempton (1961) defined a general equation for the effective stress in unsaturated soils building upon the relationship of Bishop (1959) that considers the relative compressibility values of the soil skeleton and soil particles and the effects of saturation:

$$\sigma' = \sigma - \left(1 - \frac{c_s}{c}\right) S_\chi u_w \qquad \text{Eq. 2.6}$$

where σ' is the effective stress, c_s is the compressibility of the grains, c is the compressibility of the granular skeleton, u_w is the pore water pressure, and S_χ is a scaling parameter for saturation

defined using the χ value used in Bishop's (1959) definition of effective stress. Skempton (1961) used this equation to evaluate the need for considering the role of pore water pressure in stiffer materials like rock and concrete. This equation indicates that the definition of a single-value effective stress for both saturated and unsaturated soils requires knowledge of the material properties of the soil.

Difficulties were encountered in selecting an appropriate definition of the effective stress parameter due to issues such as hysteresis and volume change (Blight 1967). In attempting to overcome these issues, while also eliminating the necessity to define the effective stress parameter, Lu and Likos (2006) referred to the second term in Equation 2.6 as the suction stress σ_s, a material relationship that is a function of suction or the degree of saturation, S_r. Lu and Likos (2006) defined σ_s as a macroscopic stress that collectively incorporates the effects of capillarity, soil- and pore fluid-specific forces such as van der Waals forces, electrical double-layer repulsion forces, and the net attraction forces arising from chemical cementation at the grain contacts. The functional relationship between suction stress and suction for a given soil under a certain stress state was referred to as the suction stress characteristic curve (SSCC).

Lu and Likos (2006) proposed an empirical approach to determine the SSCC using shear strength failure envelopes defined from drained shear strength tests performed on saturated and unsaturated soil specimens under controlled values of matric suction as shown in Figure 2.6. Although the failure envelopes are plotted as a function of net normal stress in this figure, they still represent effective failure envelopes as they should be defined from drained tests. Lu and Likos (2006) assumed that the suction stress σ_s at a given suction ψ is equal to the apparent tensile strength, which could be calculated from the intercept of the failure envelopes with the normal stress axis as follows:

$$\sigma_s = \frac{c}{\tan(\phi')} \qquad \text{Eq. 2.7}$$

where c is the apparent cohesion of the soil due to the effects of suction and □′ is the effective friction angle. To define the SSCC shown in the schematic in Figure 2.6, the apparent cohesion for saturated soils tested under drained conditions is assumed negligible, which is the case for uncemented soils, and the friction angle is assumed to be constant with confining stress. Further, it is assumed that the friction angle does not change when different suction values are applied to the soil (Escario 1980; Nishimura and Fredlund 2000). This assumption may only be valid for the case of rigid soils that do not change in volume during changes in matric suction (e.g., sands, silts, and clays of low plasticity). Changes in σs and the effective stress parameter χ with suction have been evaluated for different soils using the approach similar to that shown in Figure 2.6 (Khalili and Khabbaz 1998; Lu and Likos 2006; Khosravi et al. 2012).

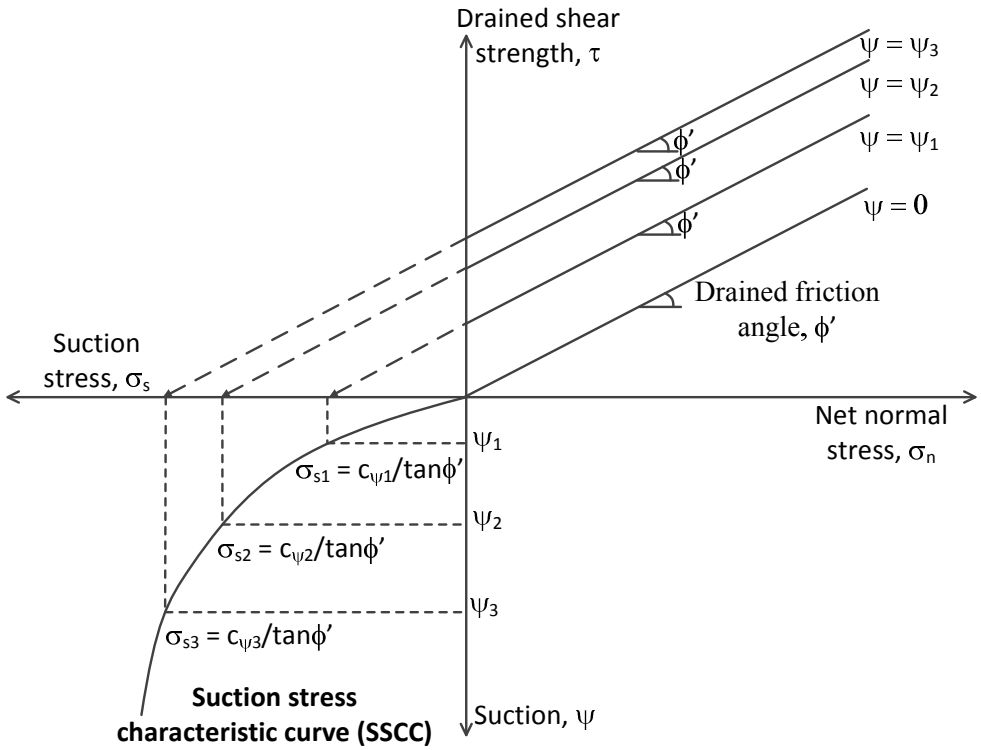

Figure 2.6 Schematic showing the definition of the suction stress vs. matric suction relationships using shear strength failure envelopes (after Lu and Likos 2006)

It is a common assumption that the effective stress parameter is related to the degree of saturation when interpreting the shear strength of soils (Bishop and Donald 1961; Oberg and Sallfors 1997) and in elasto-plastic constitutive relationships (Hassanizadeh and Gray 1990; Houlsby 1997; Gray and Schrefler 2001; Gallipoli et al. 2003; Wheeler et al. 2003; Tamagnini 2004; Nuth and Laloui 2008; Alonso and Romero 2011). This assumption may not work well for some soils, and relatively large discrepancies have been observed in some early studies (Bishop and Blight 1963). Other studies have used the effective saturation [$S_e = (S-S_{res})/(1-S_{res})$] as the effective stress parameter successfully to evaluate the shear strength and elastic modulus of unsaturated soil (Vanapalli et al. 1996; Lu et al. 2010; Khosravi and McCartney 2012). More complicated functions of degree of saturation have also been proposed (Toll and Ong 2003; Sheng et al. 2008), while some studies have shown the utility of empirical relationships. Khalili and Khabbaz (1998) defined the effective stress parameter as a power-law relationship involving the ratio of the suction and the air entry suction, which has been applied in constitutive models (Loret and Khalili 2002) and in re-examining data from the literature (Khalili et al. 2004). Khalili and Khabbaz (1998) introduced a unique relationship between χ and a ratio known as the suction ratio, ratio of matric suction over the air entry suction, ψ_{aev}, as follows:

$$\chi = \psi \left\{ \frac{\psi}{\psi_{aev}} \right\}^{-\Omega}, \ \psi \geq \psi_{aev} \qquad \text{Eq. 2.8}$$

where Ω is a fitting parameter. A value of Ω of 0.55 was found to fit most experimental data from the literature (Khalili and Khabbaz 1998). Khalili and Zargarbashi (2010) performed staged triaxial tests on unsaturated soil specimens during wetting, and observed that the effective stress parameter is sensitive to hydraulic hysteresis. Further, they found that the use of an effective stress parameter equal to the degree of saturation may not be suitable for all soils during hydraulic hysteresis. Nonetheless, Khosravi and McCartney (2012) found that the effective stress

parameter defined as the effective saturation also permits reasonable assessment of changes in shear modulus during hydraulic hysteresis. It is also possible that application of net stresses may also affect the effective stress parameter, as volume changes may affect the shape of the SWRC especially at low suction magnitudes (Ng and Pang 2000).

A closed-form equation for the suction stress was proposed by Lu et al. (2010) by employing the effective saturation as the effective stress parameter χ. This permits integration of the van Genuchten (1980) SWRC into the definition of the suction stress. The suction stress can be predicted by combining Equation 2.4 with Equation 2.5, as follows (Lu et al. 2010):

$$\sigma_s = \frac{(u_a - u_w)}{\left(1 + [\alpha_{vG}(u_a - u_w)]^{N_{vG}}\right)^{\frac{N_{vG}-1}{N_{vG}}}} \qquad u_a - u_w \geq 0 \qquad \text{Eq. 2.9}$$

where N_{vG} and α_{vG} are the parameters fitted to experimental SWRC data points. Further, by substituting Equation 2.9 into Equation 2.5, the effective stress can be defined for unsaturated soils as follows (Lu et al. 2010):

$$\sigma' = (\sigma - u_a) + \frac{(u_a - u_w)}{\left(1 + [\alpha_{vG}(u_a - u_w)]^{N_{vG}}\right)^{\frac{N_{vG}-1}{N_{vG}}}} \qquad u_a - u_w \geq 0 \qquad \text{Eq. 2.10}$$

Lu et al. (2010) validated Equation 2.10 for both sands and clays using suction stress values obtained from shear strength tests using Equation 2.7, albeit primarily for low suction magnitudes (up to 1500 kPa) and relatively high degrees of saturation (in the range of 1.00 to 0.35). They found that the predicted SSCC for clay increased monotonically with suction, while the predicted SSCC for sand increased to a maximum value, then decreased back to zero. Lu et al. (2010) also proved that fine-grained soils like silt and clay should experience a monotonic increase in inter-particle stresses when the van Genuchten (1980) model parameter N_{vG} is greater than 2. Khosravi et al. (2012) and Lu et al. (2010) also observed an increasing trend in suction

stress with suction for a sand-silt mixture and a clay, respectively, verifying this prediction for low suctions. However, the suitability of extrapolating the analytical expression for effective stress in Equation 2.10 to high suction magnitudes has not been evaluated.

Evaluation of the SSCC equation of Lu et al. (2010) indicates that the suction stress at high suction magnitudes is very sensitive to the value of N_{vG}. A parametric analysis of the impact of N_{vG} on the shapes of the SWRC and SSCC for a constant value of α_{vG} = 0.60 kPa^{-1} fitted to experimental results obtained from this study is shown in Figures 2.7(a) and 2.7(b) in terms of the SWRC and SSCC, respectively. The results in these figures indicate that relatively small changes in N_{vG} can have a significant impact on the amount of water stored in the soil as well as the magnitude of suction stress at high suctions. Specifically, larger values of N_{vG} lead to a decrease in the volume of water stored in the soil as well as a lower suction stress. The results in Figure 2.7(a) indicate that soils with higher N_{vG} values will experience a significantly greater increase in suction stress with suction compared with soils having only slightly smaller values of N_{vG}.

Similar parametric analysis of the impact of α_{vG} on the shapes of the SWRC and SSCC for a constant value of N_{vG} = 1.60 fitted to experimental results obtained from this study is shown in Figures 2.8(a) and 2.8(b) in terms of the SWRC and SSCC, respectively. The results in these figures indicate that changes in α_{vG} can have the same significant impact on the magnitude of suction stress at high suctions. Increasing the value of α_{vG} led to shift the SWRC into a smaller air entry suction value, and thus reduction of the volume of water stored in the soil as well as a lower suction stress.

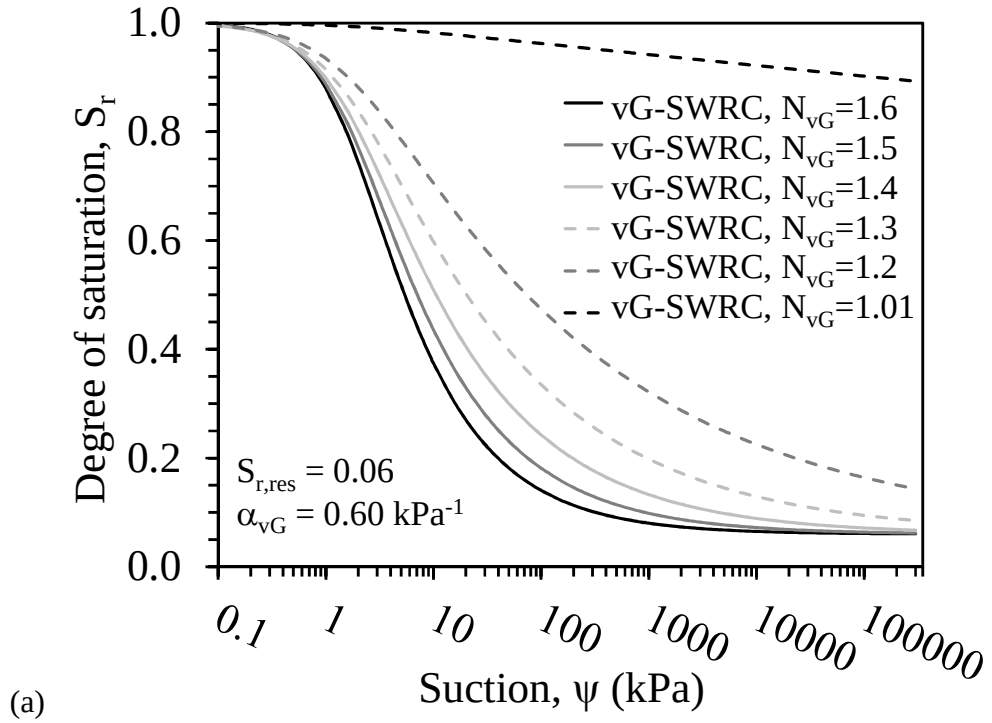

(a)

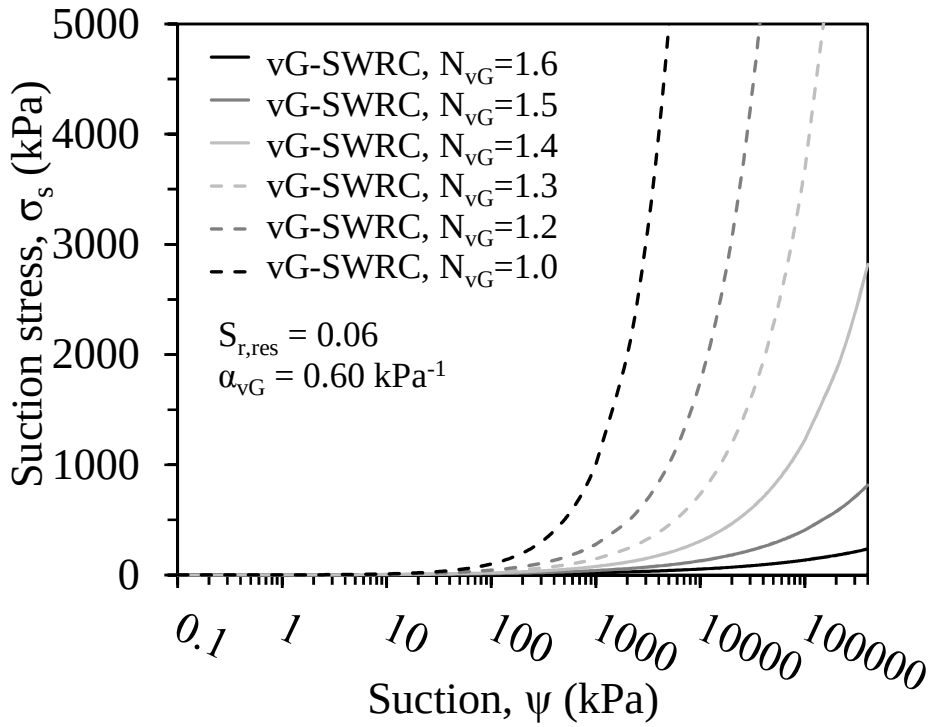

(b)

Figure 2.7: Impact of N_{vG} on the shapes of the SWRC and SSCC (constant value of α_{vG} = 0.60 kPa^{-1}): (a) SWRC; (b) SSCC

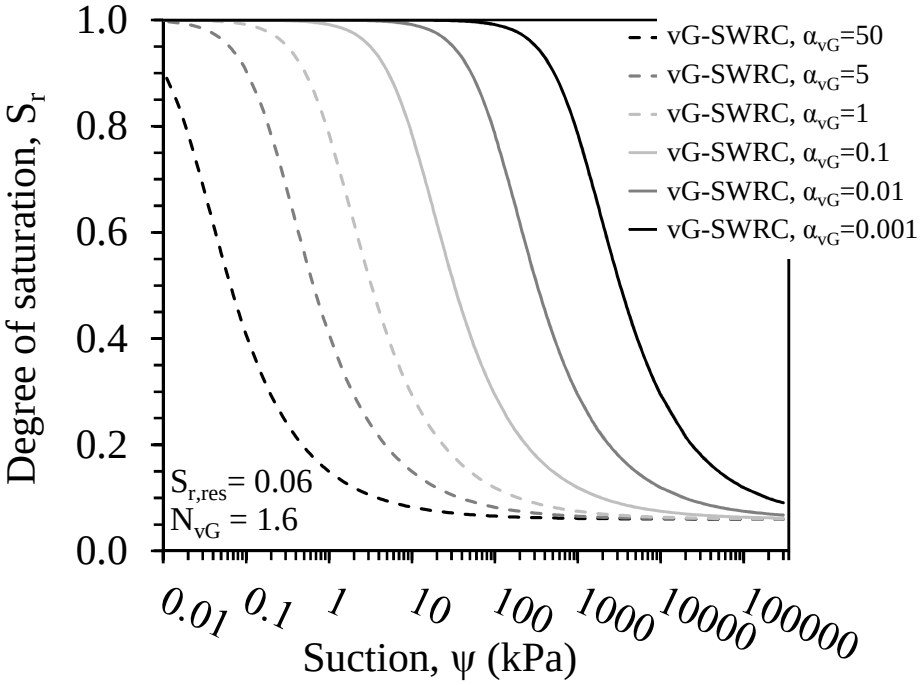

(a)

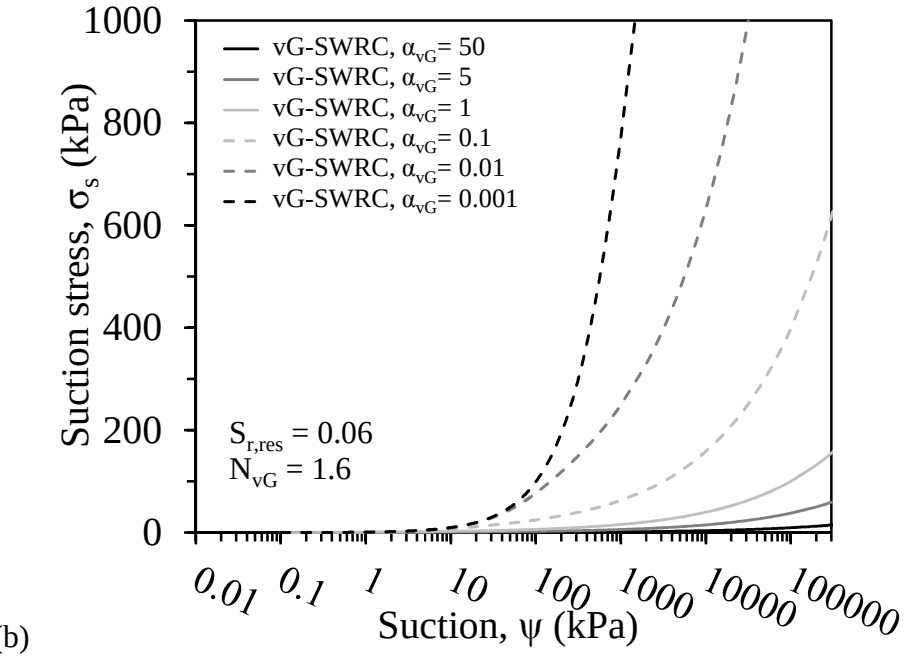

(b)

Figure 2.8: Impact of α_{vG} on the shapes of the SWRC and SSCC (constant value of N_{vG} = 1.60): (a) SWRC; (b) SSCC

2.5.Volume Change Behavior of Unsaturated Soils

2.5.1.Effects of Suction on Volume Change Behavior of Unsaturated Soils

The volume change behavior of unsaturated soils has been studied by a number of investigators. Rahardjo et al. (2003) performed CD and CW triaxial tests on residual soil from

the Jurong sedimentary formation. Results from this study showed that compacted specimens at high matric suction relative to net confining stress exhibit post-peak softening and dilatancy behavior similar to the behavior of overconsolidated soils. However, the behavior of compacted soil under low matric suctions relative to the net confining stress is controlled by the effect of net confining stress, which induces the characteristics of a normally consolidated soil. Estabragh and Javadi (2012) performed constant suction isotropic consolidation triaxial tests on compacted silt to investigate the suction effect on the compressibility of unsaturated soils. The results indicated that the air entry value and yield point have important role in the behavior of unsaturated soils and dilation depends on the value of suction at a given confining pressure where higher suctions cause more dilatancy.

2.5.2.Effects of Temperature on Volume Change Behavior of Soils

Thermal effects on the volume change behavior of saturated and unsaturated soils are complex due to coupling between temperature, suction and stress history. Accordingly, the approaches used by investigators include an evaluation of soil behavior during changes in the temperature of a specimen under a constant effective stress state, or evaluation of the soil mechanical behavior at various temperatures under isothermal conditions. A summary of the conclusions drawn from the different studies on the impact of temperature on the behavior of saturated soils is as follows:

- The compression index of soils is not sensitive to temperature for saturated soils (Campanella and Mitchell 1968; Eriksson 1989; Graham et al. 2001) and unsaturated soils (Saix et al. 2000; Uchaipichat and Khalili 2009)
- Heating of normally consolidated or lightly overconsolidated soils under constant effective stress and drained conditions leads to volumetric contraction (Paaswell 1967; Campanella

and Mitchell 1968; Plum and Esrig 1969; Baldi et al. 1988; Hueckel and Baldi 1990; Towhata et al. 1993; Boudali et al. 1994; Delage et al. 2000, 2004), and thus a reduction in the void ratio. A greater amount of contraction is noted with increasing plasticity index (Demars and Charles 1982).

- Heating of heavily overconsolidated soils under constant effective stress and drained conditions leads to volumetric expansion (Demars and Charles 1982; Baldi et al. 1988; Hueckel and Baldi 1990; Belanteur et al. 1997; Delage et al. 2000, 2004; Sultan et al. 2002; Cekeravac and Laloui 2004), although heating of these soils above a threshold temperature may lead to contraction (Hueckel and Baldi 1990; Delage et al. 2000, 2004; Cekeravac and Laloui 2004). A summary of the impact of OCR on the thermal volumetric strain for different types of soils is presented in Figure 2.9

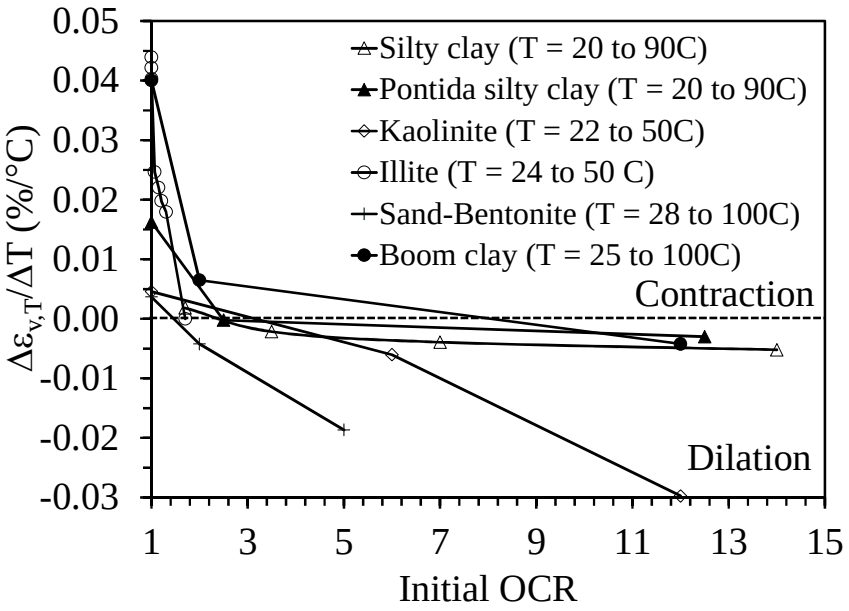

Figure 2.9: Influence of OCR on the thermal volumetric strain by Towhata et al. (1993); Baldi et al. (1988); Cekerevac and Laloui (2004); Plum and Esrig (1969); Graham et al. (2001); Sultan et al. (2002), respectively as in the legend in the figure

- Coccia and McCartney (2013) observed that anisotropic stress states may lead to thermal expansion and contraction in different directions in the same soil specimen. For a specimen

of saturated Bonny silt, expansion was observed in the direction of greater overconsolidation ratio (lower stress), while contraction was observed in the direction of lower overconsolidation ratio (greater stress).

- Multiple cycles of heating and cooling may lead to a gradual accumulation of permanent volumetric contraction in soils regardless of the stress history due to thermal creep or kinetic thermal hardening (Campanella and Mitchell 1968; Burghignoli et al. 1992; Vega and McCartney 2014).
- For most soils, an increase in temperature leads to a softening effect corresponding to a reduction in the apparent preconsolidation (or yield) stress as shown in Figure 2.10 (Campanella and Mitchell 1968; Habibagahi 1973; Demars and Charles 1982; Eriksson 1989; Tidfors and Sällfors 1989; Hueckel and Baldi 1990; Boudali et al. 1994; Graham et al., 2001; Francois et al. 2007; Uchaipichat and Khalili 2009).
- Heating then cooling of normally consolidated soils may cause an increase in the apparent preconsolidation stress (Plum and Esrig 1969). This may indicate that the thermal softening observed in other studies may not be permanent upon cooling.

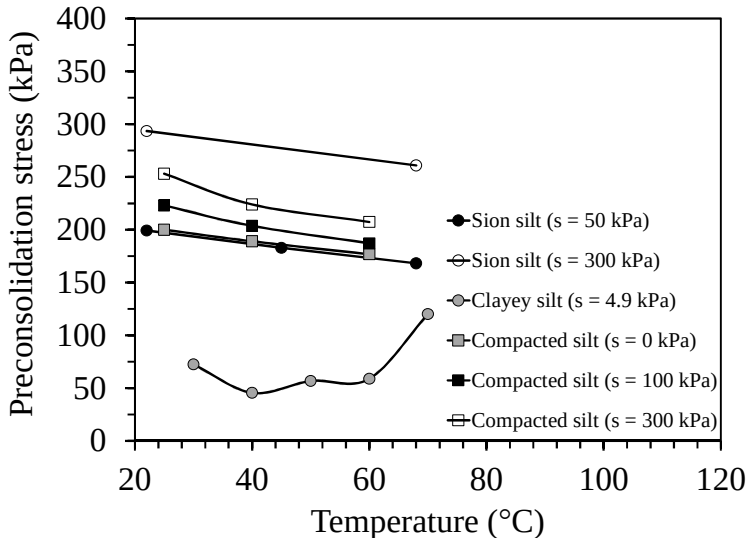

Figure 2.10: Influence of temperature on the preconsolidation stress of Sion silt (Francois et al. 2007) and compacted silt (Uchaipichat and Khalili 2009)

The volume change behavior of unsaturated soils during heating has been investigated in several studies (Romero et al. 2003; Francois et al. 2007; Salager et al. 2008; Tang et al. 2008; Uchaipichat and Khalili 2009). Tang et al. (2008) performed thermo-mechanical tests on unsaturated, heavily-compacted MX80 bentonite following a wetting path from an initial suction of 110 MPa to a target suction of 9 MPa. The results from tests at constant confining stress showed that heating led to expansion under low values of confining stress and high suction, and led to contraction at high values of confining stress and low suction as presented in Figure 2.11. This indicates that stress history also plays an important role in the thermal response of unsaturated soils. Uchaipichat and Khalili (2009) performed drained heating tests on silt specimens at matric suctions up to 300 kPa and net confining stresses up to 200 kPa, and found that heavily overconsolidated specimens experienced reversible thermal expansion with introducing larger irreversible thermal contraction at lower overconsolidation ratio as shown in Figure 2.12. Further, for a given net mean stress, the amount of thermal contraction increased with increasing suction.

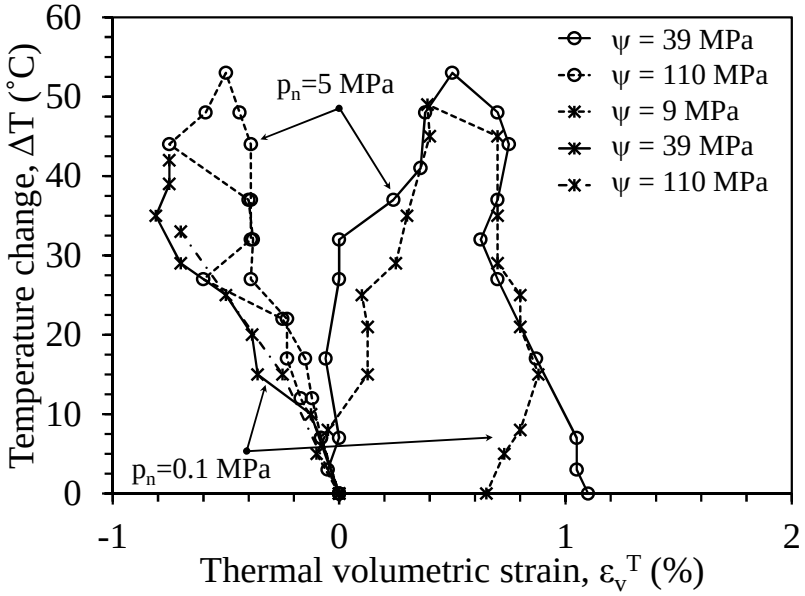

Figure 2.11: Thermal volumetric strain versus temperature during heating (Tang 2008)

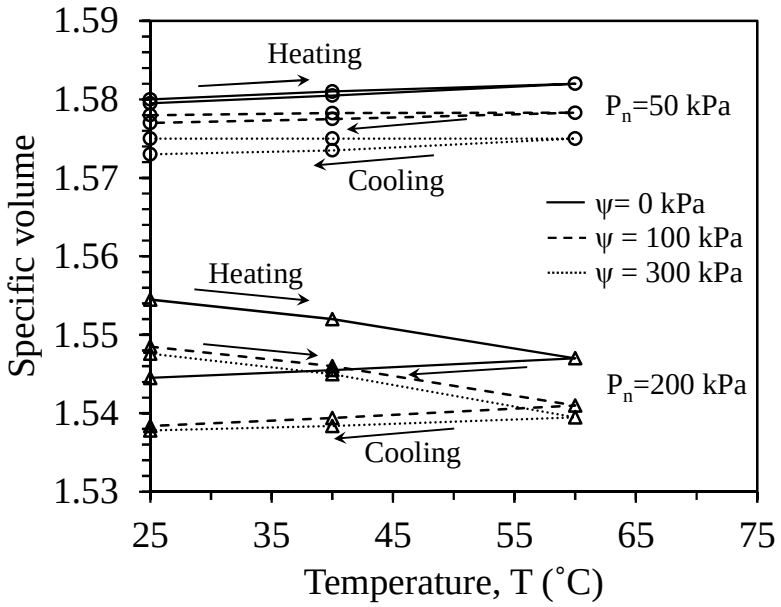

Figure 2.12: Thermal volume change behavior of silt at varies suction values and net confining stresses (Uchaipichat and Khalili 2009)

2.6.Shear Strength of Unsaturated Soils

2.6.1.General

The drained shear strength of saturated soils is commonly described by Mohr-Coulomb failure criterion, incorporating the effective stress, as follows:

$$\tau = \sigma' \tan \phi' \qquad \text{Eq. 2.11}$$

where τ is the shear strength, σ′ is the effective stress defined using Eq. 2.10, and □′ is the drained friction angle. An extension of the Mohr-Coulomb equation to represent the shear strength of unsaturated soils can be obtained by substituting Eq. 2.10 in Eq. 2.11, as follows (Lu et al. 2010):

$$\tau = \left[(\sigma - u_a) + \frac{(u_a - u_w)}{\left(1 + \left[\alpha_{vG}(u_a - u_w)\right]^{N_{vG}}\right)^{\frac{N_{vG}-1}{N_{vG}}}} \right] \tan\phi' \qquad \text{Eq. 2.12}$$

A similar equation could have been developed using the effective stress definition of Khalili and Khabbaz (1998). Other shear strength equations have been developed for unsaturated soils using

the assumption of independent stress state variables (Fredlund and Morgenstern 1977; Vanapalli et al. 1996; Alonso et al. 1990; Sheng et al. 2008a; etc.). However, these equations have the issue that they require different shear strength parameters for saturated and unsaturated conditions.

2.6.2.Stress-Strain Characteristics for Unsaturated Soils

The shear strength characteristics of unsaturated soils in terms of stress-strain curves under isothermal conditions have been studied by many investigators (Chen 1984; Thu et al. 2006; Oh et al. 2008; Blatz 2002). Research on the effect of suction and net confining stress on the shape of the stress-strain curves and consequently on shear strength reveal that the net confining stress in comparison with the suction applied contribute to the brittle failure mechanisms. Chen (1984) performed tests under confined conditions and found that brittle failure occurs either when the specimen sheared under zero confining stress, or when the confining stress applied is higher than the current suction value. Blatz (2002) observed that the shear strength of unsaturated clay is controlled by the confining stress rather than the initial suction. Thu et al. (2006) performed constant water content triaxial tests on statically compacted silt specimens under matric suctions up to 200 kPa and confining stresses up to 350 kPa. Their test results showed evidence of strain softening at low confining stresses, and observed an increase in stiffness and shear strength with increasing net confining stresses. The same conclusion was drawn by Oh et al. (2008), who performed triaxial tests on kaolin clay compacted dry of optimum. Strain-softening stress-strain curves were observed for specimens whose confining stress is much lower than the initial suction. Hydraulic hysteresis may also affect the shear stiffness of unsaturated soils. For small strain conditions, Khosravi and McCartney (2012) found that the shear modulus increases nonlinearly with suction during drying from saturated conditions, but remains high during subsequent wetting due to suction-induced hardening.

2.6.3.Experimental Assessment of Suction Effects on Unsaturated Soil Shear Strength

Many studies have evaluated the role of suction on the shear strength of unsaturated soils. Most of the testing has been performed under isothermal conditions with low suction magnitudes controlled using the axis translation technique. Blight (1967) conducted consolidated-drained (CD) triaxial tests for specimens of unsaturated silt and he has found that the shear strength of the soil increases with increasing the suction applied and increasing the net normal stress. Escario (1980) performed suction-controlled direct shear tests on unsaturated soil and found that the slope of the failure envelope, (the tangent of the drained friction angle) is independent of suction. This implies that the slope of the failure envelope defined under saturated conditions should be the same as at different suction magnitudes, as indicated in Figure 2.13.

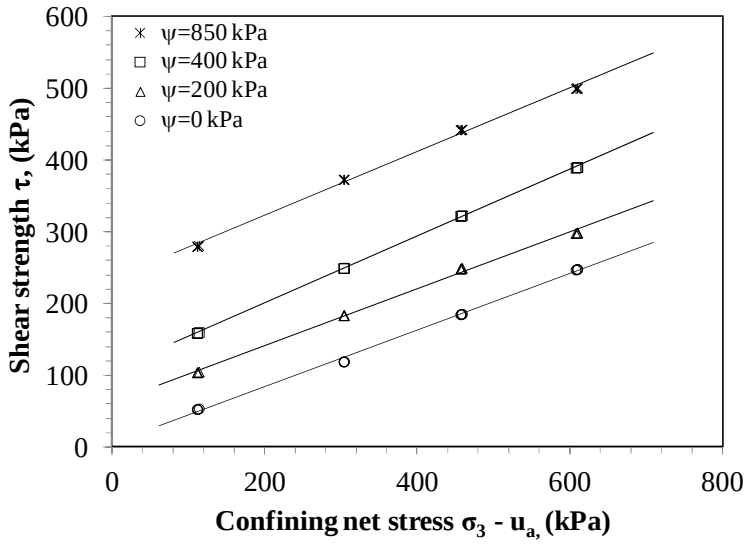

Figure 2.13: Shear strength versus confining net stress for unsaturated Madrid gray clay (Escario 1980)

Many other studies have focused on evaluating the shear strength of unsaturated soils under high suction magnitudes. Nishimura and Fredlund (2000) conducted isothermal triaxial compression tests on silty soil under high suction magnitudes. They found constant values of shear strength with increasing suction after the soil reached residual saturation, and that the rate

of increase in peak shear strength with net normal stress was similar to the effective internal friction angle for saturated conditions. Blatz (2002) examined the effect of high suction and high confining pressure on the behavior of a compacted sand-bentonite by performing a series of undrained triaxial tests. Their test results show a nonlinear increase in the strength and stiffness with increasing suction as indicated in Figure 2.14. They also suggested that the increase in shear strength was probably due to the corresponding increases in density rather than the effect of suction on the shear resistance. A ring shear apparatus adapted with suction control using the vapor equilibrium technique was used by Vaunant et al. (2007) and Merchan et al. (2008) to investigate the effect of high magnitudes of total suction on the residual shear strength of low plasticity clay, and an increase in strength was noted with increasing suction.

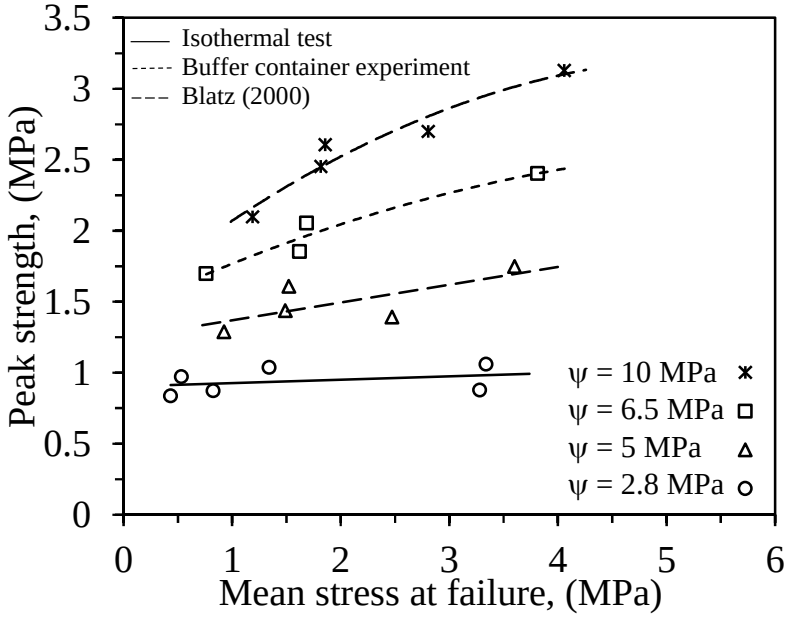

Figure 2.14: Peak strength versus mean stress at failure for lab and in-situ sets experiments at varies suction values (Blatz 2002)

2.6.4.Effects of Elevated Temperature on the Shear Strength of Soils

The influence of temperature change on the shear strength and stress-strain characteristics of saturated soils have been studied by several investigators. Sherif and Burrous (1969) performed

unconfined compression tests on saturated, normally consolidated clays and found that an increase in temperature led to a reduction in the undrained shear strength of the soil. However, this was likely due to thermally-generated excess pore water pressures that were not permitted to drain. Houston et al. (1985) performed consolidated undrained tests on saturated, normally consolidated specimens of Illite clay at different temperatures, and observed that the pore water pressure increased and effective stress decreased during heating. However, after drainage and subsequent thermal consolidation, the peak shear strength of the soil was greater than at low temperatures. Hueckel and Baldi (1990) performed drained triaxial compression tests on overconsolidated specimens of Pontida silty clay, and observed a decrease in peak shear strength with temperature. This was attributed to a reduction in the size of the yield locus (and consequently a reduction in the overconsolidation ratio), but it may also be related to the increase in void ratio during heating of the overconsolidated soil.

The uniqueness of the critical state line (CSL) was also investigated and confirmed by Hueckel and Baldi (1990) and Graham et al. (1995). These studies also observed that temperature has a negligible effect on the critical state line. However, Cekeravac and Laloui (2004) observed a slight increase in the slope of the critical state line with temperature for saturated kaolinite clay. Houston et al. (1985) also observed an increase in the slope of the critical state line with temperature for saturated illite clay, although substantial increases were only noted in tests performed at very high temperatures above 100 °C. Hueckel et al. (2009) showed examples of how the effects of temperature on the shear strength of soils could be explained using either increase in the slope of the critical state line with increasing temperature or a decrease in the preconsolidation stress with increasing temperature, and noted that the suitability of the modelling approach may depend on the particular soil. Uchaipichat and Khalili

(2009) evaluated the shear strength and volume change of unsaturated compacted silt under non-isothermal conditions for suction magnitudes less than 300 kPa. For a given suction magnitude, they observed a decrease in peak shear strength with increasing temperature as illustrated in Figure 2.15. However, the shear strength at critical state conditions was unaffected by temperature. They observed that changes in matric suction led to greater changes in the peak and critical state strength values than changes in temperature. Similar reductions in peak shear strength and increases in shear strength with suction were observed by Wiebe et al. (1998) and Ghembaza et al. (2007b). Wiebe et al. (1998) prepared specimens of sand-bentonite at different degrees of saturation using compaction at different water content, which could have led to different soil structures, but Ghembaza et al. (2007b) incorporated the vapor equilibrium technique into a triaxial cell to perform triaxial compression tests on normally consolidated, unsaturated sandy clay under a temperature of 80°C and a suction value of 8.5 MPa.

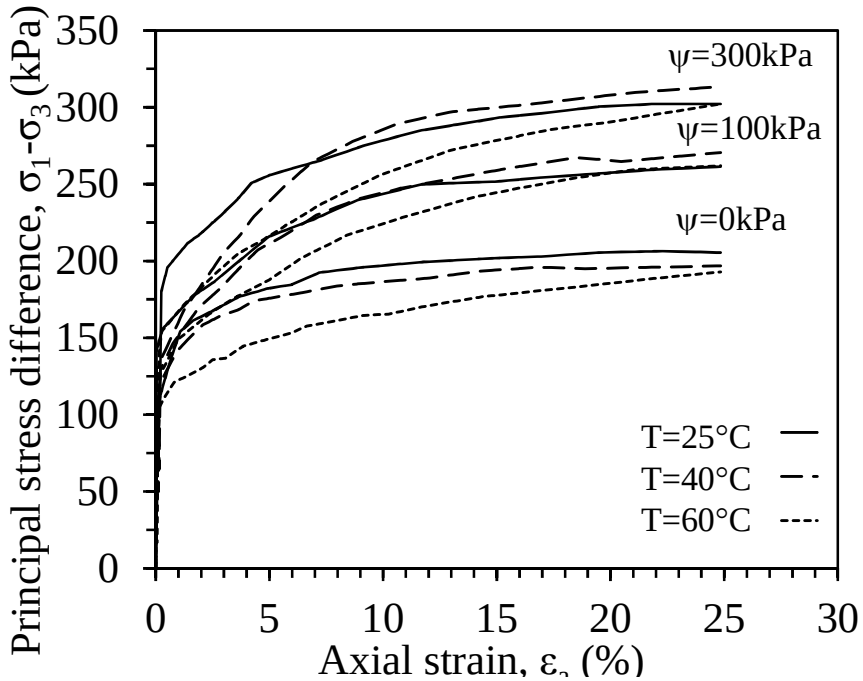

Figure 2.15: Suction- and temperature-controlled conventional compression shear tests at initial mean effective stress of 100 kPa (Uchaipichat and Khalili 2009)

2.6.5.Effects of Elevated Temperature on the Shear Strength of Soils at High Suctions

Although interesting lessons were learned from these tests on low suctions, there has not been a thorough study on the impact of temperature on the strength of unsaturated soils under higher suction magnitudes. Most research on the impact of high suction magnitudes has focused on the impact of suction on the shear strength of soils, and the impact of temperature has not been thoroughly investigated. Alsherif and McCartney (2012) performed a preliminary set of tests to assess the roles of suction and temperature on the effective stress and shear strength of unsaturated compacted silt. They found that the peak shear strength increases slightly for compacted silt under high suction magnitudes with increasing temperature, which is contradictory to the observations of Uchaipichat and Khalili (2009) for low suction magnitudes, confirming the importance of further investigation into the impacts of temperature on the shear strength of compacted silts under high suction magnitudes.

Alsherif and McCartney (2012) focused on measurement of the peak shear strength of compacted silt using constant water content triaxial tests under higher suction magnitudes controlled using saturated salt solutions. The same silt used in this study was investigated by Alsherif and McCartney (2012), and more details of this soil will be presented in Chapter 3. The triaxial tests were performed on specimens brought to suction equilibrium at temperatures ranging from 24 to 65 °C. Results from these tests indicate that increased temperature leads to an increase in the peak shear strength of soils having a constant initial suction.

The silt was first oven-dried at a temperature of 75°C for 24 h, ground using a rubber pestle, then screened through a sieve No. 40. Next, it was carefully wetted with a spray gun to a water content of 14.5%, and placed in a sealed plastic bag to cure for 24 h for allowing the water content to homogenize. Compaction was performed in three equal lifts in a mold of 35.5 mm

diameter using a manual press to reach a dry unit weight of 16.8 kN/m^3. This corresponds to an initial void ratio of 0.53. For each lift, the soil was compressed to a thickness of 24.2 mm. To avoid the presence of weak zones within the samples, the interface between the layers was scarified. A manual press was used to push the specimen downwards to remove the specimen from the mold.

The testing procedures involved bringing the specimens to equilibrium with high suction magnitudes using the vapor equilibrium technique at different temperatures (Delage et al. 2008), then measuring the shear strength of the soil specimens in constant water content triaxial tests. This is a preliminary testing program as the suction and temperature were not controlled within the triaxial setup itself. Saturated salt solutions were prepared in glass desiccators by dissolving the salt in distilled water until precipitated salt remains visible. The specimens were suspended above the salt solution on a porous disc to allow a water exchange between the liquid and vapor phases in the container headspace. The desiccator was placed within a temperature controlled chamber, shown in Figure 2.16.

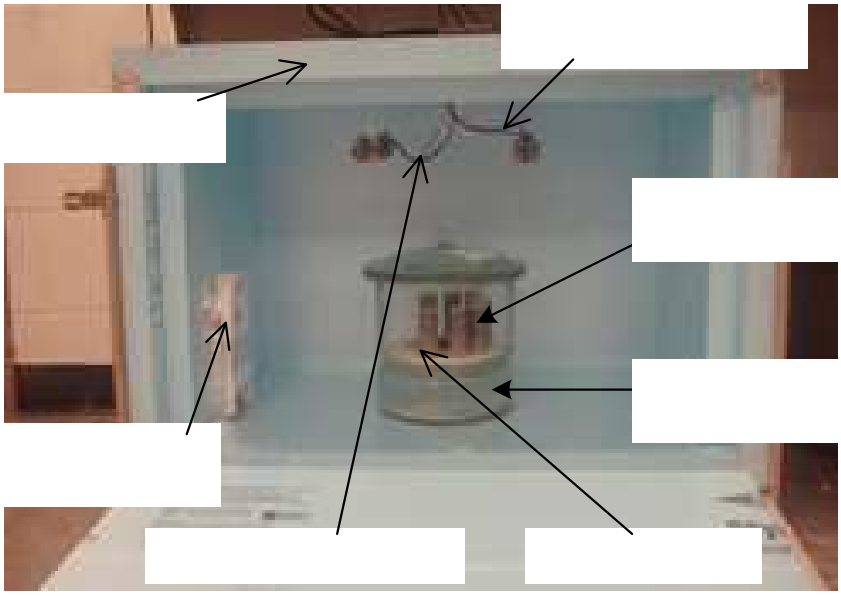

Figure 2.16: Desiccator and temperature control chamber showing soil specimen

A strip heater and a temperature controller were used to maintain a target temperature. The relative humidity and temperature were recorded hourly using a combined sensor-data logger from Lascar Electronics. This sensor can measure temperatures ranging from -35 to +80 °C with an accuracy of ±0.5°C and relative humidity values ranging from 0 to 100% with an accuracy of ±3%. The change in gravimetric water content of the soil with increasing soil suction was measured by weighing the specimen every three days until it reaches a constant mass. This step was performed in less than 15 seconds after taking the specimen out of the desiccators. This duration was found to be short enough so that water evaporation during the weighing process was negligible. Four target total suction values corresponding to four relative humidity values were implemented using four different salt solutions at temperatures of 24, 45, and 65 °C, as shown in Figure 2.17.

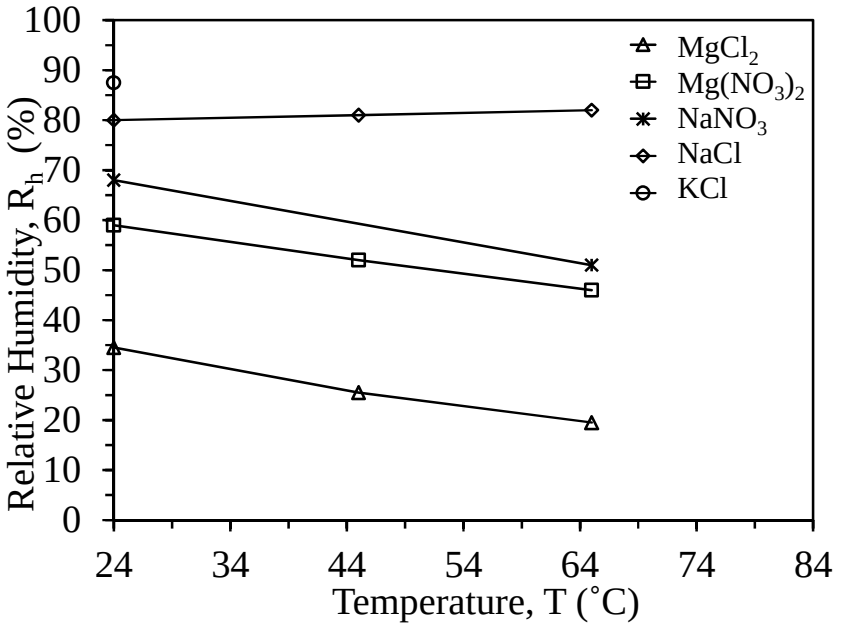

Figure 2.17: Relative humidity change with temperature for different salt solutions

The equilibration times required when imposing different total suction magnitudes using different salt solutions are shown in Figure 2.18(a). These results indicate that a shorter time is

needed to reach equilibrium at a room temperature of 24 °C as the total suction increased. Similar trends were noted for higher temperature tests in Figure 2.18(b). The soil specimens at high temperatures reach equilibrium faster than specimens at room temperature for suction values applied by the same salt solution.

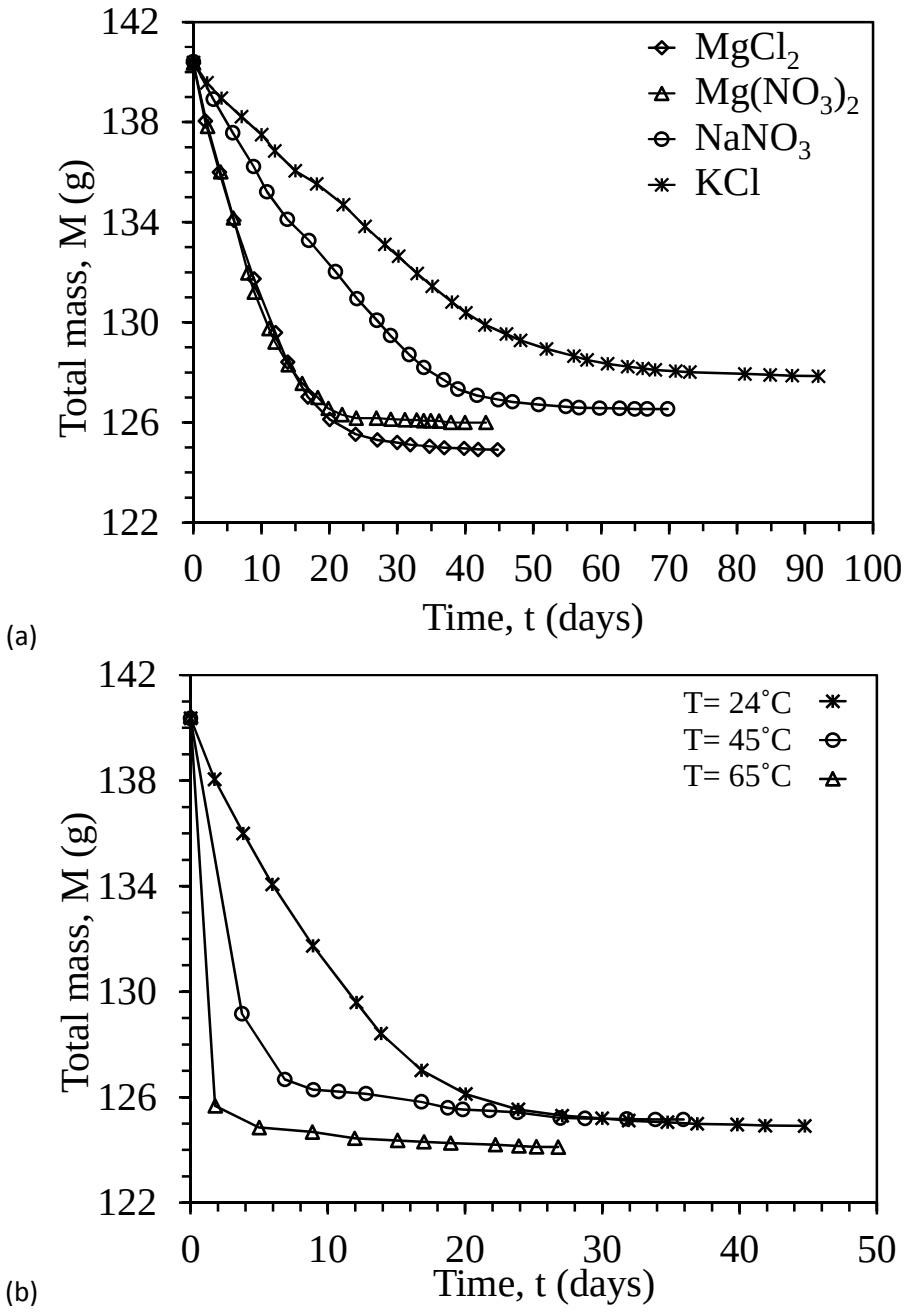

Figure 2.18: Change in mass of the soil over time for: (a) Different suction values imposed using different salt solutions at T = 24 °C, (b) Different temperatures applied to an MgCl2 salt solution

At equilibrium under the applied values of suction and temperature, the soil specimens were placed in the triaxial cell and an isotropic net confining pressure value ranging from 0 to 200 kPa was applied. Atmospheric air pressure was maintained at the top and bottom of the specimen while increasing the cell pressure and during shearing, and no access to water was permitted. The compacted specimens were relatively stiff so little volume change was noted during this process. Placement of the specimen in the triaxial cell was performed in less than 2 minutes to minimize changes in water content and temperature of the specimen. The specimens were then sheared until reaching a peak value of principal stress difference (occurring at a strain of 1.5 to 3%) at a rate of 0.127 mm/min. After shearing the specimen to failure, the final water content was measured.

The SWRC was defined by converting the equilibrium relative humidity to total suction using Kelvin's equation. The SWRC of the silt is shown in Figure 2.19(a), obtained using the axis translation technique to evaluate the air entry suction and the vapor equilibrium technique to define the tail of the SWRC, and the impact of temperature on the SWRC at high suctions is shown in Figure 2.19(b). The van Genuchten (1980) SWRC model was fit to each set of data, with the fitting parameters α_{vG} and N_{vG} reported in the figure. The fitted SWRCs indicate that temperature leads to a shift in the SWRC to the left (i.e., less water retention for a given suction value), which is consistent with results obtained by Romero et al. (2003) and Uchaipichat and Khalili (2009).

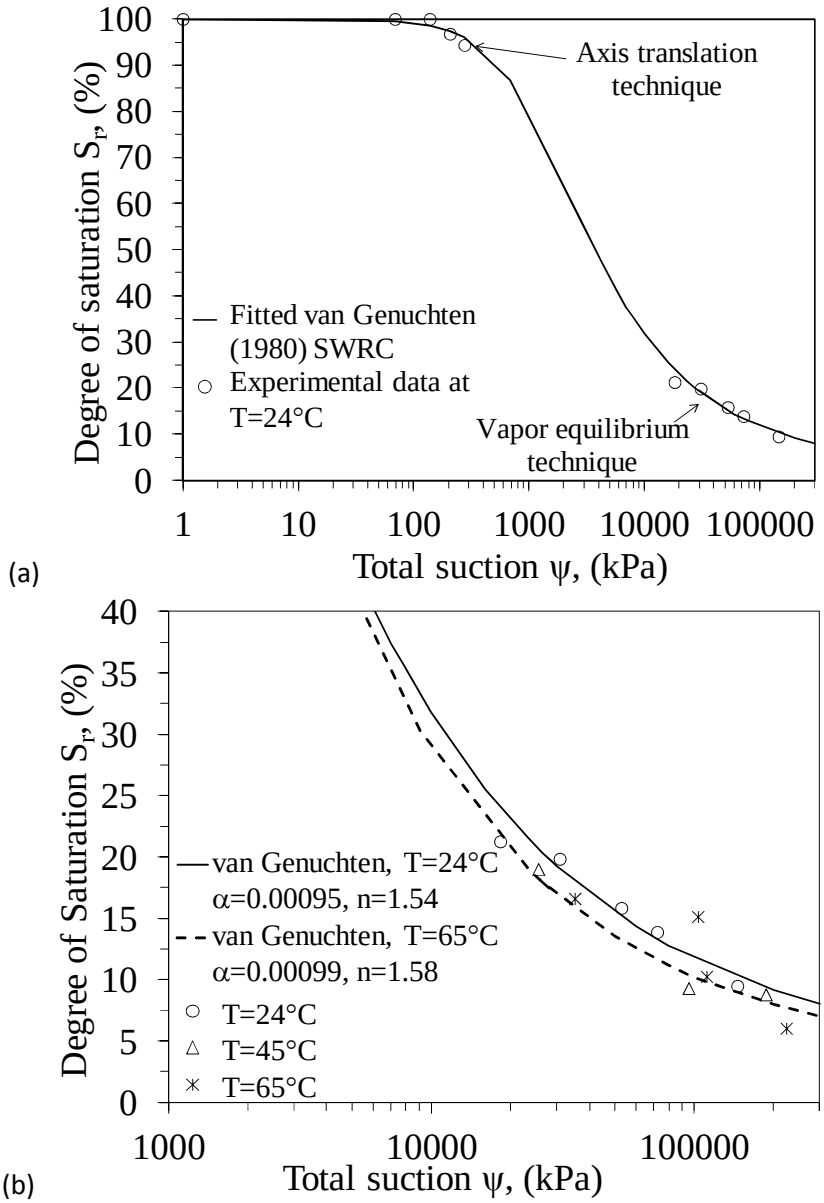

Figure 2.19: SWRCs defined for Bonny silt specimens: (a) Entire range of suction under isothermal condition, (b) High suction range under isothermal and non-isothermal conditions

The failure envelopes for specimens sheared under room temperature are shown in Figure 2.20. The results show an increase in the shear strength of the soil with increasing suction and increasing net confining pressure. Because the excess pore water pressure generation in the unsaturated soil is expected to be negligible due to the low degrees of saturation, the total stress envelopes from constant water content triaxial tests should be close to the effective stress

envelopes for these suction conditions. The friction angle for the silt specimens under high suction is larger (ϕ'=43°) than that from tests on saturated soil (ϕ'=36°). The difference may be attributed to the differences in consolidation of the unsaturated specimens from that of the saturated specimens tested in the consolidated undrained triaxial test. The total suction has similar effects on the failure envelopes to the trends observed by Nishimura and Fredlund (2000) for high suction magnitudes.

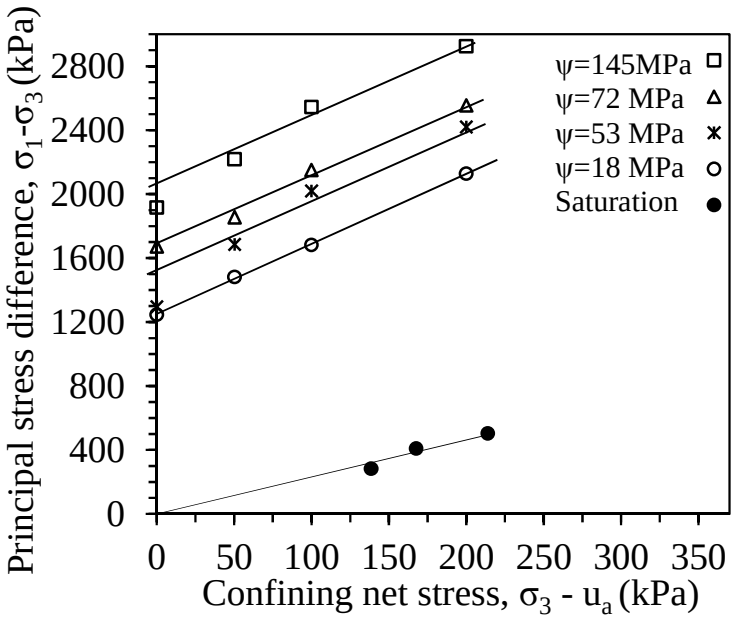

Figure 2.20: Effective stress failure envelope for saturated silt along with total stress failure envelopes for unsaturated silt at constant room temperature of 24 °C (not to scale)

The failure envelopes defined for different salt solutions and temperatures are shown in Figure 2.21. Similar to the isothermal failure envelopes in Figure 2.20, the slope of the failure envelopes does not change with either increasing suction or temperature. Due to the use of saturated salt solutions, it was not possible to maintain constant suction values and increase the temperature, so the differences in the intercept values between the failure envelopes in Figure 2.21 can be attributed to both temperature and suction.

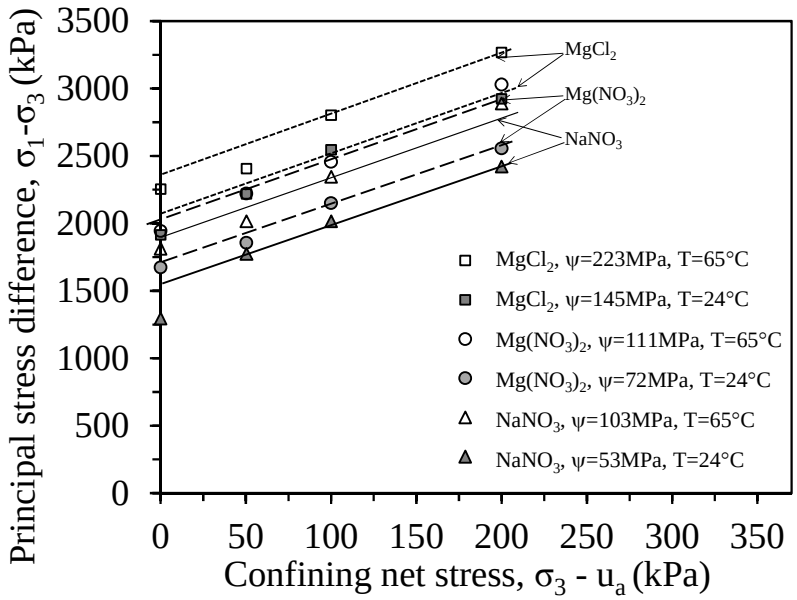

Figure 2.21: Failure envelopes for silt at different suction values and temperatures

The results in Figure 2.21 show a combined effect of temperature and suction on the shear strength. Accordingly, to better interpret the results shown in Figure 2.21 the concept of the suction stress characteristic curve (SSCC) may be used to separate the effects of suction and temperature on the constant water shear strength. First, the slope of the failure envelope along with the apparent cohesion values for unsaturated silt specimens in Figures 2.20 and 2.21 were used to back-calculate the suction stress σ_s of the soil at temperatures of 24 °C and 65 °C using Equation 2.7. The SSCC defined using Equation 2.7 for different temperatures is shown in Figure 2.22. The experimental results indicate a nonlinear increase in suction stress by up to approximately 30 kPa as the total suction increases up to 223 MPa. This interpretation of the results in Figures 2.20 and 2.21 reflects that the peak shear strength increases slightly for compacted silt under high suction magnitudes with increasing temperature, which is contradictory to the observations of Uchaipichat and Khalili (2009) for low suction magnitudes.

This may be due to the impact of temperature on the magnitude of excess pore water pressure generation during shearing in low and high suction ranges.

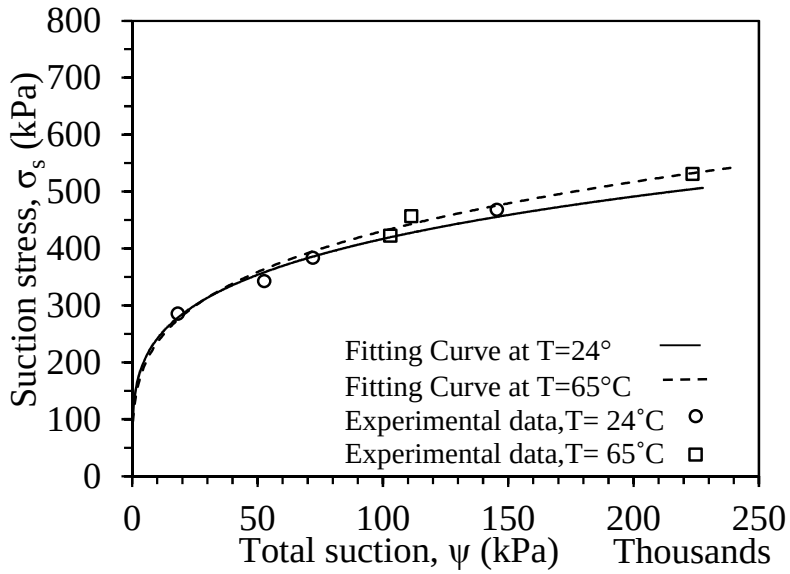

Figure 2.22: SSCCs defined for compacted silt at temperatures of 24 °C and 65 °C

In this preliminary set of tests, the specimens were brought to equilibrium outside of the triaxial cell, and then were quickly transported to the triaxial setup for shearing. Further, volume was not tracked during compression of the air voids during application of the cell pressure, or during shearing. Accordingly, these tests only provide an approximation of the effects of coupling between temperature, suction, net stress, and void ratio. In addition, the issues noted with the use of saturated salt solutions to independently control the temperature and suction in soils indicates that an alternative approach involving vapor control may be more appropriate.

The results from Alsherif and McCartney (2012) indicate that the total suction has a greater impact on the peak shear strength of soils than temperature. However, increased temperature was found to lead to a slight increase in the peak shear strength of unsaturated soils under high suction magnitudes, which is contradictory to the observed impact of temperature for low suctions. This emphasizes the importance of further investigation into the impacts of temperature

on the shear strength of compacted silts under high suction magnitudes using more advanced testing approaches.

2.7.Thermo-Hydro-Mechanical Constitutive Models for Soils

Heating will affect many aspects of unsaturated soil behavior, including the shape of the SWRC (which may affect effective stress in unsaturated soils), volume change, and elasto-plastic stress-strain behavior. Constitutive relationships have already been developed for each of these effects, although they may not be extended to the conditions representative of unsaturated conditions or more specifically high suction magnitudes.

2.7.1. Temperature-Dependent SWRC Models

With respect to the details of the temperature-dependent SWRC model, Grant and Salehzadeh (1996) defined an incremental relationship to evaluate the change in suction in a soil for a given change in temperature, as follows:

$$\frac{d\psi}{\psi} = \frac{dT}{\beta_0 + \beta_1 T} \qquad \text{Eq. 2.13}$$

where ψ is the suction, $\beta_1 = 1$, and β_0 is a parameter associated with temperature-dependent fluid properties. They integrated this relationship into the van Genuchten (1980) model:

$$\theta = \theta_r + (\theta_s - \theta_r)\left\{\frac{1}{\left[\alpha p_{c(T=T_r)}\left(\frac{\beta_0 + T_r}{\beta_0 + T_f}\right)\right]^{\lambda} + 1}\right\}^{\frac{(\lambda-1)}{\lambda}} \qquad \text{Eq. 2.14}$$

where T_r is a reference temperature, T_f is an observational temperature in Kelvin, θ is the volumetric water content (dimensionless), α (P^{-1}) and λ (dimensionless) are empirical parameters. The observed that the value of β_0 was approximately -400 Kelvin for silty soils.

Similarly, Salager et al. (2007) developed an incremental equation which accounted for the relative thermal expansion coefficients of the water β_e and solids β_s:

$$d_s = F_w d_w + \left(F_w w(\beta_e - \beta_s) + \frac{s}{\sigma_s}\frac{d\sigma_s}{dT} - s\tan\phi\frac{d\phi}{dT}\right)dT + \left[\left(\frac{\delta_s}{\delta_e}\right)_{T,\theta} - \frac{F_w w}{(1+e)}\right]de \quad \text{Eq. 2.15}$$

where *s* is the suction, *w* is the gravimetric water content, F_w is the slope of the SWRC, *e* is the void ratio, ϕ is the fluid-solid contact angle, and σ_s is the surface tension. Both studies obtained a good match with experimental SWRC data.

2.7.2.Thermo-Hydro-Mechanical Constitutive Models for Soils

Many thermal constitutive models for saturated clays have been developed by incorporating thermal yield surfaces into to the original Cam-Clay model (Hueckel and Borsetto 1990; Cui et al. 2000; Laloui and Cekeravac 2003). The yield locus equation from the original Cam-clay model can be expressed as follows:

$$f = \frac{q}{Mp'} + \ln\left(\frac{2.718\,p'}{p'_c}\right) - 1 = 0 \quad \text{Eq. 2.16}$$

where *f* is the yield locus fuction, q is the principal stress difference, M is the slope of the critical state line, p′ is the mean effective stress, and p_c' is the preconsolidation (or yield) stress. Primary consideration was given to the prediction of the changes in preconsolidation stress with temperature using empirical relationships, as this parameter governs changes in the size of the yield locus. Earlier, Hueckel and Borsetto (1990) was one of the first studies to incorporate the effect of temperature changes on the preconsolidation stress p'_c, as follows:

$$p'_C = p'_{Co}\exp\left[\frac{1}{\lambda-\kappa}(1-a_0\Delta T)(1+e_0)\varepsilon_v^p\right] + 2\left(a_1\Delta T + a_2\Delta T^2\right) \quad \text{Eq. 2.17}$$

where p'_{C0} is the initial preconsolidation stress before heating; λ and κ are the slopes of the isotropic virgin compression and recompression curves, respectively; e_0 is the initial void ratio;

the coefficients a_0, a_1, a_2 are constants and ε_v^p is the plastic volumetric strain. The last term on the right-hand side of Equation (2.17) represents the thermal softening function.

Laloui and Cekeravac (2003) proposed an expression for temperature effects on the preconsolidation stress similar to Eq. 2.17, but indicated that their equation provides a better fit for isotropic thermo-mechanical paths. Their expression is given as follows:

$$p'_C = p'_{Co} \exp\left(\frac{1+e_0}{\lambda-k}\varepsilon_v^p\right)\left[1-\gamma\log\left(1+\frac{\Delta T}{T_0}\right)\right] \qquad \text{Eq. 2.18}$$

where γ is a material parameter that is recomended to be equal to 0.4 for silty soils. T_0 is a reference temperature, and the same difintions as in Hueckel and Borsetto (1990) model were used for λ, κ, $e_{0,}$ and ε_v^p.

Cui et al. (2000) built upon the model of Hueckel and Borsetto (1990) and defined a series of three yield functions that governed changes in the preconsolidation stress with temperature (the load-yield or LY curve), the temperature at which plastic thermal strains would occur for normally consolidated soils (the temperature-yield or T-Y curve), and the temperature at which overconsolidated soils may transition from elastic expansion to plastic contraction during heating (the heating-contraction or HC curve). Cui et al. (2000) used a simplified form of Equation 2.17 to define the load yield locus (LY) curve that characterizes the effects of temperature on the preconsolidation stress, as follows:

$$p'_{CT} = p'_{C0} \exp\left(-\alpha_o \Delta T\right) \qquad \text{Eq. 2.19}$$

where p'_{C0} is the initial preconsolidation stress before heating, defined by the intersection of the LY curve with the p' axis which functions as a hardening parameter, and α_0 is a parameter governing the curvature of the LY curve, which ranges from 0.005 to 0.1.

Baldi et al. (1990) observed that lightly overconsolidated soils have a transitional behavior from elastic expansion only to a combination of elastic expansion and plastic contraction as the OCR decreased. To simulate this behavior, Cui et al. (2000) suggested a thermal yield locus, called the thermal yield (TY) curve, which was activated when the temperature reaches a certain threshold value T_c, as follows:

$$T_{CT} = (T_C - T_0)\exp(-\beta p') + T_0 \qquad \text{Eq. 2.20}$$

where T_C is a reference temperature, T_0 is the initial temperature, and β is a new hardening parameter governing the shape of the TY curve in the T - p′ plane. Cui et al. (2000) noted that the magnitude of β can range from 0.4 to 800.

Cui et al. (2000) proposed their third yield function (the HC curve) to represent the point at which an initially overconsolidated soil specimen would change in behavior from expansion to contraction during heating, as observed by Hueckel and Baldi (1990) and Cekeravac and Laloui (2004). It is given as follows:

$$p' = c_1 p'_{c0} \exp(c_2 \Delta T) \qquad \text{Eq. 2.21}$$

where c_1 is the intersection of the HC line with the p□ axis and c_2 is a shape parameter.

Below the TY curve, a soil has purely thermo-elastic behavior, and will expand during heating. The incremental elastic volumetric strain of saturated soil during either mechanical or thermal loading in terms of drained reversible thermal contraction for normally consolidated (NC) soils was modeled by Cui et al. (2000) as follows:

$$d\varepsilon_{vT}^{e} = \alpha_2 dT + \left(\frac{\kappa}{1+e_0}\right)\frac{dp'}{p'} \qquad \text{Eq. 2.22}$$

However, an increase in temperature is expected to cause irreversible, plastic thermal volumetric contraction of saturated soil. When changes in the mean effective stress are applied to

a soil that has been heated, it will encounter plastic strains after reaching the preconsolidation stress defined from the LY curve in Eq. 2.19, as follows:

$$d\varepsilon_{vTp}^{p} = \alpha_1 \frac{dp'}{p'} \qquad \text{Eq. 2.23}$$

Cui et al. (2000) developed the following expression to predict the plastic volumetric contraction which can be encountered when the temperature reaches the TY curve:

$$d\varepsilon_{vT}^{p} = \left(\frac{-\alpha_2}{1-a}\right)\left[\exp\left(\frac{-\alpha_2}{1-a}\Delta T\right) - a\right]dT \qquad \text{Eq. 2.24}$$

where α_2 is a soil constant, and α is a shape parameter close to unity that is incorporated to better predict the soil behavior at high temperatures (Cui et al. 2000). It is clear from this formulation that the plastic thermal volumetric strain is empirical, and is not derived from work-based principles like the plastic volumetric strain in the Cam-Clay model. This is an issue that deserves further study in future research. Cui et al. (2000) defined a new set of volumetric thermal plastic yield curves that allows for the prediction of plastic strains at higher OCR values. They paid specific attention to the coupling and hardening phenomena related to the combined effects of stress and temperature.

For overconsolidated (OC) soils, Cui et al. (2000) suggested that the thermal volumetric contraction varies with OCR, and that this value can be defined by determining the slope of the curve parameter α_p using the HC curve at which the total incremental volumetric strain is zero, as follows:

$$d\varepsilon_{vT}^{p} = \alpha_p\left[\exp\left(\alpha_p \Delta T\right) - a\right]dT \qquad \text{Eq. 2.25}$$

Schematics of the LY, TY, and HC curves are shown in Figure 2.23. Beneath any of these yield surface, thermo-mechanical elastic strains will be encountered, while thermo-elasto-plastic strains occur when reaching and expanding the yield surfaces.

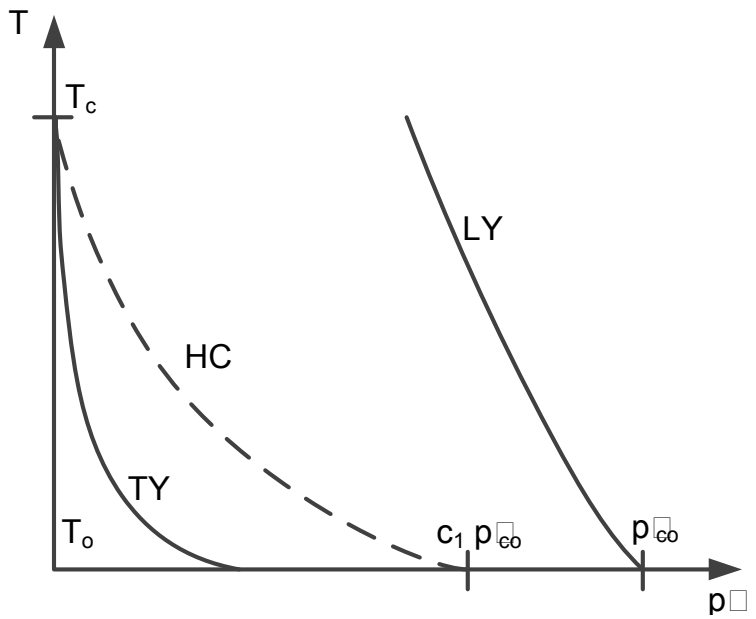

Figure 2.23: Yield loci in the *T–p´* plane. LY, loading yield; TY, thermal yield; HC, yield limit to change the expansion of overconsolidated soils into contraction due to heating

Recently, Hueckel et al. (2009) evaluated different failure conditions of saturated clays at elevated temperatures using the thermal modified Cam-clay models mentioned in this section. Hueckel et al. (2009) hypothesized that the increase in temperature may not only lead to a decrease in the preconsolidation stress, but may also affect the increase on the slope of the critical state line M. Hueckel et al. (2009) also indicated that the evolution of both the yield locus and failure is critically dependent on the history of thermo mechanical loading. They showed that as the shape and characteristic dimensions of the yield locus are controlled by two independent functions of temperature, the peak strength on a given stress path may vary non-monotonically, first decreasing and then increasing, and remain above the critical line, which was studied earlier by Hueckel et al. (1998), as shown in Figure 2.24. They explained this change in strength mode as a result of changing the yield point from the strain-softening side to the strain-hardening part of the locus ones temperature applied past the critical value. With subsequent triaxial loading at that temperature, strain-hardening allows the locus to grow until it reaches the current critical

line at M_{90}, and hence possibly shear strength much higher than the strength at critical temperature. The important conclusion by Hueckel et al. (2009) is that there is no single yield surface that can be attributed uniquely to a given temperature, and the yield limit generated during the same heating phase depends on confining stress, OCR, and the response during thermoplastic heating.

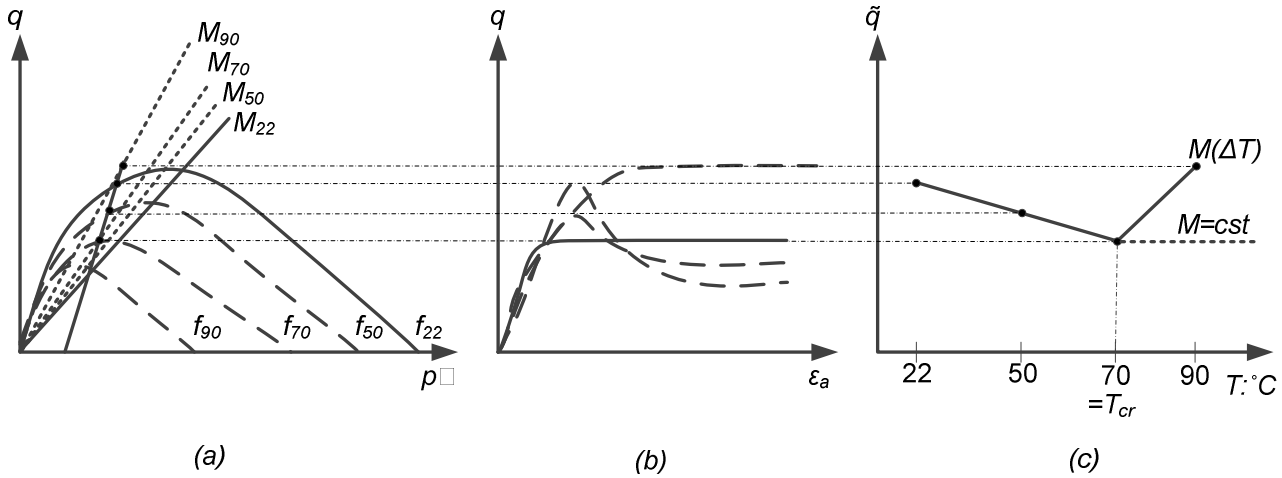

Figure 2.24: Evolution of peak strength q with temperature: (a) for peak strength at the softening part, $q > q_{crit}$, the strength can decrease with temperature, whereas for the yield locus it shrinks below $\tilde{q} < q_{crit}$, and the ultimate strength is reached through a hardening process always at the value of the stress path intersection with the current critical state line M(ΔT); (b) corresponding stress–strain curves; (c) theoretical variation of strength with temperature. Note that for a constant M value the shear strength remains constant at q_{crit} (Hueckel et al. 2009)

Although several thermo-hydro-mechanical models have been proposed in order to predict the behavior of unsaturated soils in non-isothermal conditions (Uchaipichat 2005; François and Laloui 2008a; Dumont et al. 2011; among others), only the modified Cam-Clay-type models for unsaturated conditions developed by Uchaipichat (2005) is reviewed due to its incorporation of suction and effective stress state into the yield surface. The influence of temperature on unsaturated soils can be incorporated into the isotropic yield surface by implementing a temperature function, $f(T)$, and a suction function $f(\psi)$ to define the influence of temperature on p'_c in unsaturated soils as follows:

$$f_{iso} = p' - p'_{co}\exp\left(\beta\varepsilon_v^p\right)\cdot f(\psi)\cdot f(T) \qquad \text{Eq. 2.26}$$

where $_{c0}$ is the current mean effective stress, ε_v^p is the plastic volumetric strain due to loading, and β is a soil parameter. The steady-state boundary surface (SSBS) corresponding to this equation in the normalized mean effective stress-temperature-suction space is shown in Figure 2.25. The shape of this surface indicates that an increase in temperature will cause a decrease in the mean effective preconsolidation stress, while an increase in the matric suction will cause an increase in the mean effective preconsolidation stress. Stress states located beneath the SSBS will maintain a purely-elastic soil response due to either changes in net stress, matric suction, and/or temperature. Plastic yielding will begin once the stress state makes contact with the SSBS causing both a shift in the yield surface as well as irrecoverable volumetric strains.

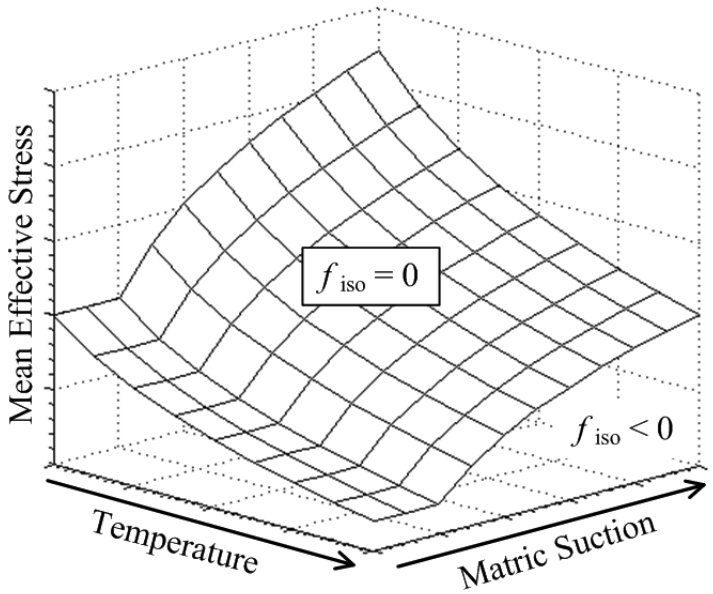

Figure 2.25: Steady-state boundary surface in the normalized p´ : T : ψ space

Uchaipichat (2005) modeled the yield locus for unsaturated silt using the following expression:

$$\frac{\left(p' - \left(p'_c / r\right)\right)^2}{\left(\left(1 - 2/r\right)p' + \left(p'_c / r\right)\right)^2} + \frac{q^2}{\left(\left(1-a\right)Mp' + \left(a/r\right)Mp'_c\right)^2} = 1 \qquad \text{Eq. 2.27}$$

where r is a spacing ratio ($r = p'_c/p'_{CSL}$), and a is a dimensionless parameter ranging from 0 to1. Uchaipichat (2005) found that the smaller values of a provide better modeling to the behavior of frictional materials, and a trial and error fitting procedure was followed to obtained this value. The evolution of the yield locus with temperature increase and matric suction for silt used in Uchaipichat (2005) is shown in Figure 2.26, and a summary of their model parameters is presented in Table 2.1. The results in Figure 2.26 indicated that temperature led to a shrinkage in the yield locus, and thus a reduction in the effective preconsolidation stress, while the increase in matric suction resulted in expanding the yield locus, and thus an increase in the effective preconsolidation stress. The temperature and suction effects on the effective preconsolidation stress by Uchaipichat (2005) can be modeled as follows:

$$\ln p'_c = \frac{N_{s,T} - N_{0,T_0}}{\lambda_{s,T} - k} + \frac{\lambda_{0,T_0} - k}{\lambda_{s,T} - k} \ln p'_{co} + \frac{v_o \varepsilon_v^p}{\lambda_{s,T} - k} \qquad \text{Eq. 2.28}$$

where $N_{s,T}$, $\lambda_{s,T}$ are the parameters of the compression curve at suction s and elevated temperature T. v_o is the initial specific volume. $N_{0,T0}$, $\lambda_{0,T0}$ are the parameters of the compression curve at saturated condition and reference temperature T_0.

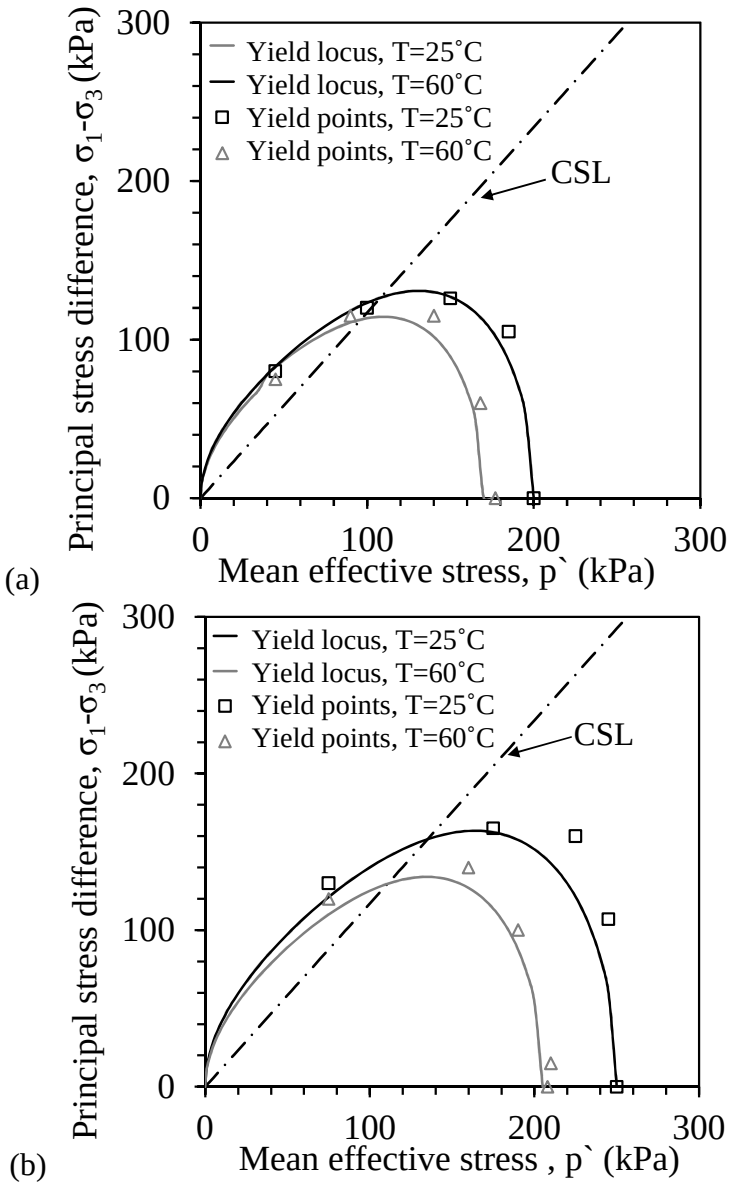

Figure 2.26: Evolution of yield locus with temperature at different matric suction: (a) 0 kPa (saturated); (b) 300 kPa (Uchaipichat 2005)

Table 2.1: Summary parameters of thermo-elastic-plastic model (Uchaipichat 2005)

Parameters	Value at T=25°C
M	1.17
λ	0.09
k	0.006
v	0.25
α	0.7
r	1.85

3. PROPERTIES OF TESTING MATERIALS

3.1 Introduction

Silt obtained from the borrow source for the Bonny Dam near the Colorado-Kansas border was used in this experimental study. The grain size distribution for this silt is shown in Figure 3.1. The plasticity index for this soil is 4, so it classified as ML according to the Unified Soil Classification Scheme. A summary of the index properties of the soil is given in Table 3.1.

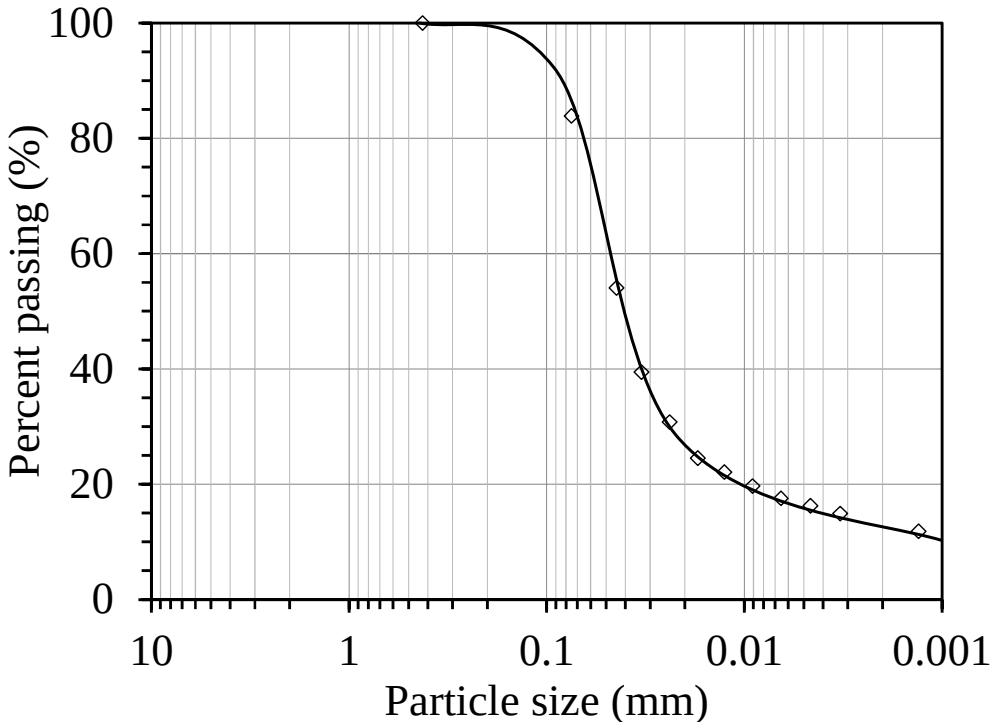

Figure 3.1: Grain size distribution for Bonny silt

Table 3.1: Geotechnical index properties of Bonny silt

Parameter	Value
Liquid limit, LL	25
Plastic limit, PL	21
Plasticity index, PI	4
Specific gravity, G_s	2.65
Standard Proctor optimum gravimetric water content, w_{opt}	13.6%
Standard Proctor optimum gravimetric dry density, $\gamma_{d,max}$	16.3 kN/m^3

3.2 Compaction Characteristics

Because statically compacted silt was used in this study, modified and standard Proctor compaction tests were performed on Bonny silt following ASTM D 698 to provide a frame of reference. The compaction curves along with the zero air voids (ZAV) line are shown in Figure 3.2. The maximum dry unit weights of the silt are 16.6 kN/m^3 and 19.1 kN/m^3 for specimens compacted using the standard and modified Proctor compaction efforts, respectively. The optimum water content for the standard Proctor effort is approximately 14%, while that for the modified Proctor effort is approximately 11%.

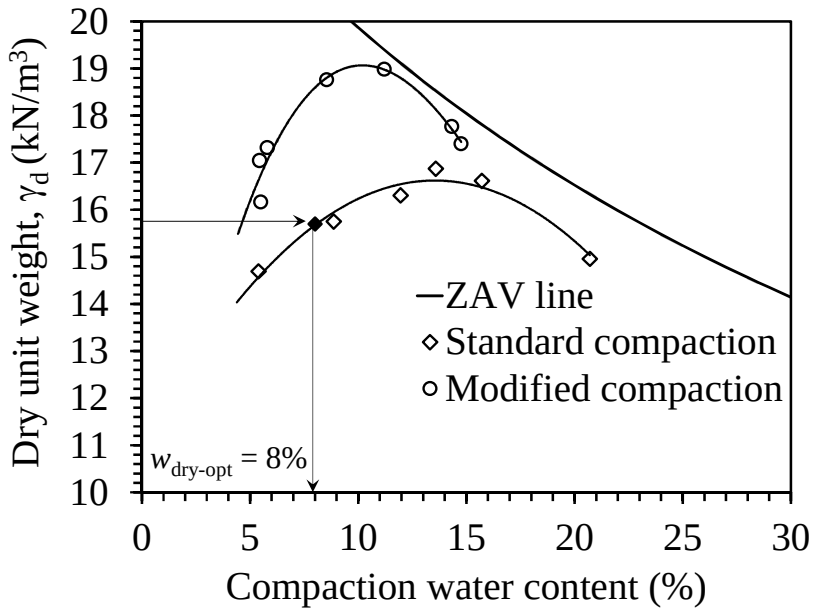

Figure 3.2: Modified and standard Proctor compaction curves for Bonny silt

3.3 Shear Strength Parameters

The effective shear strength parameters of saturated Bonny silt were determined by performing a set of consolidated undrained triaxial compression tests on back-pressure saturated soil specimens with an initial void ratio of 0.68 and a compaction water content of 10.5% under different mean effective stresses of 100, 200 and 300 kPa with pore water pressure measurement,

following ASTM D4767 for consolidated-undrained (CU) triaxial compression testing. The shear stress-strain curves are shown in Figure 3.3(a) and the excess pore water pressure (PWP) response is shown in Figure 3.3(b).

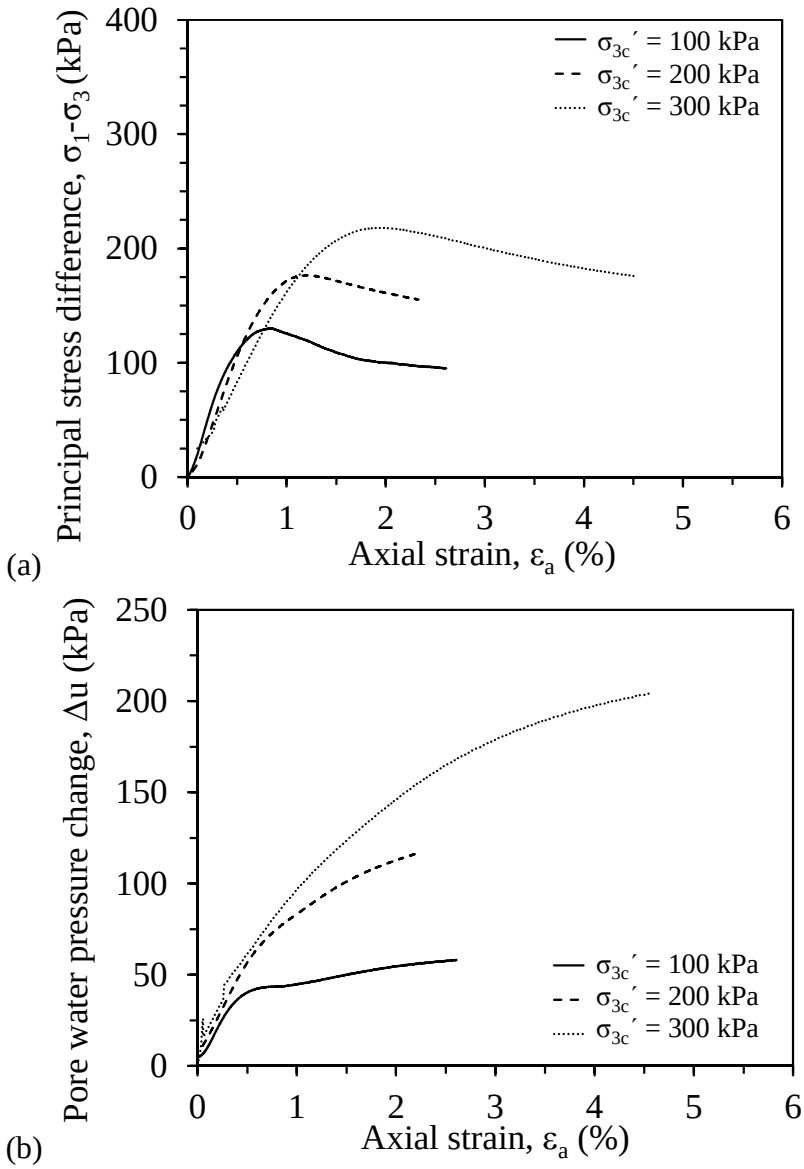

Figure 3.3: Shear strength results for saturated specimens subjected to different net confining stresses (a) Principal stress difference vs. axial strain (b) Pore water pressure vs. axial strain

The results in Figure 3.3(b) indicate that the buildup of the pore-water pressures increases as the shearing developed and continue to increase after reaching the maximum principal stress

difference. This means that the effective stresses is also continued decreasing and the soil specimens are contracting.

The stress paths in the mean effective stress plot are shown in Figure 3.4. The results in this figure indicate that during shearing of the soil specimen under all values of net confining stresses, the stress paths are consistent with the shapes representative of normally consolidated to lightly overconsolidated clays (contractile), and tend toward the same critical state line having a slope of M = 1.23. The points of failure were defined using the stress path tangency failure criterion (maximum principal stress ratio). This value of M was used to define the drained friction angle of the silt, which was calculated to be 31°.

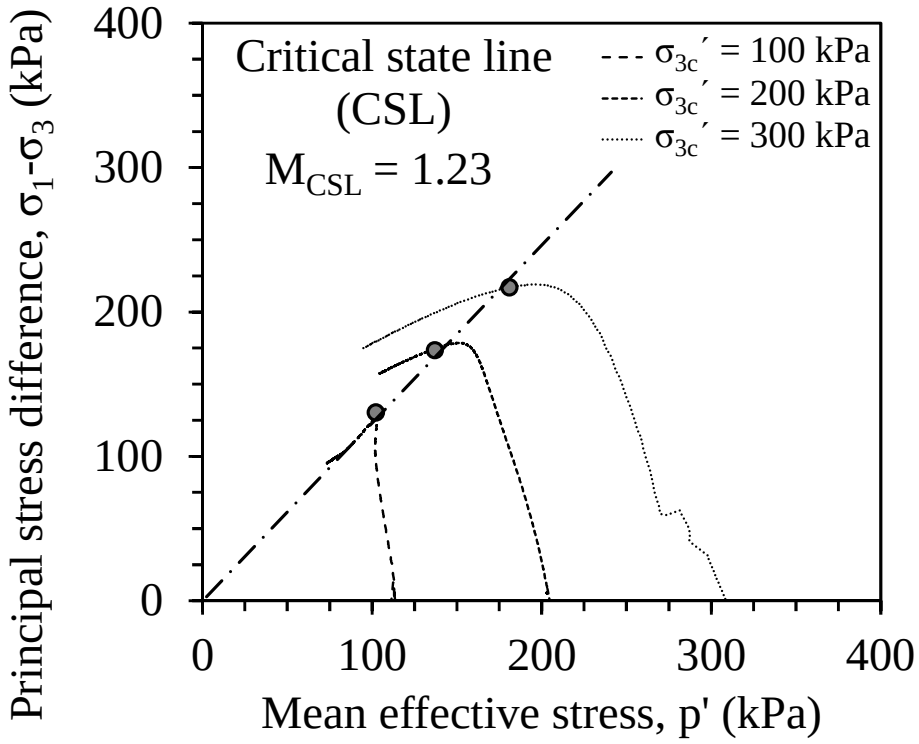

Figure 3.4: Critical state analysis for saturated Bonny silt at different net confining pressure values with the effective stress paths in the mean effective stress plot

3.4 Hydraulic Properties of Bonny Silt

The flexible-wall permeameter setup developed by McCartney and Znidarčić (2010) was used to define points on the soil water retention curve for Bonny silt at high saturation. In this test setup, they incorporate the axis translation technique for suction control and a flow pump is used to draw water from the bottom of the specimen in stages. The use of the flow pump permits careful measurement of the volume of water extracted from the specimen, which used to calculate the degree of saturation and volumetric water content. The change in suction during operation of the pump was monitored using a differential pressure transducer.

The vapor equilibrium testing setup was developed by Alsherif and McCartney (2012), who provide a summary of the method to control different high suction magnitudes and monitor equilibrium times. An interesting feature of the data points on the SWRC obtained using the vapor equilibrium technique is that the volume of the compacted specimens tended to decrease under application of the high suction magnitudes. This implies that data points for high suctions and low suctions do not necessarily have the same void ratio.

The hydraulic conductivity of the saturated silt specimen was also measured in the flexible-wall permeameter device by applying different flow rates across the saturated specimen and measuring the pressure gradient with the differential pressure transducer. The hydraulic conductivity was calculated from this information using Darcy's law. Further, the outflow data during each of the suction equilibration stages were used to determine points on the drying-path hydraulic conductivity function (HCF) using Gardner's (1958) method.

The van Genuchten (1980) SWRC relationship was used in this study to provide a functional relationship for the SWRC data from the axis translation and high suction tests. The fitting process used involved the conventional regression approach of least squares minimization. This

approach was done deliberately despite the issues in the experimental SWRC data noted earlier in this section, as this is the approach typically used in engineering practice.

The drying-path soil water retention curve (SWRC) for Bonny silt compacted to a void ratio of 0.68 was measured using a flexible-wall permeameter device for low suction magnitudes, and using the vapor equilibrium technique for high suction magnitudes. The suction equilibration points on the SWRC are shown in Figure 3.5(a) and Table 3.2. An interesting feature of the data points on the SWRC obtained using the flexible-wall permeameter device is that the points started to flatten after drying the specimen to a degree of saturation of approximately 0.65. This occurred because the water phase in the silt started to become discontinuous, making it impossible to withdraw further water from the specimen with the pump. This behavior was also observed by Khosravi and McCartney (2012) for the same soil but under different initial void ratios. A comparison between the HCF data and HCF curve predicted from the SWRC using the van Genuchten-Mualem model (van Genuchten 1980) is shown in Figure 3.5(b). The results in this figure indicate that HCF predicted from the SWRC underestimates the HCF data. The HCF curve that best fits the experimental HCF data is also shown in the figure.

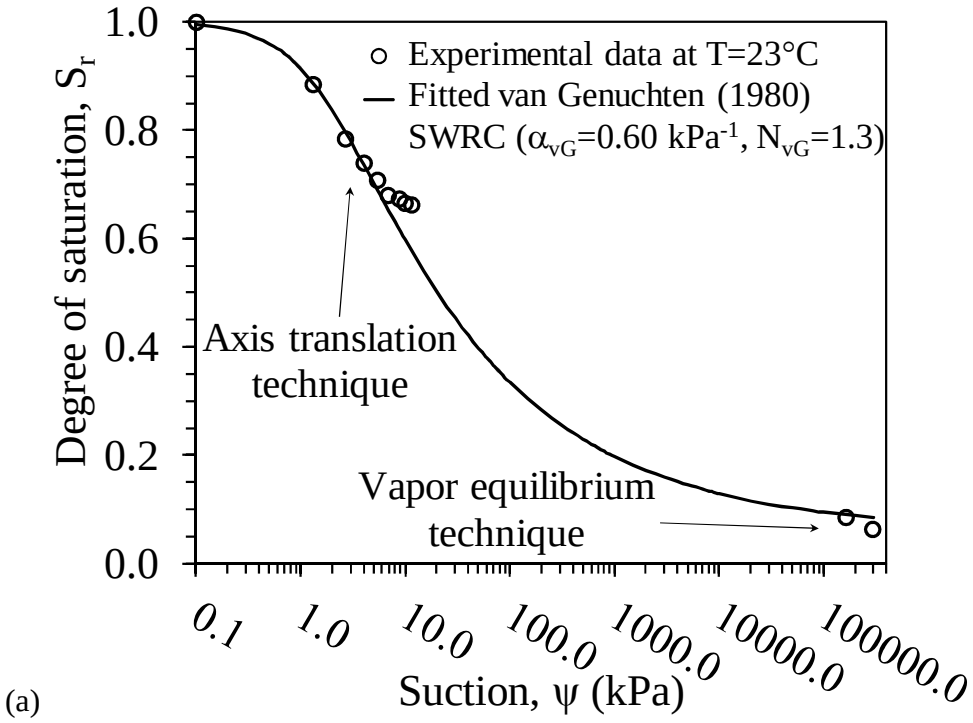

(a)

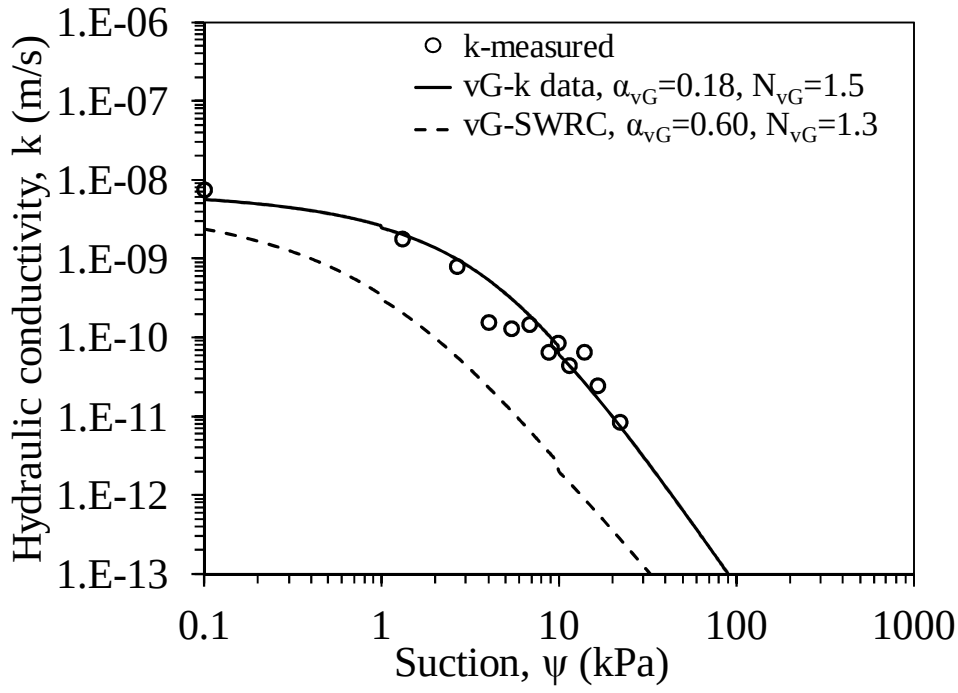

(b)

Figure3.5: Hydraulic properties of Bonny silt: (a) Soil water retention curve; (b) Drying curve HCF with the HCF predicted from the SWRC

Table 3.2: Equilibrium Points on the SWRC for Bonny silt

Suction (kPa)	Experimental results	
	Volumetric water content	Degree of saturation
0.1	0.39	1.00
1.31	0.34	0.89
2.66	0.30	0.78
4.01	0.29	0.74
5.38	0.27	0.71
6.80	0.26	0.68
8.72	0.26	0.67
9.86	0.26	0.67
11.39	0.26	0.66
162000		0.086
291000		0.064

The thermal conductivity of saturated Bonny silt was measured using a new approach developed by McCartney et al. (2013b) to measure the thermal conductivity of soils in a modified triaxial cell by inserting a thermal needle into the specimen through the top platen. The thermal conductivity and degree of saturation during a test involving saturation then drainage of silt is shown in Figure 3.6. The results in this figure indicate that the initial thermal conductivity for this particular silt in as-compacted conditions (time of zero) is 1.34 W/mK, while after saturation it is equal to 1.55 W/mK. As the degree of saturation is decreased during the drainage test to 0.94, the thermal conductivity decreased down to 1.45 W/mK. All of the triaxial tests in this study start from as-compacted conditions and get drier, so the value of thermal conductivity of 1.34 W/mK measured at the beginning of the test and corresponding to 0.41 initial degree of saturation is the upper limit on the thermal conductivity expected during the triaxial tests. The change in thermal conductivity corresponding to the change in degree of saturation is shown in Figure 3.7.

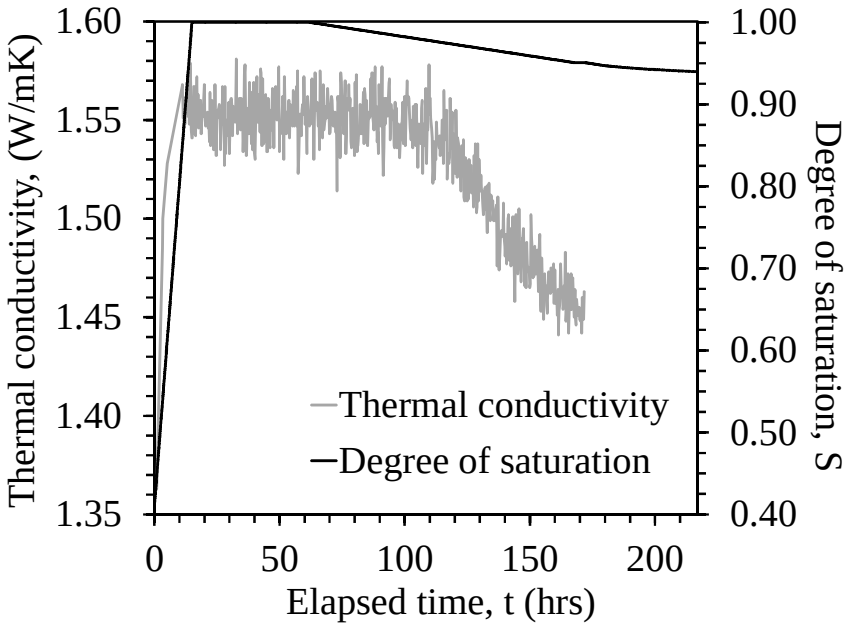

Figure 3.6: Thermal conductivity versus degree of saturation over time

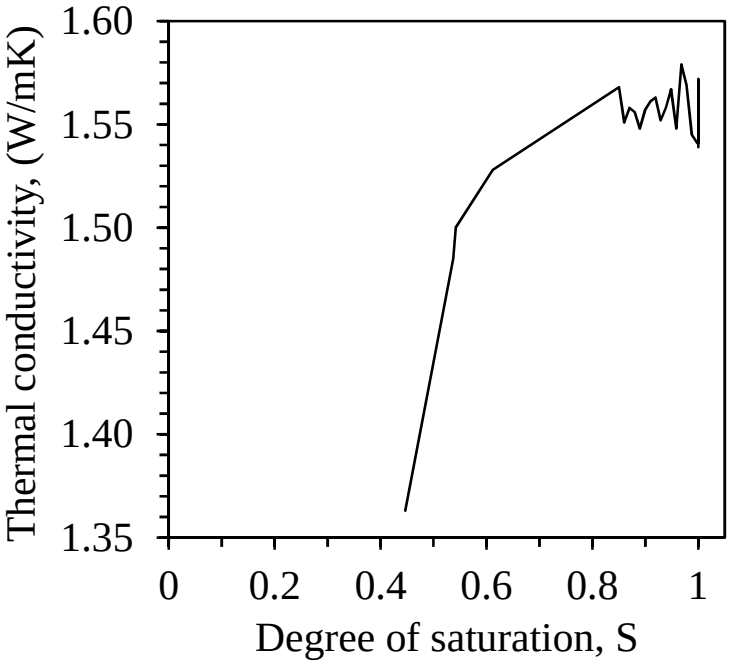

Figure 3.7: Relationship between thermal conductivity and degree of saturation

3.5 Air Permeability

The air permeability of the soil is a critical variable to the success of the new triaxial device as it uses vapor flow to apply the suction to the specimen. The air permeability is defined as the

ability of a soil to conduct air by convective flow, in which case the movement of air occurs due to a gradient of gas pressure across the specimen. Knowledge of the air permeability of the soil used in testing program is useful in selecting an appropriate flow rate applied at the bottom of the specimen. The air permeability is expected to be inversely related to soil water content, the pore size distribution, and the connectivity of the open pores in the soil.

Air permeability for a completely dry soil is considered to be equal to the intrinsic permeability of the soil. The intrinsic permeability can be calculated as follows:

$$k_i = \frac{K\mu}{\rho g} \qquad \text{Eq. 3.1}$$

where k_i is the intrinsic permeability (m^2), K is saturated hydraulic conductivity to water (m/s), μ is dynamic viscosity of water (kg/m-s), ρ is density of water (kg/m^3), g is gravitational constant (m/s^2). The typical relationship between air permeability and intrinsic permeability is expressed as follow:

$$k = k_i \cdot k_{ra} \qquad \text{Eq. 3.2}$$

where k is the air permeability and k_{ra} is the relative permeability to air. Brooks and Corey (1964) developed an expression for relative permeability to air based on Burdine's solution, as follows:

$$k_{ra} = (1 - S_e)^2 \left[1 - S_e^{\frac{2+\lambda}{\lambda}} \right] \qquad \text{Eq. 3.3}$$

where S_e is the effective degree of saturation, defined as $S_e = \frac{S - S_r}{1 - S_r}$, λ is the Brooks-Corey pore size distribution index, which is equal to 1.82 for Bonny silt. All values of the parameters are presented in Table 3.3.

Table 3.3: Summary of parameters for air permeability calculation

Parameters	Value at T=23°C
k_{sat}, (m/min)	7.56×10^{-09}
S_{res}	0.064
λ	1.82
ρ_w, (kg/m^3)	997.62
μ_w , (kg/m-min^2)	0.000933
g, (m/min^2)	3600

Combining Equations 3.1 and 3.3 into Equation 3.2 results in the following expression:

$$k_{ra} = (1-S_e)^2\left[1-S_e^{\frac{2+\lambda}{\lambda}}\right]\frac{K\mu}{\rho g} \qquad \text{Eq. 3.4}$$

The theoretical change in air permeability of unsaturated Bonny silt compacted to initial void ratio of 0.68 as a function of the degree of saturation is shown in Figure 3.8. The air permeability is observed to increase by 7 orders of magnitude of the full range of degree of saturation for Bonny silt.

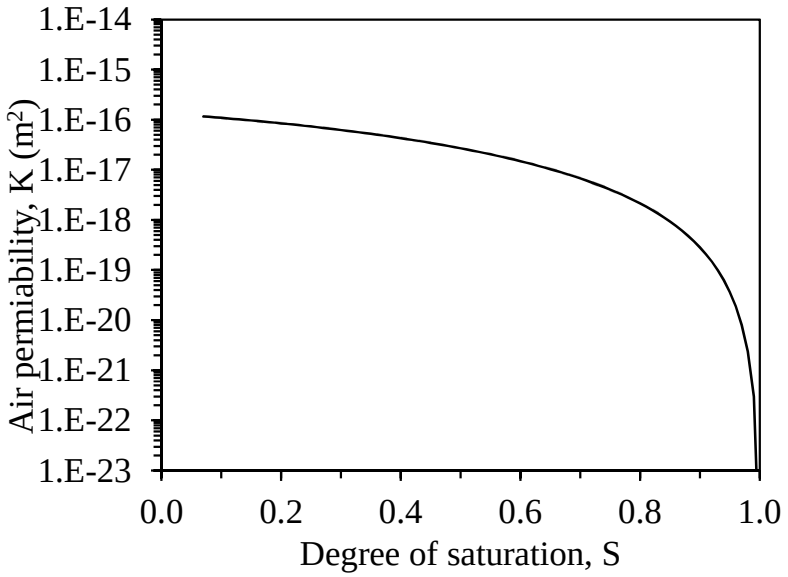

Figure 3.8: Theoretical values of air permeability of unsaturated Bonny silt compacted to initial void ratio of 0.68.

The intrinsic permeability can also be written in accordance with Darcy's law as follows:

$$k_a = \left(\frac{Q_{AV}}{\Delta P} \frac{L}{A} \mu \right) \times \left(10^{12} \frac{darcy}{m^2} \right) \quad \text{Eq. 3.5}$$

where k_a is the intrinsic air permeability (Darcy/m^2), Q_{AV} is the average gas flow rate (m^3/s), ΔP is the differential pressure across soil specimen (kPa), L is the height of the specimen (m), A is the cross-section area (m^2), μ is the dynamic viscosity of the gas (kPa-s). Equation 3.5 is used in this study to evaluate the experimental value of air permeability through soil specimens. Results regarding air permeability from this study are presented in Chapter 6.

3.6.Isothermal and Nonisothermal Volume Change Properties

The compression properties of saturated and unsaturated Bonny silt were measured using a standard oedometer test following the procedures in ASTM D2435, although loading increments were applied only until reaching the end of primary consolidation at each stress level. The compression curve for a specimen compacted to the target condition used in this experimental study as described later in Section 5.2 is shown in Figure 3.9. The results in Figure 3.9(a) show the compression curve with the parameters for the consolidated test performed on saturated soil specimen, and the results in Figure 3.9(b) show the compression curve with the parameters for the consolidated test performed on unsaturated soil specimen. Results in this figures indicate that the value of preconsolidation pressure is 90 kPa and for saturated specimen and 390 kPa for unsaturated specimen. A comparison between the saturated and unsaturated test results is presented in Figure 3.10. A summary of test parameters and the converted Cam-Clay model parameters are presented in Table 3.4.

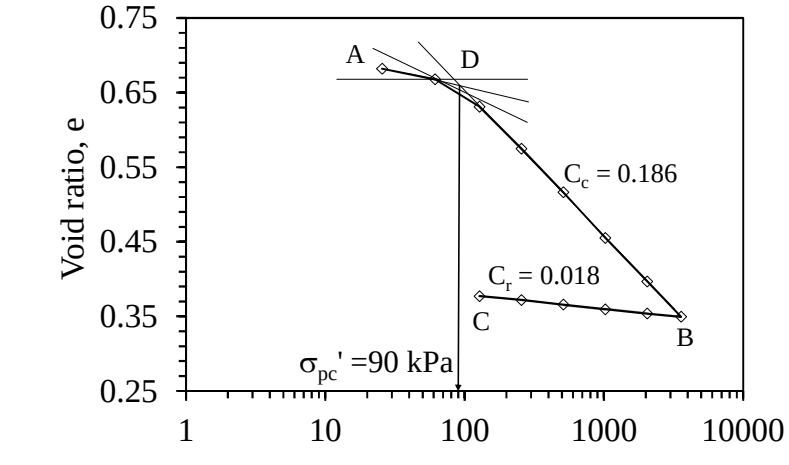

(a)

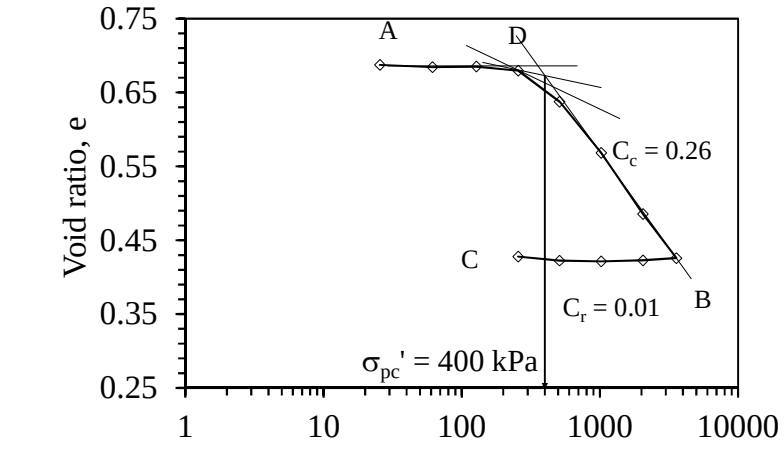

(b)

Figure 3.9: Compression curves for: (a) Saturated specimen; (b) Unsaturated specimen

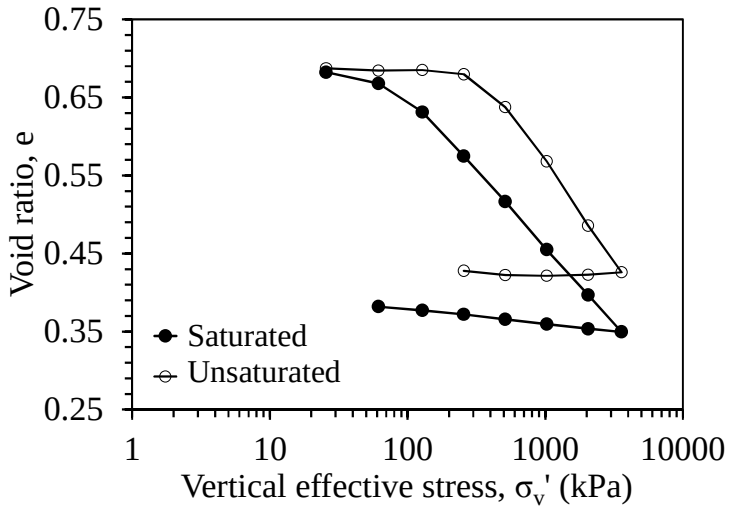

Figure 3.10: Comparison between the compression curves for saturated and unsaturated Bonny silt specimens

Table3.4: Summary of the compression curve parameters for the saturated and unsaturated Bonny silt specimens, along with the interpreted parameters for the Cam-clay model

Parameters	Value at T=23°C
$P'_{c\ sat}$ (kPa)	90
$C_{c\ sat}$	0.186
$C_{r\ sat}$	0.018
λ_{sat}	0.08
κ_{sat}	0.02
$P'_{c\ unsat}$ (kPa)	400
$C_{c\ unsat}$	0.25
$C_{r\ unsat}$	0.01
λ_{unsat}	0.11
κ_{unsat}	0.03

The impact of cyclic heating and cooling on the thermally induced volume change of saturated compacted Bonny silt under different stress states was measured using a temperature-regulated oedometer with back-pressure control by Vega and McCartney (2014). The permanent thermal axial volume change as a function of OCR for each of the heating-cooling cycles is shown in Figure 3.11, which clearly reveals an upward shift in the curves at low OCRs with increasing numbers of heating-cooling cycles. The results in this figure indicate that the normally consolidated silt specimens were observed to show permanent contraction while the overconsolidated silt specimens were observed to show expansion. In addition, during additional heating and cooling phases, the specimens all showed a small amount of additional contraction, regardless of the stress state. The normally consolidated specimen showed the greatest amount of additional permanent contraction.

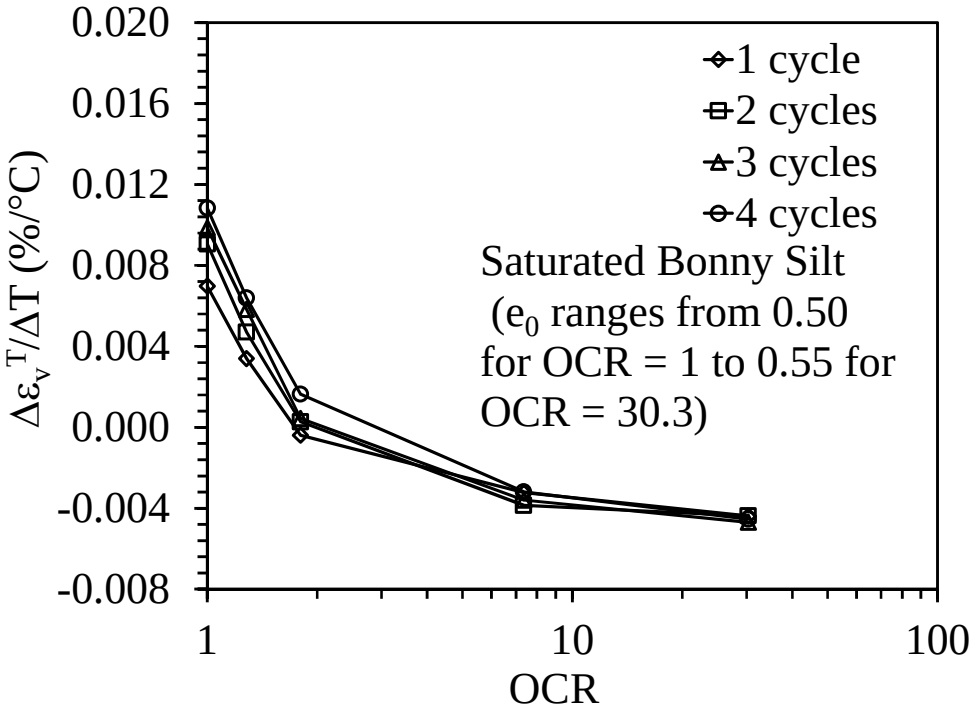

Figure 3.11: Permanent strain of saturated Bonny silt as a function of OCR for different numbers of heating cycles by Vega and McCartney (2014)

4. THERMO-HYDRO-MECHANICAL TRIAXIAL EQUIPMENT

4.1 Introduction

In this chapter, details of the new triaxial cell developed for characterization of the nonisothermal shear strength of unsaturated soils under high suction magnitudes are presented. This includes a discussion of the individual components, as well as an assessment of the thermal response of the system without soil. Specifically, a detailed description of the control systems in the triaxial setup is presented in Section 4.2 and an evaluation of the triaxial wall and seal and the suction implementation described in Sections 4.3 and 4.4, respectively. The calibration procedure and results are discussed in Sections 4.5 and 4.6.

4.2 Testing Apparatus

4.2.1. Triaxial Cell

A new triaxial cell was designed to accommodate elevated temperatures and the application of high suction magnitudes to a soil specimen using the vapor flow technique. A drawing of the new triaxial cell with its different components is shown in Figure 4.1. Duran Borosilicate glass tubing having an outer diameter of 180 mm, a wall thickness of 9 mm and a length of 381 mm is used as the pressure vessel for the triaxial cell. This material is selected because the ultimate use of the triaxial cell is to evaluate the nonisothermal shear strength of soils under high suction magnitudes. Duran Borosilicate glass has a high resistance to thermal shock, a low coefficient of thermal expansion, low creep potential, and high chemical resistance. However, a shortcoming of this material is that internal pressures are limited to 630 kPa. A picture of the triaxial cell is shown in Figure 4.2.

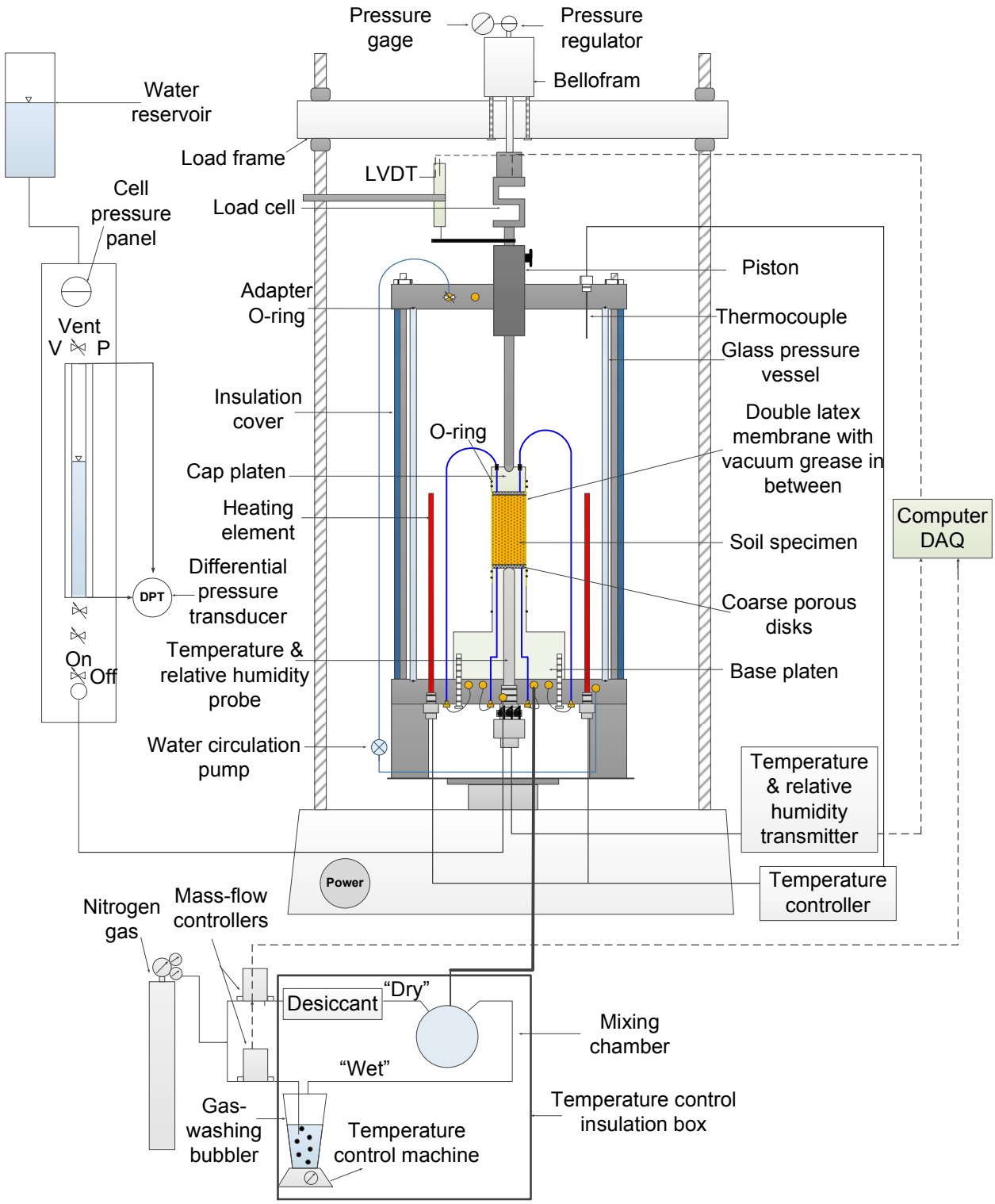

Figure 4.1. Schematic of the nonisothermal triaxial cell for unsaturated soils under high suction magnitudes

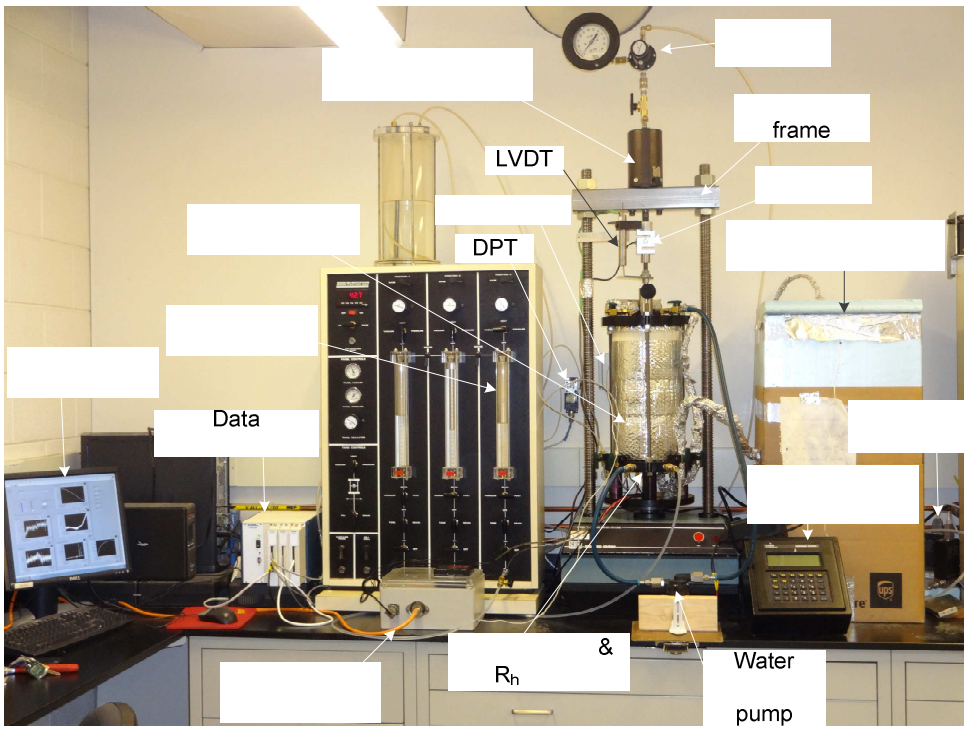

Figure 4.2. Picture of thermo-hydro-mechanical triaxial system

4.2.2 Suction Control System

The upper and lower platens in the triaxial cell were designed to allow unrestricted gas flow through initially unsaturated soil specimens. Unrestricted gas flow will only occur in soils at an initially low degree of saturation (approximately less than 50%), where the gas phase is continuous. The gas flow system was designed to permit automated control of the relative humidity of the pore air being supplied to the base of the soil specimen (and consequently control of the total suction applied to the soil specimen) while making sure that the temperature of the gas stream is the same as that within the specimen to avoid condensation. A schematic and picture of the automated humidity-control system is shown in Figures 4.3(a) and 4.3(b), respectively. During application of a total suction value, N2 gas is passed from a pressure-regulated bottle through 6.3 mm-diameter PFA (perfluoroalkoxy) tubing. The flowing gas is split into two separate streams through a pair of computer-controlled mass-flow valves (MKS

Instruments, Type 1179A). These valves can regulate the flow of each gas stream between zero and 3.3×10-6 m3/s based on a control voltage supplied by a National Instruments LabView data acquisition program. The first gas stream is vapor-saturated by bubbling it upward through a tank filled with distilled water that is resting on a hot plate. The second gas stream is dried to zero relative humidity by passing it through a Hammond cylinder filled with color-indicating drierite desiccant media (calcium sulfate, >98% CaS04, >2% CaCl2). The two gas streams (wet and dry) are then reintroduced into a mixing chamber. The combined gas stream, which has a relative humidity that is a direct function of the 'wet' to 'dry' (w/d) gas flow ratio, is then passed through the soil specimen within the triaxial cell. The bubbling chamber, Hammond cylinder, and mixing chamber are all contained within an insulated box whose temperature is controlled by the hot plate and is the same as that imposed on the soil specimen. The top of the specimen is connected to an insulated flask that is vented to atmosphere. In addition, all the 6.35 mm perfluoroalkoxy (PFA) tubing connected to the system is insulated to reduce loss of temperature. For the tests performed in this study, the N2 gas pressure was 40 kPa at the base of the specimen and 0 kPa at the top of the specimen.

A differential pressure transducer (DPT) connected to the top and bottom of soil specimen is used to monitor the differential pressure across the specimen, which can be used to assess when steady-state conditions have been reached. After reaching steady-state gas flow through the specimen at a combined flow rate of 3.3×10-6 m3/s, the relative humidity of the gas is adjusted using a feedback-control system that involves monitoring of the relative humidity and temperature at the bottom of the specimen with a probe (Model HMT330 from Vaisala, Inc.). This probe is connected to the bottom of the soil specimen through the platen allowing for continuous measurement and monitoring during testing. This probe can be pressurized up to 407

kPa. It was observed to work well for all values of relative humidity under temperatures ranging from -70 to +180 °C, and also has a high resistance to corrosion. A rigid porous disk separates the bottom of the specimen from the head of the probe to avoid the issue of any possible influence of the sensor on the mechanical performance of the specimen. The probe is connected to a transmitter that transfers the recorded data to the LabView control program. Signals from the humidity probe provide feedback for automated regulation of the 'wet' to 'dry' gas flow ratio using the two mass-flow controllers. A second relative humidity sensor is placed within the insulated flask connected to the top of the specimen to monitor the relative humidity of the gas passing out of the specimen. When the relative humidity values of the N2 gas at the inlet and outlet of the specimen are the same, the total suction in the specimen can be calculated using Kelvin's law. This assumption is based on the idea that constant relative humidity is applied to the bottom of soil specimen and the flow of gas is through one axial direction from bottom to top of specimen. This means that the decrease in relative humidity over time is in the axial direction to the top of the specimen until equilibration occurs.

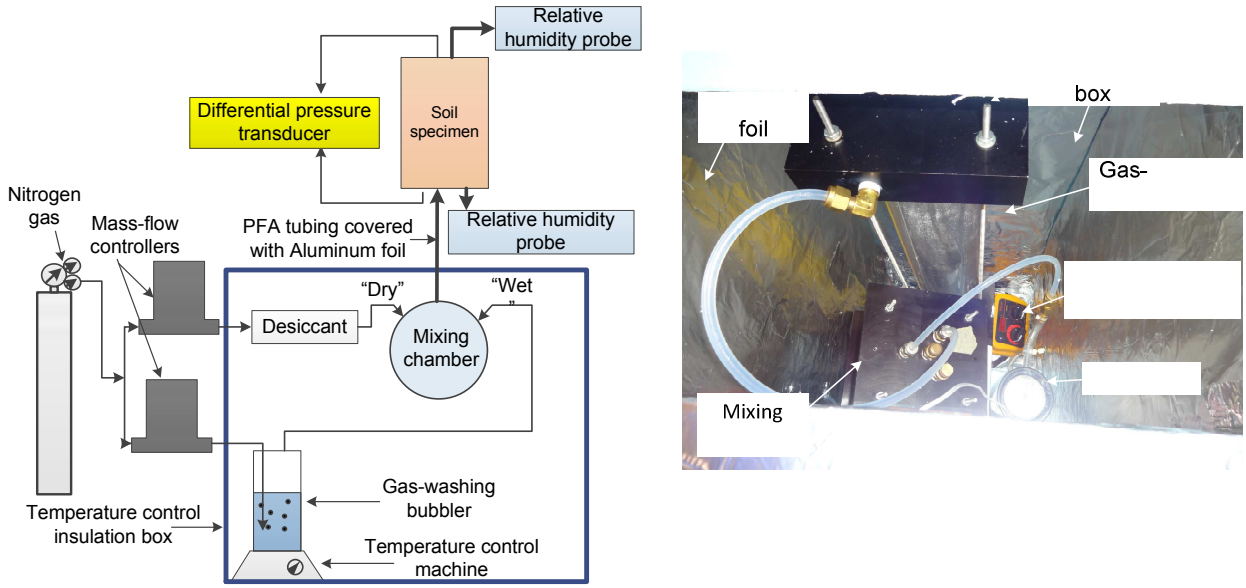

(a) (b)

Figure 4.3. Vapor flow technique for suction control: (a) Schematic; (b) Picture

4.2.3 Temperature Control System

The temperature in the fluid within the triaxial cell is imposed using three heating elements in a triangular array around the specimen. A temperature control unit from Omega Instruments is used to control the temperature and rate of heating, and uses a thermocouple installed through the top of the cell for feedback. A pump (Model TS5 15PV from TopsFlo Inc.) is used to circulate the pressurized water inside the cell to ensure uniform temperature distributions. The pump is capable of operating under pressures up to 1000 kPa and temperatures up to 100 °C.

4.2.4 Mechanical Loading System

A Brainard-Kilman Model S-600 triaxial load frame was adapted to operate in either load-control or displacement-control conditions. In normal operation, this load frame can be used to apply constant displacement rates to shear a soil specimen in displacement-controlled conditions. A pneumatic piston was incorporated into the top beam of the load frame to apply load-controlled conditions to the specimen. Load-control conditions should be applied during suction application or during temperature changes so that the specimen can deform freely in the axial direction while maintaining a constant axial load. The pneumatic piston can be locked off so that the soil specimen can be sheared in displacement-controlled conditions. In either configuration, a load cell is used to record axial loads, and a linearly variable differential transformer (LVDT) is used to track axial displacements. The volume change of the soil specimen during changes in suction, temperature, or shearing is also monitored by recording the water level in a graduated burette connected to the water supply line of the cell pressure using a differential pressure transducer.

4.2.5 Computer Program

All components of the system including the load cell, LVDT, temperature and relative humidity probe and the differential pressure transducer were connected to the computer through data acquisition system. A LabVIEW program was used to control the target relative humidity applied and consequently control the suction implemented to the soil specimen in addition to recording the percentages of the dry and wet Nitrogen gas corresponding to each relative humidity measured. A picture of the front screen of the LabVIEW program is shown in Figure 4.4.

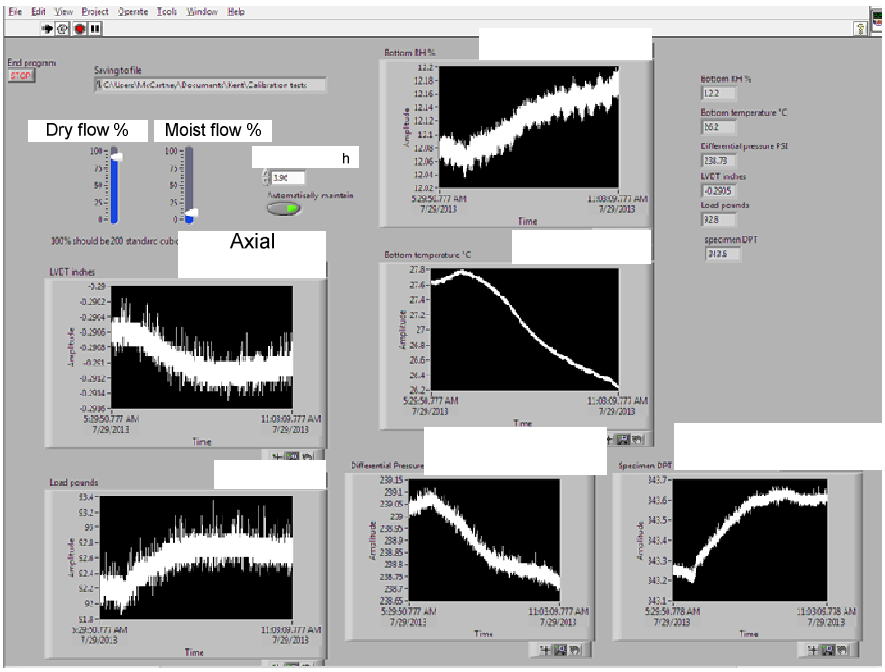

Figure 4.4. Picture of the main screen of the LabVIEW program used for controlling and monitoring suction and temperature application

4.3 Triaxial Cell Wall and Seal Assessment

After the triaxial cell components were connected and sealed and before starting the calibration tests, the material used for the cell wall and all sealing and connections were assessed to ensure that it withstand the applied pressures at elevated temperatures. A pressure up

to 500 kPa was applied first to the triaxial cell at room temperature, and then the temperature was raised up to 70 °C and kept constant for two days a long with checking the bottom sealing surround the relative humidity probe. No adverse effects of the temperature on the performance of the glass cylinder or the sealing were detected.

4.4 Suction Application Assessment

An assessment of the best procedure for suction implementation was achieved by performing two preliminary tests on soil specimens at room temperature. The first test was performed by connecting the nitrogen gas flow line to the bottom of the soil specimen for implementing the desired relative humidity and monitoring the relative humidity at the top to reach equilibrium condition. The second test was performed by connecting the nitrogen gas flow line to the top of the soil specimen for applying the desired relative humidity and monitoring the relative humidity at the bottom to reach equilibrium condition. The soil specimens are assumed to be in equilibrium when the measured values of relative humidity at the top and bottom of the soil specimen are the same. The results from the two tests are presented in Figures 4.5(a) and 4.5(b), respectively. The results in these figures indicate that the best procedure for suction implementation was by applying suction through the application of relative humidity at the bottom of the soil specimen and wait the top of the specimen to reach the same value.

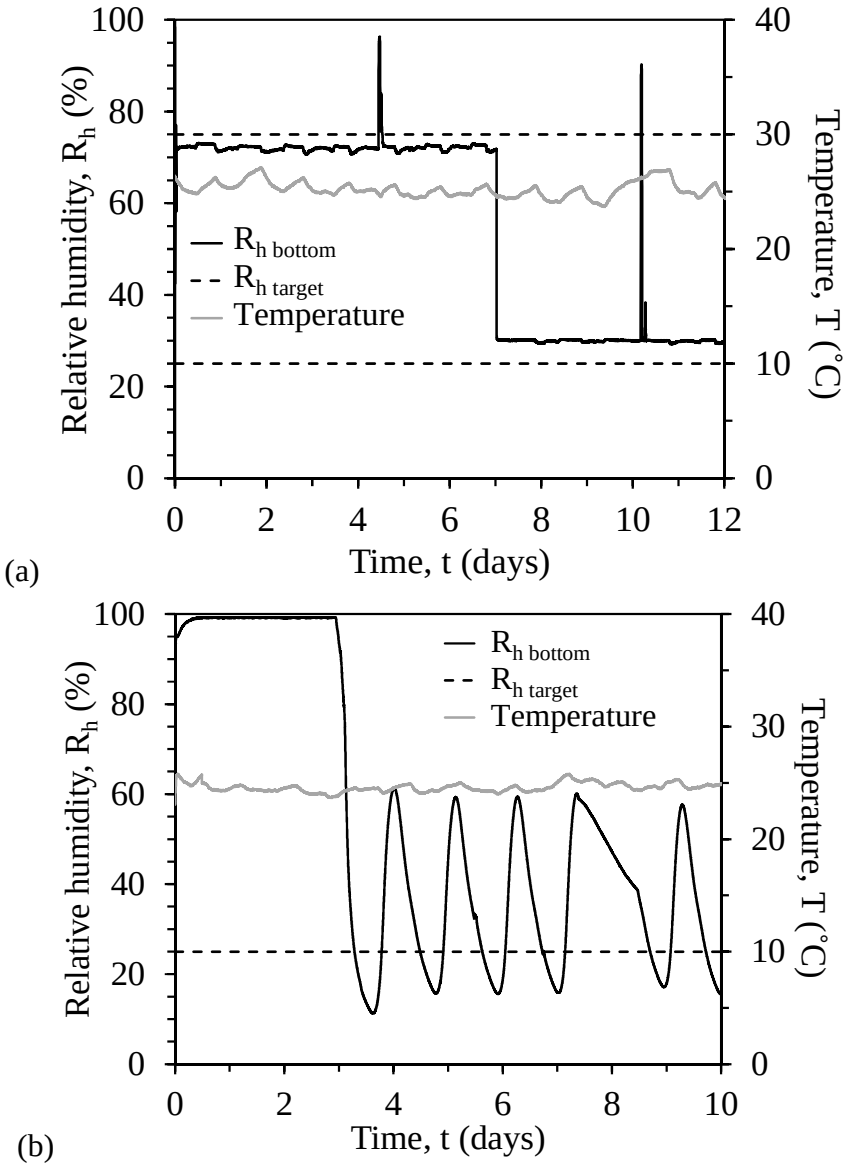

Figure 4.5. Measurements of relative humidity and temperature over time showing: (a) Hydration by applying suction on bottom of the soil specimen, (b) Hydration cyclic during application of suction on top of the soil specimen

It is clear from the results in Figure 4.5(a) that the flow of Nitrogen gas through the bottom of the soil specimen where the relative humidity probe is located allows shorter time to reach constant value of relative humidity (target value). However, when the gas flow through the top of the specimen instead of the bottom, higher percentage of dry Nitrogen was applied for longer time at the top of the specimen in order to the probe at the bottom to reach the target relative

humidity value, which resulted in drying the top of the soil specimen to lower relative humidity value than the target value. This condition forces the automated humidity system to push more moisture air to the top to recover the drop in relative humidity as shown in Figure 4.5(b), which resulted in applying suction cyclic and consequently non homogenous distribution of the volumetric water content and suction.

The suction implemented to the soil specimen was assessed at elevated temperatures imposed to the triaxial cell before covering the humidity system with insulation box. The test was performed by controlling the relative humidity at the bottom of a course pore stone specimen and applying thermal loading cyclic. The tests began by applying the target relative humidity to the bottom of specimen at room temperature and wait until the relative humidity reach a constant value in approximately two hours. Then, the degree of temperature was raised inside the cell to the target value and the corresponding change in relative humidity was recorded using the relative humidity probe. The results from tests performed to assess the target relative humidity values of 25, 50, and 75% are shown in Figures 4.6(a), 4.6(b) and 4.6(c), respectively. In all figures, the results indicated a drop in the relative humidity and an increase in suction due to a temperature increase. In addition, regardless of the initial relative humidity at room temperature, the drop in relative humidity stabilizes at a value of 10% at a temperature of 70 °C in these tests.

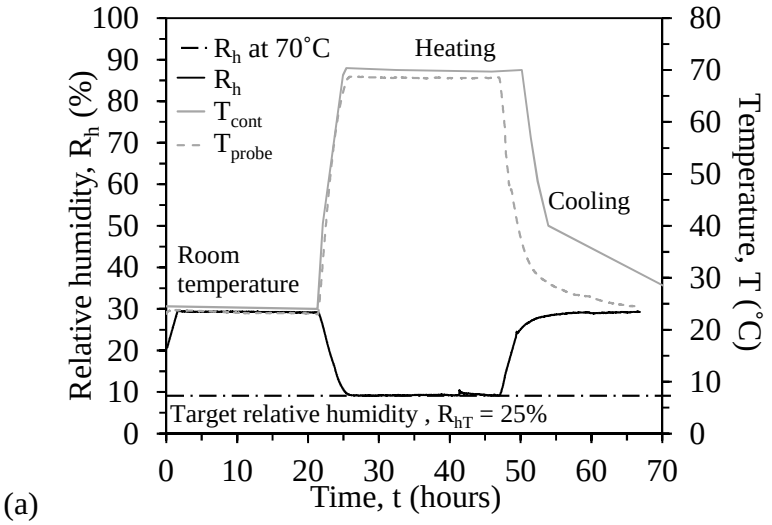

(a)

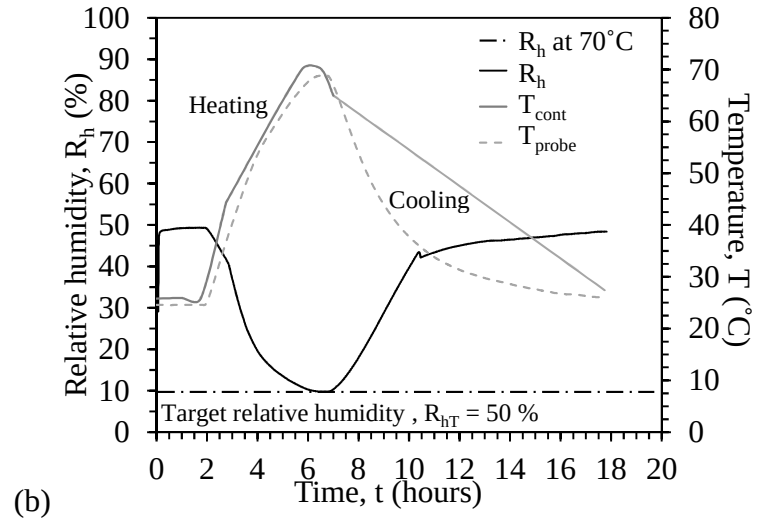

(b)

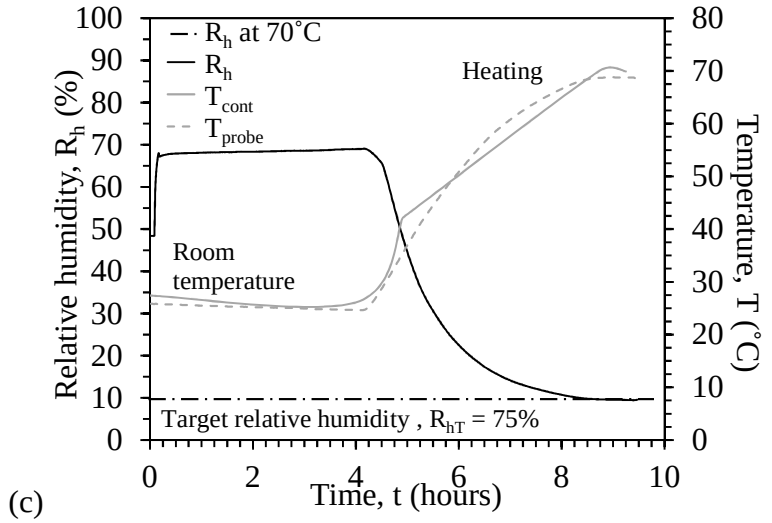

(c)

Figure 4.6: Thermal loading cyclic at target relative humidity values of: (a) 25%; (b) 50%; (c) 75%

The explanation of the drop in relative humidity at the time of 25 hours in Figure 4.6(a), 7 hours in Figure 4.6(b) and 9 hours in Figure 4.6(c) is related to the temperature difference between the triaxial cell and the automated humidity system, which was exposed to room temperature, a thermo-dynamic problem was created and the Nitrogen gas applied to the bottom of the specimen was not able to hold higher percentage of moisture in order to recover the relative humidity drop and keep it constant with increasing the degree of temperature. In order to resolve this issue, a closed box made of thermal insulation that was covered on the inside with hard aluminum foil was used to bring the suction control system to the same temperature as that of the triaxial cell. A temperature-controlled heating plate was placed within the insulated box to control the temperature.

4.5 Calibration of Measurement Devices

The measurement devices used in the new triaxial equipment including the differential pressure transducers (DPT), the temperature sensor, the thermocouple, the load cell transducer and the linearly variable differential transformer (LVDT) individually were calibrated prior to the start of the testing program to ensure its efficiency in measuring the correct data. Calibration data for DPTs connected to soil specimen and water level in the graduated burette are shown in Figures 4.7(a) and 4.7(b), respectively. Also, the overall test equipment response to the increase in temperature was calibrated and corrections to the measured values were presented. Two different set of calibration tests were performed: the first type of calibration tests was performed to report the applied and measured relative humidity relationship, and the second set of calibration tests were performed to account for the temperature effect on the thermal expansion of the whole system components.

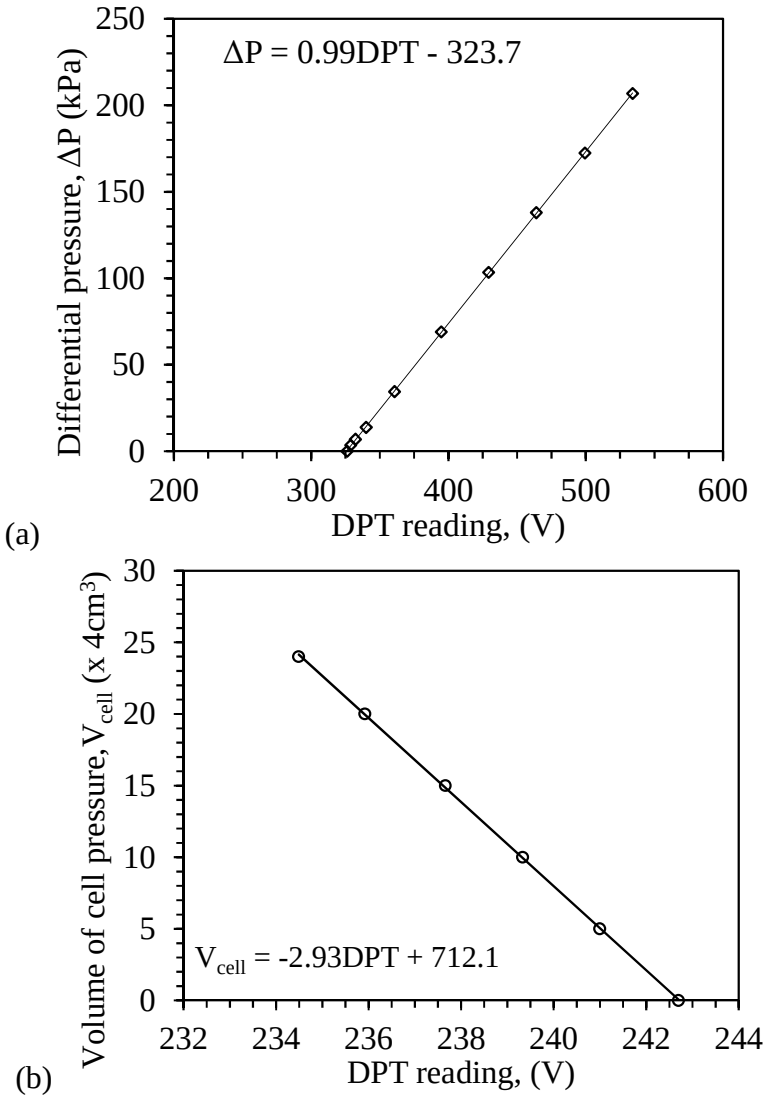

Figure 4.7: Calibration results of differential pressure transducers connected to: (a) top and bottom of the soil specimen to measure differential pressure; (b) Measurements from graduated burette connected to the cell pressure used to measure water inflow or outflow from the cell

4.6 Relative Humidity Calibration Tests

4.6.1.Relative Humidity Calibration Test Procedure

The controlled relative humidity using the automated humidity system was also calibrated by performing two relative humidity calibration tests on a specimen consists of a set of coarse pore stone which was used for the propose of speeding up the equilibrium time. The first test was performed under room temperature by applying the desired relative humidity ($R_{h\,T}$) to the course

pore stone specimen and monitoring the corresponding relative humidity ($R_{h\ bottom}$) recorded by the probe until it reaches equilibrium, and also recorded the wet and dry Nitrogen gas percentages corresponding to each relative humidity recorded. Then repeat the same steps at different target relative humidity values and the automated system adjusts the wet and dry Nitrogen gas percentages to new values. The same test was repeated at elevated temperature of 60 °C to evaluate the effect of increasing temperature on the relative humidity applied. This test began by increasing the degree of temperature in one step up to 60 °C in both the triaxial cell and the insulation box and waiting until the temperature reached equilibrium. Then the target relative humidity was applied and the corresponding relative humidity was recorded using the relative humidity probe at the base of the specimen.

4.6.2.Relative Humidity Calibration Test Results

The results from the relative humidity calibration test at room temperature on specimen of course porous disks are shown in Figure 4.8. This figure shows the relative humidity recorded from the relative humidity and temperature probe at the bottom of the specimen at ambient temperature over time in addition to the relative humidity values at the top of the specimen ($R_{h\ top}$) tracked using Lascar data logger. The results show a good match between the applied and recorded relative humidity particularly at 50% relative humidity and the corresponding top relative humidity was also following application of the target relative humidity. However, a difference between the top and bottom relative humidity values was observed initially, so time was permitted for these to reach a similar value before applying the next target relative humidity value. The corresponding total suction applied to each relative humidity with respect to time is shown in Figure 4.9. The results in this figure indicate the wide range of total suction can be applied to unsaturated soils using this triaxial setup.

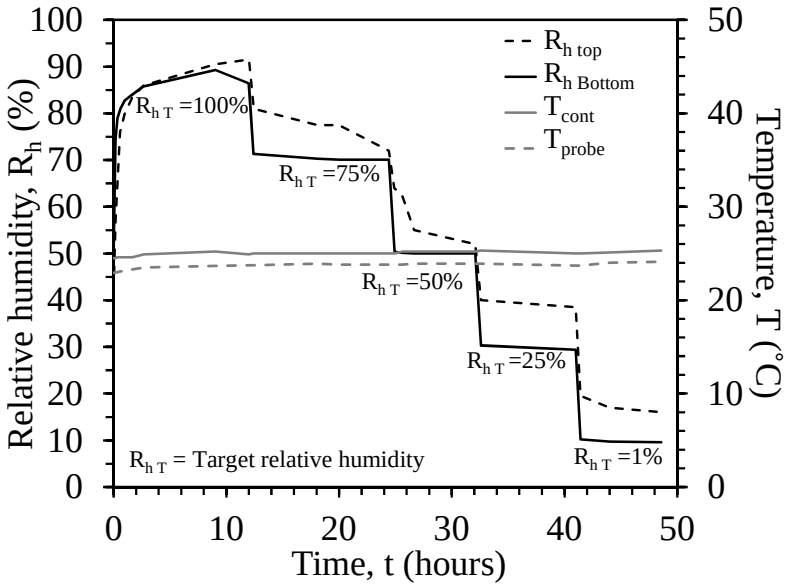

Figure 4.8: Relative humidity corresponding to each target value over time at room temperature

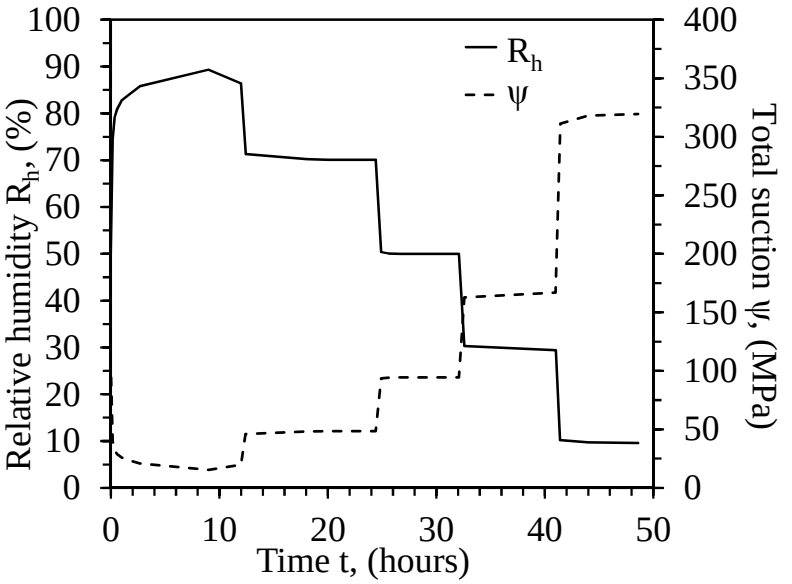

Figure 4.9: Relative humidity and corresponding total suction values applied to the specimen with respect to time

In order to insure that the target relative humidity matching the applied relative humidity to the soil specimen, the target relative humidity was compared to the equilibrium relative humidity recorded using the relative humidity probe, as shown in Figure 4.10. A difference up to 9% was recorded at the bottom of the specimen from the target values.

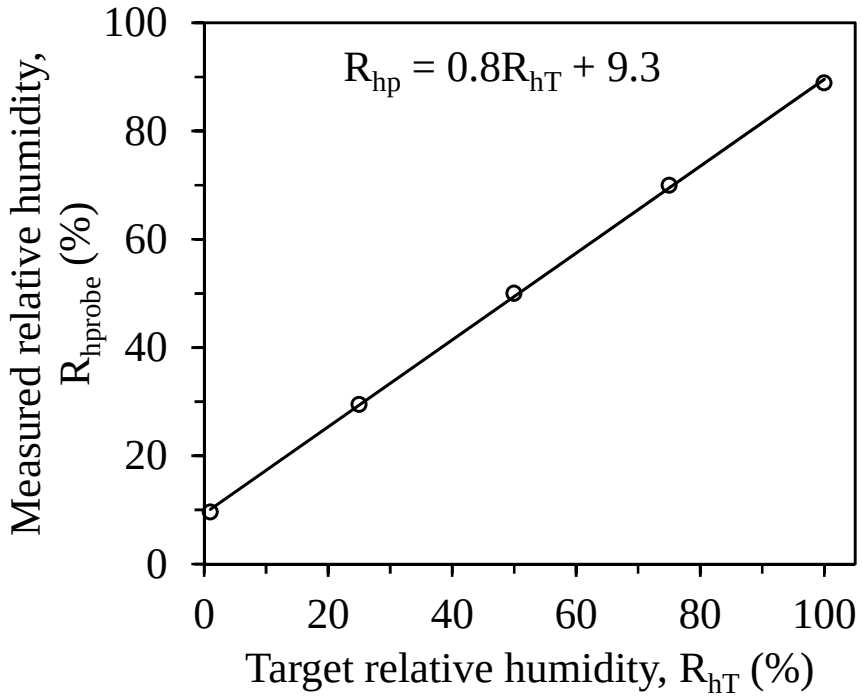

Figure 4.10: Relationship between the target relative humidity and the measured relative humidity at the base of the specimen

The relative humidity recorded from the relative humidity calibration test at elevated temperature with respect to time is shown in Figure 4.11. The results show that after using the insulation box, the automated system was capable of maintaining constant relative humidity value during the heating cooling cycle. However, maintaining constant relative humidity at high temperatures does not mean maintaining constant suction according to Kelvin's law. An adjustment to the value of target relative humidity should be made to maintain a constant suction into soil specimens, as shown in Figure 4.12.

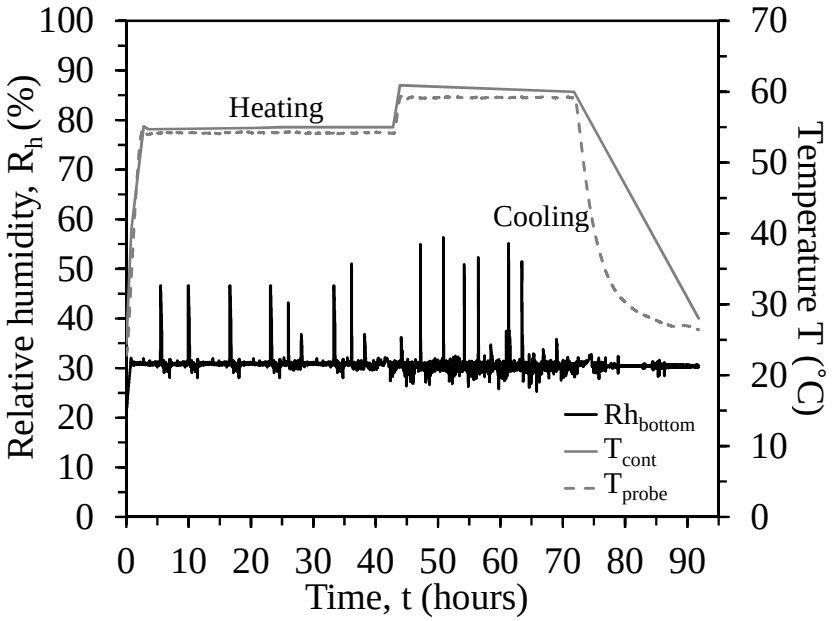

Figure4.11. Relative humidity over time at elevated temperature

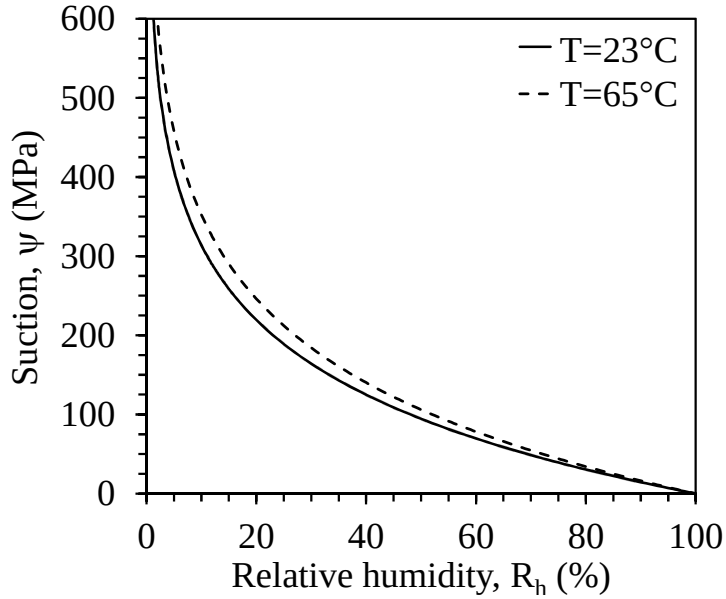

Figure 4.12: Relative humidity and corresponding suction at various temperatures according to Kelvin's law

4.6.3 Thermal Calibration Test Procedure

The thermal expansion of the different components of the triaxial cell including porous stones, piston, drainage lines, and the water filling them due to a temperature increase may affect the volume change measurements of the unsaturated soil specimen measured using the LVDT

and cell water inflow or outflow. In order to calculate the actual volume change of the soil Specimen during temperature changes, it is necessary to perform a thermal calibration tests. A solid aluminum cylinder having a diameter of 35.5 mm and a height of 71 mm, having a known value of coefficient of volumetric thermal expansion of 6.9×10^{-5} m/m°C was used to assess the thermal expansion of the triaxial cell.

After placing the aluminum specimen inside the triaxial cell and applying the target value of confining pressure (100 kPa, 200 kPa and 300 kPa) with the piston closed, the pressure regulator was adjusted to maintain an anisotropic condition with K_0 equals to 0.5. The next step after opening the piston and placing the LVDT on top of it is to increase the temperature by one step up to 65 °C over the course of approximately 6 hours and monitoring the temperature at the bottom of the aluminum cylinder using the temperature probe until it reaches constant value. Then, reduce the temperature to room temperature and let the system cool. Through the heating and cooling process, the overall volume change was estimated using DPT connected to the water level in graduated burettes connected to the confining cell pressure. The same procedures were also followed to calibrate for temperature effect by increasing temperature on stages. the increase in temperature were performed in three steps of 35, 50, and 65 °C, and enough time was allowed for water level in graduated burette to equilibrate after each step of temperature increase.

4.6.4 Thermal Calibration Test Results

In order to insure that the cell temperature matching the soil specimen temperature, the controlled degree of temperature (T_c) applied to the water inside the triaxial cell using the temperature controller was compared to the equilibrium temperature degree (T_m) recorded using the temperature probe. Less than 1°C difference was observed between the temperature applied

to the temperature controller and the measured temperature at the bottom of the specimen using the probe as shown in Figure 4.13.

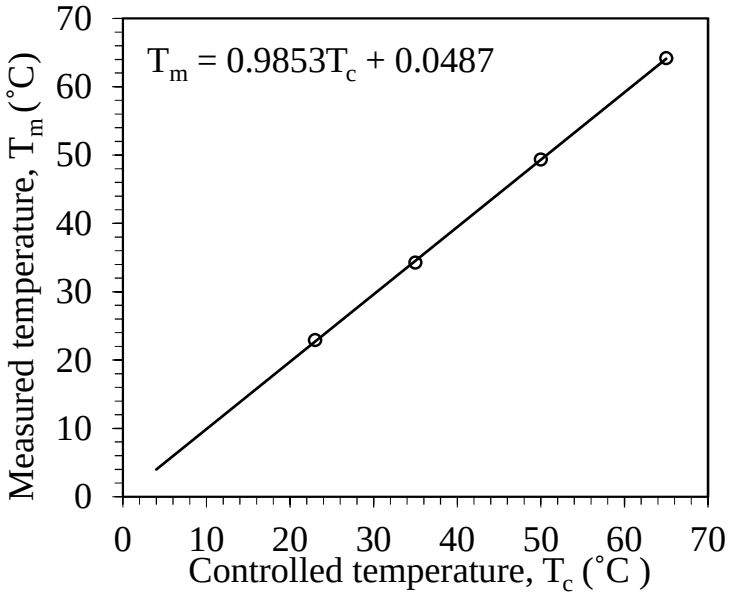

Figure 4.13: Controlled temperature versus measured temperature

The axial deformation due to temperature change at different confining pressure was tracked using the LVDT and corrections should be applied to the axial deformation in order to accurately calculate the axial strain. The observed axial deformation due to thermal dilatation and shrinkage of the piston was corrected for the known value of axial thermal expansion and shrinkage of the metallic sample during the heating. The correction of the axial deformation was calculated by subtracting the known axial deformation of the aluminum specimen from the total measured axial deformation as follow:

$$\Delta H_{Therm,machine} = \Delta H_t - H_o \Delta T \alpha_{alum} \qquad \text{Eq. 4.1}$$

where $\Delta H_{Therm,machine}$ is the axial deformation correction for the piston due to temperature increase to be subtracted from triaxial tests on soil specimen; ΔH_t is the total axial deformation; H_o is the original height of the aluminum specimen at ambient temperature; ΔT is the increase in temperature from the room temperature; and α_{alum} is the linear thermal coefficient of expansion,

equal to $23x10^{-6}$ /˚C at 21˚C. Typical results of measured and corrected values of thermal axial deformation for machine deflection and aluminum specimen for heating on one stage and heating and cooling on stages tests are presented in Figures 4.14(a) and 4.14(b), respectively. Results of the axial deformation correction from calibration tests performed in one step increase in temperature up to 65 ℃ are shown in Figure 4.15. The results in this figure show the axial deformation corrections as a function of temperature change for various confining pressures.

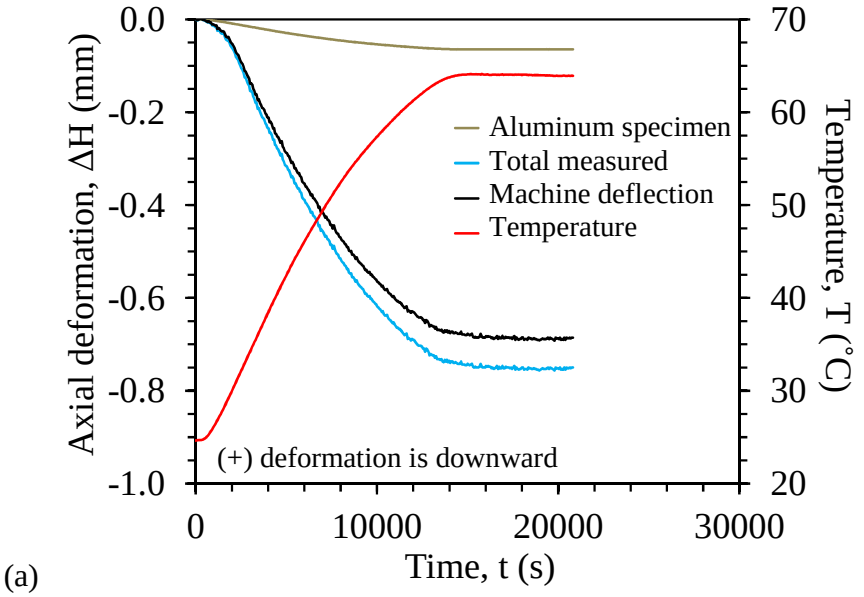

(a)

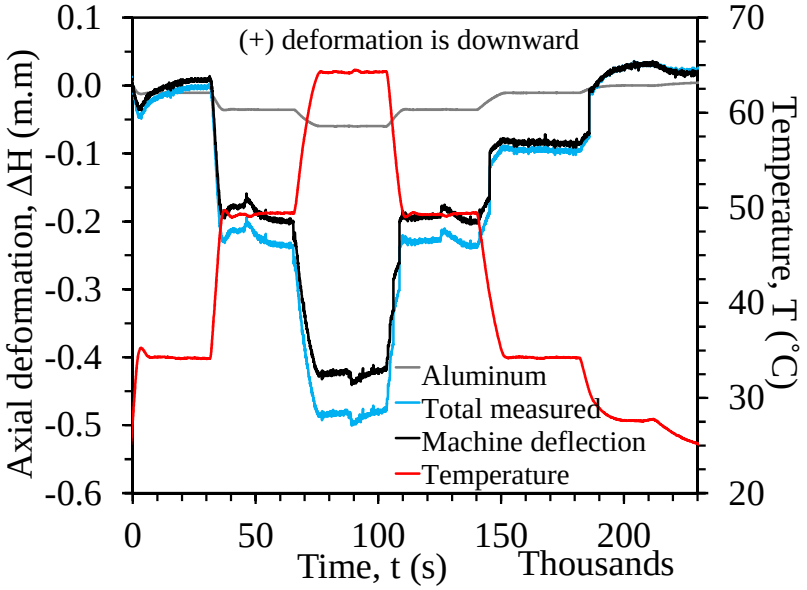

(b)

Figure 4.14: Measured and corrected values of thermal deflections for calibration test performed at: (a) Heating of one stage; (b) Heating and cooling of stages

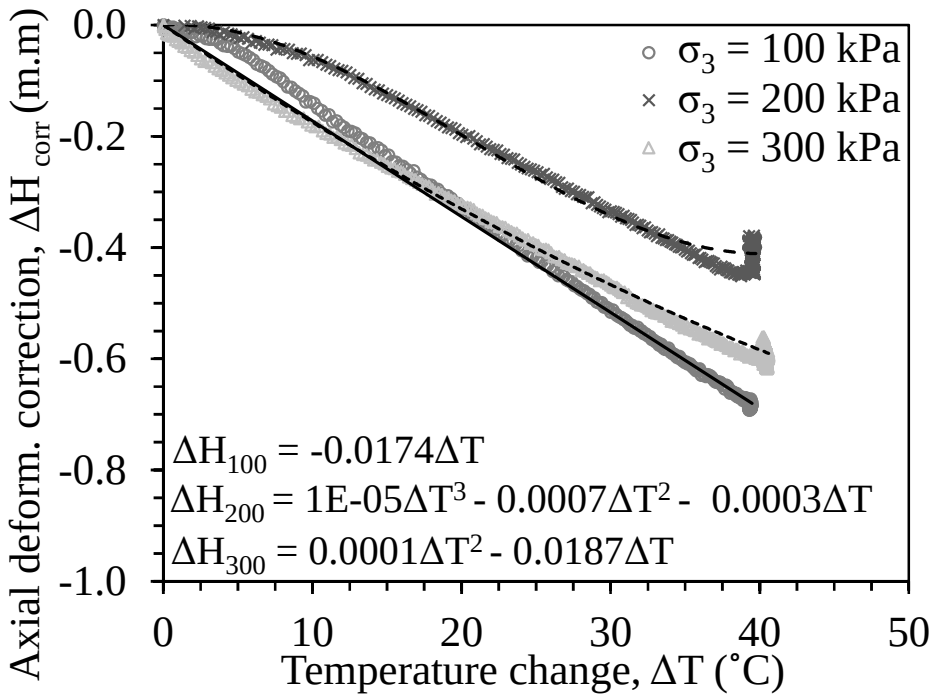

Figure 4.15: Axial deformation correction versus temperature change at various confining pressures for one step of increase in temperature

The observed volume change due to thermal dilatation and shrinkage of the drainage system was corrected for the known value of volumetric thermal expansion and shrinkage of the metallic sample during the heating cooling cycles respectively. The known volume change of the aluminum specimen was subtracted from the total measured volume change, as follows:

$$\Delta V_{Therm,machine} = \Delta V_t - V_o \Delta T \beta_{alum} \qquad \text{Eq. 4.2}$$

where $\Delta V_{Therm,machine}$ is the corrected volume change for the triaxial cell parts due to temperature increase; ΔV_t is the total volume change; V_o is the original volume of the aluminum specimen at ambient temperature; and β_{alum} is the volumetric thermal coefficient of expansion of aluminum, equal to 23×10^{-6} /˚C at 21˚C . The calibrated volume change with respect to testing temperature change and confining pressure of 100 kPa for tests performed in three steps of increase in temperature is shown in Figure 4.16(a). The axial deformation corrections for the same test are shown in Figure 4.16(b). The calibrated volume change with respect to testing temperature

change and the axial deformation corrections at confining pressures of 200 kPa and 300 kPa are presented in Figures 4.17(a), 4.17(b), 4.18(a), and 4.18(b), respectively.

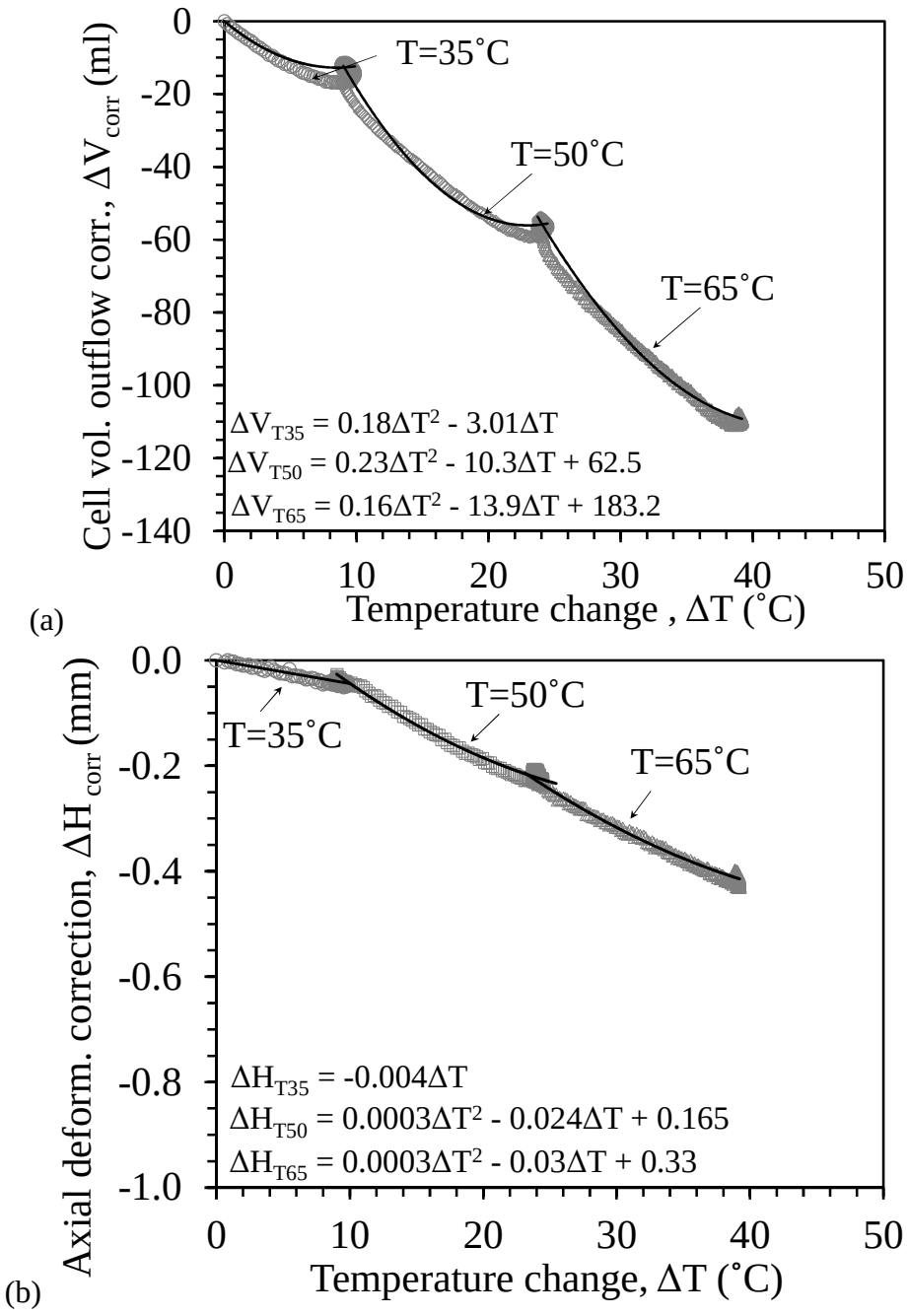

Figure 4.16: Results of calibration tests performed in three steps of increase in temperature and confining pressure of 100 kPa: (a) Volume change correction; (b) Axial deformation correction

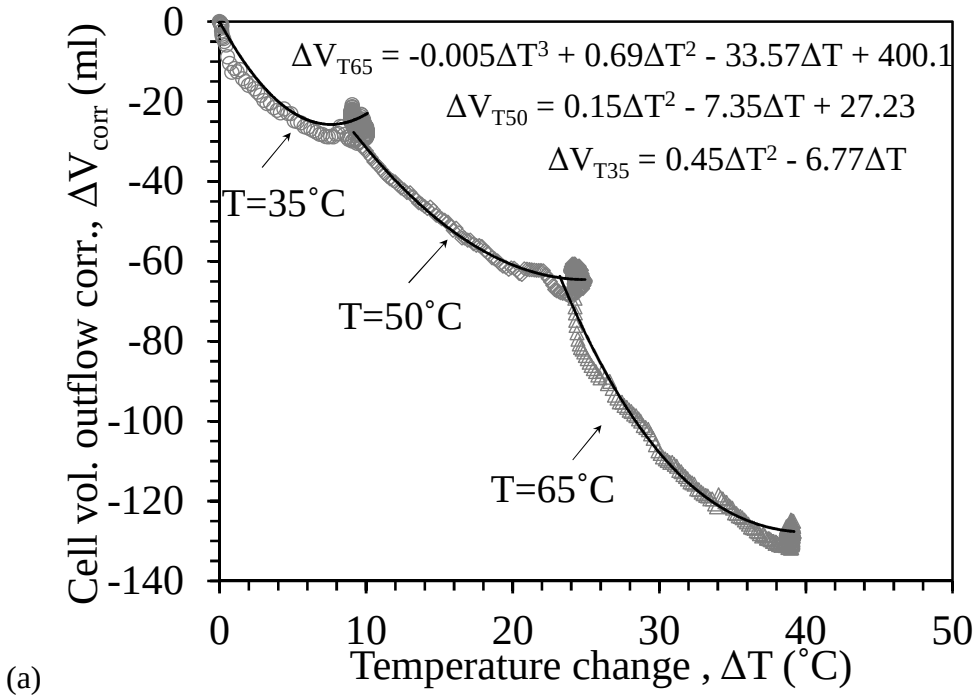

(a)

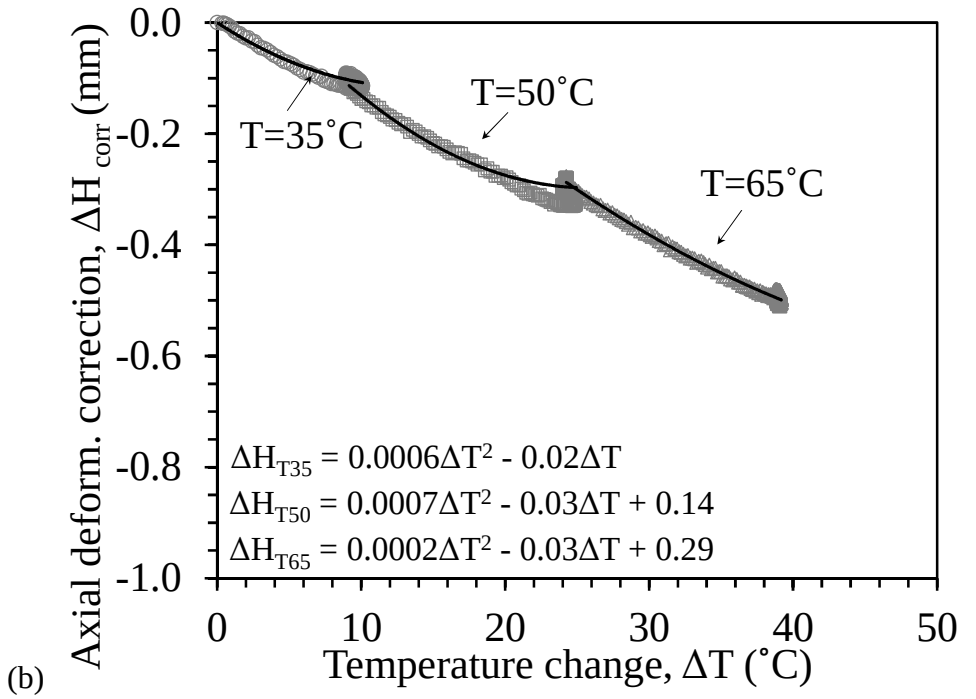

(b)

Figure 4.17: Results of calibration tests performed in three steps of increase in temperature and confining pressure of 200 kPa: (a) Volume change correction; (b) Axial deformation correction

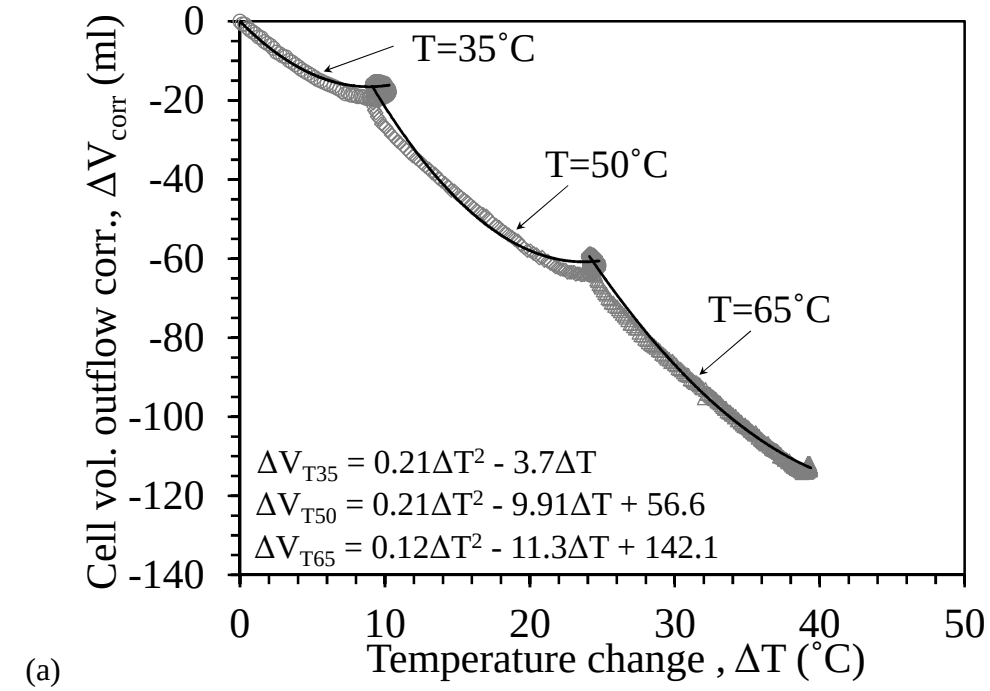

(a)

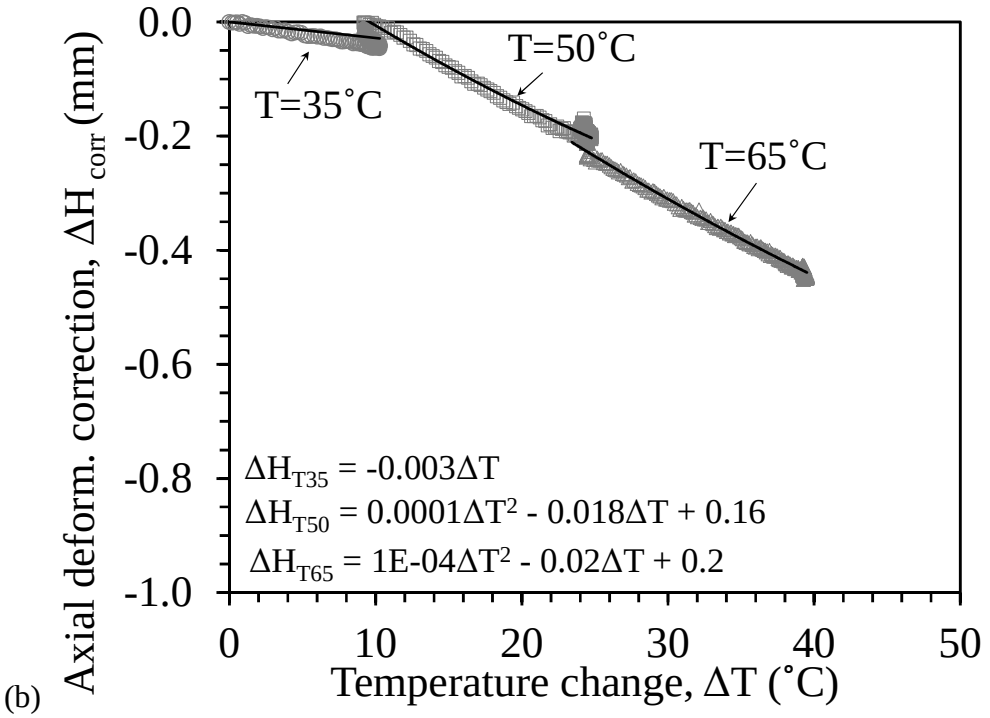

(b)

Figure 4.18: Results of calibration tests performed in three steps of increase in temperature and confining pressure of 300 kPa: (a) Volume change correction; (b) Axial deformation correction

5. EXPERIMENTAL INVESTIGATION AND PROCEDURES

5.1. Overview

In this chapter, a detailed description of the steps followed for performing desaturated consolidated-drained compression triaxial tests is presented. The soil specimen preparation procedures are explained in Section 5.2, followed by details of how the soil specimen is placed inside the triaxial cell in Section 5.3. A description of the procedures followed in performing the isothermal and nonisothermal shear strength tests at high suctions is presented in Section 5.4. This section presents the details of different thermo-mechanical testing paths investigated in this study, including tests where temperature is applied first before suction application, and tests where suction is applied before temperature application. Finally, the procedures to apply machine deflection corrections to the measurements from the triaxial setup are explained in Section 5.5.

5.2. Specimen Preparation

The specimens evaluated in all tests in this study were prepared using static compaction. Prior to compaction, the soil was oven-dried at a temperature of 110 °C for 24 h, ground using a rubber hammer, and screened through a No. 40 sieve. It was then carefully wetted with a spray gun to an initial water content of 10.5% and placed in a sealed plastic bag to cure for 24 hours so that the water content could homogenize. A compaction water content of 10.5% corresponds to a water content that is 8% dry of optimum. The reason for selecting such a low compaction water content was to prepare specimens with a low enough initial degree of saturation such that their air permeability would be high enough to permit rapid gas flow through the specimen in the vapor flow technique, leading to faster suction equilibration. The soil, having a specific gravity of 2.65, was compacted using a mechanical press in three lifts having thicknesses of 24 mm in a

35 mm-diameter mold to a dry unit weight of 15.7 kN/m^3 and initial degree of saturation of 0.41. This corresponds to an initial void ratio of 0.68. To avoid the presence of weak zones within the samples, the interfaces between lifts were scarified with a blade. The sample was then weighed and the dimensions were measured using a Vernier caliper.

5.3. Specimen Set Up

After preparing a soil specimen and before placing the soil specimen on the top platen, the relative humidity probe and thermocouple were connected to the bottom and top caps of the cell, respectively. Then, a coarse porous stone and a filter paper having the same diameter as the specimen were placed atop the lower platen of the triaxial cell. The specimen was placed atop this assembly. Another filter paper, coarse porous stone and the top platen were placed atop the specimen. A 0.635 mm-thick latex membrane was placed around the soil specimen. Two "O"-rings were placed around the latex membranes on the top and bottom platens to provide a reliable seal at low confining stresses. Next, the glass cell was placed between the top and bottom caps of the triaxial cell, and the cell was filled with de-aired water at room temperature and placed on the load frame. An LVDT was mounted to the piston to monitor axial displacements.

The differential pressure transducer used to monitor the air pressure gradient across the specimen was attached to the top and bottom ports to the specimen. The ports for the automated humidity system were connected to the cell. At this stage the water circulation pump was started and the desired confining stress was applied to the triaxial cell. The pump operation was not affected by the increase in pressure within the cell, and the pump did not affect the cell volume change measurements. A constant axial load was applied to the top of the soil specimen using the Bellofram piston at the same time as the cell pressure was applied by opening the air pressure valve connected to the piston at the same time as applying the cell pressure. The change in cell

volume and the change in height were monitored during this process using the cell volume burette on the pressure panel and the LVDT attached to the triaxial cell piston, respectively. The pictures in Figure 5.1 illustrate the steps for the triaxial assembly.

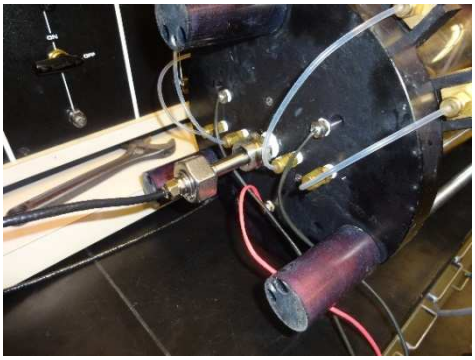

(a)

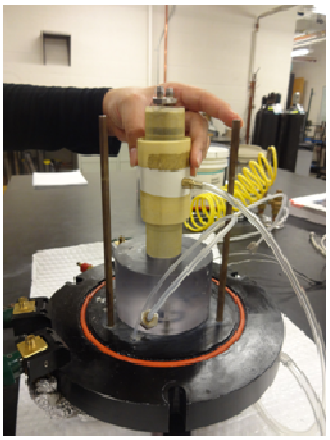

(b)

(c)

(d)

(e)

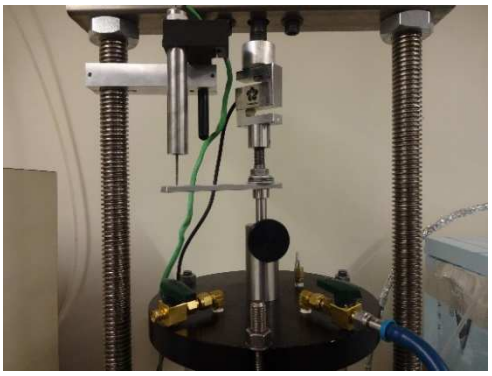

(f)

Figure 5.1: Pictures present the triaxial assembly: (a) Placing the relative humidity probe; (b) Covering the specimen by double latex membrane; (c) Sealing the specimen; (d) Placing the glass cell and piston on top of specimen; (e) filling the cell with deaired water (f) Placing the triaxial cell in the loading frame and connecting the piston to the load cell and LVDT

5.4.Testing Procedures

After assembly of the triaxial cell, all of the tests performed in this study start with application of a confining stress (100, 200 or 300 kPa) and K_0 consolidation under as-compacted conditions, using a value of K_0 of 0.5 that corresponds approximately with the value calculated from Jaky's equation and the friction angle of the compacted silt. The average air pressure in the specimens is approximately 20 kPa, so the net confining stress values were 20 kPa smaller than the cell pressure. Next, tests following four different paths were performed to understand the effects of suction and temperature on the volume change and shear strength behavior of compacted Bonny silt. The different testing paths are illustrated in Figure 5.2. The first set of tests was performed by applying a high suction magnitude to soil specimens under ambient laboratory temperature (approximately 23 °C), as shown in Figure 5.2(a). This set of tests provides a baseline case for the behavior of Bonny silt under high suction values. The second set of tests were performed by heating soil specimens to a target cell fluid temperature of 65 °C in a single stage under as-compacted conditions, then applying a high suction magnitude as shown in Figure 5.2(b). Tests following this procedure are referred to as T-S (temperature-suction) path tests. The third set of tests were performed by applying a suction magnitude to the soil specimens under ambient temperature, then heating them in three stages to target cell fluid temperatures of 35, 50, and 65 °C, as shown in Figure 5.2(c). Tests following this procedure are referred to as S-T (suction-temperature) path tests. Finally, a fourth type of test was performed following the S-T path but was cooled back to ambient temperature after heating, as shown in Figure 5.2(d). After following any of the testing paths, the soil specimens were sheared at a constant displacement rate of 1.27×10^{-4} m/min. During shearing, the pore air was permitted to drain freely. The suction control system continued to operate during shearing, which means that the tests were performed

at a constant relative humidity. It was assumed that excess pore water pressure generation is negligible under these low degrees of saturation, and the measured relative humidity values at the top and bottom of the specimen did not change, so it was assumed that these tests represent drained conditions.

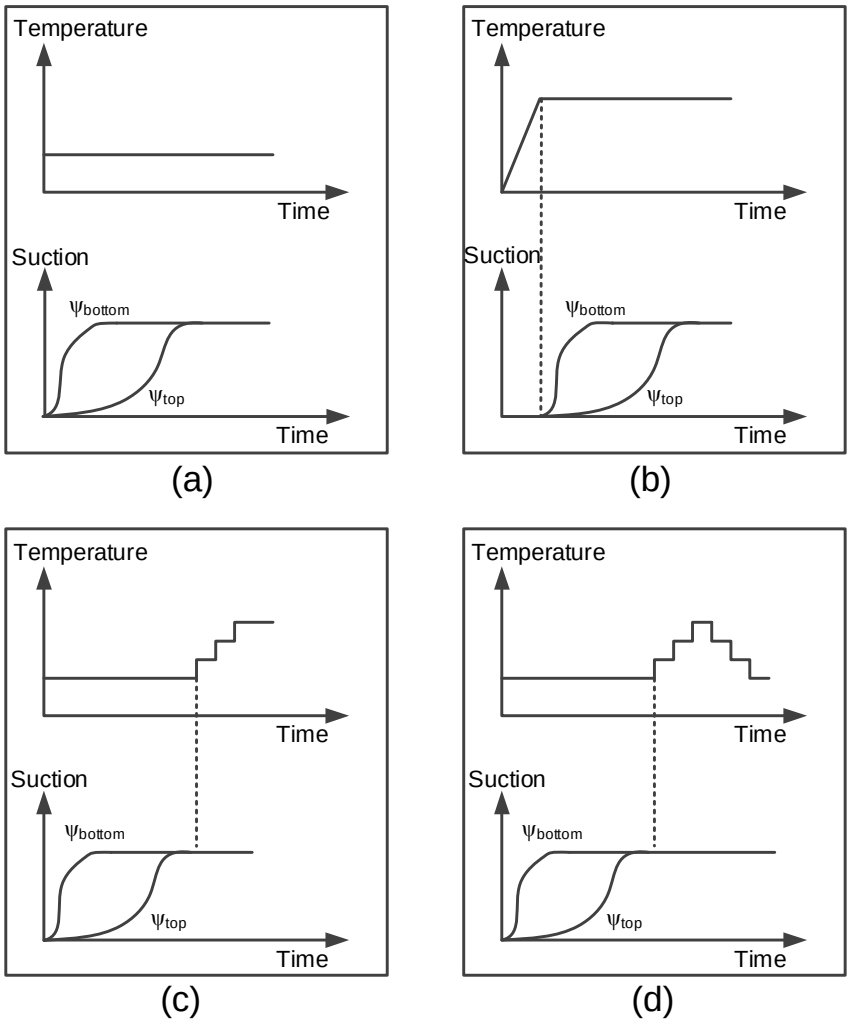

Figure 5.2: Testing paths followed in this study: (a) Suction applied under isothermal conditions; (b) Suction applied under nonisothermal conditions (T-S path); (c) Suction applied under isothermal conditions followed by thermal loading (S-T path); (d) Suction applied under isothermal conditions followed by thermal loading unloading

5.4.1.*Test Procedures under Isothermal Conditions*

In this set of triaxial compression tests, the unsaturated soil specimens were brought into suction equilibrium at room temperature under various net confining stresses then sheared to

failure. After following the stages mentioned in Section 5.3 for assembly of the triaxial cell, the automated humidity control system was utilized to apply a specified value of total suction to the specimen by applying a target relative humidity to the bottom of the specimen. Time was permitted for suction equilibration, defined as the time required for the relative humidity at the top and bottom to reach the same value. Two hours were needed for the relative humidity at the bottom to reach the target value, while an average of two weeks were needed for the relative humidity at the top to reach the same target value. After the target relative humidity at the top of the specimen was attained, at least six additional hours were allowed for uniformity of total suction throughout the soil specimen. This period of time is matched with Likos and Lu (2003) test results where they indicated that 2 to 5 hours were the time needed to reach constant water content and they allowed time from 9-12 hours to allow water content uniformity.

After this, the soil specimen was assumed to be in equilibrium under the externally applied stresses and internally applied suction when the axial deformations, recorded using the mounted LVDT, remained constant for at least 24 hours. After the soil specimen reaches equilibrium, the load frame was switched from load-control conditions to displacement control conditions. A constant displacement rate of 1.27×10^{-4} m/min was applied to shear the soil specimen. This rate was found to allow drained conditions during shearing (i.e., no change in relative humidity at the boundaries was noted). The unsaturated specimens evaluated in this study have degrees of saturation of less than 0.11, which is very close to the residual degree of saturation. It is not expected that there is sufficient water in the pores to become pressurized during the shearing process. Further, the relative humidity control system was operated during shearing to ensure that the suction remained constant during shearing. After shearing, the final water content of the soil specimen was measured and recorded.

5.4.2.*Test Procedures under Nonisothermal Conditions*

Three different testing paths were followed to investigate the influence of temperature on unsaturated silt behavior as shown in Figure 5.3. The first testing path was to increase temperature in one step up to a target value of 65 °C after applying the confining pressure, and then use the vapor flow technique to impose suction on the soil specimen (T-S Path, ABCD). The second testing path was to bring the soil specimen to suction equilibrium at room temperature, and then start increasing the temperature up to a target value in stages (S-T Path, ABEFGD).

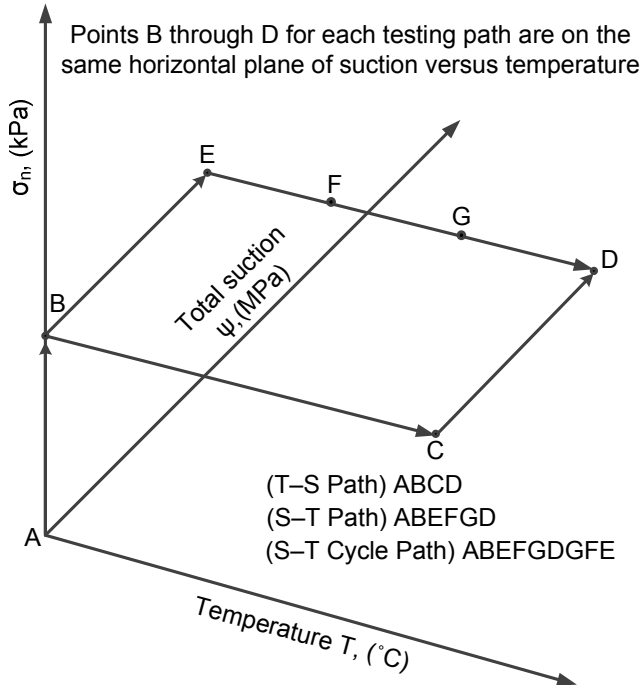

Figure 5.3: Testing paths investigated for suction and temperature control

In either testing path, the automated humidity control system was used to apply a specified value of total suction to the specimen following the same procedure described in Section 5.4.1. For tests following the T-S path, the temperature of the soil specimen was increased up to the target value 65 °C in one step and sufficient time was allowed for thermal equilibration (approximately 6 hours), before applying the target relative humidity at the bottom of soil

specimen. Then, an average of 1 to 2 weeks was allowed to ensure equilibration and uniformity of total suction throughout the soil specimen under the target temperature and no changes in axial strain measurements for at least 24 hours was recorded. The soil specimen at this point was assumed to be in equilibrium under the externally applied stresses and internally applied suction and target temperature, and the specimen was sheared under the same constant displacement rate used in the isothermal tests.

For the S-T path in Figure 5.3, suction was applied using the same procedure described in Section 5.4.1.Next, the temperature was increased in stages before finally shearing the specimen at point D. The axial strain is measured continuously. One thermal cyclic loading was performed in this study following the same procedure for S-T path tests with the exception that after the soil specimen reached thermal equilibrium at the target temperature of 65 °C, thermal unloading was applied in the same steps of 65, 50, 35 and 25 °C before finally shearing the specimen at room temperature.

5.5.Corrections to Testing Program Data

5.5.1.Corrections to Isothermal Volume Change Measurements

The volume change measurements due to suction application recorded from triaxial tests performed at room temperature have been affected by the temperature fluctuation inside the lab. Using the cooling calibration data from the calibration tests, a correction factor was applied to volume change values as shown in Figure 5.4 for various confining stresses, as follows:

$$\Delta V_{cell,correction} = -2.47\Delta T_{ambient} + 1.06 \qquad \text{Eq. 5.1}$$

where $\Delta V_{cell,correction}$ is the volume of water that should be subtracted from the cell water outflow to account for room temperature fluctuations, and $\Delta T_{ambient}$ is temperature change in ambient room temperature from a reference temperature at the beginning of the test.

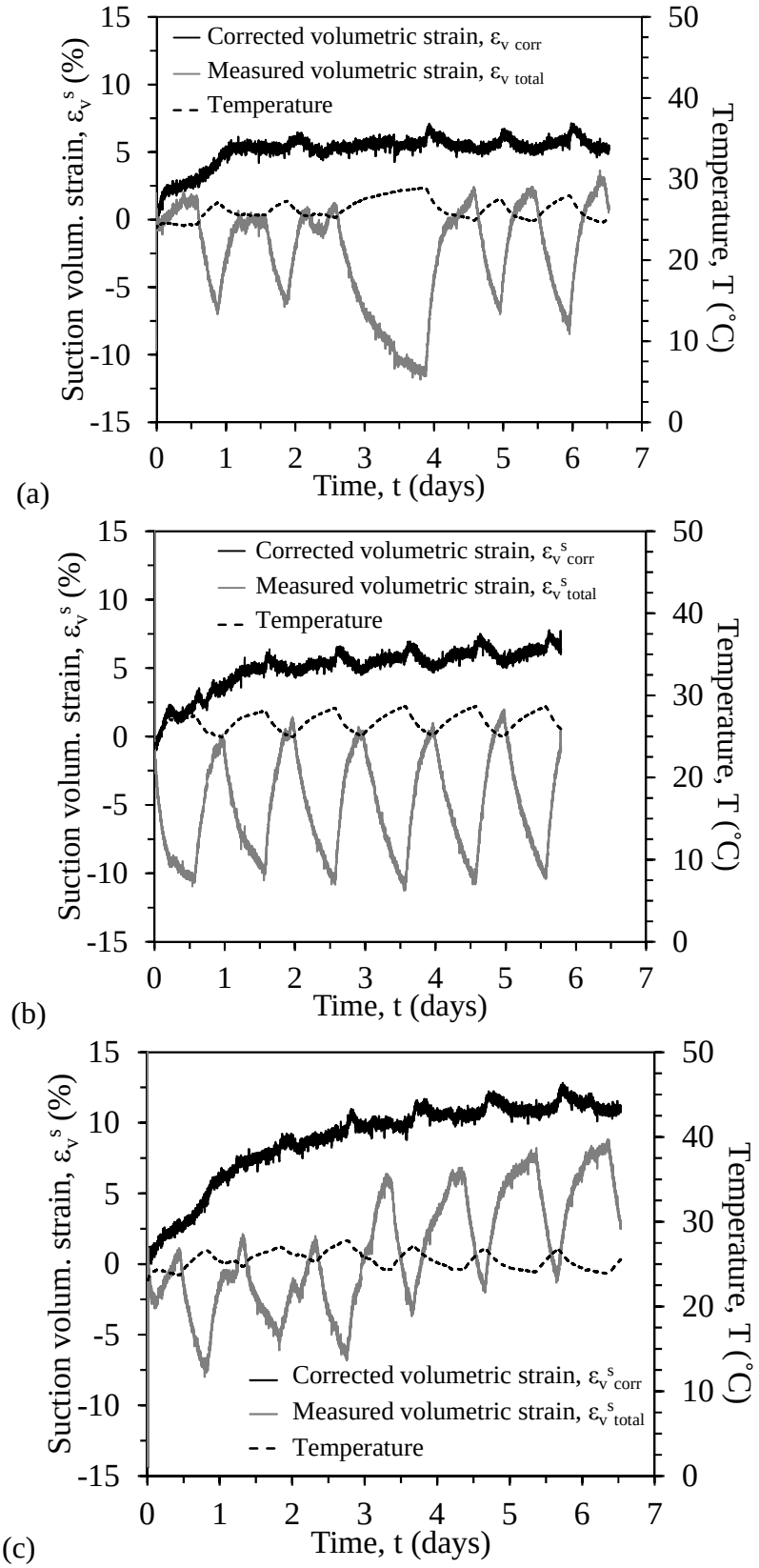

Figure 5.4: Suction volumetric strains corrected from room temperature fluctuations at confining stresses of: (a) 100 kPa; (b) 200 kPa; (c) 300 kPa

5.5.2.Corrections to Nonisothermal Axial Displacement and Volume Change Data

The measurements of axial deformation and cell water outflow under elevated temperatures were corrected using the calibration test results. The axial deformation of soil specimen is calculated as follows:

$$\Delta H_{soil} = \Delta H_{total} - \Delta H_{Therm,machine} \quad \text{Eq. 5.2}$$

where ΔH_{total} is the total measured axial deformation, $\Delta H_{Therm,machine}$ is the axial deformation correction from the calibration tests. Results of applying calibration corrections to the axial deformation of soil specimens that heated in one step at various confining stresses are presented in Figure 5.5, and results of applying calibration corrections to the axial deformation of soil specimens that heated in steps at various confining stresses are presented in Figure 5.6. The correction to the cell water outflow was applied to calculate soil volume change as follow:

$$\Delta V_{soil} = \Delta V_{total} - \Delta V_{Therm,machine} \quad \text{Eq. 5.3}$$

where ΔV_{total} is the total measured cell water outflow, $\Delta V_{Therm,machine}$ is the cell water outflow correction from the calibration tests. Results of applying cell water outflow corrections to tests data at various confining stresses are presented in Figure 5.7.

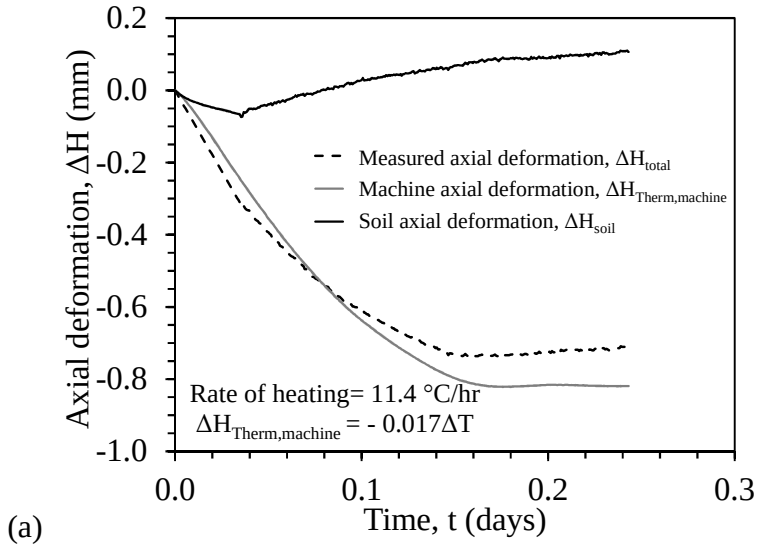

(a)

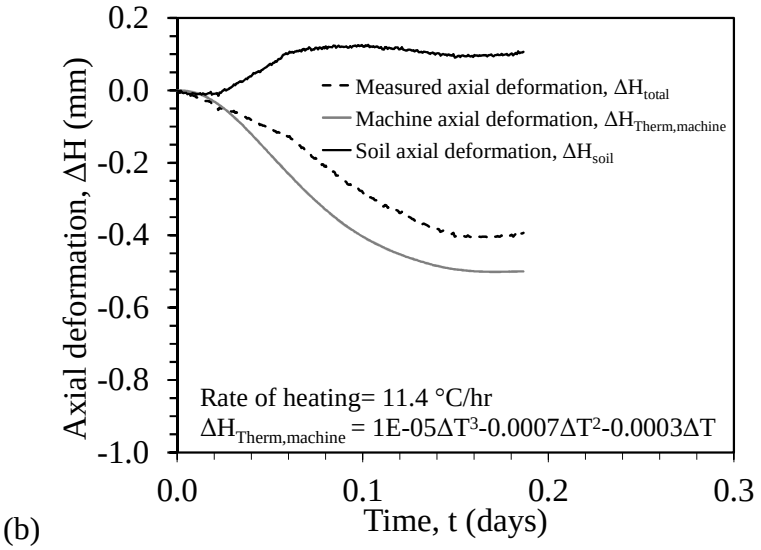

(b)

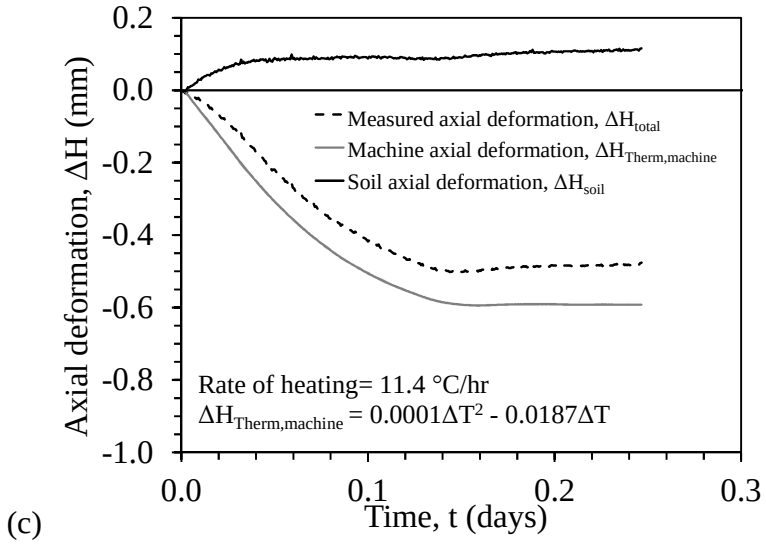

(c)

Figure 5.5: Machine corrections to the measurements of axial deformation at temperature of 65°C following test T-S Path at confining stress of: (a) 100 kPa; (b) 200 kPa; (c) 300 kPa

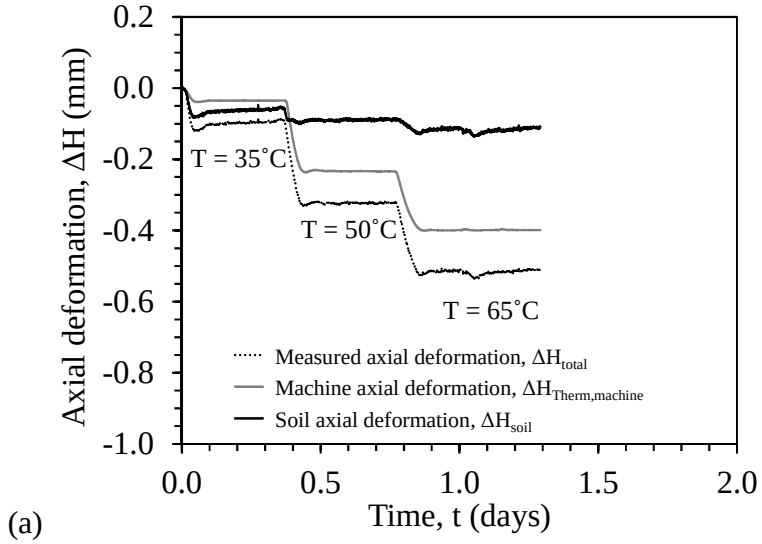

(a)

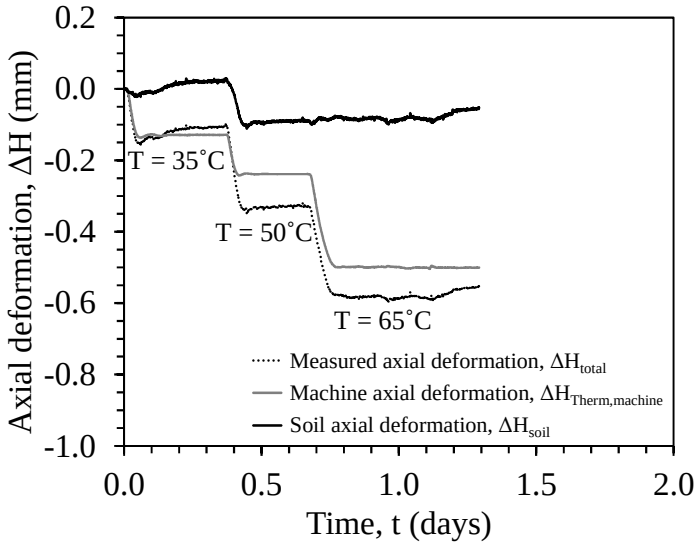

(b)

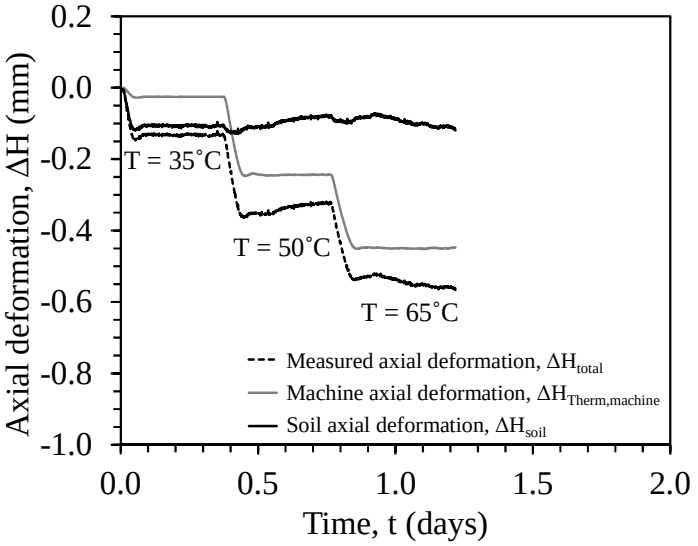

(c)

Figure 5.6: Machine corrections to the measurements of axial deformation heating on stages following test S-T Path at confining stress of: (a) 100 kPa; (b) 200 kPa; (c) 300 kPa

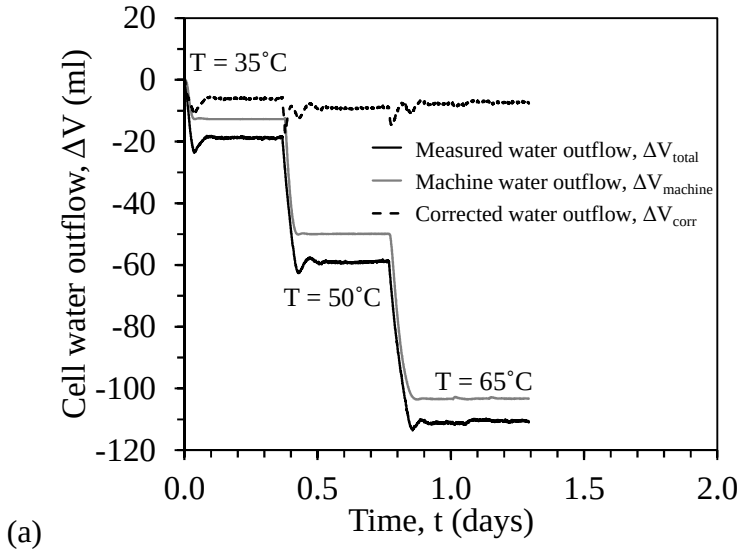

(a)

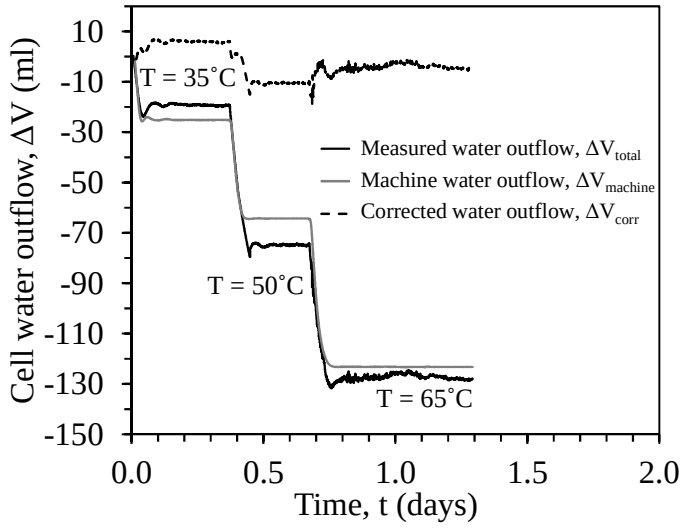

(b)

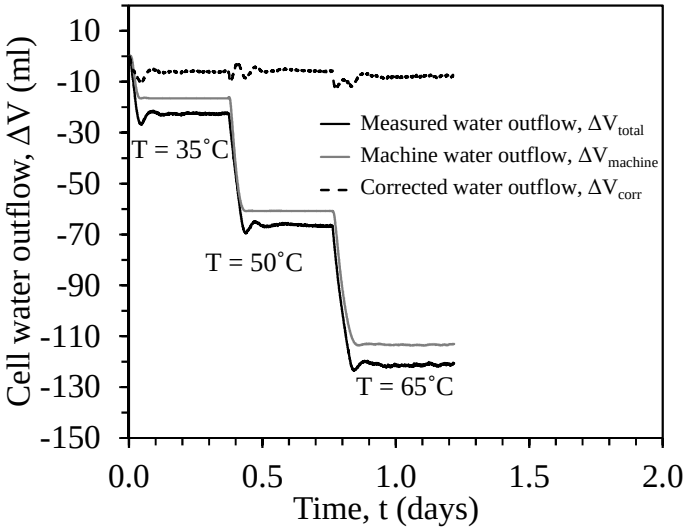

(c)

Figure 5.7: Machine corrections to the measurements of cell water outflow due to heating on stages following test S-T Path at confining stress of: (a) 100 kPa; (b) 200 kPa; (c) 300 kPa

5.5.3.Corrections to Triaxial Compression Test Data

Corrections should be applied to the triaxial compression data in order to obtain accurate results. Standard corrections to account for the effects of the double membrane and the change in area during shearing were considered in this study because of its significant magnitudes (ASTM D4767, BR5755). The corrected cross-sectional area of the specimen is calculated using the following equation:

$$A = \left(\frac{1 - \varepsilon_v}{1 - \varepsilon_a} \right) A_o \qquad \text{Eq. 5.4}$$

where Ao is the initial cross-sectional area of the specimen, and εv and εa are volumetric and axial strains respectively for the given axial load and can be obtained from:

$$\varepsilon_v = \frac{\Delta V}{V_o} \qquad \text{Eq. 5.5}$$

$$\varepsilon_a = \frac{\Delta H}{H_o} \qquad \text{Eq. 5.6}$$

in which, ΔV and ΔH are the changes in volume and height of the sample. Vo and Ho are the initial volume and height of the soil specimen. The membrane correction to be subtracted from the measured principal stress difference is calculated by the following equation:

$$\Delta(\sigma_1 - \sigma_3) = 4E_m t_m \varepsilon_a / D \qquad \text{Eq. 5.7}$$

where D is the diameter of specimen, Em is the Young's modulus for the membrane material, and tm is the thickness of the membrane. Due to the shearing stage in the triaxial tests was performed under drained condition, it is necessary to correct the cell volume using the following equation:

$$V_{cell\text{-}corr} = V_{cell} - (\Delta H \times A_p) \qquad \text{Eq. 5.8}$$

where Vcell-corr is the corrected cell volume, Vcell is the cell volume, ΔH is the displacement reading from loading frame, and Ap is the area of the piston.

6. ANISOTROPIC CONSOLIDATED-DRAINED TRIAXIAL TEST RESULTS

6.1.Introduction

In this study, three different groups of tests were performed to fully characterize the effects of suction and temperature on the shear strength and volume change behavior of unsaturated silt. Isotropic consolidated, undrained triaxial tests were performed on saturated specimens of Bonny silt at three different effective confining stresses to define the effective failure envelope. This failure envelope provides a baseline case to evaluate the results from tests on specimens at high suction magnitudes, and it can also be used to define the critical state line. In addition, two sets of isothermal anisotropic consolidated, drained triaxial tests were performed on unsaturated specimens at suction values of 162 and 291 MPa (corresponding to degrees of saturation of 0.11 and 0.06, respectively) under confining stresses of 100, 200 and 300 kPa. The ratio of vertical to radial stress in these tests was 0.5, which is approximately equal to the at-rest coefficient of earth pressure calculated using Jaky's equation ($K_0 = 1 - \sin\square$). Results from tests performed at room temperatures on saturated and unsaturated specimens are presented in Section 6.2. Also, two sets of nonisothermal anisotropic consolidated, drained triaxial tests were performed on unsaturated specimens at suction value of 291 MPa following two different testing paths. Results from tests performed at elevated temperatures on unsaturated specimens are presented in Section 6.3.

6.2.Isothermal Anisotropic Consolidated-Drained Triaxial Test Results

6.2.1.Results of Relative Humidity and Suction Equilibration

The relative humidity and temperature at the bottom and top of the specimen during suction equilibrium is shown in Figure 6.1. Two hours were needed for the relative humidity at the bottom ($R_{h\ bottom}$) to reach the target value ($R_{h\ target}$), while an average of one to two weeks were needed for the relative humidity at the top ($R_{h\ top}$) to reach the same target value. Figure 6.1(a)

presents a typical relative humidity and temperature measurements at top and bottom of the soil specimen for target relative humidity of 30%, and Figure 6.1(b) presents a typical relative humidity and temperature measurements at top and bottom of the soil specimen for target relative humidity of 12%. Figure 6.1(c) shows the corresponding suction at top and bottom of soil specimens to each target relative humidity.

6.2.2.Axial Strain and Volume Change Measurements during Isothermal Tests

The axial deformation during all testing stages was recorded with time using the LVDT placed on top of the piston, and the axial deformations were converted to axial strain by dividing by the original height of the specimen. The results of axial strain over time due to suction implementation corresponding to changes in relative humidity at the top of the soil specimen for confining stresses of 100 kPa, 200 kPa, and 300 kPa are shown in Figures 6.2(a), 6.2(b) and 6.2(c), respectively.

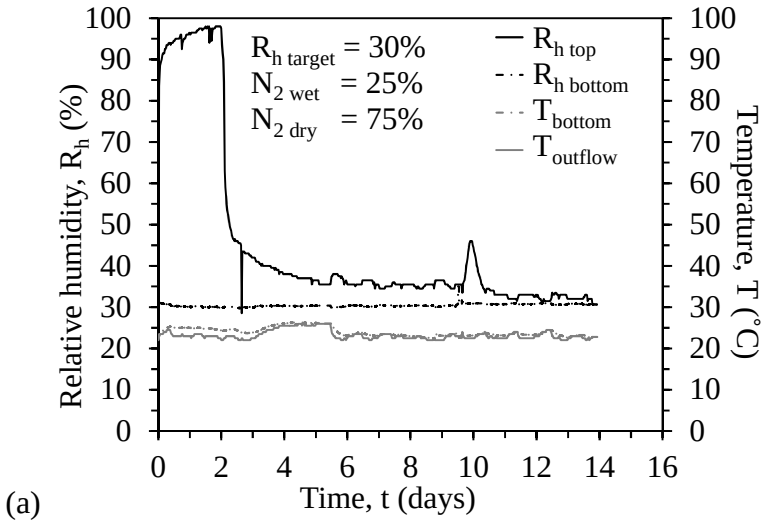

(a)

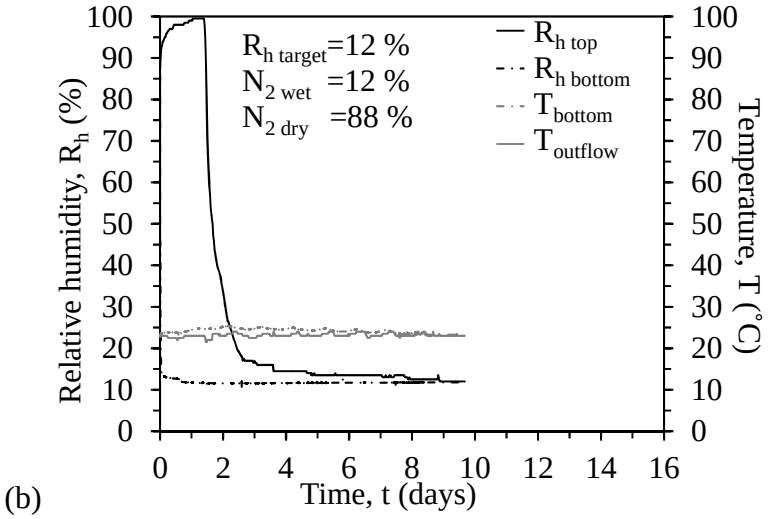

(b)

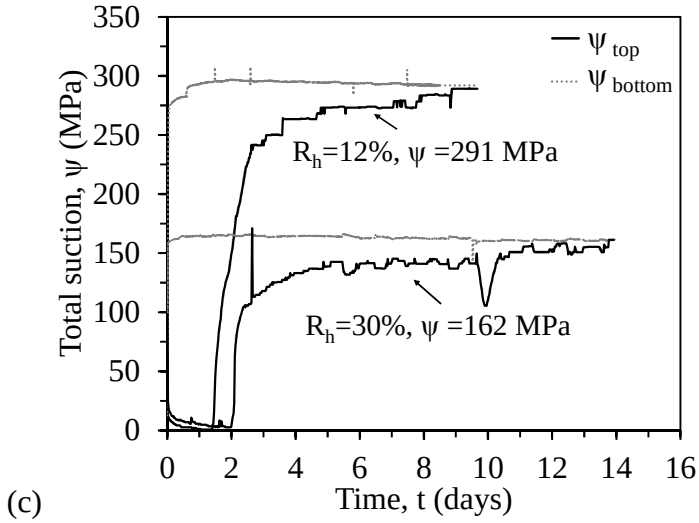

(c)

Figure 6.1: Equilibration of relative humidity at a confining stress of 200 kPa under isothermal condition: (a) Relative humidity and temperature with time for a relative humidity at equilibrium of 30%; (b) Relative humidity and temperature for a relative humidity at equilibrium of 12%, (c) Total suction calculated from the measured relative humidity over time

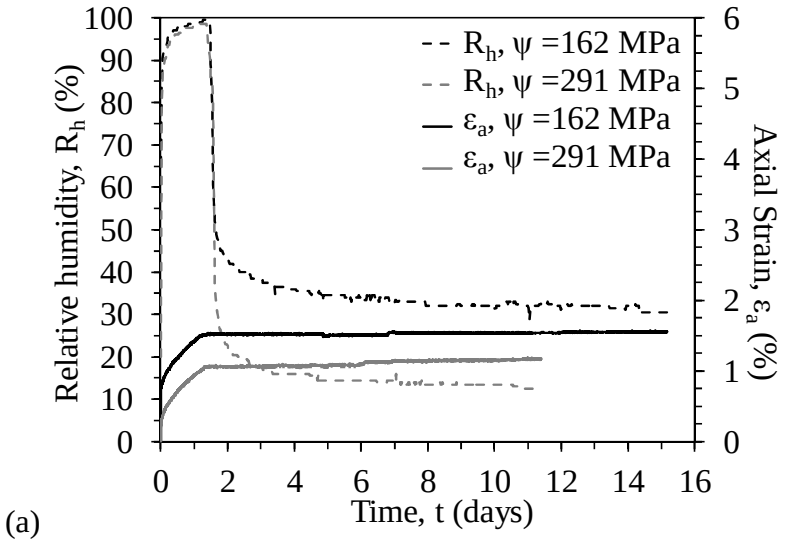

(a)

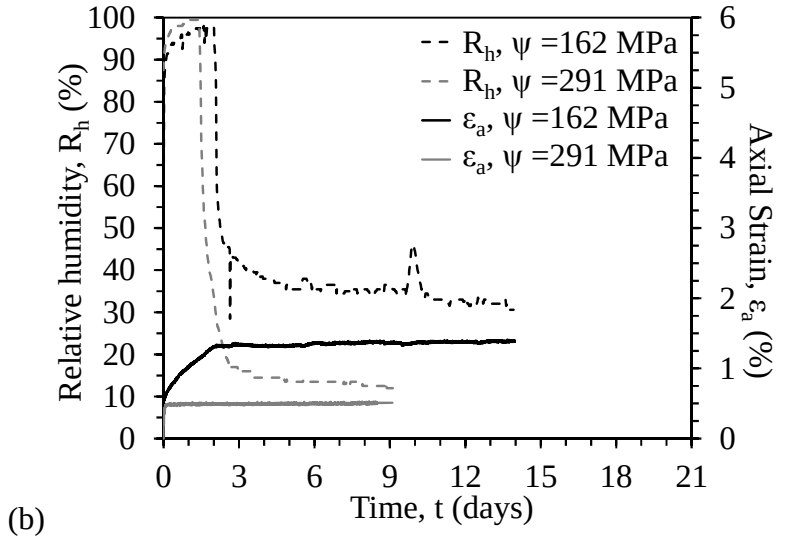

(b)

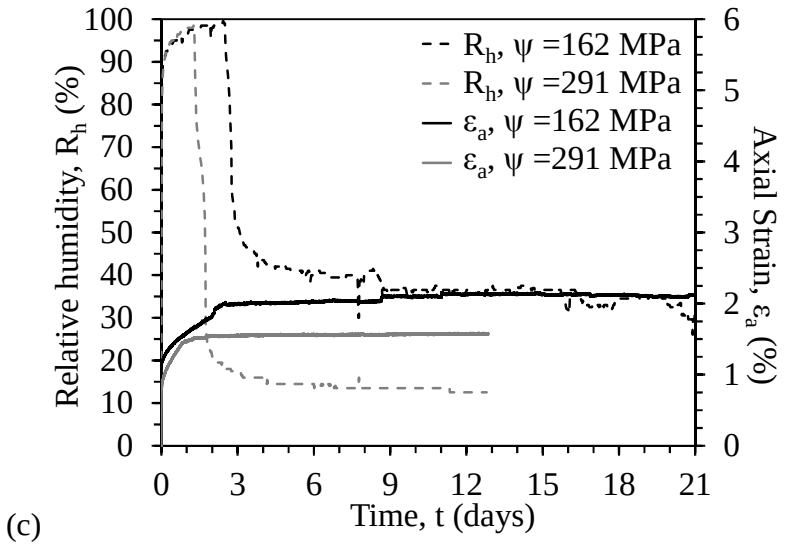

(c)

Figure 6.2: Change in axial strain during equilibration of relative humidity recorded at top of soil specimen at confining stresses of: (a) 100 kPa; (b) 200 kPa; (c) 300 kPa

The void ratios of the specimens before shearing (i.e., after equilibration under the net confining stress and after application of high suction magnitudes for the unsaturated specimens, and after consolidation under the effective confining stress for the saturated specimens) are shown in Figure 6.3. The confining stress was applied to the unsaturated specimens before application of the target suction value. The results shown in Figure 6.3 indicated that the void ratio decreased with increasing suction and net confining stress, and a greater reduction in void ratio was observed when applying high suctions to specimens under an initially high net confining stress. It is possible that a difference in the equilibrium void ratio may have been different if high suction magnitudes were applied to the specimens before application of the confining stress, as the stiffness of the soil was expected to change significantly after application of high suction magnitudes.

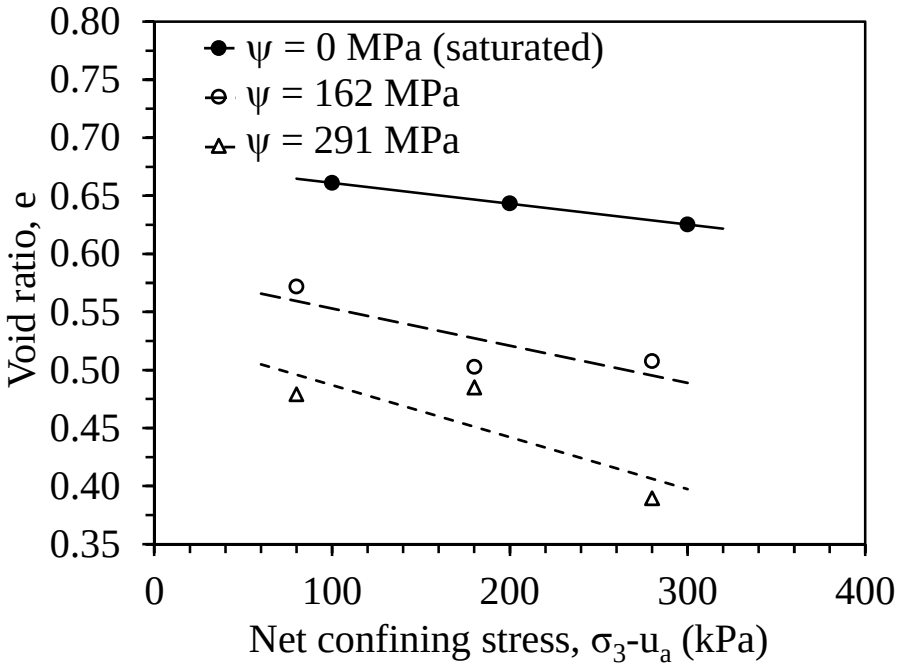

Figure 6.3: Initial void ratios of the silt specimens before shearing under different net confining stress values (i.e., after consolidation and equilibrium under the applied suction)

6.2.3.Results of Triaxial compression during Isothermal Tests

The stress–strain curves for the saturated and unsaturated specimens are shown in Figures 6.4(a) to 6.4(c) for the three different confining stress values. The results in Figure 6.4 clearly indicated that the maximum principal stress difference and axial strain at failure increased as the suction value and the confining stress increased. Further, a brittle failure mode was observed in the stress-strain curves for the specimens under high suction magnitudes, which differed significantly from the relatively smooth stress–strain curves of the saturated specimens.

In Figure 6.4(c), the stress–strain curve corresponding to 162 MPa suction showed hardening at the beginning of the test due to the brief accidental application of a fast shearing rate to the specimen when checking the contact of the loading piston and specimen before the actual start of shearing at the conventional rate. Although the stiffness from this test was not reliable, the results from this test still showed reasonable peak shear strength behavior. Because of the brittle failure mechanism noted in the unsaturated specimens, it was not possible to reach critical state conditions. Accordingly, only the peak shear strength values from the consolidated drained tests on the unsaturated specimens were used in the analysis.

The volumetric strain results of the tests performed on specimens at high total suction values of 162 and 291 MPa are shown in Figures 6.5(a) and 6.5 (b), respectively. Both figures show a clear dilation during shear for the specimens at high suction magnitudes. This difference in behavior between the saturated and unsaturated specimens was likely due to the reduction in void ratio during application of the high suction values and also likely due to an increase in apparent preconsolidation stress with increasing suction.

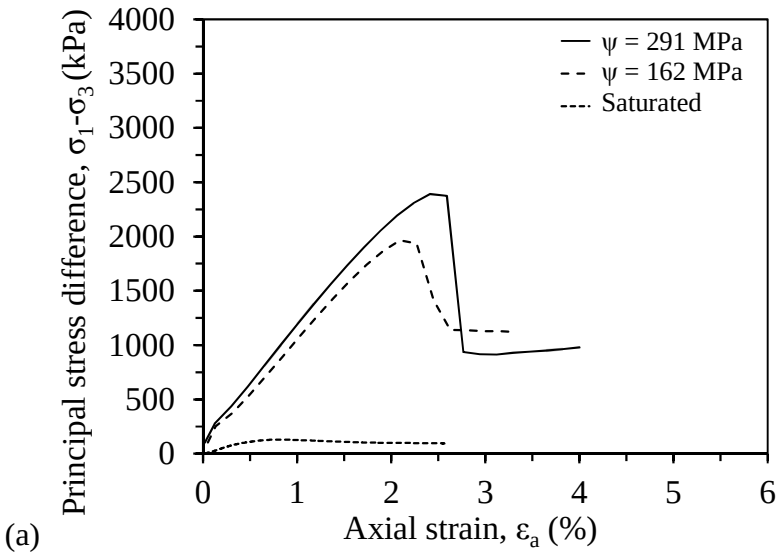

(a)

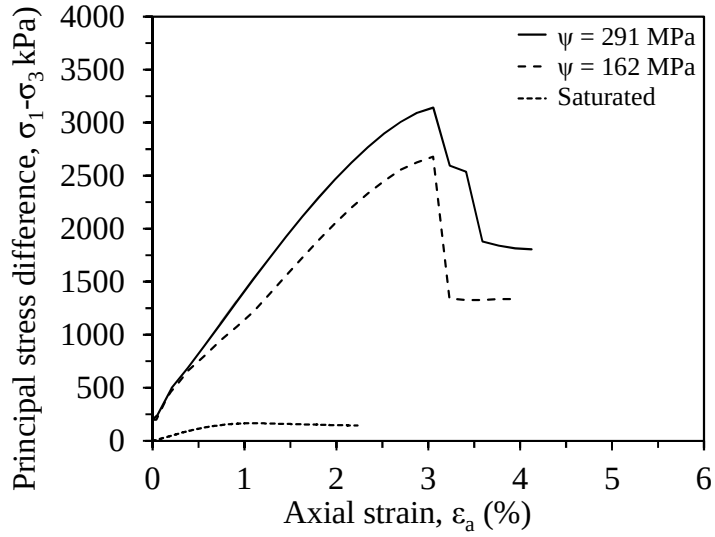

(b)

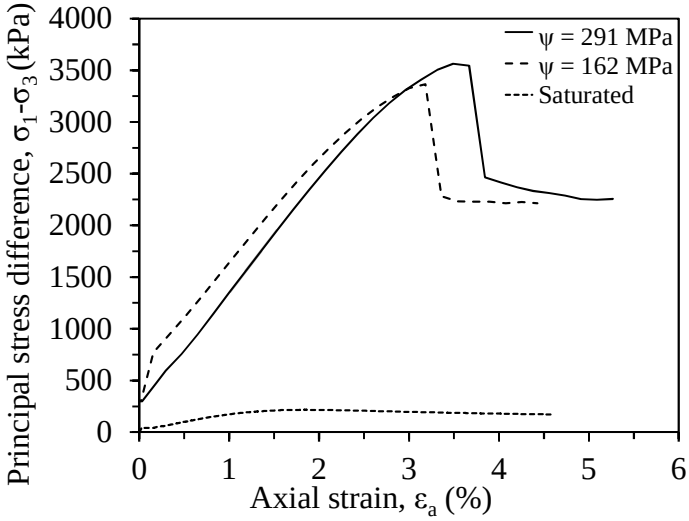

(c)

Figure 6.4: Stress-strain curves for saturated and unsaturated Bonny silt specimens under different confining stresses (note that unsaturated specimens have u_a = 20 kPa): (a) 100 kPa; (b) 200 kPa; (c) 300 kPa

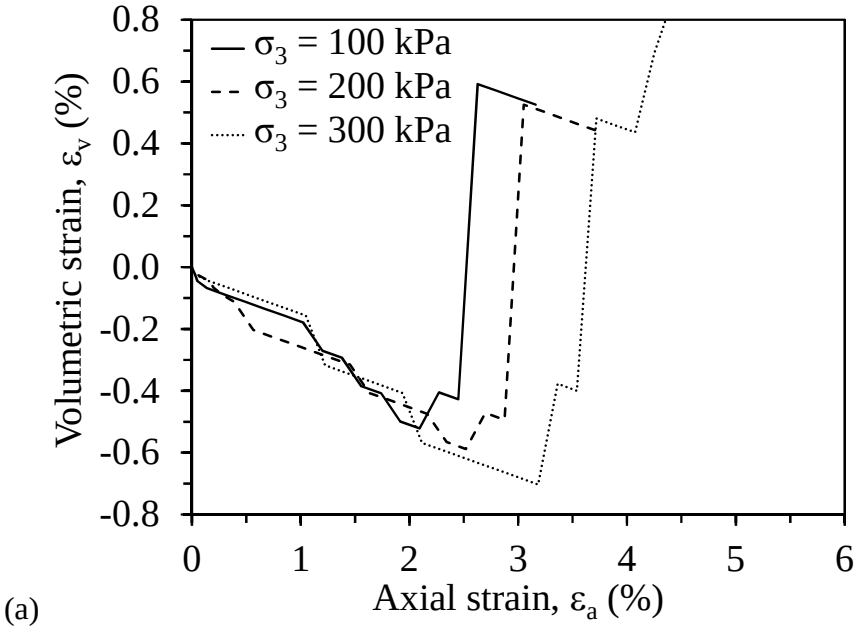

(a)

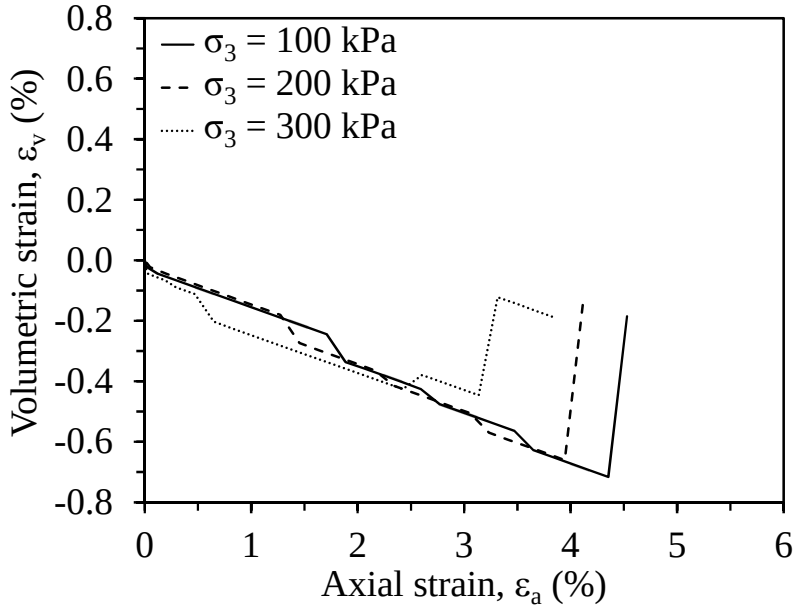

(b)

Figure 6.5: Volume change as a function of axial strain for the unsaturated silt specimens at various confining stresses at suction values of: (a) 162 MPa; (b) 291 MPa

It can also be observed from Figure 6.5(a) that the amount of dilation increased with net confining stresses for the range of net confining stresses evaluated in this study. This was different from the decrease in the amount of dilation with net confining stress observed in Figure 6.5(b) for the specimens at the higher suction value.

The drained failure envelopes for the saturated and unsaturated specimens sheared under room temperature are shown in Figure 6.6(a) in terms of net confining stress. The results showed an increase in the shear strength of the soil with increasing suction and net confining stress. The fact that the unsaturated specimens still had an increase in shear strength with increasing confining stress indicated that they still behave as frictional materials (i.e., that application of high suction magnitudes did not cause them to behave like cemented materials). Because it was assumed that unsaturated specimens have negligible excess pore water pressure generation during shearing, the failure envelopes from the CD triaxial tests represented drained failure envelopes even when plotted as a function of net normal stress. This trend was similar to the total suction failure envelopes reported by Nishimura and Fredlund (2000) for high suction magnitudes. The peak friction angle for the silt specimens at high suction magnitudes sheared under drained conditions ($\phi = 51°$) was larger than the effective friction angle defined from tests on saturated silt specimens ($\phi' = 31°$) corresponding to critical state conditions. The larger peak friction angle for the unsaturated specimens at high suction magnitudes may have been due to an increase in preconsolidation stress and the shape of the steady state boundary surface due to suction application, and to the large decrease in initial void ratio before shearing induced by application of the high suction magnitude. The void ratio at failure as a function of the maximum principal stress difference for both the saturated and unsaturated specimens at different suction values are shown in Figure 6.6(b). The results in this figure indicate that the shear strength increased with decreasing void ratio at failure and that the results from saturated and unsaturated specimens followed the same nonlinear trend. The rate of increase in maximum principal stress difference decreased more substantially at very high suction values. A summary of the initial conditions from the compression triaxial tests on unsaturated specimens at ambient temperature

is presented in Table 6.1. A summary of the results from compression triaxial tests on unsaturated specimens at ambient temperature is presented in Table 6.2.

Table 6.1: Summary of the initial conditions from the compression triaxial tests on unsaturated specimens at ambient temperature

Conf. stress at consol. σ_3 (kPa)	Rel. hum. at bottom R_h (%)	Suction ψ (MPa)	Initial Temp. at bottom T (°C)	Initial deg. of sat. S_r	Initial Void ratio e_0	Average air pressure u_a (kPa)	Axial stress at consol. σ_a (kPa)	Initial mean net stress p_{net} (kPa)	Temp. at bottom shearing T (°C)
100	30.5	162	22.7	0.41	0.68	20	200	113	22.7
200	30.6	161	22.8	0.41	0.68	20	400	247	22.8
300	29.8	165	23.8	0.41	0.68	20	600	380	23.8
100	12.0	289	22.9	0.40	0.69	20	200	113	22.9
200	11.8	292	23.2	0.42	0.66	20	400	247	23.2
300	12.0	289	22.6	0.41	0.68	20	600	380	22.6

Table 6.2. Summary of the results from compression triaxial tests on unsaturated specimens at ambient temperature

Suction ψ (MPa)	Temp. at bottom shearing T (°C)	Void ratio at shear e_s	Princ. stress diff. $\sigma_1-\sigma_3$ (kPa)	Exp. suction stress σ_s (kPa)	Initial shear stress q_0 (kPa)	Initial mean effective stress p'_0 (kPa)	Mean net stress at peak p_n (kPa)	Mean effective stress at peak p' (kPa)	Final void ratio e_f	Final degree of sat. S_r
162	22.7	0.572	1965	202	100	128	735	937	0.576	0.10
161	22.8	0.503	2679	202	200	261	1073	1275	0.507	0.11
165	23.8	0.508	3364	202	300	390	1401	1603	0.513	0.12
289	22.9	0.48	2392	263	100	128	877	1140	0.49	0.05
292	23.2	0.49	3142	263	200	261	1227	1490	0.51	0.08
289	22.6	0.39	3563	263	300	390	1468	1731	0.40	0.06

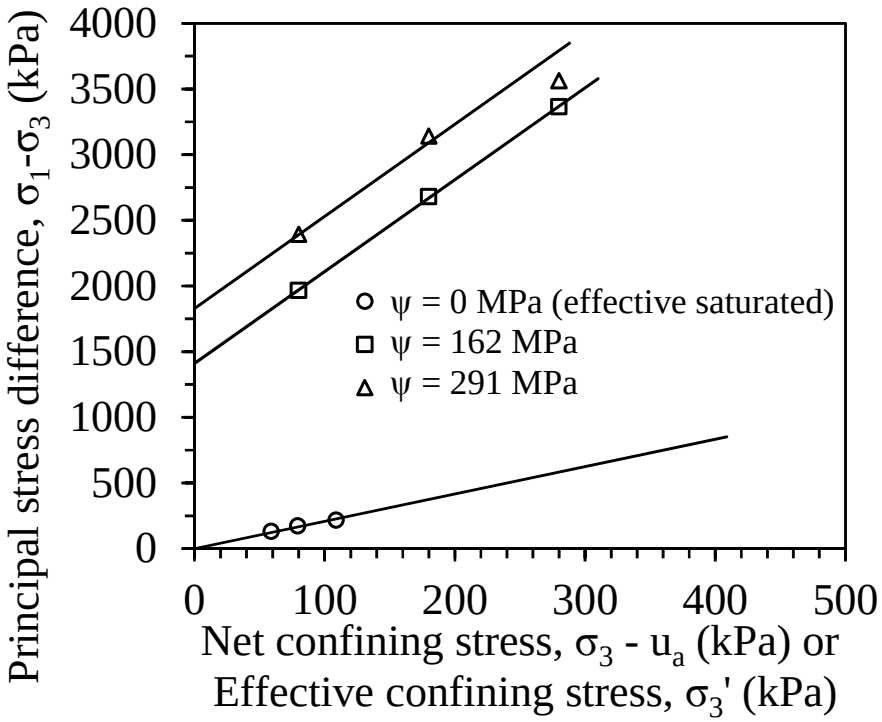

(a)

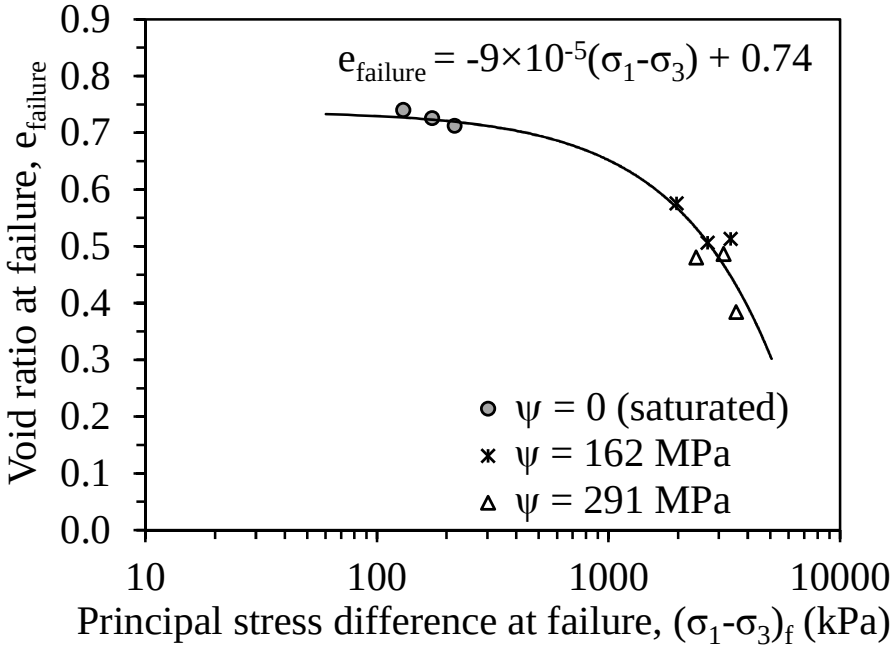

(b)

Figure 6.6: Results from triaxial tests on saturated and unsaturated silt specimens at a constant temperature of 23 °C: (a) Effective and total stress failure envelopes for saturated and unsaturated silt (not to scale); (b) Void ratio at failure versus principal stress difference for different suction magnitudes

6.3.Nonisothermal Anisotropic Consolidated - Drained Triaxial Test Results

6.3.1.Results of Relative Humidity and Suction Equilibration

An example set of relative humidity and temperature measurements at the bottom and top of the specimen during suction equilibrium for tests performed at elevated temperatures following the T-S testing path for a target relative humidity of 15% is shown in Figure 6.7(a) and the corresponding suction at the top and bottom of the soil specimen is shown in Figure 6.7(b). The temperature at the bottom of the specimen (T_{bottom}) was very stable during suction application, and was 64 °C for the test following the T-S path. Although the temperature at the top of the specimen was not measured, the temperature of the gas flowing out of the top of the specimen ($T_{outflow}$) was measured within the insulated flask. Despite the insulation of the flask, the outflow temperature was sensitive to the room temperature due to the presence of the vent. For the example test shown in Figure 6.7, the outflow temperature stabilized at 61 °C after the relative humidity of the outflow gas stabilized. At this point the outflow rate is also stable. In all tests, approximately two hours were needed for the relative humidity at the bottom ($R_{h\ bottom}$) to reach the target value ($R_{h\ target}$), while an average of one to two weeks was needed for the relative humidity at the top ($R_{h\ top}$) to reach the same target value.

The target relative humidity for the tests following the T-S path in this study was slightly different than the tests following the S-T path because the total suction calculated using Kelvin's law is sensitive to temperature. Although the target suction was 291 MPa for all of the nonisothermal tests, the suction in the tests following the T-S path was 317 MPa due to difficulty in reaching the exact target relative humidity that corresponds the target suction. Nonetheless, both suction values are within residual saturation conditions for Bonny silt, so it is assumed that they are close enough for comparison. After the target relative humidity at the top of the soil

specimen was attained and the differential pressure across the soil specimen was constant, the suction was maintained for at least six additional hours to ensure uniformity of total suction throughout the specimen.

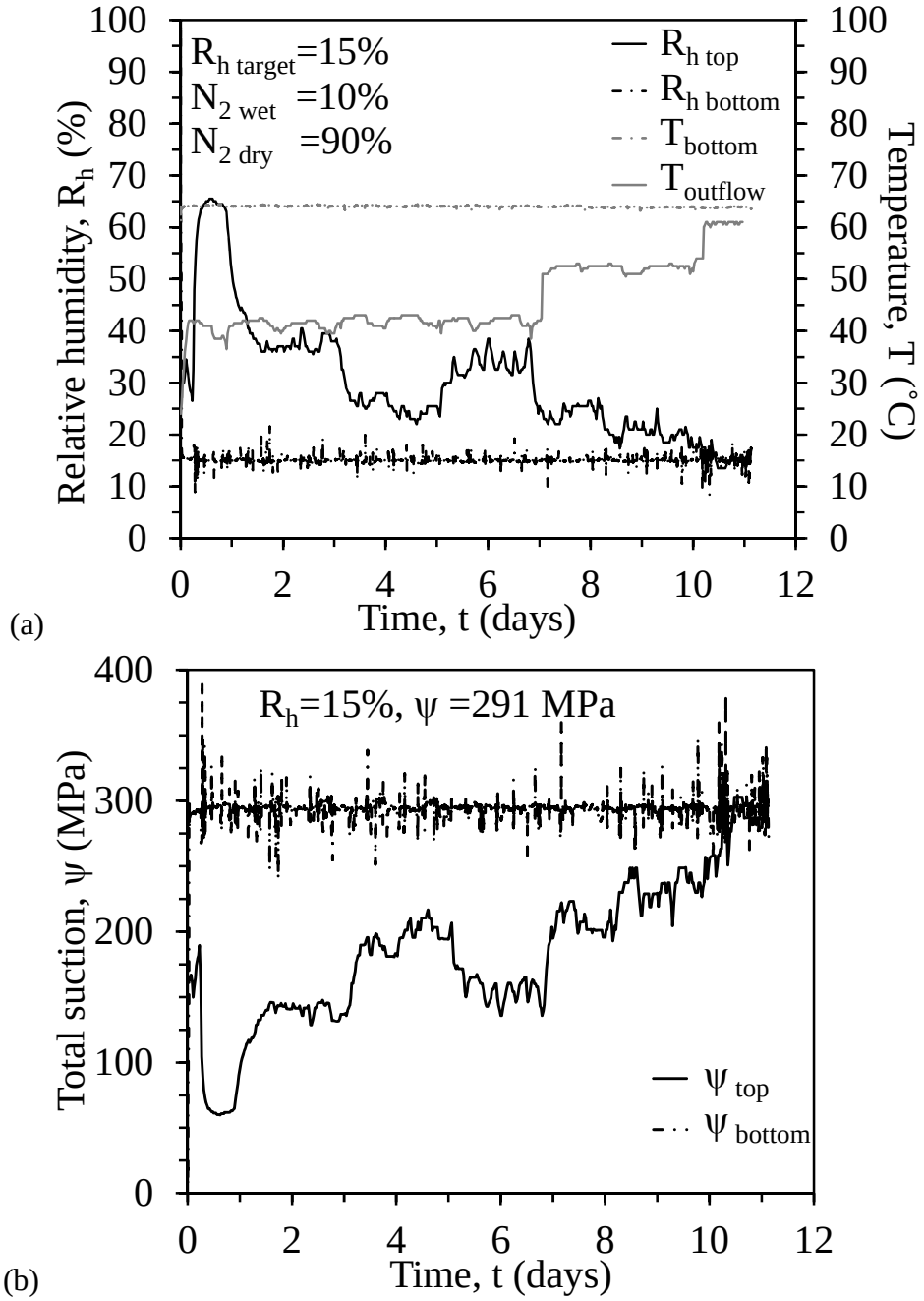

Figure 6.7: Equilibration of relative humidity at a confining stress of 300 kPa under nonisothermal condition for T-S testing path: (a) Relative humidity and temperature with time for a relative humidity at equilibrium of 15%; (b) Total suction calculated from the measured relative humidity

6.3.2.Axial Strain and Volume Change Results during Suction application

The measurements of axial strain as a function of time during suction equilibration at room temperature following the S-T testing path and at elevated temperature of 64˚C following the T-S testing path are shown in Figures 6.8(a) and 6.8(b), respectively. Approximately 2 days was required for equilibration for the S-T path while less than a day was required for the T-S path. The faster equilibration at higher temperatures is likely due to the effect of vaporization of water in the specimen under higher temperatures.

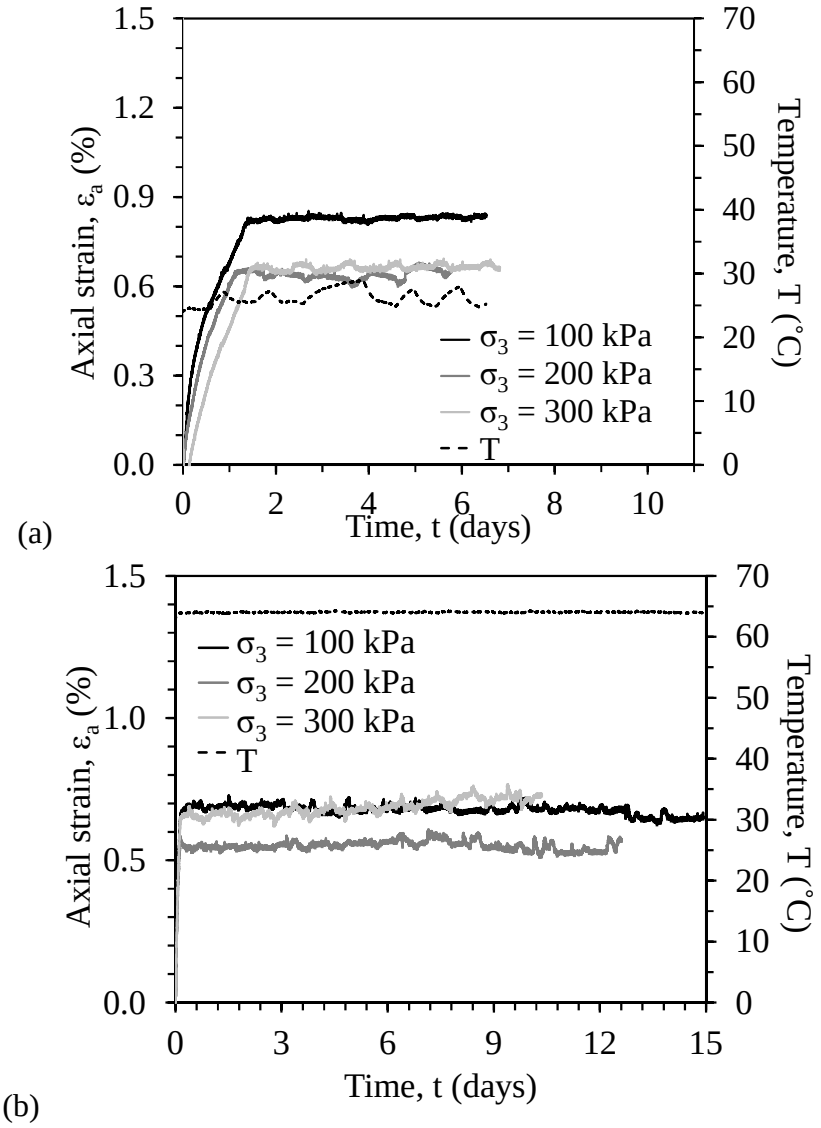

Figure 6.8: Axial strain over time for various confining stresses due to suction application at: (a) Room temperature of 25˚C (S-T path); (b) Elevated temperature of 65˚C (T-S path)

Following S-T Path, The volume change measurements corresponding to changes in total suction at the top of the soil specimen over time for confining stresses of 100 kPa, 200 kPa, and 300 kPa are illustrated in Figures 6.9(a), 6.9(b) and 6.9(c), respectively. The results in these figures indicate that the volumetric strain increases with increasing suction applied up to 300 MPa and confining stresses up to 300 kPa.

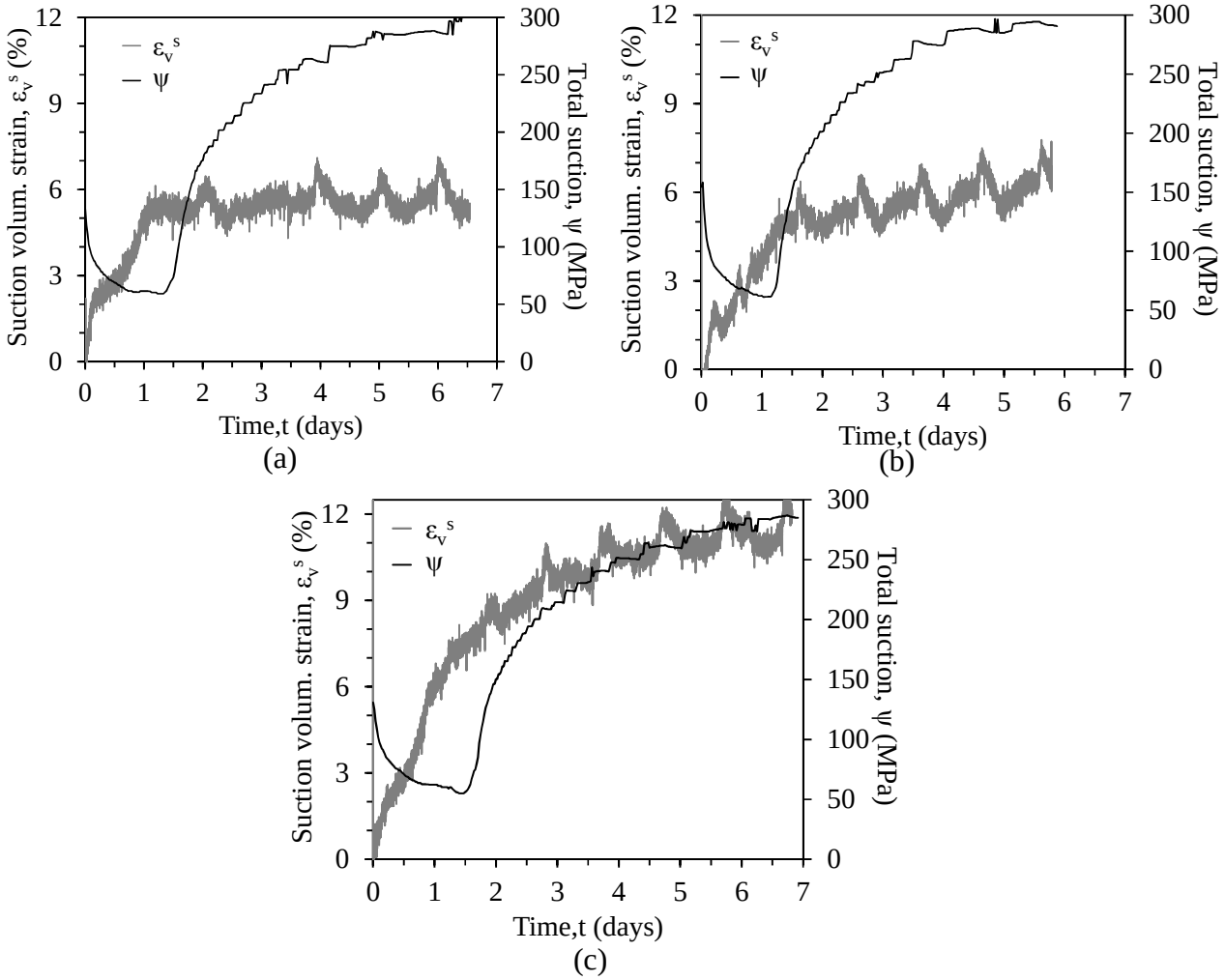

Figure 6.9: Change in volumetric strain during equilibration of total suction recorded at top of soil specimen following S-T Path at confining stresses of: (a) 100 kPa; (b) 200 kPa; (c) 300 kPa

6.3.3.Axial Strain and Volume Change Results during Heating

The volumetric strains as a function of the change in cell fluid temperature for different testing paths and confining stresses are presented in Figure 6.10. When following the T-S path,

the soil specimens were heated in a single stage at a constant heating rate of 10.5 to 11.5 °C/hour. The thermal axial strains for the unsaturated silt specimens following this path shown in Figure 6.10(a) indicate that the specimen tends to contract more with increasing confining stress. Similar trends are observed in the thermal volumetric strains for these specimens in Figure 6.10(b), albeit with a more uniform contraction with temperature. The soil specimens in the tests following the S-T path were heated under the as compacted conditions (initial S_r of 0.41) before application of suction. In this case, heating likely causes generation of excess pore water pressure, which drained and resulted in permanent contraction. The slight axial expansion of the specimens tested under lower confining stresses may have occurred due either transient drainage effects or heating of the lightly overconsolidated specimens above the contraction threshold temperature observed by Hueckel and Baldi (1990). The difference in the trends in thermal axial and volumetric strains with the change in temperature may have occurred due to the effects of the anisotropic stress state as observed by Coccia and McCartney (2013). Specifically, the trend in the thermal axial strains is similar to lightly overconsolidated conditions while the trend in the thermal volumetric strain is similar to normally consolidated conditions. The thermal axial strains following the S-T path shown in Figure 6.10(c) differ from those following the T-S path, and show expansion during staged heating similar to heavily overconsolidated soils heated below the contraction threshold temperature (Hueckel and Baldi 1990; Delage et al. 2000, 2004; Cekeravac and Laloui 2004). Similar trends in volumetric expansion are also observed for these specimens, as shown in Figure 6.10(d). After application of high suction magnitudes, these specimens have a degree of saturation of approximately 0.06 prior to heating, so it is unlikely that there is significant generation of excess pore water pressures. Application of high suction magnitudes likely results in an increase in mean effective stress, as well as an increase in mean

preconsolidation stress. If the increase in preconsolidation stress is greater than the effective stress, this would lead to an increase in the OCR causing the silt to behave like a heavily overconsolidated soil. Further, application of high suction values lead a reduction in volume (which will be discussed later). Despite the relatively low water content of the soils following the S-T path, the results in Figures 6.10(c) and 6.10(d) indicate that stress history still plays an important role in the thermal volume change of unsaturated soils under high suction magnitudes.

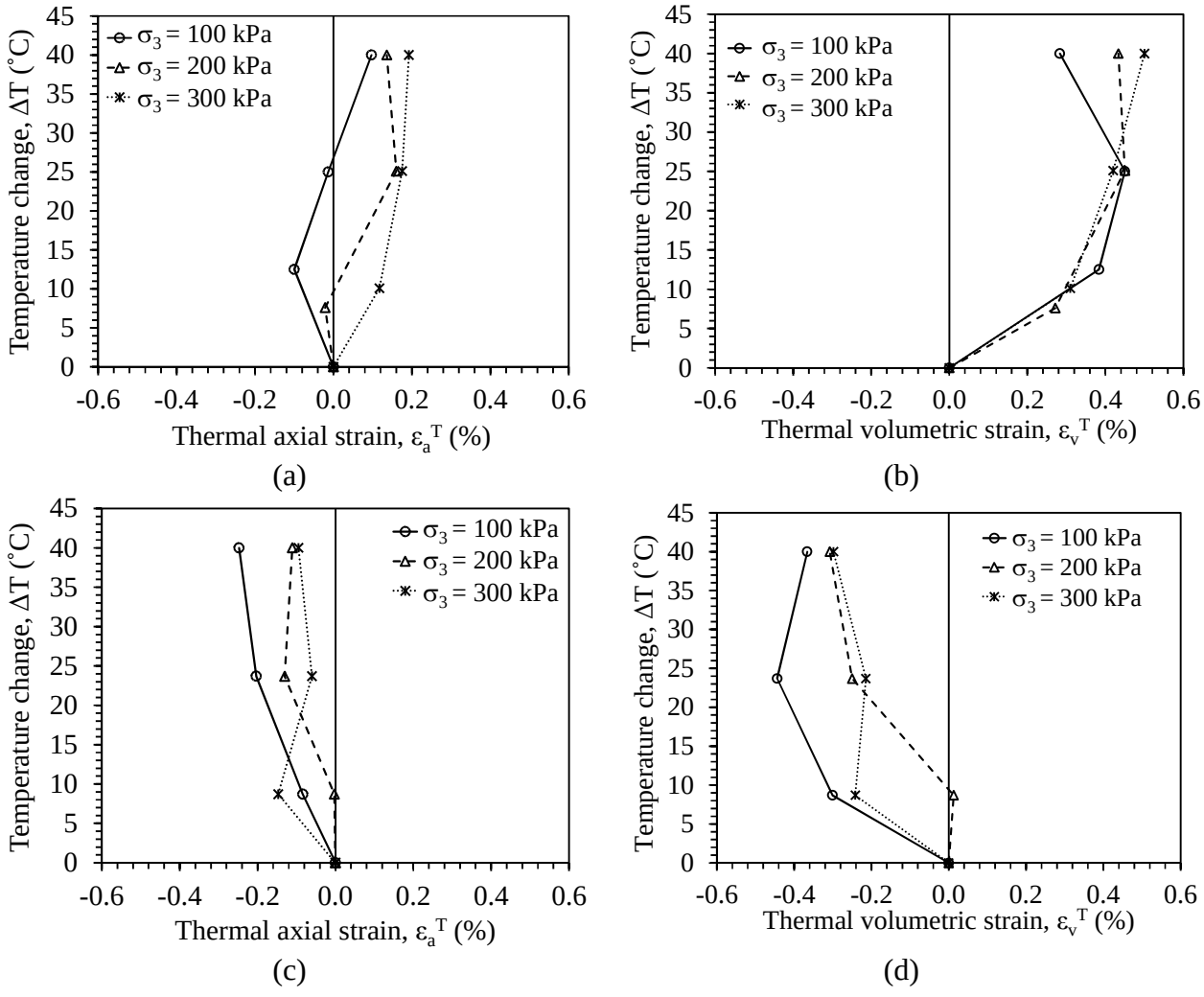

Figure 6.10: Thermal strains as a function of temperature change at various net confining stresses for tests following the: (a) Thermal axial strains for the T-S path; (b) Thermal volumetric strains for the T-S path; (c) Thermal axial strains for the S-T path; (d) Thermal volumetric strains for the S-T path

The thermal volumetric strains during a change in temperature of 41˚C for test performed at 300 kPa confining stress following S-T Path with one heating cooling cycle are presented in Figure 6.11. The same expansion reported in Figure 6.10(b) was observed in Figure 6.11 due to the increase in temperature. However, further cooling of the soil specimen led to permanent contraction, which is similar to the behavior observed by Vega and McCartney (2014).

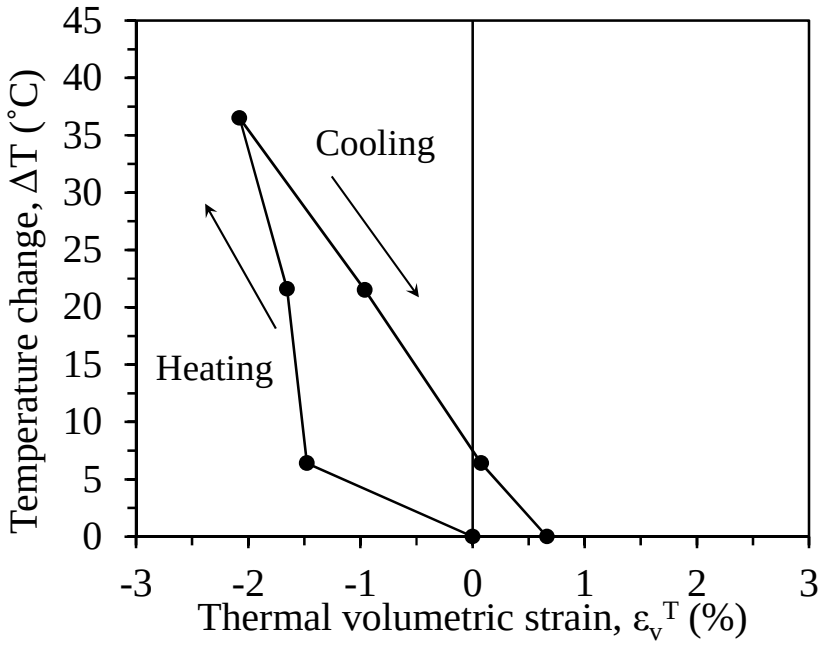

Figure 6.11: Thermal volumetric strain over temperature change at confining stress of 300 kPa for test following S-T Path with a heating-cooling cycle

6.3.4.Results of Air Permeability during Suction and Temperature Application

Typical results of air permeability calculated using Eq. 3.5 during application of high suction values are shown in Figure 6.12. The results in this figure present the differential pressure between top and bottom of the soil specimen over time and the corresponding air permeability. The data in this figure indicates that the differential pressure between soil boundaries was high at the beginning of suction application and then decreased as the soil dried, and thus increasing the air permeability until it reaches a constant value at suction equilibrium.

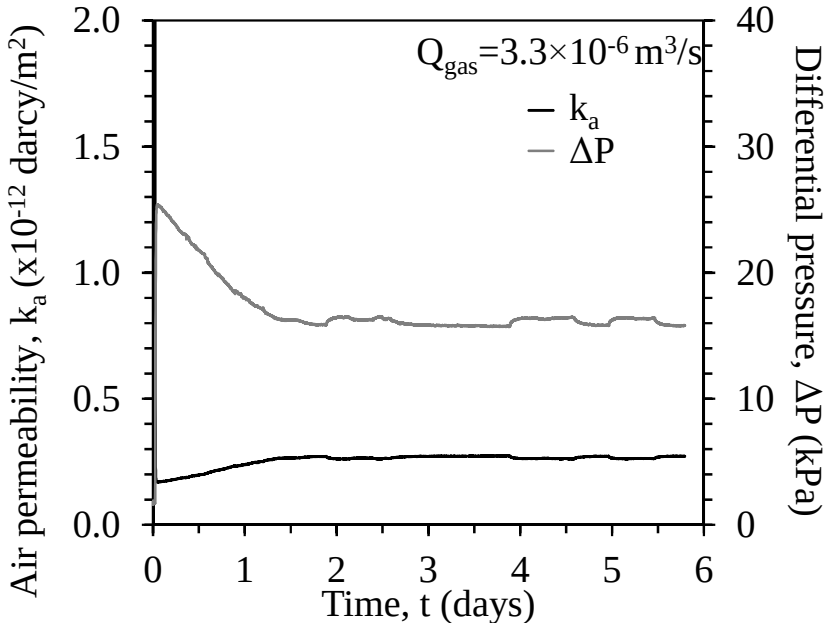

Figure 6.12: Measurements of differential pressure across the specimen and air permeability due to suction application

The effect of a change in temperature from room temperature of 23˚ up to 64˚C on the differential pressure between top and bottom of soil specimen over time along with corresponding changes in Nitrogen gas viscosity is illustrated in Figure 6.13(a). The corresponding change in air permeability due to temperature change is presented in Figure 6.13(b). The results in Figure 6.13 indicate that the increase in temperature increases the differential pressure and gas viscosity, and thus reduction in air permeability. A Summary of air permeability at different net confining pressure through stages of confining, suction, and heating for the test following the S-T Path is shown in Figure 6.14.

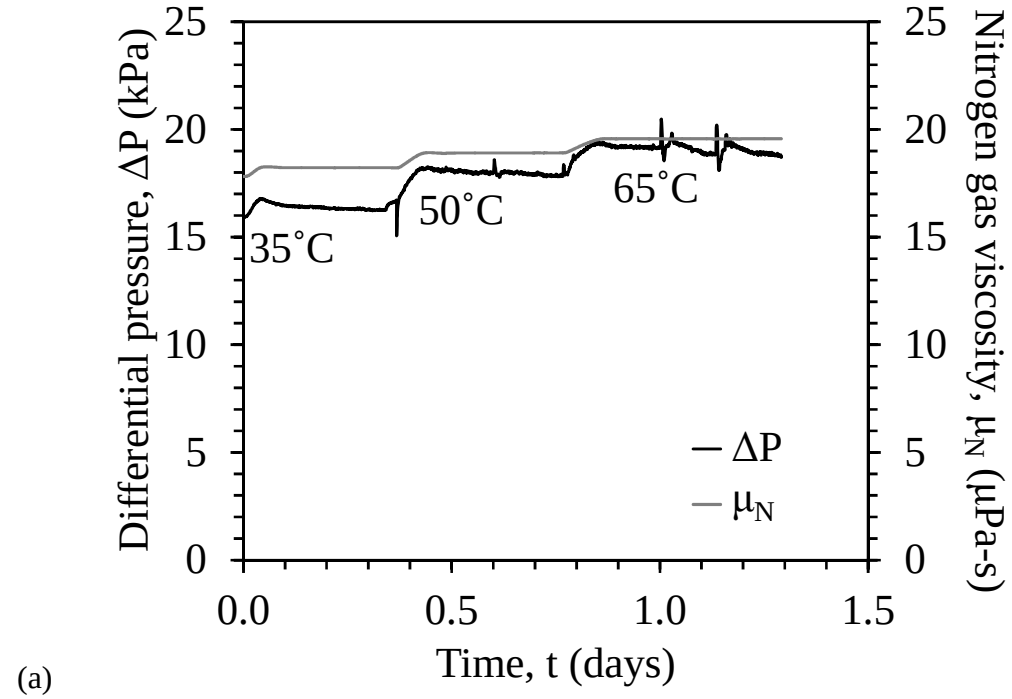

(a)

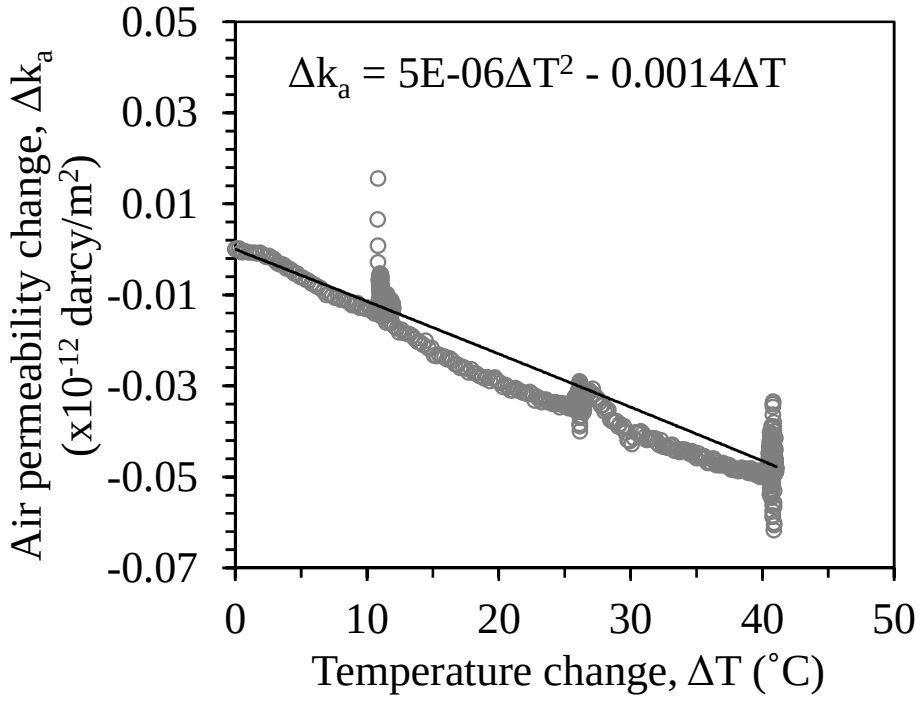

(b)

Figure 6.13: Thermal effect on air permeability at confining pressure of 100 kPa: (a) Differential pressure and gas viscosity over time; (b) Air permeability change as a function of the change in temperature

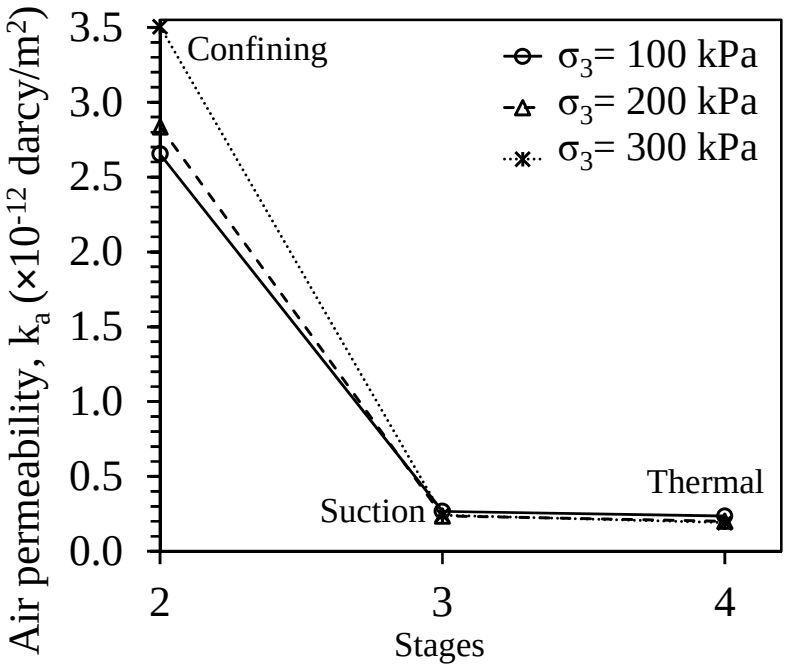

Figure 6.14: Summary of air permeability of unsaturated Bonny silt over different test stages for tests following the S-T Path

6.3.5.Results of Triaxial Compression Testing during Nonisothermal Tests

The stress-strain curves for the soil specimens that had reached thermal equilibrium following different testing paths are shown in Figure 6.15. The shear stress-strain curves for the specimens tested at ambient temperature and various suction magnitudes and at elevated temperature following different testing paths for cell pressures of 100, 200, and 300 kPa are shown in Figures 6.15(a), 6.15(b), and 6.15(c), respectively. A brittle failure mode was observed in the stress-strain curves for all specimens under high suction magnitudes regardless of the temperature. This failure mode differed significantly from the relatively ductile failure mode observed in tests on saturated conditions tested in isotropic consolidated-undrained triaxial compression tests shown in Figure 6.4. Because of the brittle failure mode, it was not possible to shear the specimens tested under high suction magnitudes to critical state conditions and that was confirmed by the slip failure observed in all specimens tested in this study regardless of

temperature. The results in Figure 6.15 indicate that the peak shear strength of the specimens tested following the T-S path was consistently smaller than those tested under ambient temperature conditions, while the peak shear strength of the specimens tested following the S-T path was greater. A Summary of the initial conditions from the compression triaxial tests on unsaturated specimens at elevated temperature of 64˚C, and different testing paths are presented in Table 6.3. A summary of the results from the triaxial compression tests on unsaturated specimens at elevated temperature of 64˚C, and different testing paths are presented in Table 6.4. The temperatures measured using the relative humidity probe below the specimen were slightly lower than the target cell fluid temperature, which was 65 °C.

Table 6.3. Summary of the initial conditions from the compression triaxial tests on unsaturated specimens at elevated temperature of 64˚C for different testing paths

Test path	Initial Temp. at bottom T (°C)	Initial deg. of sat. S_r	Initial Void ratio e_0	Average air pressure u_a (kPa)	Conf. stress at consol. p (kPa)	Axial stress at consol. σ_a (kPa)	Initial mean net stress p_n (kPa)	Rel. hum. at bottom R_h (%)	Suction ψ (MPa)	Temp. at bottom shearing T (°C)
T-S	23.1	0.41	0.67	20	100	200	113	12.5	317	64.0
	23.0	0.41	0.67	20	200	400	247	12.5	317	64.0
	23.8	0.42	0.67	20	300	600	380	13.0	311	63.9
S-T	24.1	0.42	0.67	20	100	200	113	14.9	291	63.9
	23.5	0.41	0.68	20	200	400	247	15.0	290	63.9
	23.1	0.41	0.68	20	300	600	380	15.1	289	63.9
S-T Cycle	23.7	0.42	0.67	20	300	600	380	18.0	235	25.2

Table 6.4. Summary of the results from the triaxial compression tests on unsaturated specimens at elevated temperature of 64˚C, and different testing paths

Test path	Suction ψ (MPa)	Temp. at bottom shearing T (°C)	Void ratio at shear e_s	Princ. stress diff. σ_1-σ_3 (kPa)	Exp. suction stress σ_s (kPa)	Initial shear stress q_0 (kPa)	Initial mean effective stress p'_0 (kPa)	Mean net stress at peak p_n (kPa)	Mean effective stress at peak p' (kPa)	Final void ratio e_f	Final deg. of sat. S_r
T-S	317	64.0	0.56	2235	235	100	128	825	1060	0.56	0.06
	317	64.0	0.52	2986	235	200	261	1175	1410	0.53	0.06
	311	63.9	0.48	3408	235	300	390	1416	1651	0.49	0.06
S-T	291	63.9	0.53	2707	313	100	128	982	1295	0.54	0.04
	290	63.9	0.47	3480	313	200	261	1340	1653	0.47	0.03
	289	63.9	0.36	4135	313	300	390	1658	1971	0.37	0.04
S-T Cycle	235	25.2	0.39	3699	263	300	390	1513	1776	0.39	0.07

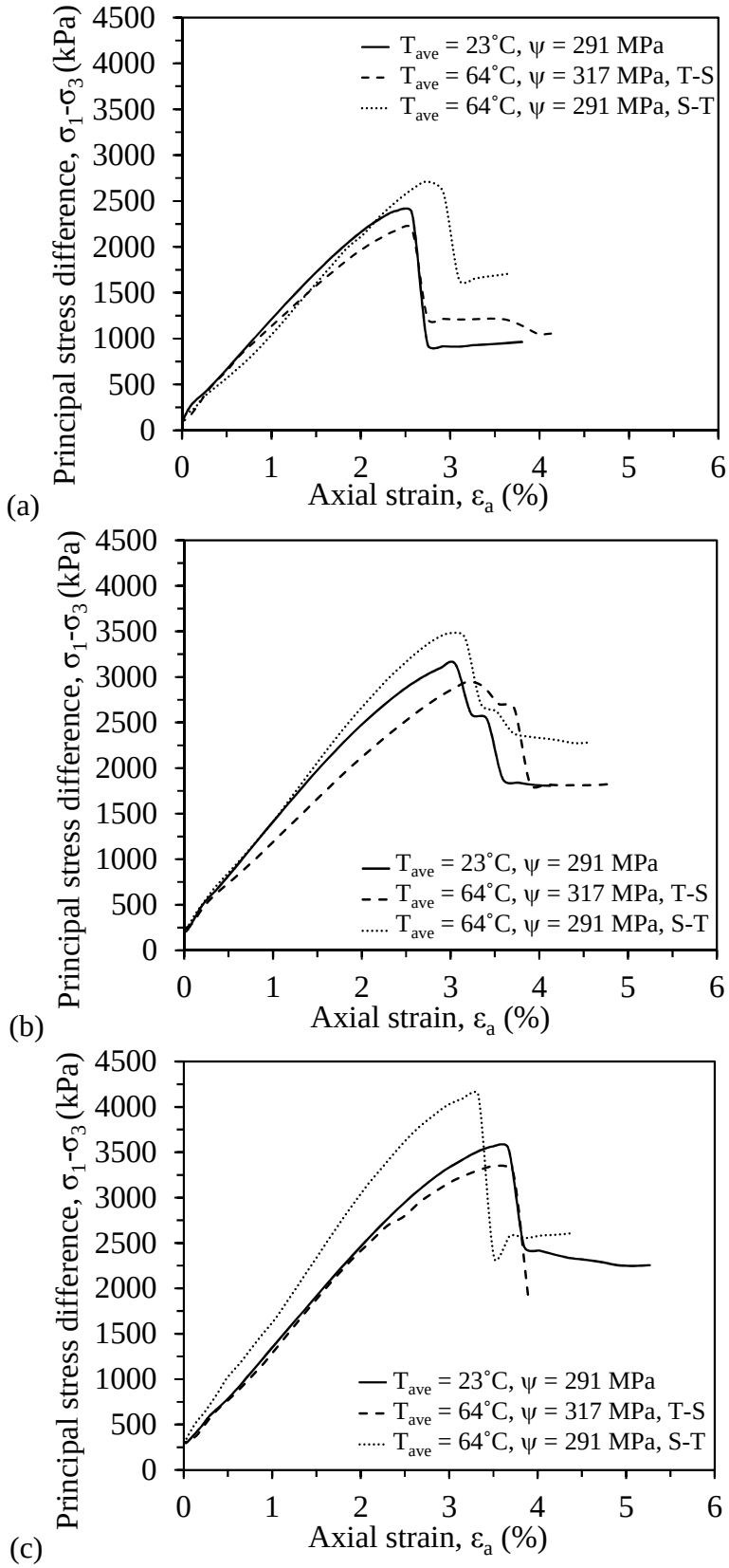

Figure 6.15: Stress-strain curves for unsaturated Bonny silt specimens tested following different testing paths and temperatures at confining stresses of: (a) 100 kPa; (b) 200 kPa; (c) 300 kPa

The volumetric strains during shearing of the unsaturated specimens at various net confining stresses following the T-S path and the S-T path are shown in Figures 6.16(a) and 6.16(b), respectively. The black points correspond to the points of peak shear strength. The results indicate that specimens tested following both the T-S and S-T paths dilate during shear, and that the amount of dilation increases with increasing confining stress for specimens tested following the T-S path tests. The specimens sheared following the S-T path tests experienced a similar amount of dilation for all three normal stresses.

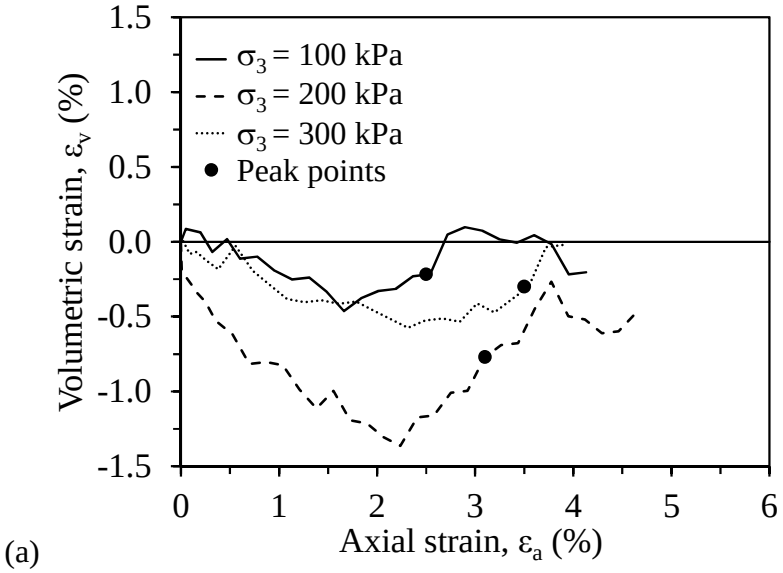

(a)

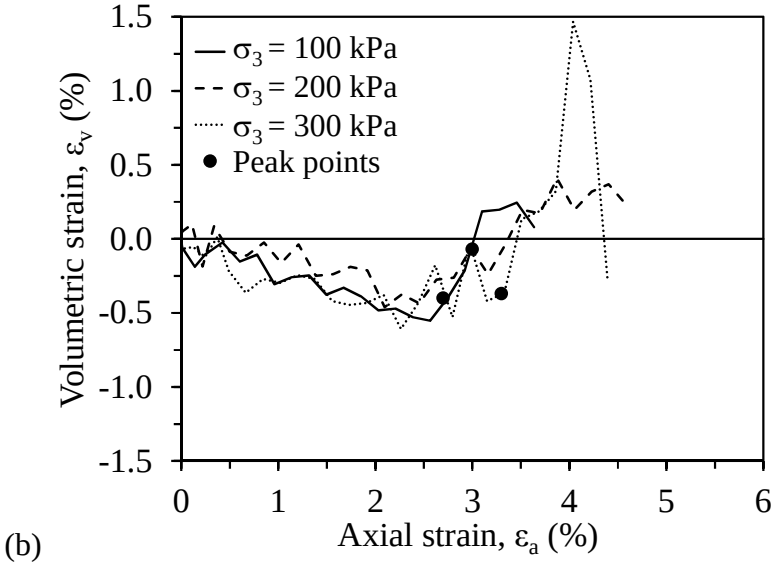

(b)

Figure 6.16: Volume change as a function of axial strain from triaxial tests at various net confining stresses: (a) T-S Path tests; (b) S-T Path tests

A summary of the void ratios at different stages of tests performed at ambient temperature is shown in Figure 6.17(a) for comparison. The void ratio is observed to decrease during application of confining stresses, as well as during application of a suction of 291 MPa. A small amount of dilation is observed after shearing. A summary of the void ratios at different stages of the tests following the T-S path is shown in Figure 6.17(b). In these tests, a similar reduction in void ratio is observed during application of the confining stress. A slight reduction in void ratio during heating corresponding to the thermal volumetric contraction of less than 1% shown in Figure 6.10(a) is then observed. The specimens contracted further during application of a suction of 291 MPa, and dilated slightly during shearing. The summary of the void ratio values at different stages of the tests following the S-T path at different confining stresses is shown in Figure 6.17(c). The results in this figure clearly indicate that the void ratio was sensitive to the confining stress and applied suction, similar to the results in Figure 6.17(a). However, heating of the specimen after it was in equilibrium at a suction of 291 MPa led to expansion of the soil specimens, which was followed by further expansion due to dilation during shearing. A comparison of the void ratio values prior to shearing in Figure 6.17(a), 6.17(b) and 6.17(c) indicates lower void ratios for the tests following the S-T path than those for the tests at ambient temperature and those following the T-S path. This may partially explain the greater peak shear strength values observed for the tests following the S-T path. The void ratio of the specimen which experienced a heating and cooling cycle after reaching suction equilibration is shown in Figure 6.17(c). Although there is a slight variability compared to the other test performed at a confining stress of 300 kPa, the void ratio at stage four for this test reflects a net contraction the specimen after cooling back to ambient temperature.

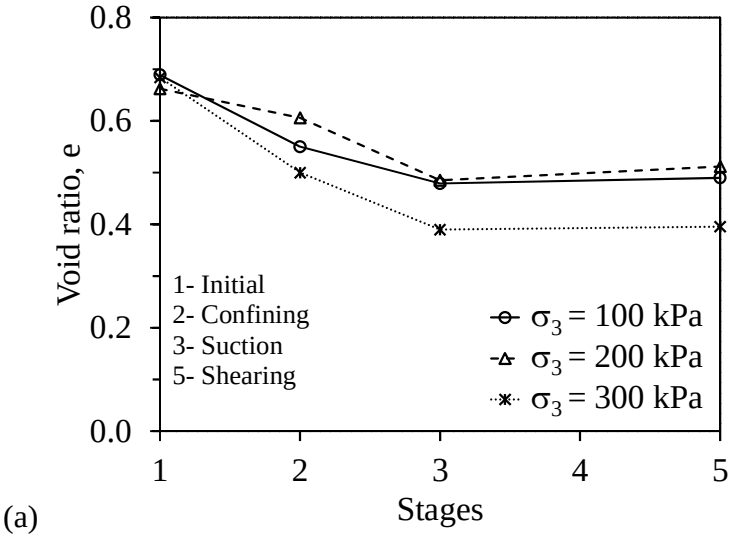

(a)

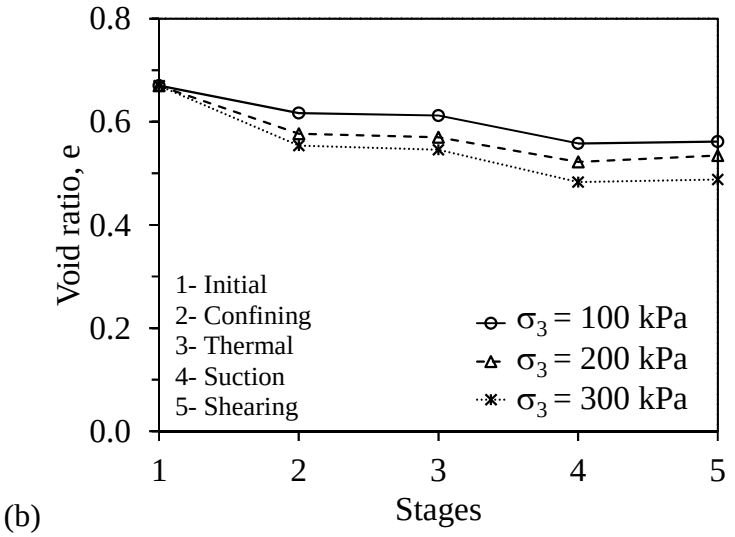

(b)

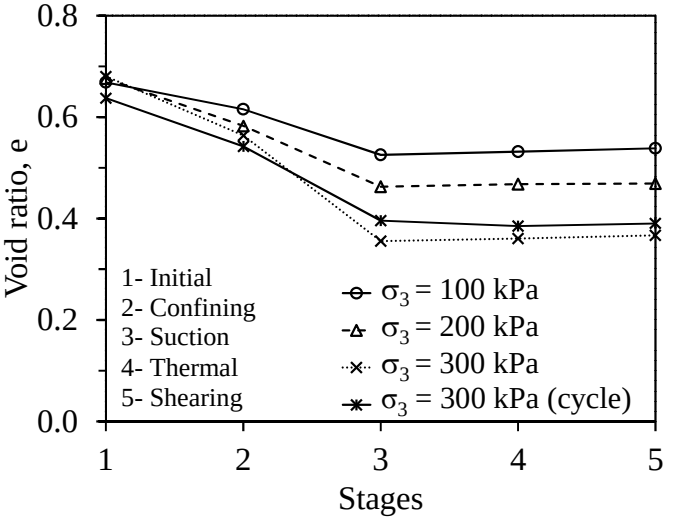

(c)

Figure 6.17: Summary of void ratios during different stages of testing: (a) Ambient temperature tests; (b) T-S path tests; (c) S-T path tests

The impact of temperature on the void ratio at failure as a function of the peak principal stress difference for different testing paths is shown in Figure 6.18. Overall, the data points follow a similar trend, which confirms that the peak shear strength is sensitive to the density of the soil at failure. However, it should be noted that the void ratio at failure for the saturated specimens at ambient temperature were at critical state conditions, while the void ratio at peak failure conditions for the unsaturated specimens at high suction magnitudes were not at critical state conditions due to the brittle failure mode.

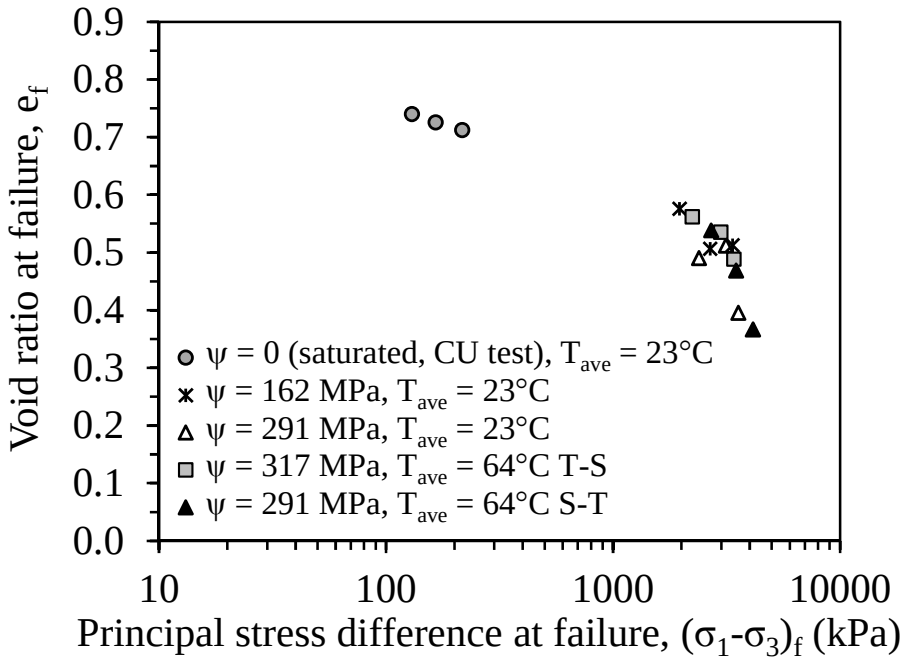

Figure 6.18: Void ratio at failure versus principal stress difference for different suction magnitudes and temperatures following different testing paths

The shearing results for the 300 kPa confining stress test following S-T Path with heating cooling cycle are presented in Figure 6.19. Similar to S-T Path results, a brittle failure mode is observed in Figure 6.19(a) and dilation is observed in Figure 6.19(b).

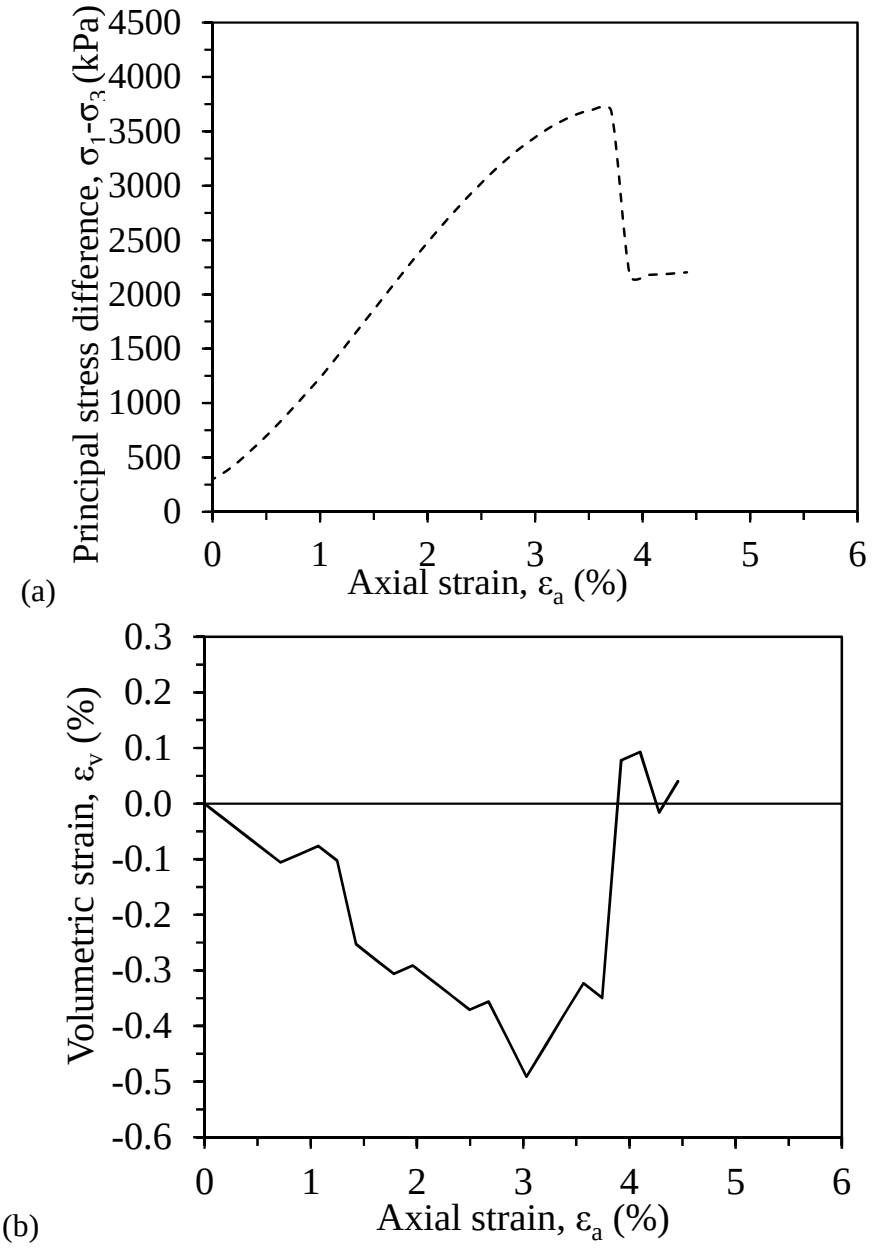

Figure 6.19: Shearing results for 300 kPa confining stress test following S-T Path with heating cooling cycle: (a) Stress-strain curve; (b) Volume change as a function of axial strain

7. ANALYSIS AND DISCUSSION OF TRIAXIAL TEST RESULTS

7.1.Overview

This chapter focuses on an analyses of the results obtained from the shear strength tests performed on Bonny silt at various suction and temperature values. First, an evaluation of the linkage between suction stress characteristic curve (SSCC) and soil water retention curve (SWRC) at ambient temperatures, along with an interpretation of the shear strength of compacted silt in terms of mean effective stress at room temperature is discussed in Section 7.2. Next, an interpretation of the effective stress of the unsaturated silt at elevated temperatures and high suction magnitudes and an evaluation of the temperature effects on soil behavior using constitutive modelling are discussed in Section 7.3, including an evaluation of the impact of temperature on the SWRC and SSCC, the preconsolidation stress, and volume change behavior.

7.2. Analysis of Isothermal Test Results

The objective of the analysis in this section was to evaluate the effective stress principle for compacted silt specimens at low degrees of saturation and assess the implications of using a single SWRC curve fitted to data obtained at low suction magnitudes to predict the effective stress state over the full range of saturation. These topics are relevant as it is possible to encounter fundamental changes in the inter-particle stresses in the transitions between the three saturation ranges of the primary drying-path SWRC (Lu and Likos 2004). The first range is the saturated range within which the soil can be considered fully saturated, which extends from zero suction up to the air entry suction. In this range, the negative water pressure can be incorporated directly into Terzaghi's definition of effective stress ($\sigma' = \sigma - u_w$). The second range is the funicular range within which air enters the pores of the soil and displaces water. A significant decrease in the degree of saturation is observed in this range. In the funicular region, the shear

strength (Blatz and Graham 2000; Rahardjo et al. 2004; Ajdari et al. 2010) and elastic moduli (Ng et al. 2009; Khosravi and McCartney 2012) of fine-grained soils increase significantly. The third range is the pendular or residual saturation range within which the pore water resides as isolated pendular menisci. In this range, van der Waals attraction forces play an important role in the inter-particle stresses in fine grained soils (Lu and Likos 2006), and several studies have found that the shear strength of soils can be significantly greater than that in the funicular range (Nishimura and Fredlund 2000; Blatz et al. 2002). The transition from the funicular to pendular ranges occurs at different degrees of saturation for different soils, and it is typically necessary to use vapor equilibrium techniques to change the water content of the soil beyond this point. The residual saturation S_{res} can be defined as the irreducible saturation at which water is bonded to the soil particles hydroscopically and can only be removed using oven drying (Brooks and Corey 1964).

7.2.1.Evaluation of Linkages between the Suction Stress Characteristic Curve and Soil Water Retention Curve at High Suction Magnitudes

To evaluate the effective stress principle in unsaturated, compacted silt under low degrees of saturation, the SSCC calculated from the failure envelopes of the soil was compared with the SSCC obtained from the predictive approach involving the SWRC proposed by Lu et al. 2010. First, the slopes of the drained failure envelopes for the unsaturated specimens shown in Figure 6.6(a) were used to back-calculate two values of suction stress σ_s using Eq. 2.7 in Section 2.4. A third point on the SSCC was defined at the origin by virtue of the fact that the effective failure envelope for the saturated soil passes through the origin of the Mohr–Coulomb diagram. This experimentally-derived SSCC could then be compared with the SSCC obtained from the predictive approach involving the SWRC proposed by Lu et al. (2010) in Eq. 2.9.

The experimental SSCC is shown in Figure 7.1(a), along with the predicted SSCC obtained from Eq. 2.9 with the fitting parameters α_{vG} and N_{vG} defined from the fitting of the van Genuchten (1980) SWRC model to the experimental SWRC in Figure 3.5(a). Although there are only two SSCC data points, the experimental SSCC indicates a nonlinear increase in suction stress with increasing suction. The predicted SSCC was found to overpredict the suction stress measured in the experiments by a significant amount. This behavior was attributed to the sensitivity of the suction stress to the value of N_{vG} observed in Figure 2.7(b). Specifically, small variations in the van Genuchten (1980) fitting parameters due to the experimental issues with the SWRC data shown in Figure 3.5(a) may have significant effects on the predicted SSCC. Accordingly, a second fitting of the van Genuchten (1980) SWRC model to the experimental SWRC data was performed to account for the error induced in the axis translation technique near the point where the water phase becomes discontinuous (approximately 0.65). The results of this fitting are shown in Figure 7.1(b) (dashed line), along with the original fitted SWRC (solid line). The new fitted SWRC still provided a reasonable fit to the experimental SWRC data, but in this case it provided a much better prediction of the experimental SSCC data in Figure 7.1(a) (dashed line). This fitting exercise emphasizes the importance of careful and informed characterization of the SWRC when predicting the SSCC at high suction magnitudes from SWRC data obtained at lower suction ranges.

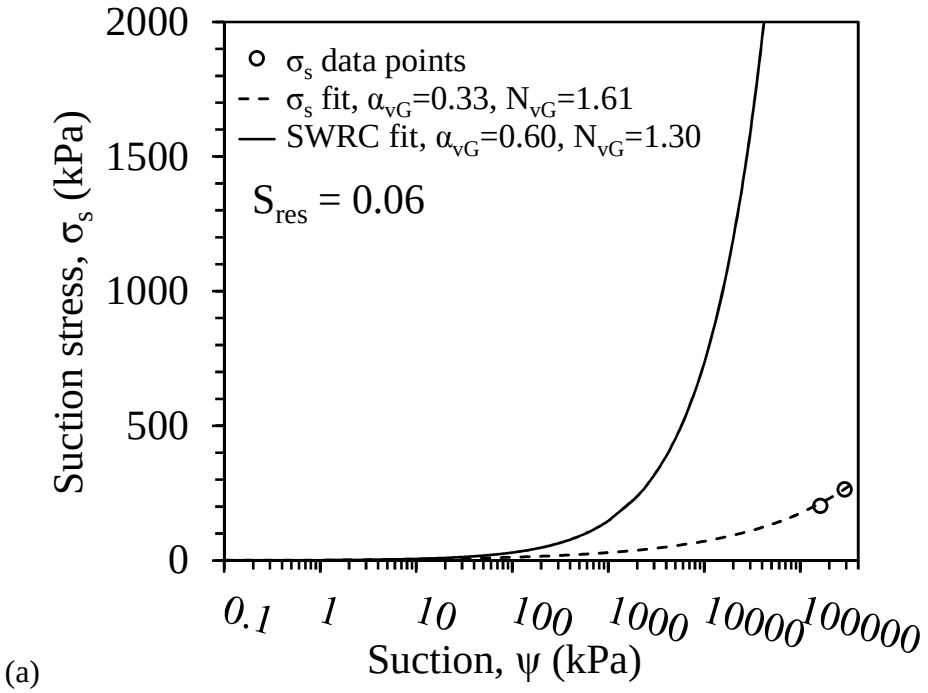

(a)

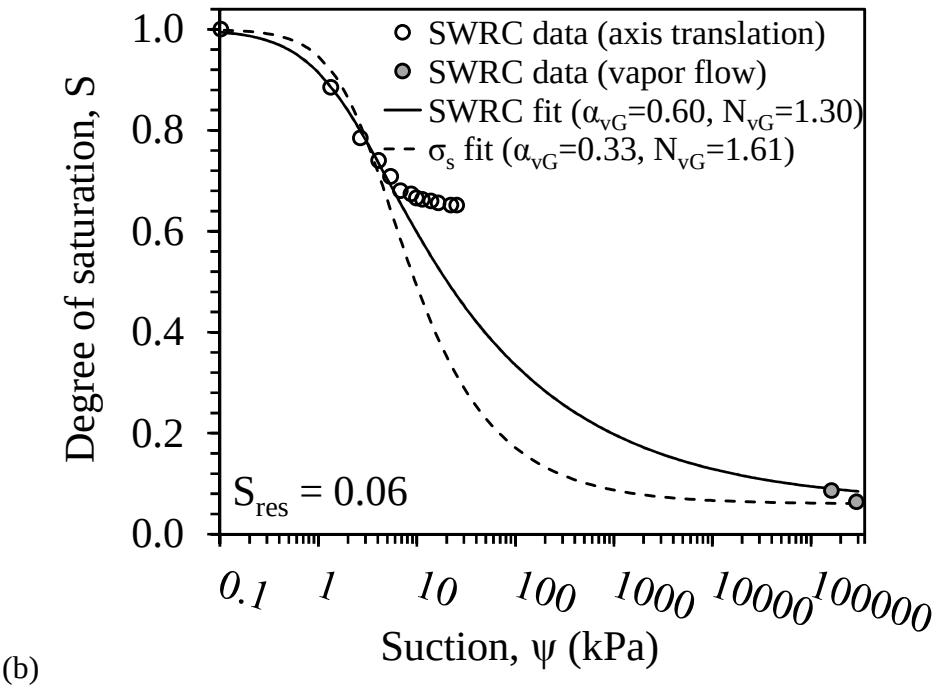

(b)

Figure 7.1: SWRCs and SSCCs fitted to the experimental data (different values of α_{vG} and N_{vG}): (a) SSCCs; (b) SWRCs

One of the possible reasons for the overprediction of suction stress using the SWRC curve fitted to the data at low suctions might be the assumption that stresses arising from capillarity

may still have a major contribution to the suction stress in the pendular range of saturation. Also, it is important to notice that the application of high suctions using the vapor equilibrium technique has a major impact on the void ratio of the silt specimens evaluated in this study. The results in Figure 6.3 in Section 6.2.2 clearly show a large decrease in void ratio as the suction increase, which means that a SWRC defined using data from high and low suction values will not be for a constant void ratio. This means that predicting the SSCC from a SWRC with points having different void ratios can lead to inaccurate predictions in effective stress.

7.2.2.Evaluation of the Critical State Line for High Suction Magnitudes at Room Temperature

The effective stress paths for the CU triaxial tests performed on saturated and CD tests on unsaturated specimens are shown in Figure 7.2. The effective stress paths for saturated specimens presented in this figure show behavior similar to normally consolidated soils where the effective stresses continue to decrease during shearing due to the increase in the pore-water pressure and specimens experienced a contraction for the specified range of normal stresses. The effective stress paths for the unsaturated specimens were calculated by plotting the measured values of principal stress difference versus the mean effective stress calculated using Equation (2.10) using the experimentally-fitted SSCC parameters from Figure 7.1(a) and the suction values back-calculated from the relative humidity measured at the bottom of the soil specimen during the shearing process. The effective stress paths for the unsaturated specimens shown in Figure 7.2 have a slope of 1:3, which is the same as the theoretical slope of the expected effective stress path in a drained triaxial test. This indicates that negligible excess pore water pressures were generated during shearing of the unsaturated specimens at low degrees of saturation. To better interpret the values of effective stress, the van Genuchten (1980) SWRC

parameters fitted to the experimental suction stress data in Figure 7.1(a) were used to calculate the effective stress according to Equation (2.10).

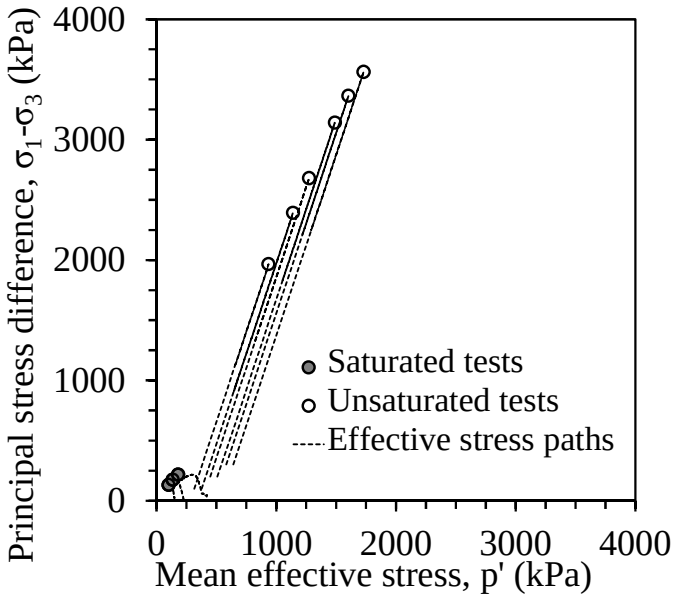

Figure 7.2: Critical state and peak shear strength analysis for Bonny silt at different suction values obtained using the experimental SSCC parameters: Effective stress paths obtained using suction stress values calculated from the suction applied to bottom of the specimen

An evaluation of the critical state line (CSL) in terms of mean effective stress is shown in Figure 7.3. Different from the Mohr–Coulomb failure envelopes shown in Figure 6.6(a), all of the shear strength values converge on a single peak shear strength failure envelope when the data is interpreted in terms of mean effective stress with a slight shift to the left. It is clear that the peak shear strength failure envelope for the unsaturated specimens has a greater slope (M_{peak}) than that of the CSL defined from the shear strength tests on the saturated specimens (MCSL). This was expected, as the application of high suctions to the specimens was expected to cause the specimens to behave like heavily overconsolidated soils, which by definition have a peak shear strength that is greater than the shear strength at critical state. Because the stress–strain curves for the specimens exhibited a brittle shape, it was not possible to characterize the critical state shear strength of the unsaturated specimens. Nonetheless, the fact that the shear strength of

the unsaturated specimens tested at different net normal stresses and high suction magnitudes had peak shear strength values that converged on a single failure envelope reflected the validity of the effective stress principle at high suction magnitudes.

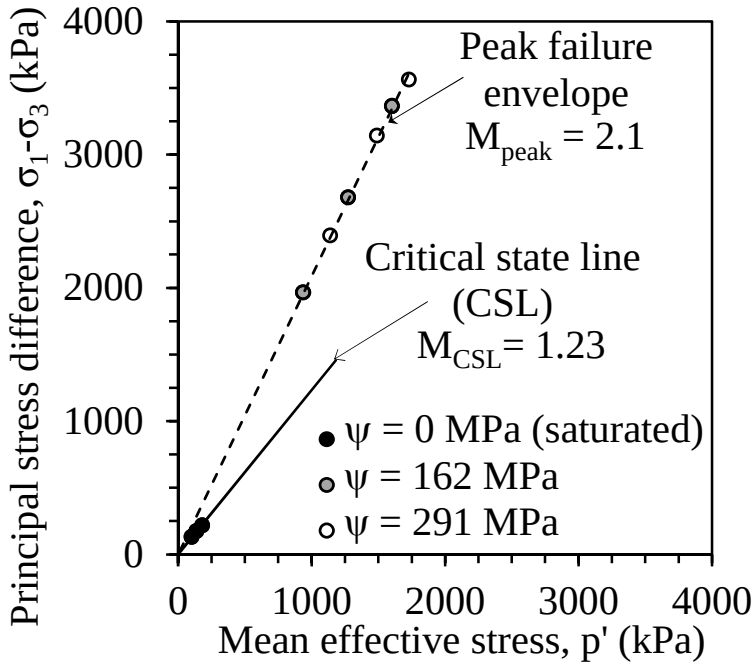

Figure 7.3: Critical state analysis for Bonny silt at different suction values obtained using the experimental SSCC parameters: Mean effective stress plot with mean effective stress obtained using the experimental SSCC

Another interesting observation from the results in Figure 7.3 is the fact that the specimens exhibited a clear linear relationship between peak shear strength and mean effective stress. This indicated that the effective stress definition of Skempton (1961) in Eq. 2.6 in Section 2.4 is not necessary to describe the effective stress state in unsaturated silt under low degrees of saturation. In other words, the compressibility of the soil skeleton, which increased significantly during application of the high suction magnitudes, is likely still much greater than that of the soil particles. This conclusion may have been different if suction was applied to the specimens before the application of the net normal stress value, which is a topic that deserves further study in the future.

*7.3.*Analysis of Nonisothermal Test Results

7.3.1.Evaluation of the Critical State Line for High Suction and High Temperature

The drained failure envelopes for the specimens tested at ambient temperature and those tested following the T-S and S-T paths are shown in Figure 7.4(a). The peak shear strength increases linearly with net confining stress, and the total friction angle appears to not be affected by temperature or suction. However, the apparent cohesion in this total stress plot was affected by changes in both temperature and suction. Despite having a slightly greater suction magnitude, the specimens following the T-S path consistently have a lower peak shear strength than the specimens tested at ambient temperature and a suction of 291 MPa. This may imply that the softening effect due to heating at a relatively high degree of saturation was greater than the hardening effect associated with suction application. This behavior is consistent with the observations of Hueckel and Baldi (1990) for the effects of temperature on the peak shear strength of saturated, heavily-overconsolidated clay. The specimens tested following the S-T path consistently have a greater peak shear strength than the specimens tested at ambient temperature. Although the results in Figure 9 for the tests following the S-T path and the ambient temperature tests indicate that there is some variability in the void ratio at the end of suction application, the specimens tested following the S-T path should ideally have a slightly greater void ratio due to the thermal expansion. The main difference between these tests was the lower degree of saturation for the tests following the S-T path due to drying during heating. If the effective saturation were used as the effective stress parameter, as assumed by Lu et al. (2010), this should lead to a lower effective stress and a lower shear strength. The results from the S-T tests indicate that the degree of saturation may have the opposite effect on the effective stress at high suction magnitudes and high temperatures than that expected at low suction magnitudes.

Heating of a soil under relatively dry conditions may cause the water in adsorbed films to expand and collect around the particle contacts for greater particle interaction. For the test performed with a heating-cooling cycle, the peak shear strength was found to be slightly higher than that from the test performed at the same net confining stress and suction that had not experienced heating. This gain in peak shear strength can be attributed to the slightly greater decrease in void ratio during suction application, as well as the slight permanent contraction upon cooling.

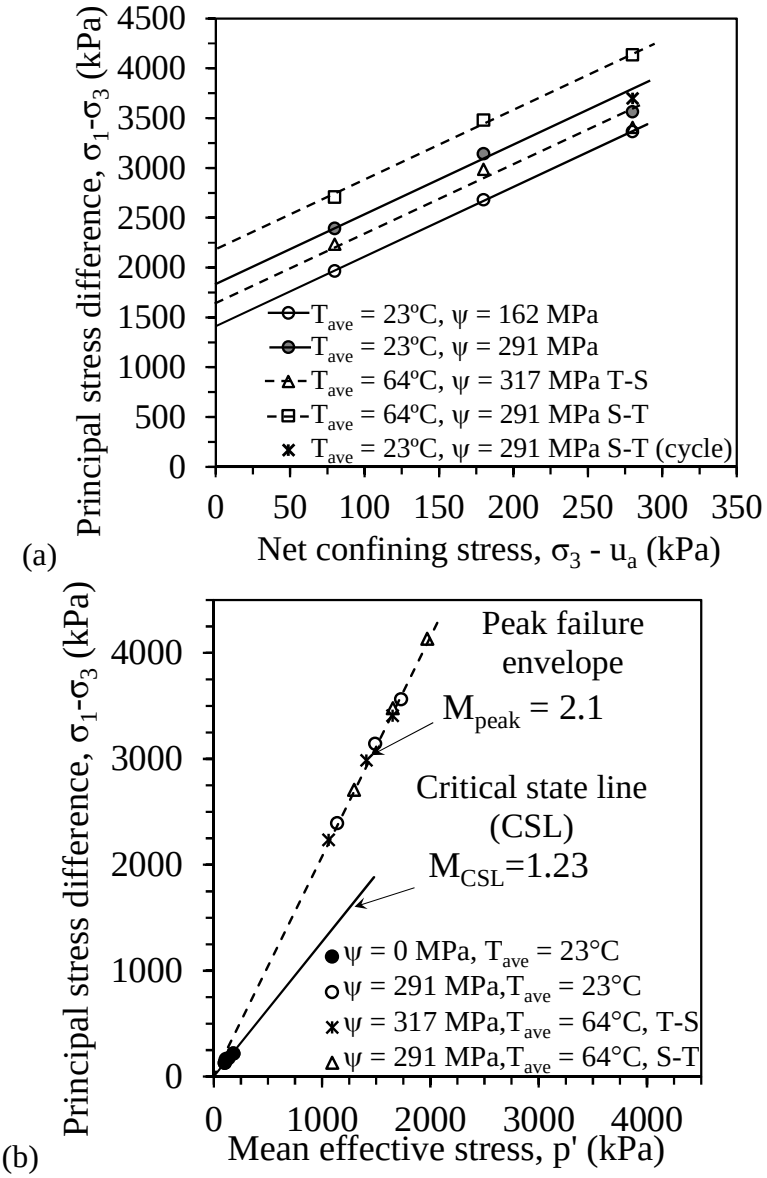

Figure 7.4: Triaxial compression results for specimens following different testing paths: (a) Total stress analysis of peak failure envelopes (not to scale); (b) Effective stress analysis of peak shear strength and critical state lines

As the soils appear to still show a frictional response under high suctions, the principle of effective stress can be investigated for these conditions. The effective stress was defined following similar procedure to the one followed in defining the effective stresses in Figure 7.3. It is assumed that the suction stress values calculated from each of the failure envelopes and reported in Tables 6.2 and 6.4 fall onto different SSCCs that depend on the temperature and testing path. Despite the high suction magnitudes considered in this study, the magnitudes of experimental suction stress listed in Tables 6.2 and 6.4 are on the same order of magnitude as the mean net stress at the beginning of shearing, indicating that it is reasonable for the soil to exhibit the frictional response observed in Figure 7.4(a). The peak shear strength values plotted as a function of the mean effective stress calculated using the experimentally-derived suction stress values are shown in Figure 7.4(b). Regardless of the temperature and testing path, the peak shear strength values define a single peak failure envelope having a slope of M = 2.1. The critical state line (CSL) extrapolated from the tests on saturated specimens tests in isotropic consolidated undrained tests are also shown in Figure 7.4(b). It is clear that the peak failure envelope is steeper than the CSL, confirming that the brittle failure mechanism prevented the specimens from reaching critical state. Nonetheless, the fact that the shear strength of the unsaturated specimens tested at different net normal stresses and high suction magnitudes and temperatures have peak shear strength values that converge on a single failure envelope reflects the validity of the effective stress principle at high suction magnitudes and high temperatures. The behavior of the specimens at high suctions is consistent with the behavior of heavily overconsolidated soils, which reach a peak shear strength value when the effective stress path intersects the steady-state boundary surface.

To better interpret the impact of testing path on the behavior of unsaturated specimens tested following the T-S and S-T paths, the secant moduli at an axial strain of 0.5%, which is assumed to represent elastic conditions, were calculated from the shear stress-strain curves in Figure 6.15. The change in secant moduli for the specimens sheared under elevated temperature with respect to the moduli for the specimens tested at a similar net confining stress and ambient temperature is shown in Figure 7.5. In general, specimens that were heated after application of high suction (S-T path) experienced an increase in secant modulus, while those that were heated under as-compacted conditions followed by application of high suction do not experience a significant change in secant modulus except at low net confining stresses. This increase in secant modulus may be attributed to the further removal of pore water during heating in the tests following the S-T path, which generally had a degree of saturation that was 3% lower than the other tests. This explanation indicates that a reduction in the degree of saturation when heating soils near residual saturation induces hardening and an increase in stiffness.

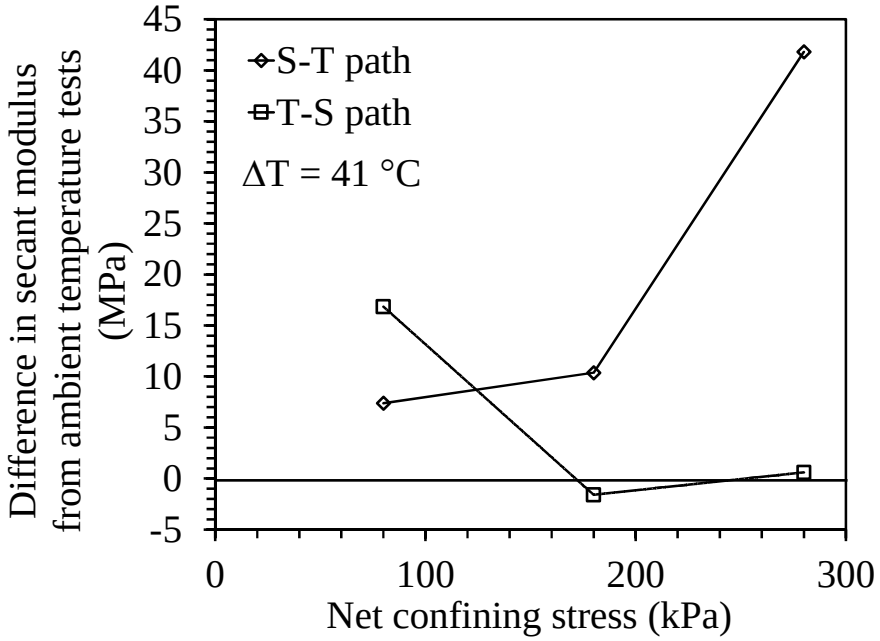

Figure 7.5: Influence of temperature changes on the change in secant modulus from the value at ambient temperature for tests following different paths

7.3.2 *Constitutive Modelling of Temperature Effects on Soil Behavior*

7.3.2.1 Impact of Temperature on SWRC and SSCC

As the suction stress concept was found to be useful in interpreting the shear strength of the specimens tested under different temperatures and following different paths, linkages between the SWRC and SSCC for high suctions and temperatures were first explored using the nonisothermal SWRC model of Grant and Salehzadeh (1996). Their model is given as follows:

$$S_e = \frac{S_r - S_{r,res}}{1 - S_{r,res}} = \left\{ \frac{1}{\left[\alpha_{GS} \psi_{(T=T_r)} \left(\frac{\beta_0 + T_r}{\beta_0 + T_f} \right) \right]^{\lambda_{GS}} + 1} \right\}^{\frac{(\lambda_{GS}-1)}{\lambda_{GS}}} \quad \text{Eq. 7.1}$$

The values of T_r and T_f in this equation should be defined in Kelvin. A value of β_0 of -400 K was used in this analysis as Grant and Salehzadeh (1996) and She and Sleep (2008) observed that this was a reasonable value for silts during drainage. The results of this model for an initial temperature of T_r = 296 K and final temperatures of T_f = 296 K (ambient temperature tests) and 337 K (elevated temperature tests) are shown in Figure 7.6(a). The Grant and Salehzadeh (1996) model corresponds well with the SWRC points at ambient temperature from Figure 3.5(a) in Section 3.4. For elevated temperatures, the Grant and Salehzadeh (1996) model predicts a decrease in the air entry suction, and an overall downward shift in the SWRC in the direction of lower degrees of saturation. The model is not able to consider the decrease in the residual water content with temperature that is observed in the data. Lu et al. (2010) assumed that the suction stress was equal to the product of the effective saturation and the suction, so the effective saturation from Eq. 7.1 can be used to predict the SSCC from the shape of the Grant and Salehzadeh (1996) SWRC, as follows:

$$\sigma_s = (u_a - u_w)\left\{\frac{1}{\left[\alpha_{GS}\psi_{(T=T_r)}\left(\frac{\beta_0 + T_r}{\beta_0 + T_f}\right)\right]^{\lambda_{GS}} + 1}\right\}^{\frac{(\lambda_{GS}-1)}{\lambda_{GS}}} \quad \text{Eq. 7.2}$$

The SSCCs predicted using the Grant and Salehzadeh (1996) SWRC model and the parameters reported in Figure 7.6(a) are presented in Figure 7.6(b). The suction stress points defined from the peak shear strength envelopes shown in Tables 6.2 and 6.4 are also shown in this figure for comparison. The SSCC predicted from the Grant and Salehzadeh (1996) corresponds well with the points from the ambient temperature tests. The lower values of degree of saturation predicted using the Grant and Salehzadeh (1996) model at elevated temperatures lead to a decrease in suction stress, albeit by a greater amount than that observed in the experiments. Alternatively, the suction stress can also be characterized using the effective stress parameter of Khalili and Khabbaz (1998) using Eq. 2.8 in Section 2.4, as follow:

$$\sigma_s = \psi\left\{\frac{\psi}{\psi_{aev}}\right\}^{-0.55}, \psi \geq \psi_{aev} \quad \text{Eq. 7.3}$$

The SSCCs predicted with Equation 7.3 using the air entry suction values from the Grant and Salehzadeh (1996) SWRC curves shown in Figure 7.6(a) are also shown in Figure 7.6(b). This model has a slightly different trend in suction stress with increasing suction, and generally provides a better fit to the ambient temperature and T-S path data.

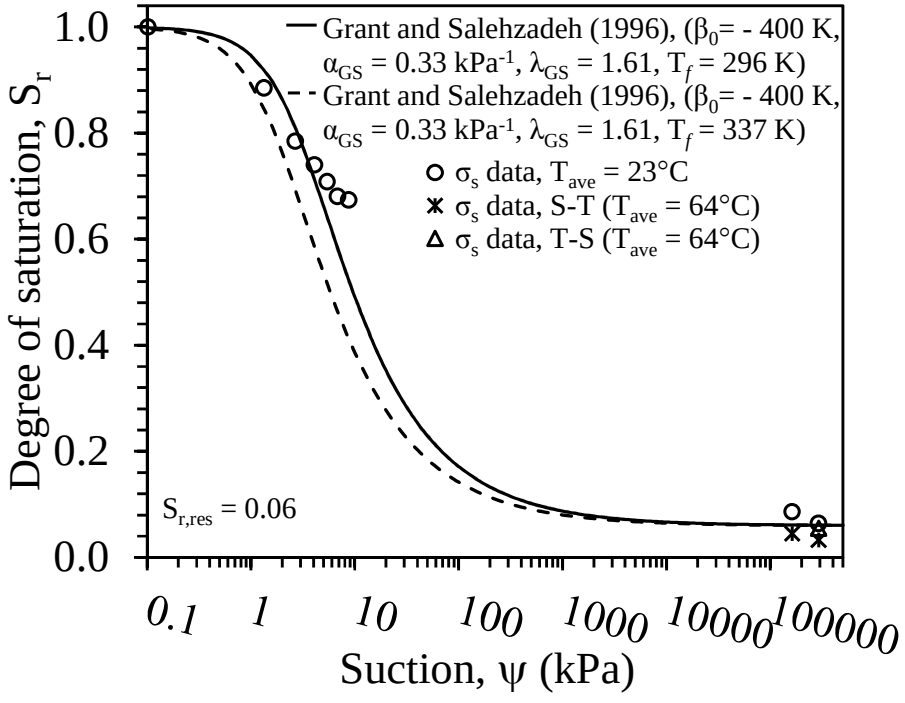

(a)

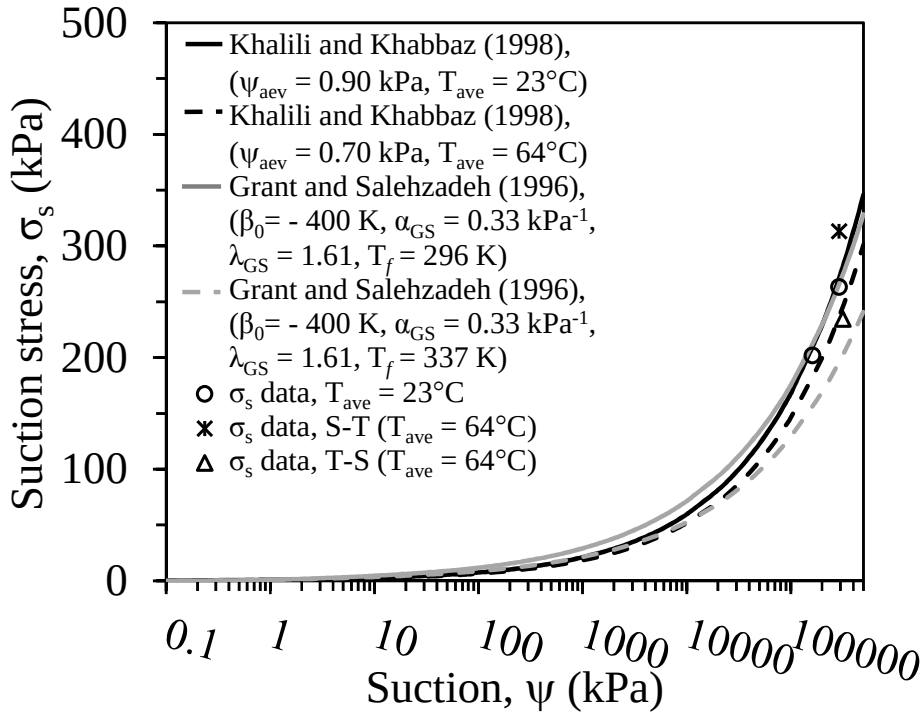

(b)

Figure 7.6: (a) Comparison of measured SWRC data with the Grant and Salehzadeh (1996) SWRC model; (b) Measured SSCC data and predicted SSCC curves

A comparison between the experimental suction stress values with those predicted using Equation 7.3 with the air entry suction values from Figure 7.6(a) is shown in Figure 7.7. Although Equation 7.3 provides a good match for the specimens tested at ambient temperature and following the T-S path, it is clear that it underestimates the suction stress for the specimens tested following the S-T path. A possible explanation is that the specimens tested following the S-T path may have experienced a reduction in the pore size distribution during the volumetric contraction associated with application of high suction magnitudes, leading to an increase in the air entry suction (Ng and Pang 2000). Further changes may have occurred due to drying during heating, leading to a greater air entry suction than at ambient temperature. A greater value of air entry suction of 1.17 kPa was found to provide a good fit to the experimental suction stress value for the S-T path tests using Equation 7.3. This data point is also plotted in Figure 7.7. More research is required to understand that effects that the nonisothermal testing path may have on the shape of the SWRC.

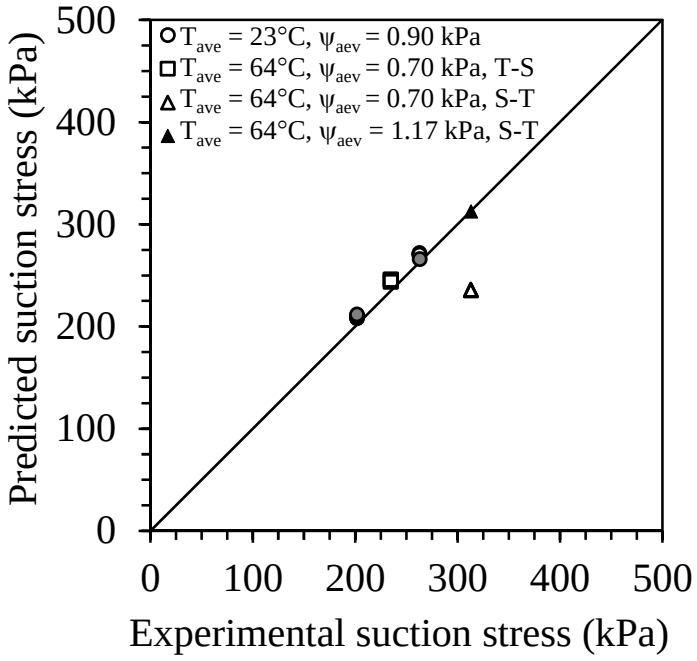

Figure 7.7: Comparison of measured suction stress values and values predicted from the model of Khalili and Khabbaz (1998)

7.3.2.2 Impact of Temperature on the Preconsolidation Stress

The thermo-mechanical constitutive model developed by Uchaipichat (2005) was used to interpret the impact of temperature on the yield surface and the preconsolidation stress for the compacted unsaturated silt specimens evaluated in this study. As test results in this study can be interpreted well in terms of mean effective stress, the constitutive relationships for saturated and unsaturated conditions are expected to be similar. A summary of the parameters used for modelling the yield locus and preconsolidation stresses for saturated and unsaturated compacted Bonny silt is presented in Table 7.1. The value of M was defined from isotropic triaxial compression tests on saturated specimens, and the values of λ and k were defined from the oedometer compression tests reported in Figure 3.9(b) in Section 3.6. The preconsolidation stresses at failure for the different triaxial compression tests performed in this study were defined by assuming that the measured values of peak shear strength define points on the steady-state boundary surface (q_{peak}, p'_{peak}). Specifically, all three tests on specimens having the same suction, temperature and testing path are expected to fall on the same steady-state boundary surface. The preconsolidation stress p'_c can be estimated by fitting the model of Uchaipichat (2005) to the experimental data points. The value of p'_c can be defined by satisfying the equality of Eq.2.23. The parameter M was assumed to be the value from the saturated, isotropic CSL, the spacing ratio parameter r is equal to p'_c/p'_{CSL} and the value of α was selected to be 0.7 to fit the experimental data. The value of α is close to the value of 0.7 recommended by Uchaipichat (2005) for frictional soils.

Table 7.1: Summary of the parameters for the yield locus of Uchaipichat (2005) and the Cam-clay model parameters for compacted Bonny silt

Parameter	Value
M_{CSL}	1.23
α	0.6
r	1.4
λ	0.11
κ	0.03
$N_{initial}$	2.33
$v_{\kappa,initial}$	1.86
$N_{suction\text{-}TS}$	2.54
$v_{\kappa\text{-}suction\text{-}TS}$	1.82
$N_{heat\text{-}ST}$	2.5
$v_{\kappa\text{-}heat\text{-}ST}$	1.76

The effects of suction on the yield locus and corresponding preconsolidation stress for tests at ambient temperature are shown in Figure 7.8(a). Although the shape of the yield surface is not particularly sensitive to the preconsolidation stress for low net stress values, the data points fit relatively well with the model. The yield locus increases in size with an increase in suction from 162 to 291 MPa. The effects of temperature on the yield locus using Equation 8 for soil specimens tested following the T-S and S-T paths are shown in Figure 7.8(b). Assuming that temperature primarily controls the preconsolidation stress, the results of this analysis indicate that the yield locus shrinks with increasing temperature for specimens tested following the T-S path and expands with increasing temperature for specimens following the S-T path. Because all of the tests define a single peak failure envelope, the hypothesis of Hueckel et al. (2009) that temperature could affect the value of the slope of the CSL was not considered.

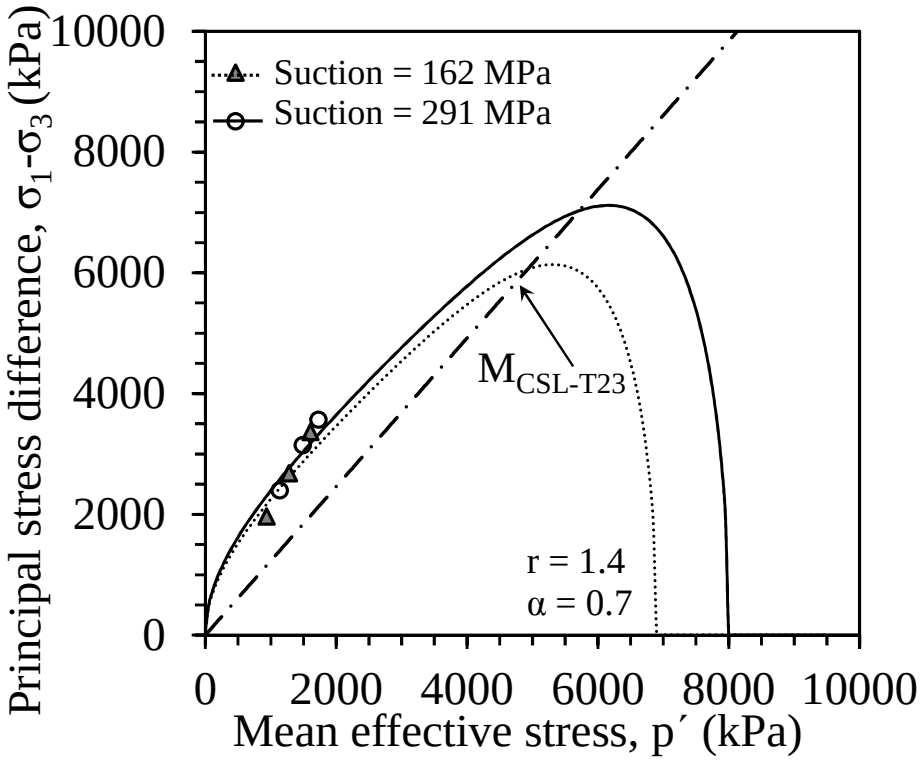

(a)

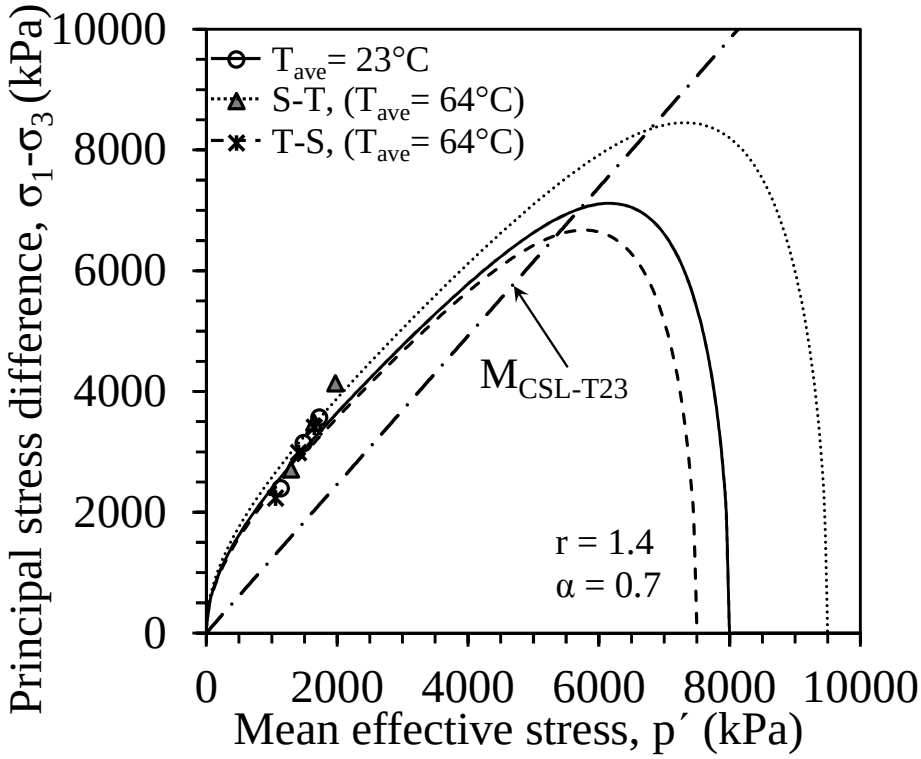

(b)

Figure 7.8: Evaluation of changes in preconsolidation stress: (a) Impact of suction and net confining stresses at ambient temperature; (b) Impact of temperature and testing path

As mentioned in the discussion of Figure 6.10 in Section 6.3.3, suction application is expected to have an effect on the effective stress and the preconsolidation stress. Using the predictive equations for effective stress (Equation 7.3 using an air entry suction of 1.17 kPa) and preconsolidation stress (analysis in Figure 7.8), the changes in effective stress, preconsolidation stress as a function of suction are shown in Figure 7.9(a) for a specimen tested following the S-T path at a confining stress of 200 kPa. The results in Figure 7.9(a) indicate that during application of a suction of 291 MPa, the increase in preconsolidation stress is much greater than the increase in the mean effective stress. The OCR for the soil calculated as the ratio of preconsolidation stress to mean effective stress is also shown in Figure 7.9(a). The OCR is observed to increase nonlinearly during application of suction. It is not possible to assess the change in OCR of the specimen during heating following the T-S path because the preconsolidation stress before suction application is not known, and is expected to be lower than the value of 400 kPa measured in the oedometer test due to the effects of thermal softening. However, the effects of suction on the preconsolidation stress for different temperatures is shown in Figure 7.9(b). As only a simple point was measured on the curves for the T-S and S-T paths, the shape of the curve was assumed to be the same as that at ambient temperature.

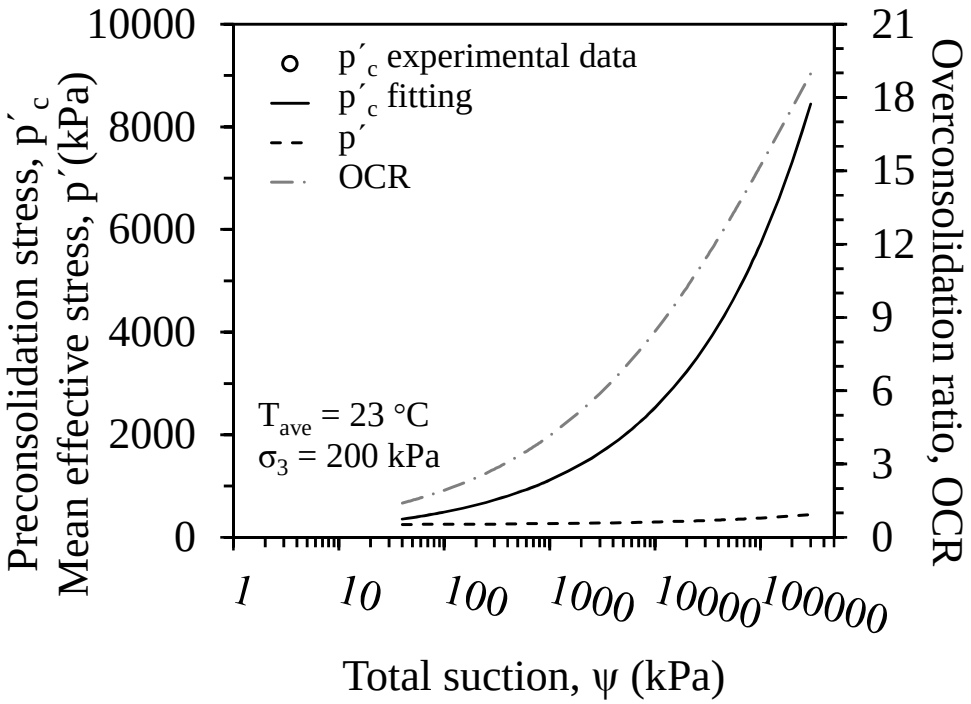

(a)

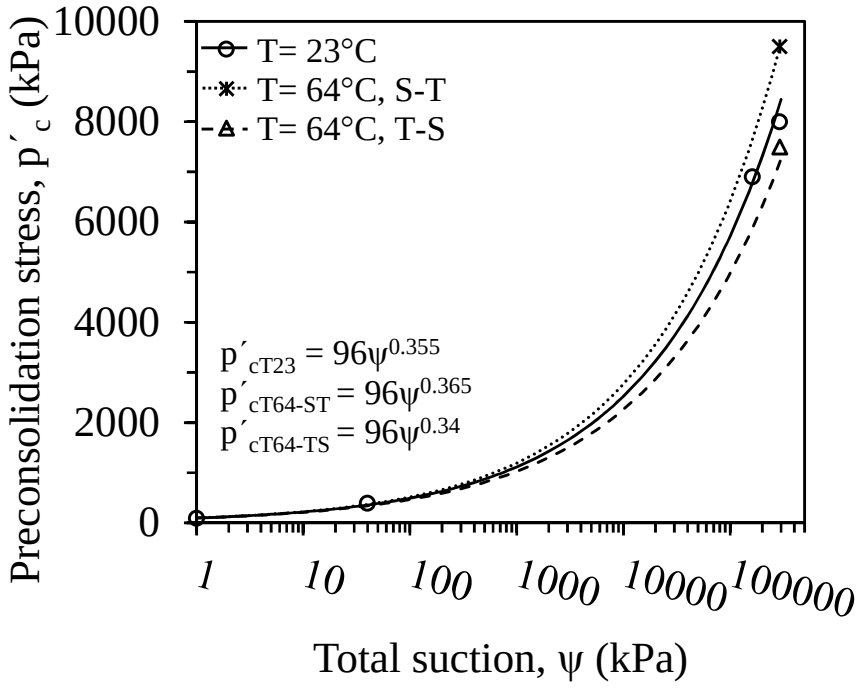

(b)

Figure 7.9: (a) Effect of suction on the effective stress, preconsolidation stress, and corresponding OCR for specimen at ambient temperature and a confining stress of 200 kPa; (b) Effect of suction on the preconsolidation stress for specimens at different temperatures and testing paths

7.3.2.3 Impacts of Temperature and Suction on the Volume Change Behavior

Using the understanding of the effective stress in unsaturated soil, along with the changes in the preconsolidation stress with suction and temperature, the effects of suction and temperature on the effective stress path in specific volume v versus the natural logarithm of the mean effective stress can be explored. In this analysis, the slopes of the CSL, recompression line (RCL), and virgin compression line (VCL) are assumed to be independent of temperature in effective stress space, but the VCL may shift to the left or right depending on path-dependent hardening or softening mechanisms. The parameters of the CSL, RCL, and VCL used in this evaluation are summarized in Table 7.1. The effective stress paths for a test following the T-S path performed at a confining stress of 200 kPa is shown in Figure 7.10(a). In this figure, the change in the specific volume was calculated using the void ratios from Figure 6.17, while the effective stress was calculated using the suction stress calculated using the Khalili and Khabbaz (1998) effective stress parameter in Equation 7.3. For the specimen following the T-S path, a small volumetric contraction without a change in effective stress was observed during drained heating, which was followed by an increase in effective stress and a large volumetric contraction during suction application. A small dilation was observed during shearing, along with an increase in the mean effective stress during drained triaxial compression. Although the decrease in effective stress due to temperature effects on the SWRC is likely the reason for the lower shear strength in the T-S path test, it is also possible that a greater amount of softening on the preconsolidation stress occurred due to the larger degree of saturation for these tests.

The effective stress path for a specimen following the S-T path performed at a confining stress of 200 kPa is shown in Figure 7.10(b). The specific volume was calculated in the same way as in Figure 7.10(a), but the effective stress was calculated by assuming that the air entry

value for the specimen following the S-T path increased. The effective stress path indicates that the specimen following the S-T path experienced an elastic contraction during initial confinement followed by a large plastic contraction during suction application. Application of a high suction also results in an increase in the mean effective preconsolidation stress, as shown in Figure 7.9. A small dilation was observed during shearing, along with an increase in the mean effective stress during drained triaxial compression.

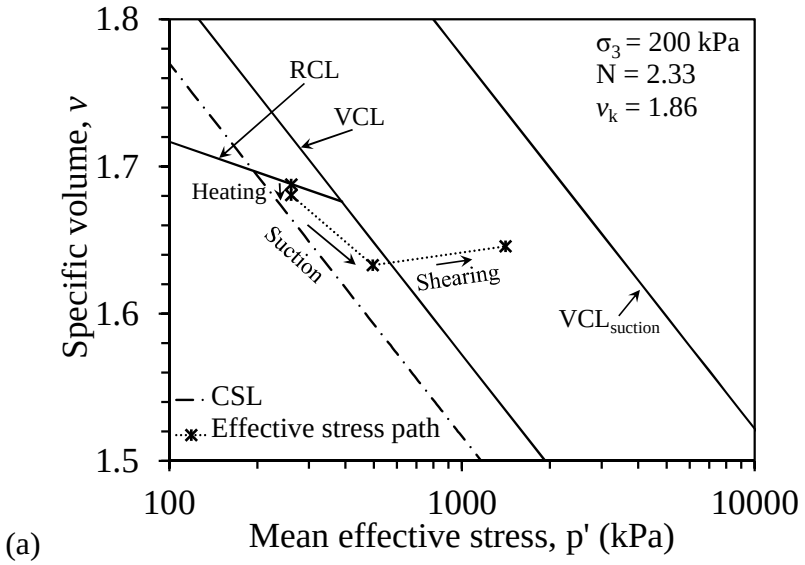

(a)

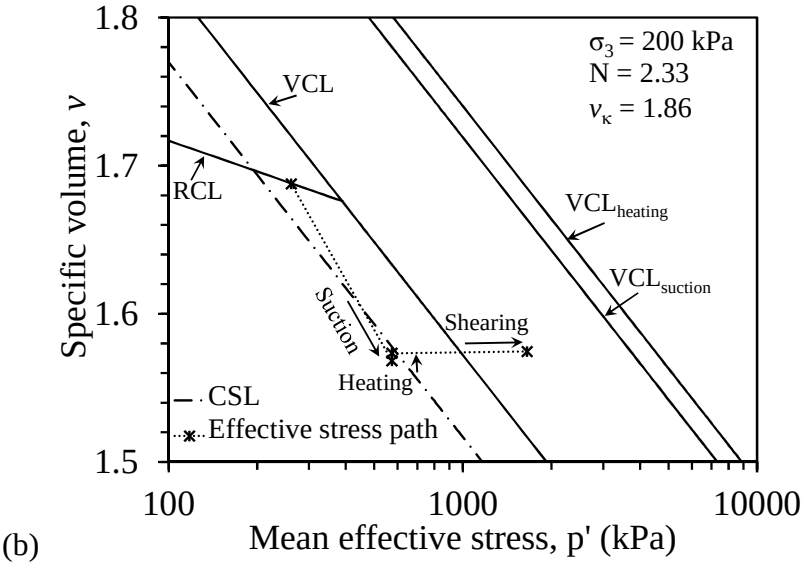

(b)

Figure 7.10: Effective stress paths during different stages of testing for specimens at a confining stress of 200 kPa: (a) T-S path, (b) S-T path

The estimated values of effective stress and preconsolidation stress at failure were used to estimate the overconsolidation ratio (OCR) of the unsaturated specimens. This permitted evaluation of the role of stress history on the ratio of the thermal volume change during heating to the change in temperature ($\Delta\varepsilon_v^T/\Delta T$) for unsaturated Bonny silt, as shown in Figure 7.11. The data for saturated Bonny silt reported by Vega and McCartney (2014) for multiple cycles of heating and cooling are shown in this figure for comparison. The trend in the saturated and unsaturated data for Bonny silt is consistent, and also follows the trends of the thermal volume change data of Uchaipichat and Khalili (2009) for compacted silt that was reinterpreted in terms of OCR by Stewart et al. (2014). During drained heating, the saturated and unsaturated specimens of Bonny silt expand under low mean effective stresses (high OCR), and contract under higher mean effective stresses (low OCR).

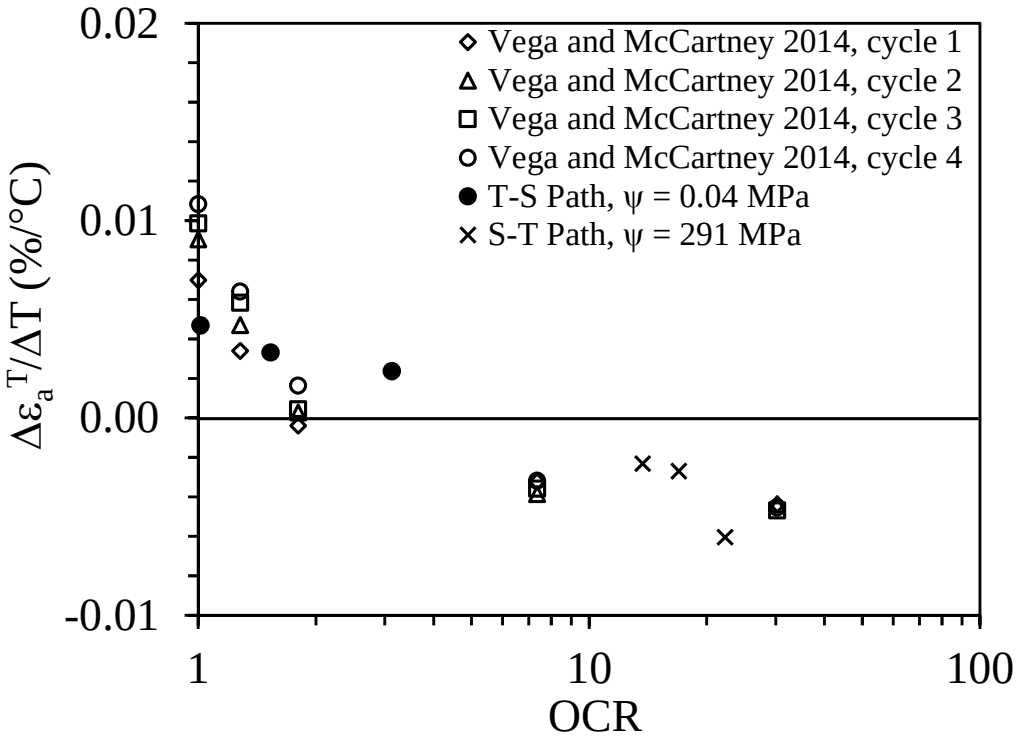

Figure 7.11: Impact of OCR on the thermal axial strains normalized by the change in temperature for compacted silt under saturated and unsaturated conditions

8. SUMMARY AND CONCLUSIONS

Isothermal and nonisothermal anisotropic drained triaxial compression tests were performed using a new triaxial cell following different testing paths to investigate the influence of high suction and temperature on the shear strength and volume change behavior of unsaturated, compacted silt. The vapor flow technique developed by Likos and Lu (2003) was shown to be an effective approach to reach high suction magnitudes in a relatively short period of time, and the temperature control system was observed to lead to uniform changes in specimen temperature. A modified mechanical loading system into triaxial testing was used successfully to assess the volume change behavior of silt during application of high suction magnitudes and elevated temperatures. The specific conclusions regarding the behavior of compacted silt under high temperatures and suctions that can be drawn from this study are as follows:

- The SWRC model parameters obtained by fitting the SWRC to data from axis translation tests at low suctions were found to overestimate the suction stress by a significant amount. This was proposed to be due to the large change in void ratio observed during application of high suction magnitudes. An alternative fitting of the SWRC model was found to provide a better prediction of the SSCC while still providing a reasonable fit to the SWRC data at low suctions, reflecting the importance of careful characterization of the SWRC when predicting the SSCC at high suctions.
- The suction stress interpreted from the peak failure envelopes in mean net stress space permitted definition of a single peak effective stress failure envelope that represented the shear strength behavior of the compacted silt in different temperatures, suctions, and following different testing paths. Although a clear peak failure envelope in terms of effective

mean stress was observed, the brittle stress strain curves did not permit evaluation of effective stresses at critical state for unsaturated specimens under high suction magnitudes. However, the slope of the peak failure envelope (M_{peak} = 2.1) was greater than the M value for critical state conditions ($M_{sat\text{-}CSL}$ = 1.23) defined using the consolidated undrained triaxial tests on saturated specimens. This behavior was consistent with that of heavily overconsolidated soils, which have a higher peak shear strength than the shear strength at critical state. This indicated that application of high suction magnitudes leads to a significant increase in preconsolidation stress in addition to the reduction in initial void ratio.

- Regardless of temperature, the shear stress-strain curves for all of the specimens tested at high suction magnitudes show a brittle failure mechanism that differed significantly from the shear stress-strains of the same soil sheared under saturated conditions. Because of this brittle failure mechanism, the unsaturated soil specimens could not be sheared until reaching critical state conditions.
- A substantial increase in shear strength was observed with total suction for the unsaturated soils under high suction magnitudes. A 30% increase in strength of the unsaturated soil was observed corresponding to an increase in total suction value of 129 MPa.
- If a suction value was imposed after heating, the shear strength was observed to decrease by 10% during a change in temperature of approximately 41 °C. If a suction value was imposed before heating, the shear strength was observed to increase by 20% during the same change in temperature.
- Silt specimens heated under as-compacted conditions before application of a high suction value experienced thermal softening that led to lower peak shear strength values than those measured in tests on specimens at high suction magnitudes performed under ambient

temperature. This behavior was consistent with that expected in the literature for overconsolidated soils.

- Greater peak shear strength values and greater secant moduli values were observed for specimens that were heated under high suction magnitudes than those observed for tests on soils at high suction magnitudes under room temperature conditions. This unexpected behavior was attributed to the lower degree of saturation of the specimens tested following S-T path, and it is hypothesized that the degree of saturation has a different effect on the stress state at high suction magnitudes near residual saturation conditions than for nearly-saturated soils.
- The thermal volume change was found to be dependent on the initial overconsolidation ratio of the unsaturated silt specimens prior to heating. Unsaturated silt specimens heated prior to suction implementation (T-S path) had an initially low overconsolidation ratio and experienced thermal contraction during heating. Unsaturated silt specimens heated after reaching suction equilibrium (S-T path) had a high overconsolidation ratio prior to heating, and experienced thermal expansion during heating.
- The data obtained from tests on specimens at high suction magnitudes indicated a shift the SWRC to a lower degree of saturation with elevated temperatures. The nonisothermal SWRC model of Grant and Salehzadeh (1996) also indicated a shift in the SWRC to a lower degree of saturation, although not at high suction magnitudes. The model also indicated a reduction in the air entry suction with temperature, which has an important effect on the effective stress.
- Different approaches were used to predict the change in suction stress with temperature. The approach of Khalili and Khabbaz (1998) to define the suction stress that uses the air entry

suction as a key parameter was observed to provide a good fit to the suction stress for the specimens sheared at ambient temperature and following the T-S path. The approach using the effective saturation to define the suction stress also provided a good fit. Neither approach was suitable to predict the increase in suction stress for specimens following the S-T path. However, a possible explanation is that suction application at ambient temperature followed by further drying during heating may have led to a change in the pore size distribution that caused an increase in the air entry suction compared to the ambient temperature tests.

- The preconsolidation stress inferred from the peak shear strength values and the shape of the Uchaipichat (2005) yield surface for soil specimens tested under high suction magnitudes was found to increase with temperature for tests following the S-T path and decrease when following the T-S path. It was also observed to be sensitive to the initial confining stress applied to the specimens. Although the change in behavior may be better explained using the possible changes in effective stress due to shifts in the SWRC, these results indicate that it is possible that a greater amount of softening during heating occurred at low suction values following the T-S path.
- The thermal axial strains for saturated and unsaturated silt specimens normalized by the change in temperature were observed to have similar magnitudes and follow a similar decreasing trend with the overconsolidation ratio estimated using the calculated effective stress and preconsolidation stress values.

REFERENCES

Abdel-Hadi, O.N. and Mitchell, J.K. (1981). "Coupled Heat and Water Flows around Buried Cables." Journal of the Geotechnical Engineering Division, ASCE. 107(11), 1461–1487.

Abuel-Naga, H.M., Bergado, D.T., Bouazza, A. and Pender, M. (2009). "Thermomechanical Model for Saturated Clays." Géotechnique. 59(3), 273–278.

Adam, D. and Markiewicz, R. (2009). "Energy from Earth-Coupled Structures, Foundations, Tunnels and Sewers." Géotechnique. 59(3), 229–236.

Ajdari, M., Habibagahi, G., Nowamooz, H., Masrouri, F. and Ghahramani, A. (2010). "Shear Strength Behavior and Soil Water Retention Curve of a Dual Porosity Silt-Bentonite Mixture." Scientica Iranica Transactions. 17, 430–440.

Alonso, E.E., Gens, A. and Josa, A. (1990). "A Constitutive Model for Partially Saturated Soils." Géotechnique. 40(3), 405-430.

Alonso, E.E. and E. Romero. (2011). "Experimental Investigation on an Effective Stress Law in Compacted Clayey/Silty Soil." Unsaturated Soils: Theory and Practice, pp. 331-336.

Alsherif, N. and McCartney, J.S. (2012). "Nonisothermal Shear Strength of Unsaturated Soils under High Suction Magnitudes." 2nd European Conference on Unsaturated Soils, Italy. 8 pg.

ASTM D2435 (2011). "Standard Test Methods for One-Dimensional Consolidation Properties of Soils Using Incremental Loading." ASTM International, West Conshohocken, PA.

ASTM D4767 (2011). "Standard Test Method for Consolidated Undrained Triaxial Compression Test for Cohesive Soils." ASTM International, West Conshohocken, PA.

ASTM D6836. (2008). "Test Methods for Determination of the Soil Water Characteristic Curve for Desorption Using a Hanging Column, Pressure Extractor, Chilled Mirror Hygrometer, and/or Centrifuge." ASTM International, West Conshohocken, PA.

ASTM D698 (2012). "Standard Test Method for Laboratory Compaction Characteristics of Using Standard Effort." ASTM International, West Conshohocken, PA.

Baldi, G., Hueckel, T. and Pelegrini, R. (1988). "Thermal Volume Changes of the Mineral-Water System in Low-Porosity Clay Soils." Canadian Geotechnical Journal. 25, 807-825.

Belanteur, N., Tacherifet, S. and Pakzad., M. (1997). "Étude des Comportements Mécanique, Thermo-mécanique et Hydro-mécanique des Argiles Gonflantes et non Gonflantes Fortement Compactées." Revue Française de Géotechnique 78, 31-50.

Bishop, A.W. (1959). “The Principle of Effective Stress.” Teknisk Ukeblad I Samarbeide Med Teknikk, Oslo, Norway. 106(39), 859–863.

Bishop, A.W. and Donald, I.B. (1961). “The Experimental Study of Partly Saturated Soil in Triaxial Apparatus.” Proceedings of the 5th International Conference on Soil Mechanics and Foundation Engineering. Paris, France. 13-21.

Blatz, J.A. and Graham, J. (2000). “A System for Controlled Suction in Triaxial Tests.” Géotechnique. 50(4), 465–478

Blatz, J.A. and Graham, J. (2003). “Elastic Plastic Modeling of Unsaturated High-Plastic Clay Using Results from a New Triaxial Test with Controlled Suction.” Géotechnique 53(1), 113–122

Blatz, A.J., Graham, J. and Chandler, N.A. (2002). “Influence of Suction on the Strength and Stiffness of Compacted Sand-Bentonite,” Canadian Geotechnical Journal. 39, 1005-1015.

Blatz, A.J., Cui, Y.J. and Oldecop, L.A. (2008). “Vapour Equilibrium and Osmotic Technique for Suction Control,” Geotech. Geol. Eng. doi:10.1007/s10706-008-9196-1.

Blight, G.E. (1967). “Effective Stress Evaluation for Unsaturated Soils.” Géotechnique. 46(2), 279-289.

Boudali, M., Leroueil, S. and Murthy, B.R.S. (1994). “Viscous Behavior of Natural Clays”. In Proceedings of the 13th International Conference on Soil Mechanics and Foundation Engineering. New Delhi. January 5-10. 1, 411–416.

Bourne-Webb, P.J., Amatya, B., Soga, K., Amis, T., Davidson, C. and Payne, P. (2009). “Energy Pile Test at Lambeth College, London: Geotechnical and Thermodynamic Aspects of Pile Response to Heat Cycles.” Géotechnique. 59(3), 237–248.

Brandl, H. (2006). “Energy Foundations and Other Thermo-Active Ground Structures.” Géotechnique. 56(2), 81-122.

Brandon, T.L., Mitchell, J.K. and Cameron, J.T. (1989). “Thermal Instability in Buried Cable Backfills.” Journal of Geotechnical Engineering. 115(1), 38-55.

Brooks, R.H. and Corey, A.T. (1964). “Hydraulic Properties of Porous Media.” Hydrology Paper No. 3. Colorado State University. Fort Collins, USA.

Burghignoli, A., Desideri, A. and Miliziano, S. (1992). “Deformability of Clays under Non-Isothermal Conditions.” Revista Italiana di Geotechnica. 4/92, 227-236.

USBR5755-89. “Procedure for Performing Consolidated-Drained Triaxial Shear testing of Soils.” United States Department of the Interior Bureau of Reclamation.

Campanella, R.G. and Mitchell, J.K. (1968). “Influence of Temperature Variations on Soil Behavior.” Journal of the Soil Mechanics and Foundation Engineering Division. 94(3), 709–734.

Cekerevac, C. and Laloui, L. (2004). “Experimental Study of Thermal Effects on the Mechanical Behaviour of a clay.” International Journal of Numerical and Analytical Methods in Geomechanics. 28(3), 209–228.

Chen, W.F. (1984). “Soil Mechanics, Plasticity and Landslides.” In: G.J. Dvorak and R.T. Shield (Editors), Mechanics of Material Behavior. Elsevier, Amsterdam, Netherlands, pp. 31-58

Coccia, C.J.R. and McCartney, J.S. (2013). “A Thermo-Hydro-Mechanical True Triaxial Cell for Evaluation of the Impact of Anisotropy on Thermally Induced Volume Changes in Soils.” Geotechnical Testing Journal. 35(2), 1-11.

Cui, Y. J. and Delage, P. (1996). “Yielding and Plastic Behavior of an Unsaturated Compacted Silt.” Géotechnique. 46(2), 291-311.

Cui, Y.J., Sultan, N. and Delage, P. (2000). “A Thermomechanical Model for Clays.” Canadian Geotechnical Journal. 37(3), 607–620.

Cunningham, M. R., Ridley, A. M., Dineen, K. and Burland, J.B. (2003). “The Mechanical Behavior of a Reconstituted Unsaturated Silty Clay.” Géotechnique 53(2):183–194

Cuisinier, O. and Masrouri, F. (2004). “Testing the Hydromechanical Behavior of a Compacted Swelling Soil.” Geotechnical Testing Journal. 27(6), 598-606.

Delage, P. and Cui, Y.J. (2000). “L'Eau Dans les Sols Non Saturés.” Techniques de l'Ingénieur, C301, Traité Construction, Vol. C2.

Delage, P., Cui, Y.J. and Sultan, N. (2004). “On the Thermal Behaviour of Boom clay.” Proceedings Eurosafe 2004 Conference, Berlin, CD-ROM, 8 pg.

Delage, P., Cui, Y.J., Yahia-Aissa, M. and De Laure, E. (1998). “The Unsaturated Hydraulic Conductivity of a Dense Compacted Bentonite.” 2nd International Conference on Unsaturated Soils. Beijing, China. pp. 27–30.

Delage, P., Silva, G.P.R.S.d., and Delaure, E., (1987). “A New Triaxial Apparatus for Non-saturated Soils.” European Conference on Soil Mechanics and Foundation Engineering,

Proceedings of the 9th ECSMFE, Groundwater Effect in Geotechnical Engineering, pp. 25-28.

Delage, P., Sultan, N. and Cui, Y.J. (2000). "On the Thermal Consolidation of Boom Clay." Canadian Geotechnical Journal. 37, 343-354.

Delage, P., Romero, E. and Tarantino, A. (2008). "Recent Developments of Controlling and Measuring Suction in Unsaturated Soils." Proceedings of the 1st European Conference on Unsaturated Soils, Durham, 33-52.

Demars, K.R. and Charles, R.D. (1982). "Soil Volume Changes Induced by Temperature Cycling." Canadian Geotechnical Journal. 19, 188–194.

Dumont, M., Taibi, S., Fleureau, J.M., Abou-Bekr, N., and Saouab, A. (2011). "A Thermo-Hydro-Mechanical Model for Unsaturated Soils Based on the Effective Stress Concept." International Journal of Numerical and Analytical Method in Geomechanics, 35(12), 1299–1317.

Escario, V. (1969). "Swelling of Soils in Contact with Water at a Negative Pressure." Proceedings, 2nd International Conference on Expansive Soils. Texas A&M Univ. pp 207-217.

Escario, V. (1980). "Suction Controlled Penetration and Shear Tests." Proceedings of the 4th International Conference on Expansive Soils. Vol II. Denver, CO. ASCE, pp. 781–797.

Escario, V., and Saez, J., (1986). "The Shear Strength of Partly Saturated Soils." Géotechnique, 36(3), 453-456.

Estabragh, A.R. and Javadi, A.A. (2012) "Effect of Suction on Volume Change and Shear Behavior of an Overconsolidated Unsaturated Silty Soil." Geomechanics and Engineering. 4(1), 55-65

Esteban Moratilla F. (1990). "Caracterizacion Experimental de la Expansividad de una Roca Evaporitica." Identificacion de los mecanismos de hinchamiento. PhD Thesis, Universidad de Cantabria, Santander, 352 p.

Eriksson, L.G. (1989). "Temperature Effects on Consolidation Properties of Sulphide Clays." In Proceedings of the 12th International Conference on Soil Mechanics and Foundation Engineering. Rio de Janeiro. August 13-18. 12: 2087-2090.

Francois, B. Salager, S., El Youssoufi, M.S., Ubals Picanyoul, D., Laloui, L., and Saix, C. (2007). “Compression Tests on a Sandy Silt at Different Suction and Temperature Levels.” GSP 157: Computer Applications in Geotechnical Engineering. 10 pg.

Fredlund, D.G. and Morgenstern, N.R. (1977). ‘‘Stress State Variables for Unsaturated Soils.’’ ABB Rev., 103(5), 447–466.

Fredlund, D.G. and Xing, A. (1994). “Equations for the Soil-Water Characteristic Curve.” Canadian Geotechnical Journal. 31, 521-532.

Gallipoli, D., Wheeler, S.J. and Karstunen, M. (2003). “Modelling the Variation of Degree of Saturation in a Deformable Unsaturated Soil.” Géotechnique. 53(1), 105-112.

Gardner W. (1958). “Some Steady-State Solutions of the Unsaturated Moisture Flow Equation with Applications to Evaporation from a Water Table.” Soil Science. 85, 228-232.

Gens, A. (2010). “Soil–Environment Interactions in Geotechnical Engineering.” Géotechnique. 60(1), 3–74.

Gens, A., Garcıa-Molina, A.J., Olivella, S., Alonso, E.E. and Huertas, F. (1998). “Analysis of a Full Scale in Situ Test Simulating Repository Conditions.” International Journal of Numerical and Analytical Methods in Geomechnics. 22, 515–548.

Ghembaza, M.S., Taïbi, S. and Fleureau, J.M. (2007). “Effet de la Température sur le Comportement Des sols Non Saturés sur les Chemins de Drainage et D’Humidification.” Canadian Geotechnical Journal. 44(9), 1061-1081.

Graham, J., Wiebe, B., Tang, X., and Onofrei, C. (1995). “Strength and Stiffness of Unsaturated Sand–Bentonite ‘Buffer’.” In Proceedings of the 1st International Conference on Unsaturated Soils, Paris. Edited by E.E. Alonso and P. Delage. A.A. Balkema, Rotterdam, pp. 89–94

Graham, J., Tanaka, N., Crilly, T. and Alfaro, M. (2001). “Modified Cam-Clay Modeling of Temperature Effects in Clays.” Canadian Geotechnical Journal. 38(3): 608–621.

Grant, S.A. and Salehzadeh, A. (1996). “Calculations of Temperature- Effects on Wetting Coefficients of Porous Solids and Their Capillary Pressure Functions.” Water Resources Research. 32, 261–279.

Gray, W.G. and Schrefler, B.A. (2001). “Thermodynamic Approach to Effective Stress in Partially Saturated Porous Media.” European Journal of Mechanics, A/Solids. 20(4), 521–538.

Habibagahi, K. (1973). “Temperature Effect on Consolidation Behavior of Overconsolidated Soils.” Proceedings, 8th International Conference on Soil Mechanics and Foundation Engineering, pp. 159-163.

Hassanizadeh, S.M. and W.G. Gray. (1990). “Mechanics and Thermodynamics of Multiphase Flow in Porous Media Including Interphase Boundaries.” Advances in Water Resources. 13(4), 169–186.

Hoffmann, C., Romero, E. and Alonso, E.E. (2005). “Combining Different Controlled-Suction Techniques to Study Expansive Clays.” Proc. Int. Symposium on Advanced Experimental Unsaturated Soil Mechanics, Trento, Italy, June 27-29, 2005. A. Tarantino, E. Romero and Y.J. Cui (eds.). A.A. Balkema, Leiden: 61-67.

Houston, S.L., Houston, W.N., and Williams, N.D. (1985). “Thermo-Mechanical Behavior of Seafloor Sediments.” Journal of Geotechnical Engineering. 111(12), 1249-1263.

Houlsby, G.T. (1997). “The Work Input to an Unsaturated Granular Material.” Géotechnique. 47(1), 193-196.

Hueckel, T. and Baldi, M. (1990). “Thermoplasticity of Saturated Clays: Experimental Constitutive Study.” Journal of Geotechnical Engineering, 116(12), 1778–1796.

Hueckel, T. and Borsetto, M. (1990). “Thermoplasticity of Saturated Soils and Shales: Constitutive Equations.” Journal of Geotechnical Engineering. 116(12), 1765-1777.

Hueckel, T., Pellegrini, R., and Olmo, C.D., (1998). “A Constitutive Study of Thermo-Elasto-Plasticity of Deep Carbonatic Clays.” International Journal for Numerical and Analytical Methods in Geomechanics. 22, 549-574.

Hueckel, T., François, B. and Laloui, L. (2009). “Explaining Thermal Failure in Saturated Clays.” Géotechnique. 59(3), 197–212.

Imbert, C., Olchitzky, E., Lassabatere, T., Dangla, P. and Courtois, A. (2005). “Evaluation of a Thermal Criterion for an Engineered Barrier System.” Engineering Geology. 1, 269–283

Jennings, J.E.B. and Burland, J.B. (1962). “Limitations to the Use of Effective Stresses in Partly Saturated Soils.” Géotechnique. 12(2), 125-144.

Kanno, T., Fujita, T., Ishikawa, H., Hara, K., and Nakano, M. (1999). “Coupled Thermo-Hydro-Mechanical Modelling of Bentonite Buffer Material.” International Journal of Numerical and Analytical Methods in Geomechanics. 23, 1281–1307.

Kayadelen, C., M.A., Tekinsoy, and T. Taskıran. (2007). “Influence of Matric Suction on Shear Strength Behavior of a Residual Clayey Soil.” Environmental Geology. 53(4), 891-901.

Khalili, N., Geiser, F. and Blight, G.E. (2004). “Effective Stress in Unsaturated Soils: Review with New Evidence.” International Journal of Geomechanics. 4(2), 115-126.

Khalili, N. and M.H. Khabbaz. (1998). “A Unique Relationship for the Determination of the Shear Strength of Unsaturated Soils.” Géotechnique. 48(5), 681–687.

Khalili, N. and Zargarbashi, S. (2010). “Influence of Hydraulic Hysteresis on Effective Stress in Unsaturated Soils.” Géotechnique. 60(9), 729–734.

Khosravi, A., Alsherif, N., Lynch, C., and McCartney, J.S. (2012). “Use of Multistage Triaxial Testing to Define Effective Stress Relationships for Unsaturated Soils.” ASTM Geotechnical Testing Journal. 35(1), 10pg.

Khosravi, A. and McCartney, J.S. (2012). “Impact of Hydraulic Hysteresis on the Small-Strain Shear Modulus of Unsaturated Soils.” ASCE Journal of Geotechnical and Geoenvironmental Engineering. 138(11), 1326–1333.

Laloui, L. and Cekerevac, C. (2003). “Thermo-plasticity of Clays: An Isotropic Yield Mechanism.” Computers and Geotechnics. 30, 649-660.

Laloui, L., Nuth, M., and Vulliet, L. (2006). “Experimental and Numerical Investigations of the Behavior of a Heat Exchanger Pile.” International Journal of Numerical and Analytical Methods in Geomechanics. 30, 763-781.

Likos, W. and N. Lu. (2003). “Automated Humidity System for Measuring Total Suction Characteristics of Clay.” Geotechnical Testing Journal, 26(2). 7 pg.

Loret, B. and Khalili, N. (2002). “An Effective Stress Elastic-Plastic Model for Unsaturated Porous Media.” Mechanics of Materials. 34, 97-116.

Lloret, A., Villar, M.V., Sanchez, M., Gens, A., Pintado, X. and Alonso, E.E. (2003). “Mechanical Behavior of Heavily Compacted Bentonite under High Suction Changes.” Géotechnique. 53(1), 27-40

Lu, N., Godt, J. and Wu, D. (2010). “A Closed-Form Equation for Effective Stress in Unsaturated Soil.” Water Resources Research. 46, 1–14.

Lu, N. and Likos, W.J. (2004). “Unsaturated soil mechanics.” John Wiley & Sons, New York.

Lu, N. and Likos, W.J. (2006). “Suction Stress Characteristic Curve for Unsaturated Soil.” Journal of Geotechnical and Geoenvironmental Engineering. 132(2), 131-142.

Matyas, E.L. and Radhakrishna, H.S. (1968). ‘‘Volume Change Characteristics of Partially Saturated Soils.’’ Géotechnique, 18, 432–448.

McCartney, J.S. (2012). “Issues Involved in Using Temperature to Improve the Mechanical behavior of Unsaturated Soils.” 5th Asia-Pacific Unsaturated Soils Conference. February 29-March 2, 2012. Pattaya, Thailand. 6 pg.

McCartney, J.S. and Murphy, K.D. (2012). “Strain Distributions in Full-Scale Energy Foundations.” DFI Journal. 6(2), 28-36.

McCartney, J.S. and Znidarcic, D. (2010). “Test System for Hydraulic Properties of Unsaturated nonwoven geotextiles.” Geosynthetics International. 17(5), 355-363.

McCartney, J.S., Ge, S., Reed, A., Lu, N., and Smits, K. (2013a). “Soil-Borehole Thermal Energy Storage Systems for District Heating.” European Geothermal Congress 2013, Pisa, Italy, June 3-7, 2013. 10 pg.

McCartney, J.S., Jensen, E., and Counts, B. (2013b). “Measurement of the Impact of Volume Change on Thermal Conductivity of Subgrade Soils.” TRB 2013. Washington, DC. January 13-17, 2013.

McKinstry, H. A. (1965). “Thermal Expansion of Clay Minerals.” The American Mineralogist, 50, 212–222.

Merchan, V., Vaunat, J., Romero, E., Meca, T. (2008). “Experimental Study of the Influence of Drying on the Residual Friction Angle of Clays.” Proceedings of the 1st European Conference on Unsaturated Soils, Durham, 423-428

Mitchell, J.K., and Soga, K. (2005). Fundamentals of Soil Behavior, 3rd ed., Wiley, NY.

Ng, C.W.W., Xu, J. and Yung, S.Y. (2009) “Effects of Imbibition-Drainage and Stress Ratio on Anisotropic Stiffness of an Unsaturated Soil at Very Small Strains.” Canadian Geotechnical Journal. 46(9), 1062-1076.

Ng, C.W.W. and Pang, Y.W. (2000). “Experimental Investigations of the Soil-Water Characteristics of a Volcanic Soil.” Canadian Geotechnical Journal. 37(6), 1252–1264.

Nishimura, T. and Fredlund, D.G. (2000). “Relationship between Shear Strength and Matric Suction in an Unsaturated Silty Soil.” Proc. UNSAT Asia. Singapore, May 18-19, 563-568.

Nishimura,T. and Fredlund, D.G. (2003). “A New Triaxial Apparatus for High Total Suctions Using Relative Humidity.” Proceedings of the 12th Asian regional conference on soil mechanics and geotechnical engineering, vol 1. Singapore, pp 65–68

Nuth, M. and Laloui, L. (2008). “Effective Stress Concept in Unsaturated Soils: Clarification and Validation of a Unified Framework.” International Journal for Numerical and Analytical Methods in Geomechanics. 32, 771–801.

Oh, W.T., Garga, V.K. and Vanapalli, S.K. (2008). “Shear Strength Characteristics of Statically Compacted Unsaturated Kaolin.” Canadian Geotechnical Journal. 45(7), 910–922.

Öberg, A., and Sällfors G. (1997). “Determination of Shear Strength Parameters of Unsaturated Silts and Sands Based on the Water Retention Curve.” Geotechnical Testing Journal. 20(1), 40-48. doi:10.1520/GTJ11419J

Olchitzky, E. (2002). “Couplage Hydromécanique et Perméabilité d’une Argile Gonflante Non saturée sous Sollicitations Hydriques et Thermiques. Courbe de Sorption et Perméabilité à l’Eau.” Ph.D. Thesis, École nationale des ponts et chaussées, Paris, France.

Passwell, R.E. (1967). “Temperature Effects on Clay Soil Consolidation.” Journal of the Soil Mechanics and Foundation Engineering Division. 93(3): 9–22.

Pintado, X., Lloret, A. and Romero, E. (2009). “Assessment of the Use of the Vapour Equilibrium Technique in Controlled-Suction Tests.” Canadian Geotechnical Journal. 46, 411-423.

Plum, R.L. and Esrig, M.I. (1969). “Some Temperature Effects on Soil Compressibility and Pore Water Pressure.” Effects of Temperature and Heat on Engineering Behavior of Soils. Highway Research Board. Washington, DC. 103: 231–242.

Preene, M. and Powrie, W. (2009). “Ground Energy Systems: From Analysis to Geotechnical Design.” Géotechnique. 59(3), 261-271.

Rahardjo, H., Hritzuk, K.J., Leong, E.C. and Rezaur, R.B. (2003) “Effectiveness of Horizontal Drains of Slope Stability.” Journal of Engineering Geology, June, 69(3-4), 295-308.

Rahardjo, H., Ong, B.H., and Leong, E.C. (2004). “Shear Strength of a Compacted Residual Soil from Consolidated Drained and Constant Water Content Triaxial Tests.” Canadian Geotechnical Journal 41(3): 421-436. doi: 10.1139/t03-093.

Romero, E. (1999). “Characterisation and Thermo-Hydro-Mechanical Behavior of Unsaturated Boom Clay: An Experimental Study.” Ph.D. Thesis. Universitat Politécnica de Catalunya. Spain.

Romero, E., Gens, A. and Lloret, A. (2001). “Temperature Effects on the Hydraulic Behavior of an Unsaturated Clay.” Geotechnical and Geological Engineering. 19: 311-332.

Romero, E., Gens, A. and Lloret, A. (2003). “Suction Effects on a Compacted Clay under Non-Isothermal Conditions.” Géotechnique. 53(1): 65-81.

Saix, C. (1991). “Consolidation Thermique par Chaleur d’un sol Non Saturé.” Canadian Geotechnical Journal. 28, 42–50.

Saix, C., Devillers, P. and El Youssoufi, M.S. (2000). “Éléments de Couplage Thermomécanique Dans la Consolidation de Sols Non Saturés.” Canadian Geotechnical Journal. 37: 308-317.

Salager, S., El Youssoufi, M.S. and Saix, C. (2007). “Influence of Temperature on the Water Retention Curve of Soils. Modelling and Experiments.” Experimental Unsaturated Soil Mechanics. 112: 251-258.

Salager, S., François, B., El Youssoufi, M.S., Laloui, L. and Saix, C. (2008). “Experimental Investigations of Temperature and Suction Effects on Compressibility and Pre-Consolidation Pressure of a Sandy Silt.” Soils and Foundations. 48(4): 453-466.

Sheng, D., Fredlund, D.G., and Gens, A. (2008a). “A New Modelling Approach for Unsaturated Soils Using Independent Stress Variables.” Canadian Geotechnical Journal, 45(4): 511–534. doi:10.1139/T07-112.

Sherif, M.A., and Burrous, C.M., (1969). “Temperature Effects on the Confined Shear Strength of Saturated, Cohesive Soil.” Proceedings of an International Conference on Effects of Temperature and Heat on Engineering Behavior of Soils, Highway Research Board, Special Report 103, pp. 267-272.

She, H.Y., and B.E. Sleep (1998). “The Effect of Temperature on Capillary Pressure-Saturation Relationships for Air-Water and Perchloroethylene-Water Systems.” Water Resources Research. 34(10), 2587–2597, doi:10.1029/98WR01199.

Sibbitt, B., McClenahan, D., Djebbara, R., Thornton, J., Wong, B., Carriere, J., and Kokko, J. (2012). “The Performance of a High Solar Fraction Seasonal Storage District Heating System – Five Years of Operation.” Energy Procedia. 30, 856–865.

Sillers, W.S., Fredlund, D.G., and Zakerzadeh, N. (2001). ‘‘Mathematical Attributes of Some Soil-Water Characteristic Models.’’ Geotechnical and Geological Engineering. 19, 243–283.

Skempton, W.A. (1961). “Effective Stress in Soils, Concrete, and Rocks.” International Conference on Pressure and Suction in Soils. Butterworth, London. 4-16.

Sultan, N., Delage, P. and Cui, Y.J. (2002). “Temperature Effects on the Volume Change Behavior of Boom Clay.” Engineering Geology. 64, 135-145.

Tamagnini, R. (2004). “An Extended Cam-Clay Model for Unsaturated Soils with Hydraulic Hysteresis.” Géotechnique. 54(3), 223–228.

Tang, A.M. and Cui, Y.J. (2005). “Controlling Suction by the Vapour Equilibrium Technique at Different Temperatures and its Application in Determining the Water Retention Properties of MX80 clay.” Can. Geotech. J. 42(1), 287-296.

Tang, A.M., Cui, Y.J. and Barnel, N. (2008). “Thermo-Mechanical Behavior of a Compacted Swelling Clay.” Géotechnique. 58(1): 45-54.

Terzaghi, K. (1925). “Principles of Soil Mechanics.” Engineering News Record. 95(19-23).

Tessier, D. (1984). “Étude Expérimentale de L’organisation Desmatériaux Argileux: Hydratation, Gonflement et Structuration au Cours de la Dessiccation et de la Reéhumectation.” Ph.D. thesis, Université de Paris VII, Paris, France.

Thomas, H.R., Sansom, M. and Rees, S.W. (2001). Non-Isothermal Flow. In: Schrefler, B.A. ed. Environmental Geomechanics, CISM International Centre for Mechanical Sciences Courses and Lectures, vol. 417. Springer, pp. 131-169.

Thu, T.M., Rahardjo, H. and Leong, E.C. (2006). “Shear Strength and Pore Water Pressure Characteristics during Constant Water Content Triaxial Tests.” Journal of Geotechnical and Geoenvironmental Engineering. ASCE. 136(3): 411-419.

Toll, D.G., and Ong, B.H. (2003). “Critical State Parameters for an Unsaturated Residual Sandy Clay.” Geotechnique 53(1):93–103. doi:10.1680/geot.2003.53.1.93.

Towhata, I., Kuntiwattanakul, P., Seko, I. and Ohishi, K. (1993). “Volume Change of Clays Induced by Heating as Observed in Consolidation Tests.” Soils and Foundations, 33(4): 170–183.

Uchaipichat, A. (2005). “Experimental Investigation and Constitutive Modeling of Thermo-Hydro-Mechanical Coupling in Unsaturated Soils.” PhD Dissertation. University of New South Wales. 293 pg.

Uchaipichat, A. and Khalili, N. (2009). “Experimental Investigation of Thermo-Hydro-Mechanical Behavior of an Unsaturated Silt.” Géotechnique. 59(4): 339-353.

Vanapalli, S.K., Fredlund, D.G., Pufahl, D.E. and Clifton, A.W. (1996). “Model for the Prediction of Shear Strength with Respect to Soil Suction.” Canadian Geotechnical Journal. 31: 379-392.

van Genuchten, M.T. (1980). “A Closed Form Equation for Predicting the Hydraulic Conductivity of Unsaturated Soils.” Soil Science Society of America Journal. 44: 892-898.

Vaunat, J., Merchan, V., Romero, E. and Pineda, J. (2007). “Residual Strength of Clays at High Suctions.” In Proc. of the 2nd Int. Conf. on Mech. of Unsat. Soils, Weimar, Germany, vol. 2, 151–162.

Vega, A. and McCartney, J.S. (2014). “Cyclic Heating Effects on the Thermal Volume Change of Silt.” ASCE GeoCongress 2012. Oakland, CA. March 25-29th 2012. 10 pg.

Villar, M.V. (1999). “Investigation of the Behavior of Bentonite by Means of Suction-Controlled Oedometer Tests.” Engineering Geology. 54, 67-73.

Villar, M.V. (2000). “Caracterizacion Termo-Hidro-Mecanica Deuna Bentonita de Cabo de Gata.” Ph.D. Thesis, Universidad Complutense de Madrid, Madrid, Spain.

Villar, M. V. and Gomez, R. (2007). “Retention Curves of Two Bentonites at High Temperature.” Experimental Unsaturated Soil Mechanics pp267-274

Wheeler, S.J., Sharma, R.J. and Buisson, M.S.R. (2003). “Coupling of Hydraulic Hysteresis and Stress-Strain Behavior in Unsaturated Soils.” Géotechnique. 53(1): 41-54.

Wiebe, B., Graham, J., Tang, G.X.M. and Dixon, D. (1998). “Influence of Pressure, Saturation, and Temperature on the Behaviour of Unsaturated Sand-Bentonite.” Canadian Geotechnical Journal. 35:194–205.